MICROBIAL AND GEOCHEMICAL IRON REDOX CYCLING IN CHOCOLATE POTS HOT SPRINGS, YELLOWSTONE NATIONAL PARK

By

Nathaniel W. Fortney

A dissertation submitted in partial fulfillment of

the requirements for the degree of

Doctor of Philosophy

(Geoscience)

at the

UNIVERSITY OF WISCONSIN-MADISON

2018

Date of final oral examination: 5/22/2018

The dissertation is approved by the following members of the Final Oral Committee:

Eric E. Roden, Professor, Geoscience
Eric S. Boyd, Assistant Professor, Thermal Biology Institute, Montana State University
Clark M. Johnson, Professor, Geoscience
Katherine D. McMahon, Professor, Bacteriology
Shaomei He, Scientist, Geoscience

To my children Charlie and Max,
for giving me the motivation to finish my PhD,
and most importantly for giving me a sense of purpose.

Acknowledgements

Science doesn't take place in a vacuum and there are a whole host of people I need to thank, acknowledge, and sing praises to for helping me get to this point. I hope I don't forget anyone.

First, to my advisor, Eric Roden, thank you for meeting with me for coffee all those years ago when I was still in the process of applying to graduate school. I remember saying I wanted to work on extremophiles, but had no ideas for projects or any clue about graduate research, and now that I've spent all this time investigating the microbes at Chocolate Pots, I hardly think of them as being "extreme" anymore. I quickly learned that "grabbing a coffee" would be commonplace and has been a great way to discuss results, new experiments, and life. Not only has Eric had a tremendous influence on my lab work, my ability to think about research, and my writing, but he has also been there for moral support during some of the greatest and most challenging points in my life. Eric genuinely has cared about and continues to care about the wellbeing of my family and myself, and that has meant wonders to me. Thank you.

Thank you to Eric Boyd for serving on my committee throughout my graduate career and for introducing me to Yellowstone. Thanks for accompanying us on our first field campaign, and letting me borrow your lab members on my return trips. To Clark Johnson I owe a debt of gratitude for being the PI of two NASA Astrobiology Institute grants. UW Madison being a NAI center was what drew me to the department in the first place, and the second grant supported me throughout my graduate career. Shaomei He introduced me to the world of metagenomics, and I now feel that bioinformatics is my greatest strength in leaving the department. Thank you for patiently explaining the command line to me and writing the numerous scripts that have helped me in my research.

Brandon Converse is no longer a member of our lab group, but he introduced me to the command line and gave me my introduction to bioinformatics that I am truly appreciative of. Though Brian Beard was not officially a member of my PhD committee, I feel as though he has played an equivalent role in my graduate career. Iron isotope analyses are challenging and Brian has been an incredible help with instrument troubleshooting and data interpretation. Thank you also to the postdocs in the isotope geochemistry group, Aaron Satkoski, Xinyuan Zheng, and Piyali Chanda, for more troubleshooting efforts, staying up late with me on the mass spec and coming in at odd hours to help tune the instrument.

To the lab group of Michael Friedrich in Bremen, Germany, thank you so much for adopting me for the few weeks I was working with you on stable isotope probing. Thank you especially to Ajinkya Kulkarni and Charlotte Holz for your experimental troubleshooting during the month prior to my arrival, your friendship, and the numerous coffee breaks!

Thanks to my fellow graduate students for welcoming me into the department, being my friends these past several years, and supporting each other in solidarity as we make our way through grad school. I felt like an outsider at first by being a microbiologist among a bunch of geologists, but now I'm proud to say I'm a GeoBadger! To my officemates, current and former, Stephanie Napieralski, Nick Levitt, Thiru Reddy, Bre Hashman, and Liz Percak-Dennett, thank you for listening to me go on about my research, teaching me about your own research, commiserating about the struggles of graduate school and life, but mostly thank you for being my friend.

Thank you to my friends and family for supporting me in everyway possible during my graduate career. For feeding me, for motivating me, for listing to me, for taking care of Katie and the kids during my absence for research or at conferences, for taking care of my children, I could

go on… “thank you” doesn’t seem like enough, but thank you. A special thanks to my parents for supporting my education, and encouraging me to continue pursuing it.

I will never be able to acknowledge the amount of support and patience from my loving wife, Katie, during my graduate career. I think graduate school has been a more trying experience for her than it was for me. I couldn’t have done this without her. She has kept me sane, and took care of our two children. I owe her big time. To my children, Charlie and Max, I know you’re probably too young to fully understand what I spent the past six years doing, but my hope is that it will allow me to provide for you better, and I hope to instill some of my curiosity and wonder about the world around us in you. Thank you.

TABLE OF CONTENTS

List of Tables

List of Figures

ABSTRACT

Hydrothermal vent systems, both terrestrial and oceanic, are important environments for astrobiological research because of the hypothesized origin of life on Earth occurring at such environments. Recent and increasing evidence for relic vent deposits on Mars has further piqued the interest of astrobiologists and have become the target for future investigations for potential Martian life. While the origin of life is still highly debated, the redox gradients formed near hydrothermal vents and the energetic advantage this gives life living in such environments is undeniable. Hyperthermophilic prokaryotic organisms are phylogenetically deeply rooted, which supports the notion of originating near hydrothermal vents. Furthermore, many of these deeply rooted organisms encode Fe redox cycling based metabolic pathways suggesting dissimilatory Fe reduction (DIR) and Fe(II) oxidation are ancient microbial metabolisms. Chocolate Pots hot springs (CP) are a collection of Fe-rich circumneutral-pH hydrothermal springs located in northwestern Yellowstone National Park. For the past two decades, one of the more prominent features has been investigated with interest in how oxygenic phototrophs (e.g. cyanobacteria) may have contributed to banded iron formation deposition in the Archean. Here we expand on previous enrichment culture based investigations of the putative Fe cycling microbial community by conducting Fe(III)-reducing incubation experiments and collecting sediment and spring water samples directly from CP to gain a better understanding of the composition of the microbial community and its metabolic potential *in situ*. High DIR activity was observed in samples collected near the hot spring vent, and diminished further downstream. Results from 16S rRNA gene amplicon and shotgun metagenomic sequencing revealed taxa related to *Thermodesulfovibrio* and Ignavibacteria which encoded putative extracellular electron transfer

pathways as potential indication of the *in situ* Fe(III)-reducing microbial community. Fe isotope fractionation that occurs as a result of DIR has been recognized as a potential biomarker of microbial activity in the rock record and in modern environments. Although natural variability obfuscated results, samples collected from the vent pool and sediment cores revealed fractionation suggestive of DIR. These studies provide constraint on the potential pathways and signatures of both extant and ancient Fe-based microbial life on Earth, Mars, and other rocky planets.

INTRODUCTION

Chocolate Pots hot springs (CP) is an iron (Fe)-rich, circumneutral-pH geothermal environment in Yellowstone National Park. Relic hydrothermal systems have been identified on Mars, and modern systems that support active Fe redox cycling like CP hot springs give us an understanding of how life could have functioned in such environments. The distribution, abundance, and activity of dissimilatory Fe(III)-reducing bacteria (DIRB) at CP is not well understood, and although indirect oxidation of Fe(II) promoted by oxygenic phototrophs, e.g. cyanobacteria, has been well-studied, the investigation of lithotrophic Fe(II) oxidation has been limited. Furthermore, Fe isotope fractionation linked to dissimilatory Fe(III) reduction (DIR) is recognized as an indicator of microbial activity in both the rock record and modern Fe redox cycling environments. The studies encompassed in the three chapters of this dissertation couple a metagenomic perspective of the *in situ* microbial community with geochemical evidence of microbial activity, including stable Fe isotope ratios, to gain insight into how Fe redox cycling may function in this and other modern Fe-rich environments, and potentially have functioned in astrobiologically relevant locations, like early Earth and ancient Mars.

In chapter one, an *in vitro* incubation experiment was conducted to assess the Fe(III)-reducing ability of the un-enriched microbial community from the CP vent, and two other locations along the flow path. Incubations were conducted with and without additional carbon and electron donor (acetate) to gain an understanding of the potential limitation *in situ*. High levels of Fe(III) reduction activity were observed at the vent with diminished activity downstream, suggesting carbon and electron donor limitation within a few meters of the vent. Follow-up stable isotope probing (SIP) incubation experiments using ^{13}C-labeled acetate were

combined with 16S rRNA gene amplicon and shotgun metagenomic sequencing to gain an understanding of the active *in situ* DIRB community at CP. Metagenome assembled genomes (MAGs) of known and putative DIRB, including *Geobacter*, Ignavibacteria, and *Thermodesulfovibrio* encoded homologs to genes in extracellular electron transfer (EET) systems involved in Fe redox transformations. These results suggested DIRB are actively involved in Fe redox cycling within Fe/Si oxide deposits located at the hot spring vent.

In chapter two, a culture-independent approach was used to determine the distribution of putative Fe cycling microorganisms in the CP vent pool and along the outflow channel of CP. Spring water was filtered from the vent source and sediment cores were collected along the flow path for DNA extraction and using 16S rRNA gene amplicon and shotgun metagenomic sequencing. High coverage MAGs derived from the sediment microbial community were related to taxa previously identified at CP, including *Thermodesulfovibrio* and Ignavibacteria, and encoded putative EET systems corroborating documented Fe(III) reduction activity from this location from earlier studies (Chapter 1). MAGs were identified encoding both putative EET systems and CO_2 fixation pathways, inferred to be lithoautotrophic Fe(II)-oxidizing bacteria and were related to the known lithoautotrophic Fe(II) oxidizer, *Sideroxydans*. A relatively low abundance in the microbial communities of the vent pool and sediment cores was consistent with the expectations for this metabolic process, and while they may still play an important role in Fe(II) oxidation at CP overall, this process along with CO_2 fixation appears to be dominated by the cyanobacterial population.

Chapter three examined the Fe geochemistry and stable Fe isotopic composition of CP spring water and sediment core samples collected from along the flow path. Geochemical results were consistent with previous studies of the activity of the Fe(III)-reducing microbial community

at CP in that no DIR activity was observed beyond the vent pool as evidenced by a lack of Fe(II). The isotope composition of sequential HCl extracted Fe phases from an Fe(III)-reducing incubation experiment was obscured by high Fe(II) concentrations in the 0.5 M HCl extracted phase, however fractionation estimates between Fe(II) and Fe(III) phases ranged between ca. -1.8‰ and -3.2‰, which is on the order of expected fractionation for DIR. Fe isotope ratios were similarly obscured in the *in situ* samples due to high Fe(II) concentrations in the 0.5 M HCl extracted phase. An Fe isotope fractionation of approximately -1.5‰ was measured between Fe(II) and Fe(III) in the vent pool deposits, however this fractionation was apparent only in the top few centimeters of the sediment core, beyond which extrapolated uncertainties become too great.. No fractionation was observed in the more distal core samples. These results suggest that under a modern oxidizing atmosphere, relic microbially produced Fe(II) quickly oxidizes resulting in no net fractionation thereby erasing any biosignature of DIR. Thus, Fe isotope ratios may only be a useful biosignature for active Fe redox cycling environments in near-surface hydrothermal environments.

Taken together the findings reported in these studies provide the first comprehensive examination of the microbiology and geochemistry of Fe(III) reduction and other Fe redox-associated processes in Chocolate Pots hot springs. Such studies provide key constraints on the potential pathways and signatures of both extant and ancient Fe-based microbial life on Earth, Mars, and other rocky planets.

CHAPTER 1

Stable Isotope Probing for Microbial Iron Reduction in Chocolate Pots Hot Spring, Yellowstone National Park

Nathaniel W. Fortney,[a] Shaomei He,[a] Ajinkya Kulkarni,[b] Michael W. Friedrich,[b] Charlotte Holz,[b] Eric S. Boyd,[c] Eric E. Roden[a]

[a]Department of Geoscience, NASA Astrobiology Institute, University of Wisconsin-Madison, Madison, Wisconsin, USA
[b]Microbial Ecophysiology Group, Faculty of Biology/Chemistry & Center for Marine Environmental Science (MARUM), University of Bremen, Bremen, Germany
[c]Department of Microbiology and Immunology, NASA Astrobiology Institute, Montana State University, Bozeman, Montana, USA

Fortney NW, He S, Kulkarni A, Friedrich MW, Holz C, Boyd ES, Roden EE. 2018. Stable isotope probing of microbial iron reduction in Chocolate Pots hot spring, Yellowstone National Park. Appl Environ Microbiol 84:15. doi:10.1128/AEM.02894-17.

ABSTRACT

Chocolate Pots hot springs (CP) is a circumneutral-pH Fe-rich geothermal feature located in Yellowstone National Park. Previous Fe(III)-reducing enrichment culture studies with CP sediments identified close relatives of known dissimilatory Fe(III)-reducing bacterial (FeRB) taxa, including *Geobacter* and *Melioribacter*. However, the abundances and activities of such organisms in the native microbial community are unknown. Here, we used stable isotope probing experiments combined with 16S rRNA gene amplicon and shotgun metagenomic sequencing to gain an understanding of the in situ Fe(III)-reducing microbial community at CP. Fe-Si oxide precipitates collected near the hot spring vent were incubated with unlabeled and ^{13}C-labeled acetate to target active FeRB. We searched reconstructed genomes for homologs of genes involved in known extracellular electron transfer (EET) systems to identify the taxa involved in Fe redox transformations. Known FeRB taxa containing putative EET systems (*Geobacter*, *Ignavibacteria*) increased in abundance under acetate-amended conditions, whereas genomes related to *Ignavibacterium* and *Thermodesulfovibrio* that contained putative EET systems were recovered from incubations without electron donor. Our results suggest that FeRB play an active role in Fe redox cycling within Fe-Si oxide-rich deposits located at the hot spring vent.

IMPORTANCE

The identification of past near-surface hydrothermal environments on Mars emphasizes the importance of using modern Earth environments, such as CP, to gain insight into potential Fe-based microbial life on other rocky worlds, as well as ancient Fe rich Earth ecosystems. By combining stable carbon isotope probing techniques and DNA sequencing technology, we gained insight into the pathways of microbial Fe redox cycling at CP. The results suggest that microbial

Fe(III) oxide reduction is prominent *in situ*, with important implications for the generation of geochemical and stable Fe isotopic signatures of microbial Fe redox metabolism within Fe-rich circumneutral-pH thermal spring environments on Earth and Mars.

KEYWORDS

Yellowstone National Park, metagenomics, microbial iron reduction, stable isotope probing

INTRODUCTION

Iron (Fe) is the most abundant redox-active element in Earth's crust and is also present in significant quantities on other rocky worlds, such as Mars (1, 2). In microbial energy metabolism, Fe can serve as an electron acceptor in the form of ferric iron [Fe(III)] (3) or as an electron donor in the form of ferrous iron [Fe(II)] (4, 5). Researchers have suggested that microbial Fe cycling, Fe(III) reduction and Fe(II) oxidation, have both been active microbial metabolic processes since the Archean eon (6-8).

Oxidized and reduced Fe minerals on the Martian crust form a redox gradient between the surface and subsurface (9, 10), and such gradients can serve as a potential source of oxidants/reductants supporting microbial life. Recent mineralogical studies of deposits in the Endeavor and Gale craters by the Opportunity and Curiosity rovers have identified Fe(III)-rich smectites and other clay minerals, suggesting formation in a circumneutral-pH environment (9, 10). These results are counter to the previous identification of Fe(III)-sulfate minerals (e.g., jarosite) in other regions of the Meridiani Planum, such as the Burns Formation, which are suggestive of a more acidic environment formation (11). The identification of potentially habitable circumneutral-pH environments on Mars necessitates the study of modern analogue environments on Earth.

Chocolate Pots hot springs (CP) are located approximately 5 km southwest of the Norris Geyser Basin in Yellowstone National Park and comprise a series of warm Fe- and Si-rich circumneutral-pH springs. One of the most studied features, and the subject of this research, is located along the southeastern bank of the Gibbon River. This hot spring consists of a primary hot spring vent, referred to here as CP (Fig. 1.1A), and two smaller satellite vents (not pictured) located several meters below and to either side of the main vent. CP has been studied for the

better part of the past century in regard to properties of the Fe-Si precipitates (12), groundwater chemistry (13-16), indirect photosynthetically mediated Fe(II) oxidation (15-18), stable Fe isotope geochemistry (19), and more recently, microbial dissimilatory iron reduction (DIR) (20). DIR is of particular interest at CP, as it has the potential to produce geochemical and stable isotopic signatures of microbial activity (21), with important implications for the detection of past or even present Fe-based microbial life in astrobiologically relevant places, such as Mars (22).

Enrichment culture studies with Fe-Si oxide material from CP successfully demonstrated the potential for reduction of these materials by microorganisms recovered from the *in situ* microbial community (20). 16S rRNA gene amplicon and metagenomic sequences from the enrichment cultures were related to known and potential dissimilatory iron-reducing bacteria (FeRB). Additionally, gene sequences corresponding to putative extracellular electron transfer (EET) protein complexes potentially responsible for DIR were identified in enrichment culture metagenomic libraries. Recent geochemical analyses have provided evidence for active DIR in sediments from the vicinity of the hot spring vent (N. Fortney, unpublished data), but the question remains as to which taxa are driving DIR *in situ* in CP. This study sought to identify active FeRB in CP by way of short-term ^{13}C-labeled stable isotope probing (SIP) experiments with native CP materials. Metagenomic analysis of community DNA was undertaken to identify and make inferences about the metabolic potential of Fe(III)-reducing organisms.

RESULTS

***In vitro* Fe(III) reduction experiments.** Anoxic incubation experiments were conducted with native CP materials collected on two occasions to assess *in situ* Fe(III) reduction potential

(see Materials and Methods). Fe(II) (>50 mmol L^{-1}) was produced in all treatment groups of the 2013 Fe(III)-reducing incubations of material collected from core sampling site 1, where greater than 85% of the Fe(III) oxides were reduced by 11 days (Fig. 1.2A). A smaller, but measurable, level of Fe(III) reduction activity was observed in the incubations of the site 3 material, with greatly diminished levels of activity in the incubations without an exogenous electron donor (Fig. 1.2B). A negligible level of activity was measured in the incubations of the site 5 material, with or without an added electron donor (Fig. 1.2C). No difference in Fe(III) reduction activity was observed between incubations with and without sodium molybdate, indicating that sulfate reduction was minimal; thus, Fe(III) was the main electron acceptor in these incubations. Substantial amounts of Fe(II) (ca. 40 mmol L^{-1}) were produced in the SIP incubations amended with both unlabeled acetate and [^{13}C]acetate after 10 days (Fig. 1.3). A measurable, although smaller, amount of Fe(II) (ca. 16 mmol L^{-1}) was produced in the incubations without an additional electron donor (Fig. 1.3).

Isopycnic centrifugation. Approximately 1 μg of DNA was extracted from each replicate of the sediment slurry from the Fe(III)-reducing following incubation for 10 days and was subjected to isopycnic separation. The buoyant densities of all low-density fractions were an average of 1.698 g mL^{-1} ± 0.004 g mL^{-1} and 1.718 g mL^{-1} ± 0.005 g mL^{-1} for all high-density fractions (Fig. 1.4; see also Fig. A.1.1 in the supplemental material), indicating the successful separation of ^{13}C-labeled DNA from unlabeled DNA. In all treatment groups, the concentrations and yields of DNA recovered from the low-density fractions were greater than those from the corresponding high-density fractions (Table A.1.2).

Microbial community composition of Fe(III)-reducing incubations. Bacterial 16S rRNA gene amplicon sequencing identified similar dominant taxa in the high- and low-density

fractions from all acetate-amended Fe(III)-reducing treatment groups (Fig. 1.5 and Table 1.1; see also Table A.1.3). The distinction between the 16S rRNA gene amplicon libraries from the different Fe(III)-reducing treatment groups was broken into the following three categories based on the analysis of similarity (ANOSIM) statistic *R*: indistinguishable (*R* = 0.00 to 0.25), distinct with some overlap (*R* = 0.25 to 0.50), and distinct (*R* >0.50). Using these criteria, only three pairs of 16S rRNA gene amplicon groups were significantly ($P < 0.05$) distinct from one another. These three pairs are (i) low-density unlabeled acetate and high-density [^{13}C]acetate, (ii) low-density unlabeled acetate and low-density no-electron donor (ED), and (iii) high-density [^{13}C]acetate and low-density no-ED. The similarity percentage (SIMPER) dissimilarity percentage was also greatest (i.e., 80.1%) in the high-density [^{13}C]acetate and low-density no-ED pair. Pairwise comparisons of the remaining pairs indicated that they were not significantly distinct from each other (Table A.1.4).

Dominant 16S rRNA gene operational taxonomic units (OTUs) from the high-density fractions of the [^{13}C]acetate-amended and unlabeled-acetate-amended treatments were related to *Geobacter* spp. and the class *Ignavibacteria* (Fig. A.1.3). No dominant *Geobacter*-related OTUs were identified in the no-ED treatment; however, several OTUs related to *Rhodocyclaceae*, *Thermodesulfovibrionaceae*, and *Ignavibacteria* were present. These same OTUs were present in the 16S rRNA gene amplicon libraries from the [^{13}C]acetate-amended and unlabeled-acetate-amended incubations, although at lower abundance than that of the *Geobacter*-related OTUs. The dominant OTUs from the low-density fraction of the [^{13}C]acetate-amended incubation were similarly represented in the no-ED high-density fraction, and the two contained the same relatives of *Ignavibacteria*, *Rhodocyclaceae*, *Thermodesulfovibrionaceae*, and *Comamonadaceae* (Tables 1.1 and A.1.3b). The same OTUs related to *Geobacter* spp.,

Ignavibacteria, and *Rhodocyclaceae* were present between both the high- and low-density fractions of the unlabeled-acetate-treated incubation DNA pools (Tables 1.1 and A.1.3a). The reads from the 10 most dominant OTUs comprised approximately 40 to 50% of all reads in these sequences, with the exception of the high-density fraction from the [^{13}C]acetate- amended incubations, where ca. 80% of all reads were affiliated with the 10 dominant taxa (Table 1.1).

The dominant OTUs from the archaeal 16S rRNA gene amplicon libraries were similar between all treatment groups and were distantly related to a euryarchaeote from the family *Methanomassiliicoccaceae* and a crenarchaeote from the class *Aigarchaeota* (Tables A.1.5a to f). Neither of these taxa has been implicated in DIR (23, 24). The remaining dominant taxa were most closely related to two methanogenic archaeal clones (25). Reads from the 10 most dominant OTUs comprised greater than 75% of all reads in the treatment groups.

Metagenomic analysis of Fe(III)-reducing SIP incubations. Shotgun metagenomic sequencing libraries were obtained from the low-density fraction of DNA from the Fe(III)-reducing incubations due to insufficient yield from the high-density fractions. The fact that we obtained shotgun metagenomic sequences from the low-density DNA pools from the Fe(III)-reducing incubations seems inconsequential to the answers we sought in this experiment. However, while the abundances of certain taxa differ between the 16S rRNA gene amplicon libraries of the different Fe(III)-reducing incubations, most notably the separation of libraries based on the metabolism of acetate and the physical separation of taxa that incorporated [^{13}C] into biomass, the dominant taxa are identical between high- and low-density DNA pools (Table 1.1).

Paired-end Illumina MiSeq shotgun sequencing produced a total of 7,408,844, 8,020,977, and 8,593,381 reads for the unlabeled-acetate, [^{13}C]acetate, and no-ED Fe(III)-reducing

incubations, respectively. The combined metagenomic assembly (coassembly) of the Fe(III)-reducing treatment groups contained 24,023,202 reads, following trimming and merging. The coassembled Fe(III)-reducing metagenome contained 681,666 contigs, with an average length of 958 bp and an N_{50} of 1,257 bp.

The CONCOCT algorithm identified 132 bins in the Fe(III)-reducing metagenomic coassembly; one bin was manually split, for a total of 133 bins (Fig. A.1.4). One bin was a composite of two bacterial phyla and could not be separated based on GC content, coverage, or binning algorithm. The composite bin was primarily composed of *Acidobacteria* and *Ignavibacteriae*. Sixty-four bins had completeness of greater than 50% and contamination that was less than 10% (Fig. A.1.5). Twelve bins contained a putative EET system.

Sequences encoding putative porin-like structures homologous to the porin iden- tified in the *Geobacter*-like porin-cytochrome-complex (*pcc*) gene cluster (26, 27) and that were proximal to a multiheme cytochrome *c* on assembled contigs were identified in three bins related to *Chlorobi*, *Geobacter* spp., and *Deltaproteobacteria* in the Fe(III)- reducing metagenomic coassembly (Fig. 1.6 and A.1.6). No homologs of *Shewanella*-like *mtrABC* genes (28) were identified in the metagenomic coassembly.

A search of the metagenomic coassembly for multiheme *c*-type cytochromes (*c*-cyts) proximal to putative outer membrane (OM) porins revealed the presence of several additional potential EET. The Fe(III)-reducing metagenomic coassembly contained five putative OM porins and associated *c*-cyts in bins identified as *Chthonomonas calidirosea*, *Pedosphaera parvula*, *Ignavibacterium* spp., *Thermoanaerobaculum* spp., and *Desulfomonile* spp., which were not previously identified in the search for other EET gene homologs (Fig. 1.6 and A.1.6). Four high-coverage bins identified as *Deltaproteobacteria*, *Anaerolinea thermophila*, *Acidobacteria*, and

Thermodesulfovibrio contained a putative OM porin but an incomplete set of proximal or supplemental *c*-cyts (Text A.1.2.1 for details). An additional putative OM porin accompanied by proximal multiheme *c*-cyts was identified in the *pcc*-containing *Geobacter* bin in the Fe(III)-reducing metagenomic coassembly.

DISCUSSION

Fe(III)-reducing SIP incubations. (i) 16S rRNA gene amplicon libraries. Relatives of *Geobacter* spp. were the dominant taxa in 16S rRNA gene amplicon libraries from both the [^{13}C]acetate and unlabeled-acetate incubations. The acetate stimulation can be seen by the representation of similar taxa (e.g., *Geobacter*) in all acetate-amended treatments, with the exception of the low-density [^{13}C]acetate incubations (Table 1.1; see also Fig. A.1.3 and Table A.1.3a). 16S rRNA gene amplicon libraries from the high- and low-density DNA from the unlabeled-acetate incubations are largely indistinguishable in terms of the dominant OTUs (Fig. 1.5). These results were not surprising and have been observed previously in acetate-amended Fe(III)-reducing incubations of CP materials and in other environments (3, 20), and they are most likely a result of *Geobacter* spp. outcompeting other native Fe reducers. A previous study demonstrated that *Geobacter* spp. outcompeted *Rhodoferax* spp. under conditions of acetate stimulation because of their higher growth rate (29). It seems likely that a similar phenomenon is responsible for the predominance of *Geobacter* spp. in our acetate-amended incubations.

High-density DNA was collected from the no-ED Fe(III)-reducing incubations to (i) identify which members of the microbial community might naturally fall in that range due to higher-density DNA (e.g., by virtue of having higher GC content), and (ii) demonstrate that the organisms identified in the [^{13}C]acetate-amended incubations were not simply carryover from

this naturally higher-density population but were indeed from organisms metabolizing the [^{13}C]acetate and incorporating it into biomass. The clear separation of the high-density DNA from the [^{13}C]acetate treatment group and high-density DNA from the no-ED treatments demonstrates that the SIP incubation and subsequent gradient density separation successfully captured organ- isms that metabolized and incorporated [^{13}C] into biomass (Fig. 1.5). This separation is also reflected in a notable difference in the abundant OTUs from these samples (Table 1.1), where the 16S rRNA gene library from the [^{13}C]acetate treatments is composed almost entirely of *Geobacter* OTUs, which are absent from the no-ED 16S rRNA gene amplicon libraries.

16S rRNA gene sequences from the low-density DNA pool from the [^{13}C]acetate incubations clustered with the no-ED samples (Fig. 1.5), suggesting that this DNA pool represents the non-[^{13}C]-incorporating portion of the microbial community. In summary, the response of the microbial community to the different incubation conditions for the SIP experiment resulted in a clear separation based on the ability of the organisms to metabolize acetate or not, followed by a clustering within the acetate- metabolizing population based on the physical separation of the [^{13}C]DNA from the unlabeled DNA (Fig. 1.5).

(ii) Metagenomic libraries. SIP enabled the recovery of DNA from organisms in the Fe(III)-reducing incubation that metabolized [^{13}C]acetate and incorporated the heavy isotope into DNA. Unfortunately, the quantity of [^{13}C]DNA from the Fe(III)-reducing incubations was insufficient for shotgun metagenomic sequencing. However, as mentioned above, similar taxa were recovered in the low-density unlabeled-acetate and high-density [^{13}C]acetate 16S rRNA gene amplicon libraries. Thus, the same organisms were sequenced as part of a metagenomic

library, regardless of the DNA pool from which the sequences originated, such that we were still able to assess in situ taxa and metabolic pathways in CP vent materials.

The metagenomic libraries from the Fe(III)-reducing incubations reflect the striking stimulation of certain members of the microbial community with the addition of acetate. This is most apparent in the dominant *Deltaproteobacteria* bin in the metagenomic coassembly. The *Deltaproteobacteria* bin was a minor member of the microbial community in the no-ED treatment metagenomic library, yet it increased in abundance (i.e., read coverage) by up to two orders of magnitude in the presence of acetate (2.6x, 29.5x, and 157.2x coverage of the *Deltaproteobacteria* bin in the no-ED, unlabeled-acetate, and [^{13}C]acetate libraries, respectively). This response is similar to what was observed for *Geobacter* OTUs in the 16S rRNA gene amplicon libraries. The competition among acetate-utilizing members of the microbial community is reflected by the fact that more-abundant members of the microbial community under no-ED conditions decreased in abundance under acetate-amended conditions, presumably because they were outcompeted by other acetate-utilizing taxa (e.g., *Deltaproteobacteria* or *Geobacter*).

Principal-component analyses did not show a distinct pattern of clustering of the archaeal members of the microbial community based on the unlabeled-acetate, [^{13}C]acetate, and no-ED treatment groups (Fig. A.1.2). Conversely, the bacterial portion of the microbial community had more separation between samples from the high- and low-density DNA pools from the different incubation treatments (Fig. 1.5). A contributing factor could be whether or not the archaeal microbial community is capable of utilizing acetate. Although many archaeal OTUs were (distantly) related to methanogenic species (Tables A.1.5a to f), it has been reported that the optimal pH for acetotrophic methanogenesis is greater than the average pH (ca. 5.8) of the vent

pool at CP (30, 31). Given this information, it is likely that the archaeal microbial community does not utilize acetate and was therefore unaffected by the addition of acetate to the incubations, resulting in nearly indistinguishable populations between the treatment groups. The lack of response to acetate stimulation in the archaeal community is also reflected in the metagenomic library. The three *Crenarchaeota* bins are of roughly equal read coverage under all incubation conditions (Fig. 1.6).

Relative abundances of known and potential FeRB under Fe(III)-reducing conditions. Average differential coverage of the metagenomic bins was used as an estimate of which taxa were more abundant in the incubations under Fe(III)-reducing conditions, with or without additional electron donor. Because Fe(III) reduction was observed under all incubation conditions, we hypothesized that the more abundant taxa containing a putative EET system would be involved in this metabolic process. The average coverage per treatment group of all binned contigs in the Fe(III)-reducing metagenomic coassembly was 4.7, and bins with an average coverage greater than this value were considered to be dominant members of the microbial community. While the dominant *Deltaproteobacteria* bin cannot be conclusively identified as a *Geobacter* relative, this is a likely possibility given the extremely high coverage of the metagenomic bin (Fig. 1.6) and the dominating presence of *Geobacter* spp. in the acetate-amended samples from the 16S rRNA gene amplicon library (Fig. A.1.2). Given these assumptions, the *Geobacter* relatives contributed extensively to DIR under acetate-amended Fe(III)-reducing conditions. Although not previously documented as FeRB, bins related to the genus *Ignavibacterium* ($n = 2$) had greatly increased coverage in the acetate-amended incubations. A similar increase in coverage was observed in the *Thermodesulfovibrio*-related bin. Canonically, *Thermodesulfovibrio* spp. are documented as being sulfate reducers; however, they

have also been shown to be able to reduce Fe(III) (32). The *Geobacter*-like *pcc* EET system has been identified in *Ignavibacterium album* (26), although, as described above, no putative EET systems have been identified in any of the isolated *Thermodesulfovibrio* genomes. The increased read coverage along with the presence of putative EET systems in the genomes, and in the case of the *Thermodesulfovibrio* bin, previously documented Fe(III) reduction, all support the idea that these organisms contributed to acetate-stimulated Fe(III) reduction. The *Acidobacteria*-related bin had high coverage under all incubation conditions and showed much less stimulation in the presence of acetate than the more abundant bins described above. This suggests that the *Acidobacteria* relative, while still a potentially active FeRB in the incubations, is less competitive than other FeRB in the microbial community. Interestingly, the *Acidobacteria*-related bin was the highest coverage putative FeRB in the no-ED incubations, a possible indication of its function as the dominant FeRB *in situ*.

EET pathways involved in Fe(III) reduction present at CP. The presence of the *pcc* EET system in bins related to *Geobacter*, *Ignavibacterium*, *Melioribacter*, and *Deltaproteobacteria* in the Fe(III)-reducing metagenomic coassembly (Fig. 1.6 and A.1.6) was expected based on previous comparative genomic analyses (26, 27), as well as recent CP FeRB enrichment culture experiments that revealed the presence of *pcc* in reconstructed genomes of *Geobacter* and *Ignavibacteriae* (20). Both *Geobacter* spp. and *Melioribacter* spp. are documented FeRB (33-35), and it is reasonable to expect that metagenomic bins belonging to relatives of these organisms reflect the same metabolic capacity under the imposed Fe(III)-reducing conditions. Although poorly resolved phylogenetically, the presence of *pcc* homologs in a bin identified as *Deltaproteobacteria* is also not surprising. *Ignavibacterium* and *Melioribacter* relatives were previously classified under the phylum *Chlorobi* (36), and both taxa

have been documented as having *pcc*, so it is possible that the poorly resolved *Chlorobi* bin from the Fe(III)-reducing metagenomic coassembly is related to these genera and possesses a similar genomic makeup.

Our previous study of FeRB enrichment culture studies from CP identified homologs to the *pcc* EET system in metagenomic bins related to *Thermodesulfovibrio* (20). A *pcc*-like EET system also was identified in the *Thermodesulfovibrio* bin from the Fe(III)-reducing coassembly in this study, but the gene arrangement was not directly analogous to the canonical *pcc* system described by Liu et al. (27). Although this putative *pcc*-like EET system has not been scrutinized using genomic and physiological experiments, the gene arrangement and properties (e.g., number of heme-binding sites, predicted cellular location, and transmembrane [TM] domains) suggest a function similar to that of *pcc*. Curiously, although no putative EET systems have been identified in any of the published *Thermodesulfovibrio* sp. genomes available on IMG, the ability to reduce Fe(III) has been demonstrated previously (32), which might explain the presence of putative EET genes in the *Thermodesulfovibrio*-related metagenomic bin. It should be noted that the *Thermodesulfovibrio*-related bins from the previous enrichment culture metagenome (20) and the current SIP metagenomic analysis are only distantly related to each other and to the type strains of *Thermodesulfovibrio* (ca. 90% identification, based on the V4 region of 16S rRNA gene sequences; data not shown), suggesting that the bins from the two experiments, while both identified as being related to *Thermodesulfovibrio*, are in fact not the same organism; therefore, we should not expect them to possess the same metabolic potential. Of further note, the *Thermodesulfovibrio*-related bin from the present study is only partially complete (78%; Fig. A.1.6).

Putative EET systems were also identified in bins belonging to several phyla, including *Acidobacteria*, *Chloroflexi*, *Armatimonadetes*, *Proteobacteria*, and *Verrucomicrobia*. Metagenomic analyses suggest that the *Acidobacteria* bins (n = 2), the *Desulfomonile* bin (*Proteobacteria*), and the *Pedosphaera* bin (*Verrucomicrobia*) are potentially involved in Fe(III) reduction (Text A.1.3.1). However, neither the *Desulfomonile* nor *Pedosphaera* bins are particularly abundant, especially *Desulfomonile* in the no-ED treatment, which suggests that if these taxa are indeed FeRB, they are unlikely to have a major contribution to overall Fe(III) reduction at CP (Fig. 1.6).

Summary and conclusions. The purpose of this study was to identify which members of the microbial community endemic to CP are actively involved in Fe(III) reduction under conditions meant to represent *in situ* conditions as best as possible. Previous incubation studies have demonstrated the ability of enrichment cultures of CP microorganisms to reduce Fe(III) oxides (20), but this is the first use of SIP to target the organisms responsible for this activity. By using ^{13}C-labeled acetate and isopycnic centrifugation, we were able to separate the portion of the community that had incorporated [^{13}C] into its DNA by metabolizing acetate coupled to DIR. Acetate is a universal electron donor for FeRB communities (3), including thermophilic communities (37-39), and there is good reason to suspect that acetate is also a major electron donor for DIR at CP, especially given the immediate response of the microbial community to acetate addition. 16S rRNA gene amplicon sequencing identified OTUs related to known FeRB, and metagenomic sequencing identified genes within these taxa which are involved in EET, thereby strengthening the hypothesis that these organisms are involved in DIR.

Geobacter was a dominant taxon in the acetate-containing SIP incubations. However, *Geobacter* spp. were not detected in the no-ED incubations, which also showed significant DIR

activity. This suggests that relatives of this taxon were stimulated by even a very small addition of acetate, which is consistent with previous enrichment culture experiments (20). The results from the SIP incubations also revealed the presence of other moderately abundant taxa that incorporated acetate into biomass (e.g., *Thermodesulfovibrio* and *Ignavibacteria*). Notably, these taxa were also significant members of the microbial community of the no-ED incubations. In addition, these taxa were also present, though in lower abundances, in previous enrichment culture experiments (20). The ability of *Thermodesulfovibrio* relatives native to CP to metabolize acetate and reduce Fe(III) is consistent with the abilities of isolated strains of this organism (32). Together, these results suggest that moderately thermophilic taxa, such as *Thermodesulfovibrio* and *Ignavibacteria*, are responsible for *in situ* DIR at CP.

Forthcoming research is targeting the *in situ* microbial community at CP using sediment cores and vent pool fluid to assess the role of Fe-redox transformations in generating geochemical and stable Fe isotopic signatures of microbial Fe energy metabolism within this Fe-rich circumneutral-pH thermal spring. Delineation of such signatures in modern Earth environments is a prerequisite for detecting signs of ancient terrestrial and past or present Fe-based microbial life on Mars and other rocky planets.

MATERIALS AND METHODS

Description of Chocolate Pots hot springs. CP (thermal ID: GCPNN002; 44.71008, -110.7413) is located approximately 5 km south of the Norris Geyser Basin along the southern bank of the Gibbon River, next to Grand Loop Road. The temperatures of the sampling locations where the sediment cores were collected in 2013 were 50.7°C at site 1 (hot spring vent), 48.4°C at site 3, and 42.7°C at site 5. The pHs of the sediment core sampling sites were 5.9, 6.5, and 7.8,

respectively. The temperature and pH of the vent pool were 51.5°C and 5.8, respectively, in October 2014. Subsurface water emanating from the vent pool is anoxic and contains high levels of dissolved Fe(II) and Si, at ca. 0.1 and 5 mM, respectively (16).

Sample collection. Small sediment cores and spring water were collected from the CP vent and along the flow path in August 2013 (Fig. 1.1B). Water and sediment samples were collected near the vent in October 2014. Spring water was collected from the pool (Fig. 1.1A) at the vent of the main mound of CP using a peristaltic pump. Fe-Si oxide sediment was collected from the bottom of the vent pool using a plastic scoop. Water and sediment were stored in degassed and sterilized bottles. The bottles were fitted with a stopper to ensure an airtight seal. One bottle of spring water was kept anoxic by bubbling with N_2 for 15 min; the other bottle was kept partially oxic by including an air headspace. The sediment was overlain with an approximately equal volume of spring water and degassed with N_2 for 5 min with swirling to remove any traces of oxygen in the sediment and water. Temperature, pH, and conductivity were measured at the vent pool using a WTW pH 3310 ProfiLine meter with SenTix 51 electrode (Cole-Parmer, Vernon Hills, IL).

Fe-Si oxide slurry preparation. A portion of the sediment cores collected in 2013 was used to produce a Fe-Si oxide slurry for use in small-scale incubation experiments. In an anaerobic chamber (95:5%, N2:H2; Coy Products, Grass Lake, MI), an additional volume of anoxic spring water was added to the Fe-Si sediment bottle for a final ratio of ca. 1:2 solid to liquid. The jar containing the sediment and water was swirled, and the suspended material was decanted into a beaker so that coarse sand grain-sized material remained in the bottle. Fine-grained material was withdrawn from the beaker using a needle and syringe. Fine-grained material, here referred to as CP slurry (CPS), was dispensed into a glass bottle fitted with a cap

modified to hold the top of a crimped and stoppered anaerobic pressure tube. The bottle containing CPS was removed from the anaerobic chamber, and the headspace was degassed with N_2 to remove residual H_2. CPS was prepared identically immediately upon return to the lab using the fresh sediment and spring water collected in 2014.

Fe(III) reduction experiments. CPS for the Fe(III)-reducing incubations was aliquoted into sterile anoxic serum bottles fitted with butyl rubber stoppers. All transfers were made using sterile N_2-flushed syringes and needles. Four treatments were tested for the 2013 Fe(III)-reducing incubation experiments. Reactors were prepared in duplicate with a mixture of acetate and lactate as an additional electron donor (0.5 mM final concentration), without an electron donor added (no-ED), and each treatment with and without sodium molybdate (Na_2MoO_4) to a final concentration of 0.6 mM as a specific inhibitor of bacterial sulfate reduction (40). Treatment groups are here referred to as acetate/lactate (Ac/Lac), Ac/Lac plus molybdate, Ac/Lac, no-ED, and no-ED plus molybdate, respectively.

Fe(III)-reducing incubations for the 2014 stable isotope probing (SIP) experiment were prepared in triplicate and contained 0.5 mM ^{13}C-labeled acetate ([^{13}C]H_3COONa, 99%; Cambridge Isotope Laboratories, Inc., Andover, MA), 0.5 mM unlabeled acetate, or no additional electron donor. The treatment groups are here referred to as [^{13}C]acetate, unlabeled acetate, and no-ED, respectively. All incubations were conducted at 50°C in the dark.

Fe(III) reduction activity was determined by the accumulation of acid-soluble Fe(II). Subsamples were collected approximately every 2 days, added to 0.5 M HCl, and agitated for 1 h. An aliquot of the extract was added to ferrozine colorimetric reagent (41) with and without the addition of 10% hydroxylamine hydrochloride to quantify total Fe and Fe(II), respectively. The amount of Fe(III) was determined by the difference between total solubilized Fe and Fe(II).

Acetate-amended incubations received an additional 0.5 mM acetate after each sampling, unless there was no increase in Fe(II) since the previous sampling.

The incubations from the 2013 Fe(III)-reducing experiments were terminated after 19 days. Fe(III)-reducing incubations from the 2014 SIP experiment were terminated after 10 days. The contents of the Fe(III)-reducing serum bottles were decanted into Falcon tubes in an anaerobic chamber and then frozen at -20°C.

DNA extraction and stable isotope probing. DNA was extracted from the frozen aliquots of sediment using the Mo Bio PowerSoil DNA isolation kit (Mo Bio, Carlsbad, CA), in accordance with previously published modifications (20). Replicate samples were kept separate during DNA extraction. DNA was not extracted from the azide-amended treatments from the Fe(II)-oxidizing incubations. High-density (^{13}C-labeled) and low-density (^{12}C-labeled) DNA from the 2014 Fe(III)-reducing SIP experiment was separated using isopycnic centrifugation, according to previously published methods (42-44), with modifications described in Text A.1.1.1.

16S rRNA gene amplicon sequencing and analysis. Gradient fractions corresponding to high- and low-density pools of DNA were selected for 16S rRNA gene amplification based on fractions with the highest fluorescence measurement in the PicoGreen assay (Thermo Fisher Scientific, Darmstadt, Germany), according to the manufacturer's instructions (n = 19). Buoyant densities of fully ^{13}C-labeled and unlabeled *Escherichia coli* DNA fractions with high fluorescence were also used to select fractions for amplification and sequencing. DNA was amplified using universal 16S rRNA gene PCR primers specific to target bacteria and archaea. The PCR and amplification conditions are described elsewhere (Text A.1.1.2).

PCR amplicons from bacterial and archaeal amplifications of the gradient-density-separated Fe(III)- reducing incubation DNA (n = 38) were submitted to the University of Wisconsin Biotechnology Center (UWBC; https://www.biotech.wisc.edu/) for paired-end 2 x 300-bp Illumina MiSeq 16S rRNA gene amplicon sequencing. Microbial community sequence data were processed using the Quantitative Insights into Microbial Ecology (QIIME) pipeline version 1.8.0 (http://www.qiime.org) (45), following the protocol for handling paired-end Illumina sequence data (Text A.1.1.2). Briefly, QIIME is used to identify and cluster reads into operational taxonomic units (OTUs) for each amplicon library, which are then subjected to homology-based analyses to obtain taxonomic information about the composition of the reads within each sample. The beta diversity of the samples was calculated using weighted UniFrac metrics (46, 47). The software package PRIMER (Primer-E; http://www.primer-e.com/ [48]) was used to conduct an analysis of similarity (ANOSIM) and similarity percentage (SIMPER) to analyze the statistical significance of the differences between treatment groups in the Fe(III)-reducing incubation.

Metagenomic sequencing and assembly. The remaining non-PCR-amplified genomic DNA from the low-density fractions of the Fe(III)-reducing SIP incubations (n = 3) was submitted to the UWBC for paired-end 2 x 300-bp Illumina MiSeq shotgun metagenomic sequencing. Raw sequence data were assembled and processed using CLC Genomics Workbench 7.5.1 (https://www.qiagenbioinformatics.com/products/clc-genomics-workbench) at the UWBC computer center (Text A.1.1.3 for details).

Binning was accomplished using the automated clustering tool CONCOCT (49) on all contigs 2,500 bp and greater. Completeness, contamination, and bin heterogeneity were calculated using CheckM (50). “Contamination” is calculated by the number of multicopy

marker genes identified in each bin, generally as a result of multiple closely related organisms (e.g., strains) being binned together (50). The strain heterogeneity measurement determines how closely related multicopy genes are. A low heterogeneity measurement suggests that genes are from closely related organisms and can be thought of as redundancy, whereas high strain heterogeneity suggests that genes came from unrelated organisms and can be thought of as true contamination in a given genome bin. Highly redundant bins with high variance in average coverage were manually split based on the fold coverage of the contigs.

Taxonomic bins were visualized using Databionic ESOM Tools (51), according to previously described methods (20). Prodigal (52) and HMMer (53) were used to identify copies of the 111 conserved essential bacterial housekeeping genes (54) within the metagenomic coassembly. Amino acid sequences of the genes were aligned to the BLAST database (current as of 8 June 2016) using the BLASTp function in command-line BLAST (55). BLAST searches were performed using the computational resources and assistance of the UW-Madison Center for High Throughput Computing (CHTC) in the Department of Computer Sciences (http://chtc.cs.wisc.edu/). Output files were uploaded to MEGAN (56), and taxonomic information was exported for viewing in Dendroscope (57). The taxonomic identification of the bins was determined (Table A.1.6) using a consensus between Phylosift (58), CheckM, and MEGAN with the BLASTp input.

Differential coverage of metagenomic reads was used to determine the response of the microbial community to treatments in the Fe(III)-reducing SIP incubation experiment. Briefly, raw metagenomic sequence reads from each treatment group were paired, and sequencing adapters removed and quality trimmed. Processed reads from each treatment group were

individually mapped back to the coassembly using the read mapping function in CLC Genomics Workbench.

Metagenomic sequence analysis. The coassembly annotated in IMG/M ER was searched for genes of interest, i.e., genes involved in putative Fe cycling. A hidden Markov model (HMM) was created to search for the well-characterized *Geobacter*-like porin-cytochrome complex (*pcc*) (26, 27) EET system, as described previously (20). A list of candidate *pcc* homolog genes was refined (Text A.1.1.4). Homologs of the well-characterized EET system in the known FeRB *Shewanella* sp. (*mtrABC*) (28) were searched for in the metagenomic coassembly using command-line BLAST and the BLASTp function in IMG. Putative EET systems which were not homologous to known model systems were identified as follows: a Python script was used to search for multiheme *c*-cyts (>5 heme-binding sites) in the amino acid assembly from the metagenome. Putative OM porins were identified by investigating genes proximal to aforementioned multiheme *c*-cyts for TM domains and a predicted OM location. Genes fitting these criteria were classified as *pcc*-like. Bins containing putative EET systems were investigated further for supplemental genes predicted to be involved in Fe(III) transformation, as previously described (Table A.1.1) (59).

Accession number(s). All metagenomic contigs for the Fe(III)-reducing coassembly are available through IMG/M ER with taxon identification number 3300009943 (https://img.jgi.doe.gov/cgi-bin/m/main.cgi?section=TaxonDetail&page=taxonDetail&taxon_oid=3300009943). This targeted locus study project has been deposited at DDBJ/EMBL/GenBank under the accession no. PRJNA438487 (https://www.ncbi.nlm.nih.gov/bioproject/PRJNA438487/). The

version described in this paper is the first version, KBWS01000000 (https://www.ncbi.nlm.nih.gov/nuccore/KBWS01000000).

ACKNOWLEDGMENTS

This work was supported by National Aeronautics and Space Administration (NASA) award NNA13AA94A administered by the NASA Astrobiology Institute, and by the University of Bremen.

REFERENCES

1. Taylor SR, McLennan SM. 1985. The continental crust: its composition and evolution. Blackwell Scientific Publications, Oxford.
2. Taylor SR, McLennan SM. 2009. Mars: crustal composition and evolution, p 141-180, Planetary Crusts: Their Composition, Origin, and Evolution, vol 10. Cambridge University Press, Cambridge, UK.
3. Lovley DR, Holmes DE, Nevin KP. 2004. Dissimilatory Fe(III) and Mn(IV) Reduction. Adv Microb Physiol 49:219-286.
4. López-Archilla AI, Marin I, Amils R. 2001. Microbial Community Composition and Ecology of an Acidic Aquatic Environment: The Tinto River, Spain. Microb Ecol 41:20-35.
5. Emerson D, Moyer C. 1997. Isolation and Characterization of Novel Iron-Oxidizing Bacteria That Grow at Circumneutral pH. Appl Environ Microbiol 63:4784-4792.
6. Vargas M, Kashefi K, Blunt-Harris EL, Lovley DR. 1998. Microbiological evidence for Fe(III) reduction on early Earth. Nature 395:65-67.
7. Hafenbradl D, Keller M, Dirmeier R, Rachel R, Roßnagel P, Burggraf S, Huber H, Stetter KO. 1996. *Ferroglobus placidus* gen. nov., sp. nov., a novel hyperthermophilic archaeum that oxidizes Fe^{2+} at neutral pH under anoxic conditions. Arch Microbiol 16:308-314.
8. Emerson D. 2000. Microbial Oxidation of Fe(II) and Mn(II) at Circumneutral pH, p 31-52. *In* Lovley DR (ed), Environmental Microbe-Metal Interactions. ASM Press, Washington, D.C.
9. Grotzinger JP, Sumner DY, Kah LC, Stack K, Gupta S, Edgar L, Rubin D, Lewis K, Schieber J, Mangold N, Milliken R, Conrad PG, DesMarais D, Farmer J, Siebach K, Calef F, 3rd, Hurowitz J, McLennan SM, Ming D, Vaniman D, Crisp J, Vasavada A, Edgett KS, Malin M, Blake D, Gellert R, Mahaffy P, Wiens RC, Maurice S, Grant JA, Wilson S, Anderson RC, Beegle L, Arvidson R, Hallet B, Sletten RS, Rice M, Bell J, 3rd, Griffes J, Ehlmann B, Anderson RB, Bristow TF, Dietrich WE, Dromart G, Eigenbrode J, Fraeman A, Hardgrove C, Herkenhoff K, Jandura L, Kocurek G, et al. 2014. A habitable fluvio-lacustrine environment at Yellowknife Bay, Gale Crater, Mars. Science 343:1242777.
10. Arvidson RE, Squyres SW, Bell JF, 3rd, Catalano JG, Clark BC, Crumpler LS, de Souza PA, Jr., Fairen AG, Farrand WH, Fox VK, Gellert R, Ghosh A, Golombek MP, Grotzinger JP, Guinness EA, Herkenhoff KE, Jolliff BL, Knoll AH, Li R, McLennan SM, Ming DW, Mittlefehldt DW, Moore JM, Morris RV, Murchie SL, Parker TJ, Paulsen G, Rice JW, Ruff SW, Smith MD, Wolff MJ. 2014. Ancient aqueous environments at Endeavour Crater, Mars. Science 343:8.
11. Knoll AH, Carr M, Clark B, Des Marais DJ, Farmer JD, Fischer WW, Grotzinger JP, McLennan SM, Malin M, Schröder C, Squyres S, Tosca NJ, Wdowiak T. 2005. An astrobiological perspective on Meridiani Planum. Earth and Planetary Science Letters 240:179-189.
12. Allen ET, Day AL. 1935. Hot Springs of the Yellowstone National Park. Carnegie Institution of Washington.
13. Rowe JJ, Fournier RO, Morey GW. 1973. Chemical Analysis of Thermal Waters in Yellowstone National Park, Wyoming, 1960-65. Geol Surv Bull 1303:31.

14. Thompson JM, Yadav S. 1979. Chemical Analysis of Waters from Geysers, Hot Springs, and Pools in Yellowstone National Park, Wyoming from 1974 to 1978. U.S. Geological Survey, Menlo Park, CA.
15. Pierson BK, Parenteau MN. 2000. Phototrophs in high iron microbial mats: microstructure of mats in iron-depositing hot springs. FEMS Microbiol Ecol 32:181-196.
16. Parenteau MN, Cady SL. 2010. Microbial Biosignatures in Iron-Mineralized Phototrophic Mats at Chocolate Pots Hot Springs, Yellowstone National Park, United States. Palaios 25:97-111.
17. Pierson BK, Parenteau MN, Griffin BM. 1999. Phototrophs in High-Iron-Concentration Microbial Mats: Physiological Ecology of Phototrophs in an Iron-Depositing Hot Spring. Appl Environ Microbiol 65:5474-5483.
18. Trouwborst RE, Johnston A, Koch G, Luther GW, Pierson BK. 2007. Biogeochemistry of Fe(II) oxidation in a photosynthetic microbial mat: Implications for Precambrian Fe(II) oxidation. Geochim Cosmochim Ac 71:4629-4643.
19. Wu L, Brucker RP, Beard BL, Roden EE, Johnson CM. 2013. Iron Isotope Characteristics of Hot Springs at Chocolate Pots, Yellowstone National Park. Astrobiology 13:1091-101.
20. Fortney NW, He S, Converse BJ, Beard BL, Johnson CM, Boyd ES, Roden EE. 2016. Microbial Fe(III) oxide reduction potential in Chocolate Pots hot spring, Yellowstone National Park. Geobiology 14:255-75.
21. Johnson CM, Beard BL, Roden EE. 2008. The Iron Isotope Fingerprints of Redox and Biogeochemical Cycling in Modern and Ancient Earth. Ann Rev Earth Planet Sci 36:457-493.
22. Michalski JR, Onstott TC, Mojzsis SJ, Mustard J, Chan QHS, Niles PB, Johnson SS. 2017. The Martian subsurface as a potential window into the origin of life. Nat Geosci 11:21-26.
23. Huynh HTT, Nkamga VD, Signoli M, Tzortzis S, Pinguet R, Audoly G, Aboudharam G, Drancourt M. 2016. Restricted diversity of dental calculus methanogens over five centuries, France. Sci Rep 6:25775.
24. Takami H, Arai W, Takemoto K, Uchiyama I, Taniguchi T. 2015. Functional Classification of Uncultured "*Candidatus* Caldiarchaeum subterraneum" Using the Maple System. PLoS One 10:e0132994.
25. Chin K-J, Lukow T, Stubner S, Conrad R. 1999. Structure and function of the methanogenic archaeal community in stable cellulose-degrading enrichment cultures at two different temperatures (15 and 30°C). FEMS Microbiol Ecol 30:313-326.
26. Shi L, Fredrickson JK, Zachara JM. 2014. Genomic analyses of bacterial porin-cytochrome gene clusters. Front Microbiol 5:657.
27. Liu Y, Wang Z, Liu J, Levar C, Edwards MJ, Babauta JT, Kennedy DW, Shi Z, Beyenal H, Bond DR, Clarke TA, Butt JN, Richardson DJ, Rosso KM, Zachara JM, Fredrickson JK, Shi L. 2014. A trans-outer membrane porin-cytochrome protein complex for extracellular electron transfer by *Geobacter sulfurreducens* PCA. Environ Microbiol Rep 6:776-85.
28. Hartshorne RS, Reardon CL, Ross D, Nuester J, Clarke TA, Gates AJ, Mills PC, Fredrickson JK, Zachara JM, Shi L, Beliaev AS, Marshall MJ, Tien M, Brantley S, Butt JN, Richardson DJ. 2009. Characterization of an electron conduit between bacteria and the extracellular environment. Proc Natl Acad Sci U S A 106:22169-74.

29. Zhuang K, Izallalen M, Mouser P, Richter H, Risso C, Mahadevan R, Lovley DR. 2011. Genome-scale dynamic modeling of the competition between *Rhodoferax* and *Geobacter* in anoxic subsurface environments. ISME J 5:305-16.
30. Siegrist H, Vogt D, Garcia-Heras JL, Gujer W. 2002. Mathematical Model for Meso- and Thermophilic Anaerobic Sewage Sludge Digestion. Environ Sci Technol 36:1113-1123.
31. Demirel B, Scherer P. 2008. The roles of acetotrophic and hydrogenotrophic methanogens during anaerobic conversion of biomass to methane: a review. Rev Environ Sci Biotechnol 7:173-190.
32. Sekiguchi Y, Muramatsu M, Imachi H, Narihiro T, Ohashi A, Harada H, Hanada S, Kamagata Y. 2008. *Thermodesulfovibrio aggregans* sp. nov. and *Thermodesulfovibrio thiophilus* sp. nov., anaerobic, thermophilic, sulfate-reducing bacteria isolated from thermophilic methanogenic sludge, and emended description of the genus *Thermodesulfovibrio*. Int J Syst Evol Micr 58:2541-8.
33. Lovley DR, Giovannoni SJ, White DC, Champine JE, Phillips EJP, Gorby YA, Goodwin S. 1993. *Geobacter metallireducens* gen. nov. sp. nov., a microorganism capable of coupling the complete oxidation of organic compounds to the reduction of iron and other metals. Arch Microbiol 159:336-344.
34. Caccavo Jr. F, Lonergan DJ, Lovley DR, Davis M, Stolz JF, McInerney MJ. 1994. *Geobacter sulfurreducens* sp. nov., a Hydrogen- and Acetate-Oxidizing Dissimilatory Metal-Reducing Microorganism. Appl Environ Microbiol 60:3752-3759.
35. Podosokorskaya OA, Kadnikov VV, Gavrilov SN, Mardanov AV, Merkel AY, Karnachuk OV, Ravin NV, Bonch-Osmolovskaya EA, Kublanov IV. 2013. Characterization of *Melioribacter roseus* gen. nov., sp. nov., a novel facultatively anaerobic thermophilic cellulolytic bacterium from the class *Ignavibacteria*, and a proposal of a novel bacterial phylum *Ignavibacteriae*. Environ Microbiol 15:1759-71.
36. Iino T, Mori K, Uchino Y, Nakagawa T, Harayama S, Suzuki K. 2010. *Ignavibacterium album* gen. nov., sp. nov., a moderately thermophilic anaerobic bacterium isolated from microbial mats at a terrestrial hot spring and proposal of *Ignavibacteria* classis nov., for a novel lineage at the periphery of green sulfur bacteria. Int J Syst Evol Micr 60:1376-82.
37. Kashefi K, Holmes DE, Baross JA, Lovley DR. 2003. Thermophily in the *Geobacteraceae*: *Geothermobacter ehrlichii* gen. nov., sp. nov., a Novel Thermophilic Member of the *Geobacteraceae* from the "Bag City" Hydrothermal Vent. Appl Environ Microbiol 69:2985-2993.
38. Slobodkin AI. 2005. Thermophilic Microbial Metal Reduction. Microbiology 74:501-514.
39. Slobodkina GB, Reysenbach AL, Panteleeva AN, Kostrikina NA, Wagner ID, Bonch-Osmolovskaya EA, Slobodkin AI. 2012. *Deferrisoma camini* gen. nov., sp. nov., a moderately thermophilic, dissimilatory iron(III)-reducing bacterium from a deep-sea hydrothermal vent that forms a distinct phylogenetic branch in the *Deltaproteobacteria*. Int J Syst Evol Micr 62:2463-8.
40. Oremland RS, Capone DG. 1988. Use of “Specific” Inhibitors in Biogeochemistry and Microbial Ecology, p 285-383. *In* Marshall KC (ed), Adv Microbiol Ecol, vol 10. Plenum, New York.
41. Stookey LL. 1970. Ferrozine - a new spectrophotometric reagent for iron. Anal Chem 42:779-781.

42. Neufeld JD, Wagner M, Murrell JC. 2007. Who eats what, where and when? Isotope-labelling experiments are coming of age. ISME J 1:103-110.
43. Dunford EA, Neufeld JD. 2010. DNA stable-isotope probing (DNA-SIP). J Vis Exp doi:10.3791/2027:e2027.
44. Lueders T, Manefield M, Friedrich MW. 2004. Enhanced sensitivity of DNA- and rRNA-based stable isotope probing by fractionation and quantitative analysis of isopycnic centrifugation gradients. Environ Microbiol 6:73-78.
45. Caporaso JG, Kuczynski J, Strombaugh J, Bittinger K, Bushman FD, Costello EK. 2010. QIIME allows analysis of high-throughput community sequencing data. Nat Methods 7:335-336.
46. Lozupone C, Knight R. 2005. UniFrac: a new phylogenetic method for comparing microbial communities. Appl Environ Microbiol 71:8228-8235.
47. Lozupone C, Lladser ME, Knights D, Stombaugh J, Knight R. 2011. UniFrac: an effective distance metric for microbial community comparison. ISME J 5:169-172.
48. Clarke KR. 1993. Non-parametric multivariate analyses of changes in community structure. Aus J Ecol 18:117-143.
49. Alneberg J, Bjarnason BSr, de Bruijn I, Schirmer M, Quick J, Ijaz UZ, Lahti L, Loman NJ, Andersson AF, Quince C. 2014. Binning metagenomic contigs by coverage and composition. Nat Methods 11:1144-6.
50. Parks DH, Imelfort M, Skennerton CT, Hugenholtz P, Tyson GW. 2015. CheckM: assessing the quality of microbial genomes recovered from isolates, single cells, and metagenomes. Genome Res 25:1043-1055.
51. Ultsch A, Moerchen F. 2005. ESOM-Maps: tools for clustering, visualization, and classification with Emergent SOM. University of Marburg, Germany,
52. Hyatt D, Chen G-L, LoCascio PF, Land ML, Larimer FW, Hauser LJ. 2010. Prodigal: prokaryotic gene recognition and translation initiation site identification. BMC bioinformatics 11:119.
53. Finn RD, Clements J, Eddy SR. 2011. HMMER web server: interactive sequence similarity searching. Nucleic Acids Res 39:W29-37.
54. Albertsen M, Hugenholtz P, Skarshewski A, Nielsen KrL, Tyson GW, Nielsen PH. 2013. Genome sequences of rare, uncultured bacteria obtained by differential coverage binning of multiple metagenomes. Nat Biotechnol 31:533-538.
55. Altschul SF, Gish W, Miller W, Myers EW, Lipman DJ. 1990. Basic Local Alignment Search Tool. J Mol Biol 215:403-410.
56. Huson DH, Auch AF, Qi J, Schuster SC. 2007. MEGAN analysis of metagenomic data. Genome Res 17:377-386.
57. Huson DH, Scornavacca C. 2012. Dendroscope 3: an interactive tool for rooted phylogenetic trees and networks. Syst Biol 61:1061-1067.
58. Darling AE, Jospin G, Lowe E, Matsen FA, 4th, Bik HM, Eisen JA. 2014. PhyloSift: phylogenetic analysis of genomes and metagenomes. PeerJ 2:e243.
59. Shi L, Dong H, Reguera G, Beyenal H, Lu A, Liu J, Yu H-Q, Fredrickson JK. 2016. Extracellular electron transfer mechanisms between microorganisms and minerals. Nat Rev Microbiol 14:651-62.
60. Herlemann DPR, Geissinger O, Ikeda-Ohtsubo W, Kunin V, Sun H, Lapidus A, Hugenholtz P, Brune A. 2009. Genomic Analysis of "*Elusimicrobium Minutum*," the

First Cultivated Representative of the Phylum "*Elusimicrobia*" (Formerly Termite Group 1). Appl Environ Microbiol 75:2841-2849.

61. Sekiguchi Y, Yamada T, Hanada S, Ohashi A, Harada H, Kamagata Y. 2003. *Anaerolinea thermophila* gen. nov., sp. nov. and *Caldilinea aerophila* gen. nov., sp. nov., novel filamentous thermophiles that represent a previously uncultured lineage of the domain *Bacteria* at the subphylum level. Int J Syst Evol Micr 53:1843-1851.
62. Lefèvre CT, Frankel RB, Abreu F, Lins U, Bazylinski DA. 2011. Culture-independent characterization of a novel, uncultivated magnetotactic member of the Nitrospirae phylum. Environ Microbiol 13:538-549.
63. Henry EA, Devereux R, Maki JS, Gilmour CC, Woese CR, Mandelco L, Schauder R, Remen CC, Mitchell R. 1994. Characterization of a new thermophilic sulfate-reducing bacterium *Thermodesulfovibrio yellowstonii*, gen. nov. and sp. nov.: its phylogenetic relationship to *Thermodesulfobacterium commune* and their origins deep within the bacterial domain. Arch Microbiol 161:62-69.
64. Nepomnyashchaya YN, Slobodkina GB, Baslerov RV, Chernyh NA, Bonch-Osmolovskaya EA, Netrusov AI, Slobodkin AI. 2012. Moorella humiferrea sp. nov., a thermophilic, anaerobic bacterium capable of growth via electron shuttling between humic acid and Fe(III). Int J Syst Evol Micr 62:613-617.
65. Pradhan S, Srinivas TNR, Pindi PK, Kishore KH, Begum Z, Singh PK, Singh AK, Pratibha MS, Yasala AK, Reddy GSN, Shivaji S. 2010. Bacterial biodiversity from Roopkund Glacier, Himalayan mountain ranges, India. Extremophiles 14:377-395.
66. Jogler C, Niebler M, Lin W, Kube M, Wanner G, Kolinko S, Stief P, Beck AJ, de Beer D, Petersen N, Pan Y, Amann R, Reinhardt R, Schüler D. 2010. Cultivation-independent characterization of '*Candidatus* Magnetobacterium bavaricum' via ultrastructural, geochemical, ecological and metagenomic methods. Environ Microbiol 12:2466-2478.
67. Ettwig KF, Butler MK, Le Paslier D, Pelletier E, Mangenot S, Kuypers MMM, Schreiber F, Dutilh BE, Zedelius J, de Beer D, Gloerich J, Wessels HJCT, van Alen T, Luesken F, Wu ML, van de Pas-Schoonen KT, Op den Camp HJM, Janssen-Megens EM, Francoijs K-J, Stunnenberg H, Weissenbach J, Jetten MS, Strous M. 2010. Nitrite-driven anaerobic methane oxidation by oxygenic bacteria. Nature 464:543-548.
68. Anda D, Büki G, Krett G, Makk J, Márialigeti K, Eröss A, Mádl-Szönyi J, Borsodi AK. 2014. Diversity and morphological structure of bacterial communities inhabiting the Diana-Hygieia Thermal Spring (Budapest, Hungary). Acta Microbiol Immunol Hung 61:329-346.

Table 1.1 Bacterial community composition of the Fe(III)-reducing incubations.

DNA Fraction	SILVA Taxonomic Assignment[a]	% of total reads for the sample	Representative Species Match[b]	GenBank Accession no.	Similarity (%)	Inferred Physiology	Reference
High-density [^{13}C]acetate	*Geobacter* (g)	40.2	*Geobacter hephaestius*	AY737507.1	95	Fe(III) reduction	P. H. Janssen, unpublished data
	Geobacter (g)	12.5	*G. hephaestius*	AY737507.1	93	Fe(III) reduction	P. H. Janssen, unpublished data
	Geobacter (g)	8.4	*G. hephaestius*	AY737507.1	93	Fe(III) reduction	P. H. Janssen, unpublished data
	Geobacter (g)	3.7	*G. hephaestius*	AY737507.1	93	Fe(III) reduction	P. H. Janssen, unpublished data
	Geobacter (g)	3.3	*G. hephaestius*	AY737507.1	93	Fe(III) reduction	P. H. Janssen, unpublished data
	Deltaproteobacteria (c)	2.4	*Cystobacter armeniaca* strain DSM 14710	NR_043939.1	89	Uncharacterized	H. Reichenbach, unpublished data
	Ignavibacteria (c)	2.3	Bacterium YC-ZSS-LKJ31	KP174519.1	88	Uncharacterized moderate halophile	B. Zhao, K. Li, & K. Liu, unpublished data
	Syntrophobacteraceae (f)	1.6	Bacterium YC-ZSS-LKJ94	KP174423.1	87	Uncharacterized moderate halophile	B. Zhao, K. Li, & K. Liu, unpublished data
	Geobacter (g)	1.4	*G. hephaestius*	AY737507.1	93	Fe(III) reduction	P. H. Janssen, unpublished data
	Elusimicrobiales (o)	1.0	*Elusimicrobium minutum* strain Pei191	NR_074114.1	88	Fermenter	Herlemann et al. (60)
	Total[c]	77.1					
Low-density [^{13}C]acetate	Rhodocyclaceae (f)	5.9	Betaproteobacterium Rufe9b	AY235688.1	94	N_2 fixation	Z. Y. Tan, T. Hurek, & B. Reinhold-Hurek, unpublished data
	Ignavibacteria (c)	5.6	Bacterium YC-ZSS-LKJ31	KP174519.1	88	Uncharacterized moderate halophile	B. Zhao, K. Li, & K. Liu, unpublished data
	Syntrophobacteraceae (f)	5.4	Bacterium YC-ZSS-LKJ94	KP174423.1	87	Uncharacterized	B. Zhao, K. Li, & K. Liu, unpublished data
	Anaerolineae (c)	5.1	*Caldilinea aerophila* strain DSM 14535	NR_074397.1	86	Facultatively anaerobic heterotroph/fermentor	Sekiguchi et al. (61)
	Thermodesulfovibrionaceae (f)	4.6	*"Candidatus* Magnetoovum mohavensis" strain LO-1	GU979422.1	89	Oxidation of reduced S-species	Lefèvre et al. (62)
	Unassigned	4.3	Bacterium YC-LK-LKJ27	KP174640.1	87	Uncharacterized moderate halophile	Zhao, B., Li, K. & Liu, K., unpublished data
	Thermodesulfovibrionaceae (f)	4.1	*Thermodesulfovibrio yellowstonii* strain DSM 11347	NR_074345.1	91	Fe(III)/SO_4^{2-} reduction	Sekiguchi et al. (32) and Henry et al. (63)
	Thermodesulfovibrionaceae (f)	3.8	*T. yellowstonii* strain DSM 11347	NR_074345.1	91	Fe(III)/SO_4^{2-} reduction	Sekiguchi et al. (32) and Henry et al. (63)
	Elusimicrobiales (o)	2.9	*E. minutum* strain Pei191	NR_074114.1	88	Fermenter	Herlemann et al. (60)
	Bacteria (k)	2.3	*Moorella humiferrea* strain 64-FGQ	NR_108634.1	87	Indirect Fe(III) reduction via humic acids	Nepomnyashchaya et al. (64)
	Total[c]	43.8					
Low-density Unlabeled acetate	*Geobacter* (g)	13.5	*G. hephaestius*	AY737507.1	95	Fe(III) reduction	P. H. Janssen, unpublished data
	Ignavibacteria (c)	5.4	Bacterium YC-ZSS-LKJ31	KP174519.1	88	Uncharacterized moderate halophile	B. Zhao, K. Li, & K. Liu, unpublished data
	Rhodocyclaceae (f)	5.3	Betaproteobacterium Rufe9b	AY235688.1	94	N_2 fixation	Z. Y. Tan, T. Hurek, & B. Reinhold-Hurek, unpublished data
	Geobacter (g)	3.9	*G. hephaestius*	AY737507.1	93	Fe(III) reduction	P. H. Janssen, unpublished data
	Thermodesulfovibrionaceae (f)	3.4	*T. yellowstonii* strain DSM 11347	NR_074345.1	91	Fe(III)/SO_4^{2-} reduction	Sekiguchi et al. (32) and Henry et al. (63)
	Thermodesulfovibrionaceae (f)	3.3	*T. yellowstonii* strain DSM 11347	NR_074345.1	91	Fe(III)/SO_4^{2-} reduction	Sekiguchi et al. (32) and Henry et al. (63)
	Unassigned	3.1	Bacterium YC-LK-LKJ27	KP174640.1	87	Uncharacterized moderate halophile	B. Zhao, K. Li, & K. Liu, unpublished data
	Anaerolineae (c)	2.6	*C. aerophila* strain DSM 14535	NR_074397.1	86	Facultatively anaerobic heterotroph/fermentor	Sekiguchi et al. (61)
	Elusimicrobiales (o)	2.2	*E. minutum* strain Pei191	NR_074114.1	88	Fermenter	Herlemann et al. (60)
	Geobacter (g)	2.1	*G. hephaestius*	AY737507.1	93	Fe(III) reduction	P. H. Janssen, unpublished data
	Total[c]	44.8					
Low-density No electron donor	Rhodocyclaceae (f)	13.1	Betaproteobacterium Rufe9b	AY235688.1	94	N_2 fixation	Z. Y. Tan, T. Hurek, & B. Reinhold-Hurek, unpublished data
	Unassigned	5.4	Bacterium YC-LK-LKJ27	KP174640.1	87	Uncharacterized moderate halophile	B. Zhao, K. Li, & K. Liu, unpublished data
	Anaerolineae (c)	4.3	*C. aerophila* strain DSM 14535	NR_074397.1	86	Facultatively anaerobic heterotroph/fermentor	Sekiguchi et al. (61)
	Chloroflexi (p)	3.1	Bacterium YC-LK-LKJ27	KP174640.1	89	Uncharacterized moderate halophile	B. Zhao, K. Li, & K. Liu, unpublished data
	Chloroflexi (p)	2.9	Uncultured bacterium clone RUGL1-593	GQ420994.2	90	Uncharacterized	Pradhan et al. (65)
	Thermodesulfovibrionaceae (f)	2.8	*"Candidatus* Magnetobacterium bavaricum"	FP929063.1	89	Sulfur oxidation	Jogler et al. (66)
	Bacteria (k)	2.5	*"Candidatus* Methylomirabilis oxyfera"	NR_102979.1	86	NO_2^--driven CH_4 oxidation	Ettwig et al. (67)
	Ignavibacteria (c)	2.1	Bacterium YC-ZSS-LKJ31	KP174519.1	88	Uncharacterized moderate halophile	B. Zhao, K. Li, & K. Liu, unpublished data
	Comamonadaceae (f)	1.7	*Curvibacter delicatus* strain DHW-S121	HG974535.1	98	Uncharacterized	Anda et al. (68)
	Bacteria (k)	1.7	*M. humiferrea* strain 64-FGQ	NR_108634.1	87	Indirect Fe(III) reduction via humic acids	Nepomnyashchaya et al. (64)
	Total[c]	39.7					

[a] Abbreviations of taxonomic level: k, kingdom; p, phylum; c, class; o, order; f, family; g, genus.

[b] As determined by NCBI BLASTn.

[c] Total percent of reads comprising the 10 most dominant OTUs.

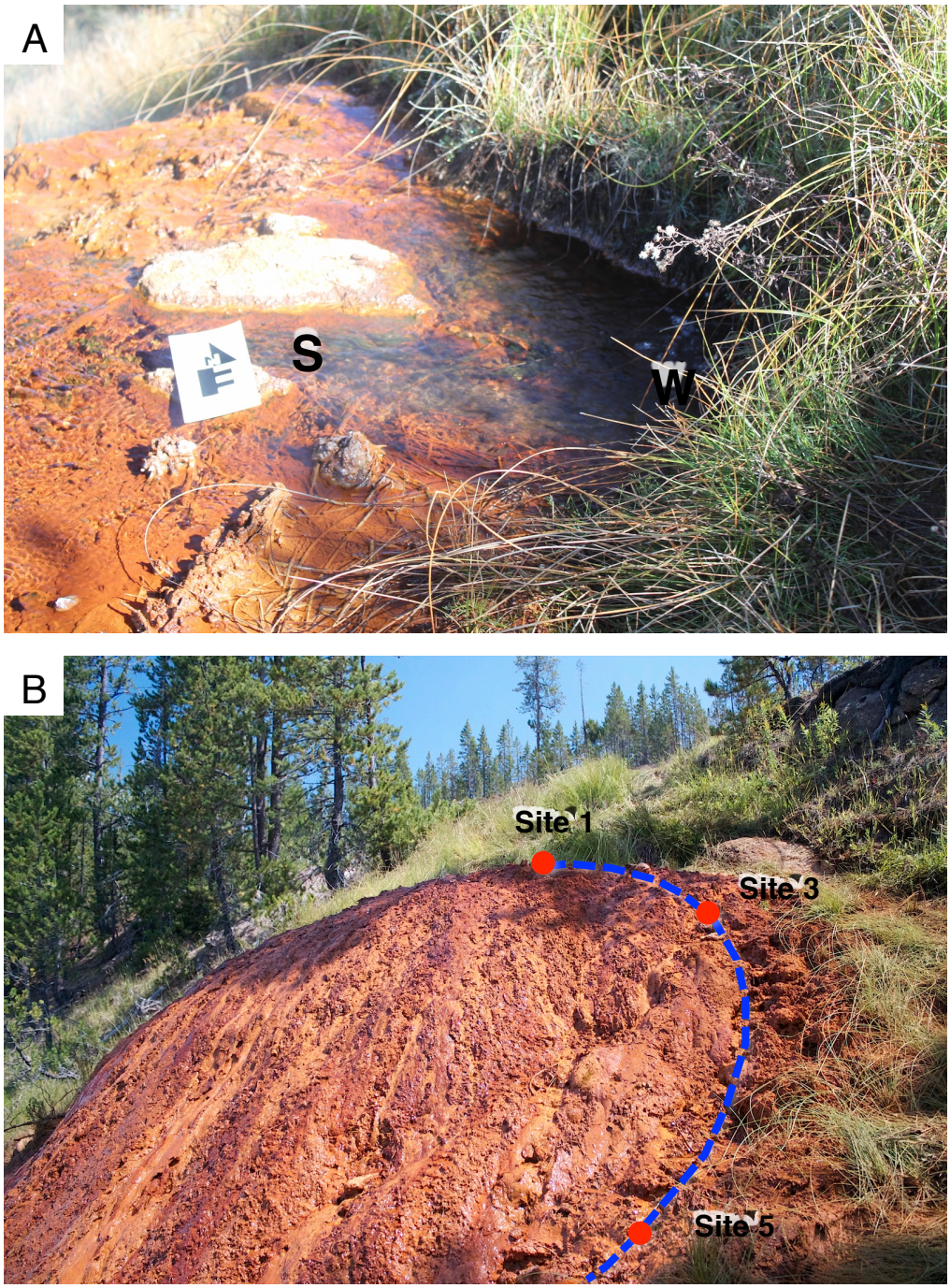

Figure 1.1. (A) Vent pool of the main mound hot spring at Chocolate Pots looking north toward the Gibbon River. Sediment used to initiate Fe(III)-reducing incubations was collected from the bottom of the pool, labeled with the letter S. Spring water was mixed with sediments to create a slurry for inoculating the Fe(III)-reducing incubations was collected near the hot spring source, labeled with the letter W. **(B)** Oblique view of the main mount vent of Chocolate Pots hot springs looking southeast toward Grand Loop Road. Approximate flow path of the hot spring water is indicated with a blue dashed line. Locations of the sampling sites of the sediment cores are labeled (1, 3, 5). Distance between Site 1 (hot spring vent pool) and Site 3 is 2.1 m and between Sites 3 and 5 is 4.7 m.

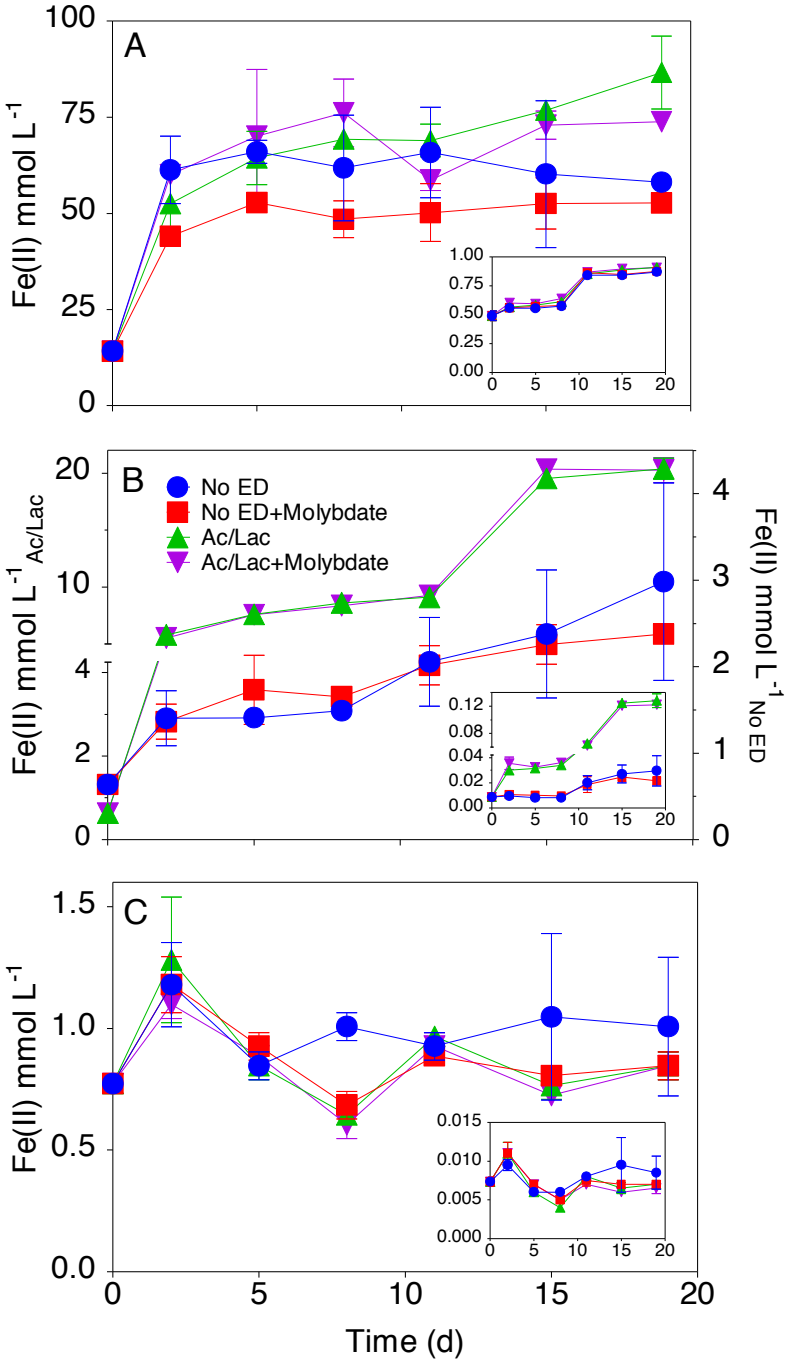

Figure 1.2. Fe(II) production for the 2013 Fe(III)-reducing incubations of Fe-Si oxide slurry prepared with CP spring water, pH 5.9. Inset panels represent the ratio of Fe(II) to total Fe at the same sampling time points. Site 1 (**A**) represents incubations of sediment samples collected from the hot spring vent pool. Sediment samples incubated from Sites 3 (**B**) and 5 (**C**) were collected along the flow path approximately 2 and 7 m downstream from the spring source, respectively. Samples were incubated at *in situ* temperatures, 50°C for Sites 1 and 3, and 43°C for Site 5. Ac/Lac amended treatments were dosed to a final concentration of 0.5 mM, and given an additional dose at Day 11. Sodium molybdate (Na_2MoO_4) containing treatments were dosed to a final concentration of 0.6 mM. Note different Y-axis scales for Fe(II) concentration measured in acetate-amended and no ED incubations in Panel (B). Data points represent single measurements on duplicate serum bottles. Error bars represent 1σ variability in the measurements; error bars not shown are smaller than the symbol. Abbreviations: No ED, No electron donor; Ac, acetate; Lac, lactate.

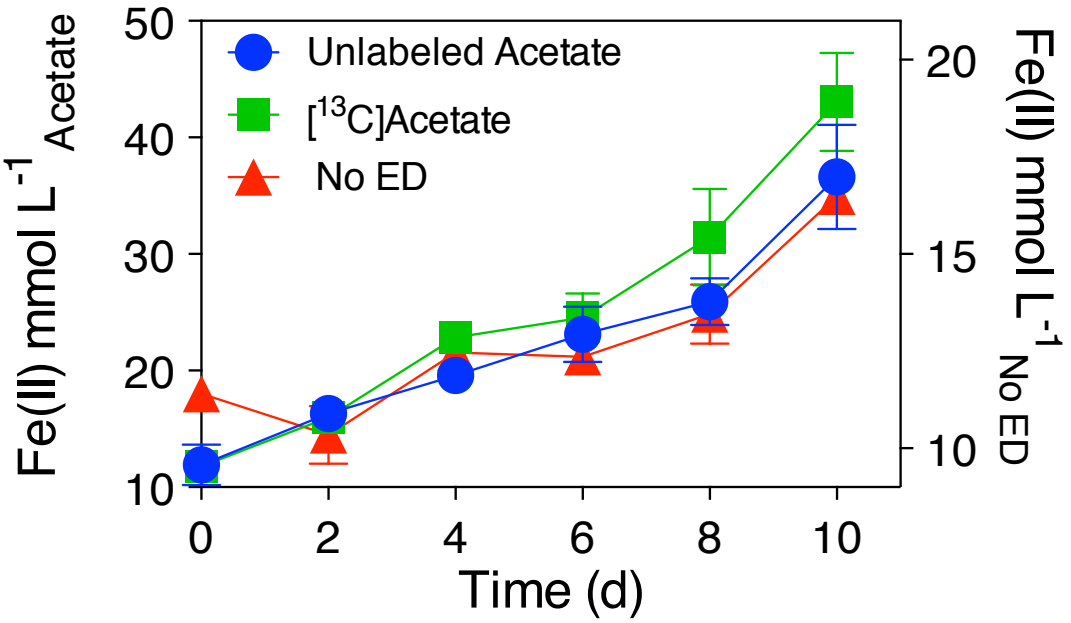

Figure 1.3. Fe(II) production in the Fe(III)-reducing incubations of Fe-Si oxide slurry prepared with CP sediments and spring water collected from the CP vent pool in October 2014. Reactor vessels were incubated at an *in situ* pH and temperature of 5.8, and 50°C. Acetate-amended incubations were amended with 0.5 mM unlabeled acetate or [^{13}C]acetate at time 0 and were provided with an additional 0.5 mM unlabeled acetate or [^{13}C]acetate every two days. Values represent the average of single measurements from triplicate incubations. Error bars represent 1σ variability in the measurements; error bars not shown are smaller than the symbol. Note different Y-axis scales for Fe(II) concentration measured in acetate-amended and no ED incubations. Final Fe(II)/Fe total ratio was approximately 0.45 for the acetate amended samples, and 0.30 for the no ED samples. Abbreviations: No ED, No electron donor.

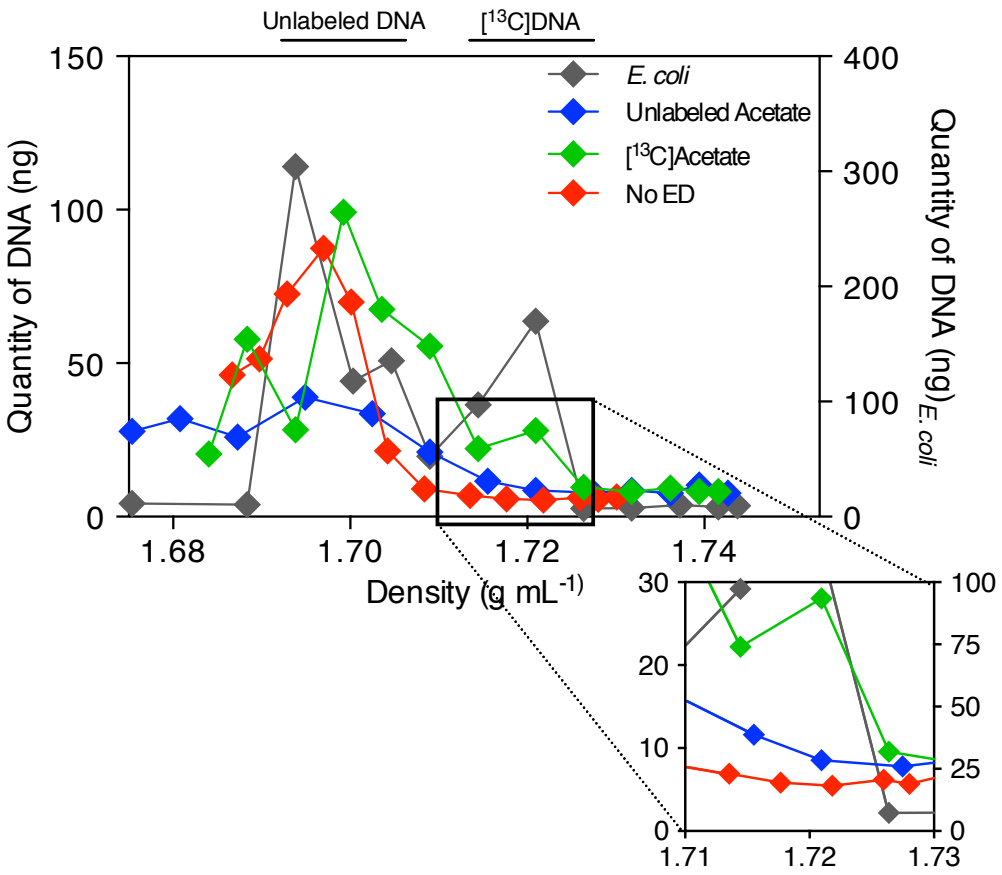

Figure 1.4. DNA quantity collected from gradient fraction replicate B following isopycnic ultracentrifugation. Densities corresponding to the fractions of greatest DNA concentration in the high- and low-density *E. coli* DNA, labeled as Unlabeled DNA and [^{13}C]DNA, respectively, were used to identify high- and low-density fractions in the DNA samples from the Fe(III)-reducing incubations. Zoomed-in panel highlights the gradient fraction (1.72 g mL^{-1}) with the peak concentration of high-density DNA collected from samples from the [^{13}C]acetate amended incubations. Note different scales for quantity of DNA measured in samples from the Fe(III)-reducing incubation (left Y-axis scale) and *E. coli* standard (right Y-axis scale). Abbreviations: No ED, No electron donor.

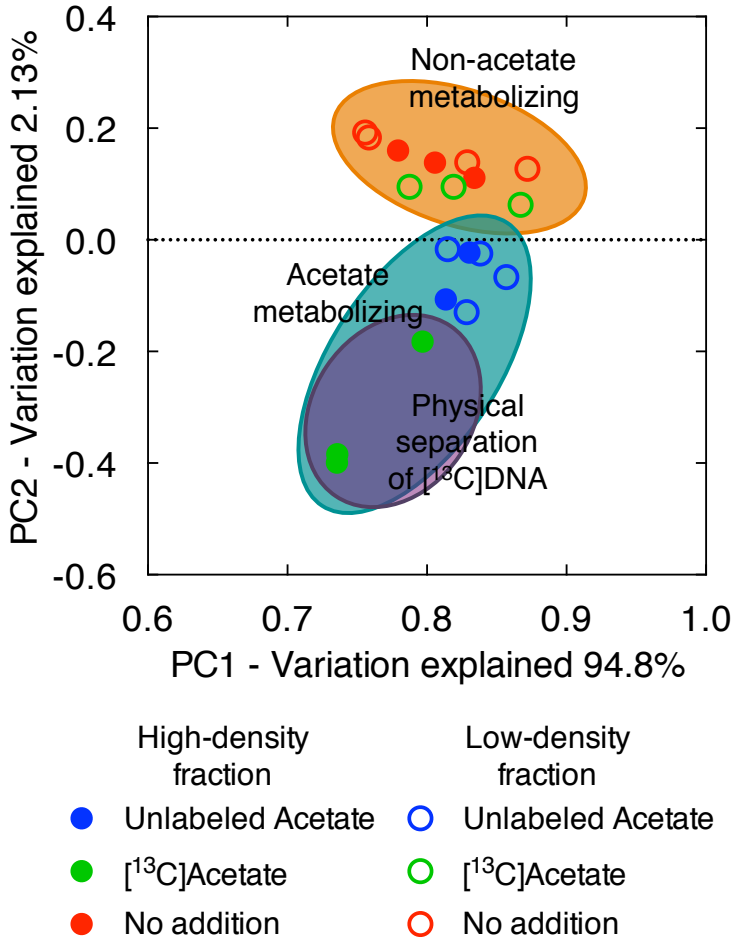

Figure 1.5. Principal components analysis of pair-wise 16S rRNA gene community dissimilarity calculated using weighted UniFrac metrics of the high- and low-density fractions (containing [^{13}C]DNA and unlabeled DNA, respectively), from the Fe(III)-reducing SIP incubations. PC2 separates non-acetate metabolizing bacterial populations (orange bubble) from acetate-metabolizing bacterial population (teal bubble, data points < 0.0). Physical separation of the [^{13}C]acetate-metabolizing bacterial population (filled green symbols, purple bubble), primarily represented by OTUs related to *Geobacter* are demarcated from the unlabeled acetate-metabolizing bacterial populations. Abbreviations: No ED, No electron donor.

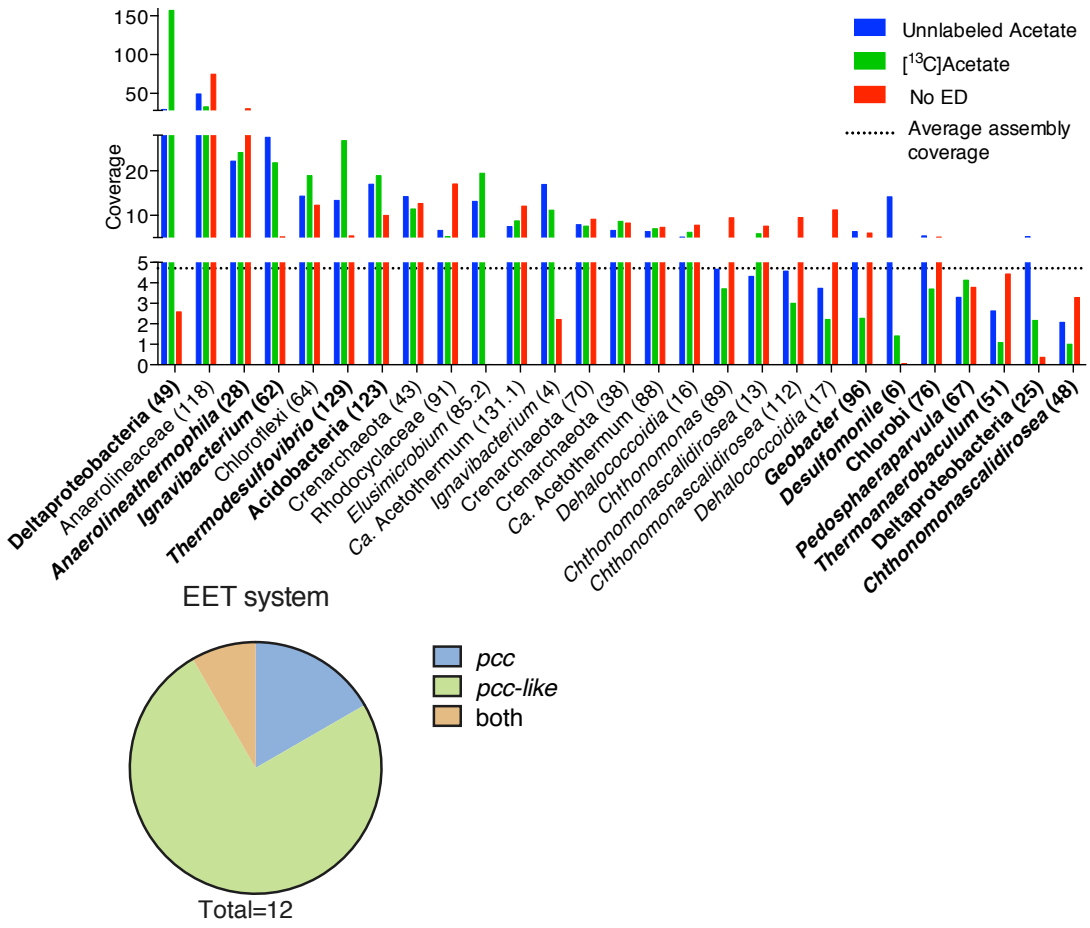

Figure 1.6. Rank abundance plot of the 20 most abundant metagenomic bins, and all bins containing putative genes of interest from the Fe(III)-reducing metagenomic co-assembly (*n*=27). Bins containing genes involved in putative extracellular electron transport (EET) pathways (*pcc*, EET genes homologous to *Geobacter*-like porin cytochrome complex; *pcc*-like, no homology to the *Geobacter*-like *pcc* system, but contains all genes necessary for a putative porin cytochrome complex EET system) are indicated in bold. Consensus taxonomic classification of each bin is listed along with the corresponding bin number in the parenthesis. Abbreviations: No ED, No electron donor; *Ca., Candidatus*.

A.1.1. SUPPLEMENTAL MATERIALS AND METHODS

A.1.1.1. Stable isotope probing details. A standard density curve was prepared using 490 μL 7.163 M CsCl and 0-130 μL Gradient Buffer (GB) in 10 μL increments, and refractive index (RI) was measured for each sample (1). All DNA solutions for gradient density separation were prepared with a ratio of CsCl, GB, and sample to achieve an RI of 1.4034, corresponding to a density of 1.725 g mL^{-1}. The entire quantity of DNA extracted from the Fe(III)-reducing incubations (ca. 1 μg) was used. DNA was not analyzed from the azide-treated Fe(III)-reducing. A standard DNA mixture of *E. coli* SB1 grown in either unlabeled or entirely ^{13}C-labeled growth media, 1.5 μg each, was prepared for each round of centrifugation to establish the density of high- and low-density DNA pools. Samples were prepared in 7 mL ultracentrifuge tubes and centrifuged for 40 hr at 45,000 rpm (ca. 174,000 *g*) using a Beckman-Coulter vTi 65.1 rotor and Optima XE-90 centrifuge (Beckman-Coulter Inc, Brea, CA). Density fractions were collected according to (1) at a flow rate sufficient to collect 16 fractions. DNA from the gradient fractions was precipitated overnight using 25 μg linear polyacrylamide and pelleted at 4°C and 14,000 *g*. DNA pellets were eluted in 30 μL diethylpyrocarbonate (DEPC)-H_2O, and concentration was measured using a Quant-iT PicoGreen dsDNA assay (Invitrogen, Carlsbad, CA).

The low-density DNA pools signify [^{12}C]DNA from no ED incubations, and incubations that received [^{12}C]acetate or DNA from the microbial community that did not metabolize [^{13}C]acetate in the [^{13}C]acetate treatment group. The high-density DNA pools signify [^{13}C]DNA from the [^{13}C]acetate incubations, or DNA from no ED or [^{12}C]acetate incubations that naturally has a higher density (e.g. higher GC content).

A.1.1.2. 16S rRNA gene amplicon sequencing and analysis. Bacterial 16S rRNA genes were amplified using universal 16S rRNA gene PCR primers (27f/907r) (2). Archaeal 16S

rRNA genes were amplified using archaeal-specific primers (109f/912r) (3). PCR reactions contained the following: AmpliTaq buffer (Life Technologies, Carlsbad, CA), dNTP (2 mM), BSA (20mg/mL), $MgCl_2$ (25mM), forward primer (10μM), reverse primer (10μM), AmpliTaq Polymerase (5U/μL), sample DNA, (ca. 0.5-2.5 ng), and DEPC H_2O to a final volume of 25 μL. Amplicons were generated using the following PCR protocol: 95°C for 5 min (initial denaturation) followed by 30 cycles of 95°C for 30 s (denaturing), 52°C for 30 s (annealing), 72°C for 60 s (extension), and a final extension at 72°C for 5 min. *Methanosarcina barkeri* DSM 800 and *E. coli* SB1 were used as positive controls. PCR product was cleaned using a Qiagen MinElute kit (Qiagen, Hilden, Germany) following manufacturer's instructions and quantified using a NanoDrop ND-1000 (PEQLAB Biotechnologie, Erlangen, Germany).

Microbial community sequence data were processed using the Quantitative Insights Into Microbial Ecology (QIIME) pipeline (http://www.qiime.org, version 1.8.0) (4). QIIME allows for *de novo* operational taxonomic unit (OTU) picking based on sequence similarity within samples, sequence alignment, and taxonomic assignment using the SILVA database. Paired-end reads were joined using the default fastq-join method (5, 6). Joined reads were quality trimmed in parallel to remove sequences with a Phred score below Q20 using the `split_libraries_fastq.py` script (7). Output sequence was validated using `validate_demultiplexed_fasta.py`. Chimeric sequences were identified using the `identify_chimeric_seqs.py` script using the usearch61 chimera detection method (8), and SILVA reference database (9, 10), release 111 (July 2012). Chimeric sequences were removed using `filter_fasta.py` command and chimeric sequence list generated in the previous step. Sequences were validated once more after chimera removal. Taxonomy was assigned to OTUs using the `pick_open_reference_otus.py` script using the usearch61 OTU picking method

and SILVA reference database, release 111. Beta diversity of the samples was calculated through the `beta_diversity_through_plots.py` script using weighted UniFrac metrics (11, 12). Sequences from the ten most abundant OTUs from each enrichment culture were analyzed using NCBI BLASTn search algorithm excluding models and uncultured/environmental sample sequences (13). BLASTn results were compared to the SILVA taxonomies identified using QIIME to potentially gather additional information about the most abundant taxa.

A.1.1.3. Metagenomic sequencing. In all samples, overlapping pairs of sequences were merged prior to adapter removal. Adapters were removed from sequence data using the Trim Sequences function within CLC Genomics Workbench using the General Adapter List library and adapter usage information provided by UWBC. Merged sequences of <50 bp or quality scores <95% were removed. Contigs for the Fe(III)-reducing incubations were generated through a combined metagenomic assembly (co-assembly) using an overlapping word length of 43 bp and minimum length of 200 bp. Reads were mapped back to contigs based on 90% length and 95% similarity. The co-assembly was uploaded to the Integrated Microbial Genomes with Microbiome Expert Reviewer (IMG/M ER) system (http://img.jgi.doe.gov/mer) for gene calling using IMG/M ER Metagenome Gene Calling method and function annotation (14).

A.1.1.4. Metagenomic sequence analysis. Candidate *pcc* homologues were eliminated if neighboring genes did not contain the canonical $Cx_{2\text{-}4}CH$ heme-binding motifs (15) found in cytochromes involved in EET. Single genes (i.e. genes without any neighboring genes) were also eliminated. Additionally, candidate *pcc* porin genes that were predicted to not be located in the cellular outer membrane (OM) by the subCELlular LOcalization predictor (CELLO v2.5, http://cello.life.nctu.edu.tw/, [16]) and PRED-TMBB (http://bioinformatics.biol.uoa.gr/PRED-TMBB/input.jsp, [17]) were not considered for further analysis.

A.1.2. SUPPLEMENTAL RESULTS

A.1.2.1. Homologs to genes involved in EET. Four high-coverage bins from the Fe(III)-reducing metagenomic co-assembly identified as *Deltaproteobacteria*, *Anaerolinea thermophila*, Acidobacteria, and *Thermodesulfovibrio* contained a putative OM porin, but an incomplete set of proximal or supplemental *c*-cyts. *Deltaproteobacteria* contained a putative *pcc*-like EET system with an OM porin flanked by extracellular (EC) and periplasmic (PP) *c*-cyts, however no homologs to an inner membrane (IM)-associated *c*-cyt (e.g. *macA*, *cbcL*, *imcH*) were identified. *A. thermophila* contained a putative OM porin and was flanked by multiheme PP and EC *c*-cyts. The bin also contained gene homologs to the IM-associated PP *c*-cyt, however no PP *c*-cyts homologs to the *Geobacter*-like *gsu1996* or *ppcA* were identified. The bin from the Acidobacteria relative did not contain an EC *c*-cyt proximal to the OM porin. The *Thermodesulfovibrio* bin contained several PP *c*-cyts, however, none were proximal to the OM porin.

A.1.3. SUPPLEMENTAL DISCUSSION

A.1.3.1 EET pathways involved in Fe(III)-reduction present at CP. Putative EET systems were identified in a bin identified as *Thermoanaerobaculum*. Neutrophilic FeRB from the phylum *Acidobacteria* have been described previously (18-20), so the identification of a putative EET system is not unprecedented. Additional *pcc*-like EET systems were identified in the Fe(III)-reducing metagenomic co-assembly in bins identified as *A. thermophila*, *Pedosphaera parvula*, *Chthonomonas calidirosea*, and *Desulfomonile*. To our knowledge, the genomes of these taxa have not been examined for potential EET systems.

The type strain *A. thermophila* UNI-1 is a strictly anaerobic, fermentative, thermophilic, filamentous bacterium isolated from soybean processing waste (21). The *in situ* conditions of CP

are amenable to the optimal growth requirements of *A. thermophila*, however, studies have demonstrated that this organism is incapable of utilizing acetate and lactate as an electron and carbon source and this is supported by our data indicating a lack of response to the addition of acetate (Fig. A.1.6). Likewise, the strain is unable to use Fe(III) (in the form of Fe(III)-NTA) as a terminal electron acceptor. As such, the presence of a full, putative *pcc*-like EET system is puzzling. However, it should be noted that the presence of a putative EET system is not a conclusive indication of the metabolic capabilities, and it has been shown that other organisms (e.g. *I. album*) possessing an EET system are incapable of DIR (22). Several other related bins (i.e. *Chloroflexi*, *Anaerolinaceae*, *Dehalococcoidia*) are present and relatively abundant in the metagenomic co-assembly (Fig. A.1.6), and likely serve the microbial community as fermenters, contributing acetate and lactate to the heterotrophic community members.

The type strain of *Chthonomonas*, *C. calidirosea* T49^{T}, is an aerobic, saccharolytic thermophile that was isolated from a geothermal environment in New Zealand that has similar physical and chemical characteristics when compared to CP (23). One bin related to this organism contained a putative EET system; despite previous studies indicating an inability to grow anaerobically. However, the aforementioned studies did not test Fe(III) as a terminal electron acceptor; unsuccessful growth was observed using elemental sulfur, sulfate, or nitrate. While results from this metagenomic analysis supported the metabolic potential of the *Chthonomonas*-related bins having the ability to grow anaerobically using Fe(III), only one bin possessed a complete EET system, and had below average read-coverage, suggesting it was not active under the Fe(III)-reducing conditions of the incubation. All three abundant *Chthonomonas*-related bins had increased coverage in the no ED incubations, suggesting these

taxa are not stimulated in the presence of acetate, and likely not involved in DIR (Fig. 1.6 and A.1.6).

Desulfomonile is a dehalorespiring bacterium which is also capable of anaerobic growth coupling thiosulfate reduction to H_2 oxidation (24, 25), although to our knowledge this organism has not been implicated in Fe-redox cycling. Even though the Fe(III)-reducing bin related to this organism has lower coverage than the most prolific putative FeRB (e.g. *Deltaproteobacteria*), it is also highly stimulated by the addition of acetate having a near negligible presence in the no ED incubations (Fig. 1.6 and A.1.6). Together, these two lines of evidence support the hypothesis of *Desulfomonile* participating as a FeRB, though likely not *in situ*.

Pedosphaera parvula Ellin514 is a member of the phylum *Verrucomicrobia* isolated from Australian pasture soil under aerobic heterotrophic conditions (26). Although it has been suggested to be an important component of the soil microbial community, little else is known about this species (26, 27). The Fe(III)-reducing bin related to this organism contains a *pcc*-like EET system along with all supplemental EET genes. Although *Pedosphaera* has not been implicated in Fe-redox cycling, to our knowledge the metabolic capability has not been tested, either. Results from our metagenomic analysis suggest the possibility of a Fe-based metabolism.

A.1.4. SUPPLEMENTAL REFERENCES

1. Dunford EA, Neufeld JD. 2010. DNA stable-isotope probing (DNA-SIP). J Vis Exp doi:10.3791/2027:e2027.
2. Lane DJ. 1991. 16S/23S rRNA sequencing, p 115-175. *In* Stackebrandt E, Goodfellow M (ed), Nucleic acid techniques in bacterial systematics. John Wiley and Sons, New York, NY.
3. Ramakrishnan B, Lueders T, Dunfield PF, Conrad R, Friedrich MW. 2001. Archaeal community structures in rice soils from different geographical regions before and after initiation of methane production. FEMS Microbiol Ecol 37:175-186.
4. Caporaso JG, Kuczynski J, Strombaugh J, Bittinger K, Bushman FD, Costello EK. 2010. QIIME allows analysis of high-throughput community sequencing data. Nat Methods 7:335-336.
5. Aronesty E. 2011. Command-line tools for processing biological sequencing data. https://code.google.com/archive/p/ea-utils/. Accessed 18 September 2015.
6. Aronesty E. 2013. Comparison of Sequencing Utility Programs. TOBioiJ 7:1-8.
7. Bokulich NA, Subramanian S, Faith JJ, Gevers D, Gordon JI, Knight R, Mills DA, Caporaso JG. 2013. Quality-filtering vastly improves diversity estimates from Illumina amplicon sequencing. Nat Methods 10:57-59.
8. Edgar RC. 2010. Search and clustering orders of magnitude faster than BLAST. Bioinformatics 26:2460-1.
9. Quast C, Pruesse E, Yilmaz P, Gerken J, Schweer T, Yarza P, Peplies J, Glöckner FO. 2013. The SILVA ribosomal RNA gene database project: improved data processing and web-based tools. Nucleic Acids Res 41:D590-D596.
10. Pruesse E, Quast C, Knittel K, Fuchs BM, Ludwig W, Peplies J, Glöckner FO. 2007. SILVA: a comprehensive online resource for quality checked and aligned ribosomal RNA sequence data compatible with ARB. Nucleic Acids Res 35:7188-96.
11. Lozupone C, Knight R. 2005. UniFrac: a new phylogenetic method for comparing microbial communities. Appl Environ Microbiol 71:8228-8235.
12. Lozupone C, Lladser ME, Knights D, Stombaugh J, Knight R. 2011. UniFrac: an effective distance metric for microbial community comparison. ISME J 5:169-172.
13. Altschul SF, Gish W, Miller W, Myers EW, Lipman DJ. 1990. Basic Local Alignment Search Tool. J Mol Biol 215:403-410.
14. Mavromatis K, Ivanova NN, Chen IM, Szeto E, Markowitz VM, Kyrpides NC. 2009. The DOE-JGI Standard Operating Procedure for the Annotations of Microbial Genomes. Stand Genomic Sci 1:63-7.
15. Thöny-Meyer L. 2000. Haem-polypeptide interactions during cytochrome *c* maturation. Biochim Biophys Acta 1459:316-324.
16. Yu C-S, Chen Y-C, Lu C-H, Hwang J-K. 2006. Prediction of protein subcellular localization. Proteins 64:643-651.
17. Bagos PG, Liakopoulos TD, Spyropoulos IC, Hamodrakas SJ. 2004. PRED-TMBB: a web server for predicting the topology of β-barrel outer membrane proteins. Nucleic Acids Res 32:W400-404.
18. Coates JD, Ellis DJ, Gaw CV, Lovley DR. 1999. *Geothrix fermentans* gen. nov., sp. nov., a novel Fe(III)-reducing bacterium from a hydrocarbon-contaminated aquifer. Int J Syst Bacteriol 49:1615-1622.

19. Losey NA, Stevenson BS, Busse H-J, Sinninghé Damste JS, Rijpstra WIC, Rudd S, Lawson PA. 2013. *Thermoanaerobaculum aquaticum* gen. nov., sp. nov., the first cultivated member of *Acidobacteria* subdivision 23, isolated from a hot spring. Int J Syst Evol Micr 63:4149-57.
20. Hartshorne RS, Reardon CL, Ross D, Nuester J, Clarke TA, Gates AJ, Mills PC, Fredrickson JK, Zachara JM, Shi L, Beliaev AS, Marshall MJ, Tien M, Brantley S, Butt JN, Richardson DJ. 2009. Characterization of an electron conduit between bacteria and the extracellular environment. Proc Natl Acad Sci U S A 106:22169-74.
21. Sekiguchi Y, Yamada T, Hanada S, Ohashi A, Harada H, Kamagata Y. 2003. *Anaerolinea thermophila* gen. nov., sp. nov. and *Caldilinea aerophila* gen. nov., sp. nov., novel filamentous thermophiles that represent a previously uncultured lineage of the domain *Bacteria* at the subphylum level. Int J Syst Evol Micr 53:1843-1851.
22. Iino T, Mori K, Uchino Y, Nakagawa T, Harayama S, Suzuki K. 2010. *Ignavibacterium album* gen. nov., sp. nov., a moderately thermophilic anaerobic bacterium isolated from microbial mats at a terrestrial hot spring and proposal of *Ignavibacteria* classis nov., for a novel lineage at the periphery of green sulfur bacteria. Int J Syst Evol Micr 60:1376-82.
23. Lee KC-Y, Dunfield PF, Morgan XC, Crowe MA, Houghton KM, Vyssotski M, Ryan JL, Lagutin K, McDonald IR, Stott MB. 2011. *Chthonomonas calidirosea* gen. nov., sp. nov., an aerobic, pigmented, thermophilic micro-organism of a novel bacterial class, *Chthonomonadetes* classis nov., of the newly described phylum *Armatimonadetes* originally designated candidate division OP10. Int J Syst Evol Micr 61:2482-2490.
24. DeWeerd KA, Mandelco L, Tanner RS, Woese CR, Suflita JM. 1990. *Desulfomonile tiedjei* gen. nov. and sp. nov., a novel anaerobic, dehalogenating, sulfate-reducing bacterium. Arch Microbiol 154:23-30.
25. DeWeerd KA, Concannon F, Suflita JM. 1991. Relationship between Hydrogen Consumption, Dehalogenation, and the Reduction of Sulfur Oxyanions by *Desulfomonile tiedjei*. Appl Environ Microbiol 57:1929-1934.
26. Sangwan P, Kovac S, Davis KER, Sait M, Janssen PH. 2005. Detection and cultivation of soil verrucomicrobia. Appl Environ Microbiol 71:8402-10.
27. Kant R, van Passel MWJ, Sangwan P, Palva A, Lucas S, Copeland A, Lapidus A, Galvina del Rio T, Dalin E, Tice H, Bruce D, Goodwin L, Pitluck S, Chertkov O, Larimer FW, Land ML, Hauser L, Brettin TS, Detter JC, Han S, de Vos WM, Janssen PH, Smidt H. 2011. Genome Sequence of "*Pedosphaera parvula*" Ellin514, an Aerobic Verrucomicrobial Isolate from Pasture Soil. J Bacteriol 193:2900-1.
28. Henry EA, Devereux R, Maki JS, Gilmour CC, Woese CR, Mandelco L, Schauder R, Remen CC, Mitchell R. 1994. Characterization of a new thermophilic sulfate-reducing bacterium *Thermodesulfovibrio yellowstonii*, gen. nov. and sp. nov.: its phylogenetic relationship to *Thermodesulfobacterium commune* and their origins deep within the bacterial domain. Arch Microbiol 161:62-69.
29. Sekiguchi Y, Muramatsu M, Imachi H, Narihiro T, Ohashi A, Harada H, Hanada S, Kamagata Y. 2008. *Thermodesulfovibrio aggregans* sp. nov. and *Thermodesulfovibrio thiophilus* sp. nov., anaerobic, thermophilic, sulfate-reducing bacteria isolated from thermophilic methanogenic sludge, and emended description of the genus *Thermodesulfovibrio*. Int J Syst Evol Micr 58:2541-8.
30. Herlemann DPR, Geissinger O, Ikeda-Ohtsubo W, Kunin V, Sun H, Lapidus A, Hugenholtz P, Brune A. 2009. Genomic Analysis of "*Elusimicrobium Minutum*," the

First Cultivated Representative of the Phylum "*Elusimicrobia*" (Formerly Termite Group 1). Appl Environ Microbiol 75:2841-2849.

31. Jogler C, Niebler M, Lin W, Kube M, Wanner G, Kolinko S, Stief P, Beck AJ, de Beer D, Petersen N, Pan Y, Amann R, Reinhardt R, Schüler D. 2010. Cultivation-independent characterization of '*Candidatus* Magnetobacterium bavaricum' via ultrastructural, geochemical, ecological and metagenomic methods. Environ Microbiol 12:2466-2478.
32. Nepomnyashchaya YN, Slobodkina GB, Baslerov RV, Chernyh NA, Bonch-Osmolovskaya EA, Netrusov AI, Slobodkin AI. 2012. Moorella humiferrea sp. nov., a thermophilic, anaerobic bacterium capable of growth via electron shuttling between humic acid and Fe(III). Int J Syst Evol Micr 62:613-617.
33. Huynh HTT, Nkamga VD, Signoli M, Tzortzis S, Pinguet R, Audoly G, Aboudharam G, Drancourt M. 2016. Restricted diversity of dental calculus methanogens over five centuries, France. Sci Rep 6:25775.
34. Chin K-J, Lukow T, Stubner S, Conrad R. 1999. Structure and function of the methanogenic archaeal community in stable cellulose-degrading enrichment cultures at two different temperatures (15 and 30°C). FEMS Microbiol Ecol 30:313-326.
35. Nunoura T, Takaki Y, Kakuta J, Nishi S, Sugahara J, Kazama H, Chee G-J, Hattori M, Kanai A, Atomi H, Takai K, Takami H. 2011. Insights into the evolution of Archaea and eukaryotic protein modifier systems revealed by the genome of a novel archaeal group. Nucleic Acids Res 39:3204-3223.
36. Huber JA, Butterfield DA, Baross JA. 2006. Diversity and distribution of subseafloor Thermococcales populations in diffuse hydrothermal vents at an active deep-sea volcano in the northeast Pacific Ocean. J Geophys Res 111.
37. Galand PE, Lovejoy C, Vincent WF. 2006. Remarkably diverse and contrasting archaeal communities in a large arctic river and the coastal Arctic Ocean. Aquat Microb Ecol 44:115-126.
38. Osburn MR, Amend JP. 2011. Thermogladius shockii gen. nov., sp. nov., a hyperthermophilic crenarchaeote from Yellowstone National Park, USA. Arch Microbiol 193:45-52.

Table A.1.1. Genes required in model Fe(III)-reducing extracellular electron transfer systems.

Model system	Model organism	Gene symbol	Gene locus tag	Gene description	Protein function ID	Predicted cellular location	Heme-binding sites	Trans-membrane domains
pcc	*Geobacter sulfurreducens* PCA		GSU2724	Cytochrome C family protein	TIGR01904	ec[a]	20	
			GSU2725	Cytochrome C family protein		pp[b]	4	
			GSU2526	Hypothetical protein		om[c]		20
		omcC	GSU2731	Cytochrome C554	pfam13435	ec	12	
		omaC	GSU2732	Cytochrome C family protein		pp	8	
		ombC	GSU2733	Hypothetical protein		om		18
		omcB	GSU2737	Cytochrome C7	pfam14552	ec	12	
		omaB	GSU2738	Cytochrome C family protein		pp	8	
		ombB	GSU2739	Hypothetical protein		om		18
		omcZ	GSU2076	Cytochrome C family protein	pfam01833	ec	8	
		gsu1996	GSU1996	Cytochrome C7	pfam14552	pp	12	
		ppcA	GSU0612	Cytochrome C3	pfam02085	pp	2	
		ppcB	GSU0364	Cytochrome C3	pfam02085	pp	2	
		ppcC	GSU0365	Cytochrome C3	pfam02085	pp	2	
		ppcD	GSU1024	Cytochrome C3	pfam02085	pp	3	
		ppcE	GSU1760	Cytochrome C3	pfam02085	pp	2	
		macA	GSU0466	Cytochrome C551 peroxidase	pfam03150	pp	2	
		imcH	GSU3259	NapC/NirT Cytochrome C family	pfam03264	im[d]/cp[e]/pp	7	
		cbcL	GSU0274	Cytochrome C3_2	pfam14537	im/cp	9	
mtr	*Shewanella oneidensis* MR-1	*mtrB*	SO1776	Outer membrane protein precursor MtrB	pfam11854	om		22
		mtrA	SO1777	Decaheme Cytochrome C MtrA	pfam14552/09699	pp	10	
		omcB	SO1778	Decaheme Cytochrome C	pfam14552	ec	10	
		omcA	SO1779	Decaheme Cytochrome C		ec	10	
		mtrF	SO1780	Decaheme Cytochrome C MtrF		ec	10	
		mtrE	SO1781	Putative outer membrane protein	pfam11854	om		22
		mtrD	SO1782	Decaheme Cytochrome C MtrD	pfam09699	pp	10	
		fccA	SO2727	Cytochrome C3_2	pfam14537	pp	4	
		cymA	SO4591	NapC/NirT Cytochrome C family	pfam03264	pp	4	

[a] Extracellular
[b] Periplasmic
[c] Outer membrane
[d] Inner membrane
[e] Cytoplasmic

Table A.1.2. DNA concentration from selected high- and low-density fractions from the Fe(III)-reducing incubations following isopycnic centrifugation.

		High density fractions			Low density fractions		
Treatment	Replicate	Fraction #	Density (g/mL)	[DNA] (ng/µL)	Fraction #	Density (g/mL)	[DNA] (ng/µL)
Unlabeled	A	ND[a]	ND	ND	11	1.70397	1.268
Acetate	B	6	1.72096	0.285	10	1.69490	1.297
					11	1.68730	0.863
	C	6	1.72523	0.273	10	1.70033	1.784
		7	1.71661	0.435			
[^{13}C]Acetate	A	8	1.72071	0.179	11	1.70502	1.054
	B	6	1.72096	0.935	10	1.69924	3.306
	C	6	1.72096	0.284	10	1.69924	1.180
		7	1.71553	0.246			
No ED[b]	A	6	1.71251	0.220	9	1.69907	2.963
	B	6	1.71354	0.230	10	1.69700	2.916
	C	6	1.71355	0.280	9	1.69907	2.864
					10	1.69597	2.871

[a] Not determined. No high-density fraction collected from unlabeled acetate treated replicate A
[b] No electron donor

Table A.1.3a. Bacterial community composition of high-density DNA from the unlabeled acetate Fe(III)-reducing incubation.

SILVA Taxonomic Assignment	% Total[a]	Representative Species Match[c]	Accession Number	Similarity (%)	Inferred Physiology	Reference
Geobacter (g)	13.2	*Geobacter hephaestius*	AY737507.1	95	Fe(III) reduction	Janssen, P.H., unpublished
Ignavibacteria (c)	6.4	Bacterium YC-ZSS-LKJ31	KP174519.1	88	Uncharacterized moderate halophile	Zhao, B., Li, K. & Liu, K., unpublished
Geobacter (g)	3.9	*Geobacter hephaestius*	AY737507.1	93	Fe(III) reduction	Janssen, P.H., unpublished
Rhodocyclaceae (f)	3.6	Betaproteobacterium Rufe9b	AY235688.1	94	N_2 fixation	Tan, Z.Y., Hurek, T. & Reinhold-Hurek, B., unpublished
Thermodesulfovibrionaceae (f)	3.5	*Thermodesulfovibrio yellowstonii* strain DSM 11347	NR_074345.1	91	Fe(III)/SO_4^{2-} reduction	Henry et al., 1994; Sekiguchi et al., 2008
Thermodesulfovibrionaceae (f)	3.3	*Thermodesulfovibrio yellowstonii* strain DSM 11347	NR_074345.1	91	Fe(III)/SO_4^{2-} reduction	Henry et al., 1994; Sekiguchi et al., 2008
Geobacter (g)	1.9	*Geobacter hephaestius*	AY737507.1	93	Fe(III) reduction	Janssen, P.H., unpublished
Elusimicrobiales (o)	1.6	*Elusimicrobium minutum* strain Pei191	NR_074114.1	88	Fermenter	Herlemann, et al., 2009
Unassigned	1.6	Bacterium YC-LK-LKJ27	KP174640.1	87	Uncharacterized moderate halophile	Zhao, B., Li, K. & Liu, K., unpublished
Unassigned	1.4	Bacterium YC-LK-LKJ2	KP174649.1	83	Uncharacterized moderate halophile	Zhao, B., Li, K. & Liu, K., unpublished
	40.5[b]					

Table A.1.3b. Bacterial community composition of high-density DNA from the no electron donor Fe(III)-reducing incubation.

SILVA Taxonomic Assignment	% Total[a]	Representative Species Match[c]	Accession Number	Similarity (%)	Inferred Physiology	Reference
Ignavibacteria (c)	9.3	Bacterium YC-ZSS-LKJ31	KP174519.1	88	Uncharacterized moderate halophile	Zhao, B., Li, K. & Liu, K., unpublished
Rhodocyclaceae (f)	8.5	Betaproteobacterium Rufe9b	AY235688.1	94	N_2 fixation	Tan, Z.Y., Hurek, T. & Reinhold-Hurek, B., unpublished
Unassigned	4.1	Bacterium YC-LK-LKJ27	KP174640.1	87	Uncharacterized moderate halophile	Zhao, B., Li, K. & Liu, K., unpublished
Unassigned	3.7	Bacterium YC-LK-LKJ2	KP174649.1	83	Uncharacterized moderate halophile	Zhao, B., Li, K. & Liu, K., unpublished
Chloroflexi (p)	3.2	Bacterium YC-LK-LKJ27	KP174640.1	89	Uncharacterized moderate halophile	Zhao, B., Li, K. & Liu, K., unpublished
Anaerolineae (c)	3.0	*Caldilinea aerophila* strain DSM 14535	NR_074397.1	86	Facultatively anaerobic heterotroph/fermentor	Sekiguchi, Y., et al., 2003
Thermodesulfovibrionaceae (f)	2.7	*Candidatus* Magnetobacterium bavaricum	FP929063.1	89	Sulfur oxidation	Jogler, C., et al., 2010
Thermodesulfovibrionaceae (f)	1.8	*Thermodesulfovibrio yellowstonii* strain DSM 11347	NR_074345.1	91	Fe(III)/SO_4^{2-} reduction	Henry et al., 1994; Sekiguchi et al., 2008
Bacteria (k)	1.7	*Moorella humiferrea* strain 64-FGQ	NR_108634.1	87	Indirect Fe(III) reduction via humic acids	Nepomnyashchaya, Y. N., et al., 2012
Thermodesulfovibrionaceae (f)	1.7	*Thermodesulfovibrio yellowstonii* strain DSM 11347	NR_074345.1	91	Fe(III)/SO_4^{2-} reduction	Henry et al., 1994; Sekiguchi et al., 2008
	39.7[b]					

[a] Number of reads out of total reads for the sample

[b] Total percent of reads comprising the ten most dominant OTUs

[c] As determined by NCBI BLASTn

Table A.1.4. Analysis of Similarity (ANOSIM) and Similarity Percentage (SIMPER) comparing 16S rRNA gene amplicon libraries from the high- and low-density DNA pools from the Fe(III)-reducing incubation treatment groups.

		ANOSIM		SIMPER
Pairs of 16S rRNA gene amplicon libraries		Distinction (*R*-value)[a]	Significance (*p*-value)[b]	Average dissimilarity (%)
Unlabeled Acetate Low	Unlabeled Acetate High	-0.214	0.733	24.90
Unlabeled Acetate Low	[^{13}C]Acetate Low	0.352	0.143	33.31
Unlabeled Acetate Low	[^{13}C]Acetate High	0.630	0.029	54.92
Unlabeled Acetate Low	No ED[c] High	0.667	0.057	37.88
Unlabeled Acetate Low	No ED Low	0.833	0.029	43.23
Unlabeled Acetate High	[^{13}C]Acetate Low	0.833	0.100	35.67
Unlabeled Acetate High	[^{13}C]Acetate High	0.333	0.300	53.06
Unlabeled Acetate High	No ED High	1.000	0.100	35.64
Unlabeled Acetate High	No ED Low	1.000	0.067	44.74
[^{13}C]Acetate Low	[^{13}C]Acetate High	0.778	0.100	74.99
[^{13}C]Acetate Low	No ED High	1.000	0.100	31.90
[^{13}C]Acetate Low	No ED Low	0.796	0.057	34.93
[^{13}C]Acetate High	No ED High	1.000	0.100	78.10
[^{13}C]Acetate High	No ED Low	1.000	0.029	80.12
No ED High	No ED Low	0.519	0.057	24.95

[a] Distinction range is defined as: indistinguishable (R=0-0.25), distinct with some overlap (R=0.25-0.5), and distinct (R>0.5)

[b] Significance value cutoff of $p<0.05$

[c] No electron donor

Table A.1.5a. Archaeal community composition of high-density DNA from unlabeled acetate amended Fe(III)-reducing incubation.

SILVA Taxonomic Assignment	% Total[a]	Representative Species Match[c]	Accession Number	Similarity (%)	Inferred Physiology	Reference
Methanomassiliicoccaceae (f)	33.3	*Methanomassiliicoccus* sp. strain clone N89-2	LN827539.1	94	Methanogen	Huynh, H. T. T., et al., 2016
Crenarchaeota (p)	13.7	anaerobic methanogenic archaeon ET1-10	AJ244286.1	87	Methanogenic cellulolytic archaeon	Chin, K.-J., et al., 1999
Crenarchaeota (p)	11.1	*Candidatus* Caldiarchaeum subterraneum fosmid clone JFF016_H02	AP011878.1	86	Chemolitho(auto)troph	Nunoura, T., et al., 2011
Crenarchaeota (p)	9.5	anaerobic methanogenic archaeon ET1-8	AJ244284.1	89	Methanogenic cellulolytic archaeon	Chin, K.-J., et al., 1999
Unassigned	9.4	*Methanomassiliicoccus* sp. strain clone N89-2	LN827539.1	90	Methanogen	Huynh, H. T. T., et al., 2016
Crenarchaeota (p)	4.7	anaerobic methanogenic archaeon ET1-10	AJ244286.1	89	Methanogenic cellulolytic archaeon	Chin, K.-J., et al., 1999
Unassigned	3.6	*Palaeococcus* sp. Ax00-33	AY559124.1	86	Fermenter	Huber, J. A., et al., 2006
Methanomassiliicoccaceae (f)	2.5	*Methanomassiliicoccus* sp. strain clone N89-2	LN827539.1	88	Methanogen	Huynh, H. T. T., et al., 2016
Crenarchaeota (p)	1.6	anaerobic methanogenic archaeon ET1-10	AJ244286.1	98	Methanogenic cellulolytic archaeon	Chin, K.-J., et al., 1999
Crenarchaeota (p)	1.2	anaerobic methanogenic archaeon ET1-8	AJ244284.1	87	Methanogenic cellulolytic archaeon	Chin, K.-J., et al., 1999
	90.6[b]					

Table A.1.5b. Archaeal community composition of high-density DNA from [13C]acetate amended Fe(III)-reducing incubation.

SILVA Taxonomic Assignment	% Total[a]	Representative Species Match[c]	Accession Number	Similarity (%)	Inferred Physiology	Reference
Methanomassiliicoccaceae (f)	18.8	*Methanomassiliicoccus* sp. strain clone N89-2	LN827539.1	92	Methanogen	Huynh, H. T. T., et al., 2016
Crenarchaeota (p)	17.0	anaerobic methanogenic archaeon ET1-10	AJ244286.1	90	Methanogenic cellulolytic archaeon	Chin, K.-J., et al., 1999
Aigarchaeota (c)	12.0	*Candidatus* Caldiarchaeum subterraneum fosmid clone JFF016_H02	AP011878.1	85	Chemolitho(auto)troph	Nunoura, T., et al., 2011
Crenarchaeota (p)	10.7	anaerobic methanogenic archaeon ET1-8	AJ244284.1	87	Methanogenic cellulolytic archaeon	Chin, K.-J., et al., 1999
Unassigned	8.0	*Methanomassiliicoccus* sp. strain clone N89-2	LN827539.1	90	Methanogen	Huynh, H. T. T., et al., 2016
Crenarchaeota (p)	5.4	anaerobic methanogenic archaeon ET1-10	AJ244286.1	90	Methanogenic cellulolytic archaeon	Chin, K.-J., et al., 1999
Unassigned	4.4	*Palaeococcus* sp. Ax00-33	AY559124.1	82	Fermenter	Huber, J. A., et al., 2006
Unassigned	2.4	Uncultured archaeon clone mrR1.11	DQ310417.1	90	Uncharacterized	Galand, P. E., et al., 2006
Crenarchaeota (p)	1.8	anaerobic methanogenic archaeon ET1-8	AJ244284.1	86	Methanogenic cellulolytic archaeon	Chin, K.-J., et al., 1999
Crenarchaeota (p)	1.7	anaerobic methanogenic archaeon ET1-10	AJ244286.1	90	Methanogenic cellulolytic archaeon	Chin, K.-J., et al., 1999
	82.3[b]					

Table A.1.5c. Archaeal community composition of high-density DNA from no electron donor Fe(III)-reducing incubation.

SILVA Taxonomic Assignment	% Total[a]	Representative Species Match[c]	Accession Number	Similarity (%)	Inferred Physiology	Reference
Methanomassiliicoccaceae (f)	30.0	*Methanomassiliicoccus* sp. strain clone N89-2	LN827539.1	92	Methanogen	Huynh, H. T. T., et al., 2016
Crenarchaeota (p)	12.9	anaerobic methanogenic archaeon ET1-10	AJ244286.1	90	Methanogenic cellulolytic archaeon	Chin, K.-J., et al., 1999
Aigarchaeota (c)	11.6	*Candidatus* Caldiarchaeum subterraneum fosmid clone JFF016_H02	AP011878.1	85	Chemolitho(auto)troph	Nunoura, T., et al., 2011
Crenarchaeota (p)	9.1	anaerobic methanogenic archaeon ET1-8	AJ244284.1	87	Methanogenic cellulolytic archaeon	Chin, K.-J., et al., 1999
Unassigned	5.8	*Methanomassiliicoccus* sp. strain clone N89-2	LN827539.1	90	Methanogen	Huynh, H. T. T., et al., 2016
Crenarchaeota (p)	4.5	anaerobic methanogenic archaeon ET1-10 16S rRNA gene, partial	AJ244286.1	90	Methanogenic cellulolytic archaeon	Chin, K.-J., et al., 1999
Unassigned	4.2	*Palaeococcus* sp. Ax00-33	AY559124.1	82	Fermenter	Huber, J. A., et al., 2006
Crenarchaeota (p)	1.6	Uncultured archaeon clone MD3057K-42	GQ994192.2	90	Uncharacterized	Wang, F., Saren, G., & Yu, X., unpublished
Crenarchaeota (p)	1.4	anaerobic methanogenic archaeon ET1-10	AJ244286.1	90	Methanogenic cellulolytic archaeon	Chin, K.-J., et al., 1999
Methanomassiliicoccaceae (f)	0.7	*Methanomassiliicoccus* sp. strain clone N89-2	LN827539.1	93	Methanogen	Huynh, H. T. T., et al., 2016
	81.7[b]					

Table A.1.5d. Archaeal community composition of low-density DNA from unlabeled acetate amended Fe(III)-reducing incubation.

SILVA Taxonomic Assignment	% Total[a]	Representative Species Match[c]	Accession Number	Similarity (%)	Inferred Physiology	Reference
Aigarchaeota (c)	21.2	*Candidatus* Caldiarchaeum subterraneum fosmid clone JFF016_H02	AP011878.1	85	Chemolitho(auto)troph	Nunoura, T., et al., 2011
Methanomassiliicoccaceae (f)	14.4	*Methanomassiliicoccus* sp. strain clone N89-2	LN827539.1	92	Methanogen	Huynh, H. T. T., et al., 2016
Crenarchaeota (p)	13.1	anaerobic methanogenic archaeon ET1-10	AJ244286.1	90	Methanogenic cellulolytic archaeon	Chin, K.-J., et al., 1999
Crenarchaeota (p)	7.8	anaerobic methanogenic archaeon ET1-8	AJ244284.1	87	Methanogenic cellulolytic archaeon	Chin, K.-J., et al., 1999
Unassigned	6.3	*Methanomassiliicoccus* sp. strain clone N89-2	LN827539.1	90	Methanogen	Huynh, H. T. T., et al., 2016
Crenarchaeota (p)	4.8	anaerobic methanogenic archaeon ET1-10	AJ244286.1	90	Methanogenic cellulolytic archaeon	Chin, K.-J., et al., 1999
Unassigned	4.6	*Palaeococcus* sp. Ax00-33	AY559124.1	82	Fermenter	Huber, J. A., et al., 2006
Unassigned	1.5	Uncultured archaeon clone mrR1.11	DQ310417.1	90	Uncharacterized	Galand, P. E., et al., 2006
Unassigned	1.5	*Thermogladius shockii* strain WB1	NG_044969.1	85	Fermenter	Osburn, M. R. & Amend, J. P., 2011
Crenarchaeota (p)	1.2	anaerobic methanogenic archaeon ET1-10	AJ244286.1	90	Methanogenic cellulolytic archaeon	Chin, K.-J., et al., 1999
	76.4[b]					

Table A.1.5e. Archaeal community composition of low-density DNA from [13C]acetate amended Fe(III)-reducing incubation.

SILVA Taxonomic Assignment	% Total[a]	Representative Species Match[c]	Accession Number	Similarity (%)	Inferred Physiology	Reference
Aigarchaeota (c)	28.6	*Candidatus* Caldiarchaeum subterraneum fosmid clone JFF016_H02	AP011878.1	85	Chemolitho(auto)troph	Nunoura, T., et al., 2011
Methanomassiliicoccaceae (f)	16.9	*Methanomassiliicoccus* sp. strain clone N89-2	LN827539.1	92	Methanogen	Huynh, H. T. T., et al., 2016
Crenarchaeota (p)	9.9	anaerobic methanogenic archaeon ET1-10	AJ244286.1	90	Methanogenic cellulolytic archaeon	Chin, K.-J., et al., 1999
Crenarchaeota (p)	6.1	anaerobic methanogenic archaeon ET1-8	AJ244284.1	87	Methanogenic cellulolytic archaeon	Chin, K.-J., et al., 1999
Unassigned	4.1	*Palaeococcus* sp. Ax00-33	AY559124.1	82	Fermenter	Huber, J. A., et al., 2006
Unassigned	4.0	*Methanomassiliicoccus* sp. strain clone N89-2	LN827539.1	90	Methanogen	Huynh, H. T. T., et al., 2016
Crenarchaeota (p)	3.3	anaerobic methanogenic archaeon ET1-10	AJ244286.1	90	Methanogenic cellulolytic archaeon	Chin, K.-J., et al., 1999
Unassigned	2.9	*Thermogladius shockii* strain WB1	NG_044969.1	85	Fermenter	Osburn, M. R. & Amend, J. P., 2011
Methanomassiliicoccaceae (f)	1.9	*Methanomassiliicoccus* sp. strain clone N89-2	LN827539.1	91	Methanogen	Huynh, H. T. T., et al., 2016
Unassigned	1.4	Uncultured archaeon clone mrR1.11	DQ310417.1	90	Uncharacterized	Galand, P. E., et al., 2006
	79.1[b]					

Table A.1.5f. Archaeal community composition of low-density DNA from no electron donor Fe(III)-reducing incubation.

SILVA Taxonomic Assignment	% Total[a]	Representative Species Match[c]	Accession Number	Similarity (%)	Inferred Physiology	Reference
Methanomassiliicoccaceae (f)	32.7	*Methanomassiliicoccus* sp. strain clone N89-2	LN827539.1	92	Methanogen	Huynh, H. T. T., et al., 2016
Aigarchaeota (c)	18.7	*Candidatus* Caldiarchaeum subterraneum fosmid clone JFF016_H02	AP011878.1	85	Chemolitho(auto)troph	Nunoura, T., et al., 2011
Crenarchaeota (p)	5.9	anaerobic methanogenic archaeon ET1-10	AJ244286.1	90	Methanogenic cellulolytic archaeon	Chin, K.-J., et al., 1999
Unassigned	5.8	*Methanomassiliicoccus* sp. strain clone N89-2	LN827539.1	90	Methanogen	Huynh, H. T. T., et al., 2016
Unassigned	5.5	*Palaeococcus* sp. Ax00-33	AY559124.1	82	Fermenter	Huber, J. A., et al., 2006
Crenarchaeota (p)	4.8	anaerobic methanogenic archaeon ET1-8	AJ244284.1	87	Methanogenic cellulolytic archaeon	Chin, K.-J., et al., 1999
Methanomassiliicoccaceae (f)	2.7	*Methanomassiliicoccus* sp. strain clone N89-2	LN827539.1	91	Methanogen	Huynh, H. T. T., et al., 2016
Crenarchaeota (p)	2.1	anaerobic methanogenic archaeon ET1-10	AJ244286.1	90	Methanogenic cellulolytic archaeon	Chin, K.-J., et al., 1999
Crenarchaeota (p)	1.5	*Candidatus* Nitrososphaera sp. strain clone N89-12	LN827538.1	95	Methanogen	Huynh, H. T. T., et al., 2016
Methanomassiliicoccaceae (f)	1.4	*Methanomassiliicoccus* sp. strain clone N89-2	LN827539.1	93	Methanogen	Huynh, H. T. T., et al., 2016
	81.1[b]					

[a] Number of reads out of total reads for the sample

[b] Total percent of reads comprising the ten most dominant OTUs

[c] As determined by NCBI BLASTn

Table A.1.6. Taxonomic assignment and statistics of metagenomic bins from Fe(III)-reducing incubation.

			Coassembly	Unlabeled Acetate	[^{13}C]Acetate	No ED[a]						Similarity to 16S	%Identity to
Bin	Avg GC%	Bin size (Mbp)	Avg assembly coverage	Avg normalized coverage	Avg normalized coverage	Avg normalized coverage	Completeness	Contamination	Strain heterogeneity	Consensus Taxonomy[b]	Taxon rank	Amplicon Library[c]	GenBank[d]
0	59.0	1.883	4.68	1.17	1.55	1.98	57.99	0	0	*Chthonomonas calidirosea*	Species	N/A[e]	
1	55.8	1.040	4.12	1.17	1.70	1.46	26.19	0	0	*Ignavibacterium*	Genus	N/A	
2	61.4	0.744	4.24	1.32	1.03	1.83	25.55	0	0	*Thermoanaerobacteraceae*	Family	N/A	
3	54.9	0.093	3.19	1.08	0.84	1.39	6.66	0	0	Euryarchaeota	Phylum	N/A	
4	33.1	0.337	25.44	16.93	11.16	2.22	16.59	0	0	*Ignavibacterium*	Genus	N/A	
5	43.6	1.180	11.07	4.56	3.10	4.46	85.36	0	0	Euryarchaeota	Phylum	N/A	
6	56.7	3.735	13.61	5.42	3.70	5.15	92.1	1.94	33.33	*Desulfomonile*	Genus	N/A	
7	68.0	1.091	5.70	1.44	0.53	3.65	31.54	1.02	25	Acidobacteria	Phylum	N/A	
8	56.6	0.156	3.78	0.97	1.07	1.81	17.36	0.85	0	Parcubacteria	Phylum	N/A	
9	60.3	1.738	4.48	1.16	0.91	2.40	32.83	1.94	0	*Desulfobacteraceae*	Family	N/A	
10	53.7	3.568	8.44	2.55	3.11	3.18	79.53	4.22	12.5	*Desulfomonile*	Genus	N/A	85.48
11	67.1	2.255	15.96	3.27	1.33	11.00	83.04	0	0	*Dehalococcoidia*	Class	99.54[f]	89.74
12	31.6	1.648	4.97	4.31	0.98	0.56	62.66	1.81	50	Acidobacteria	Phylum	N/A	
13	58.5	2.026	17.36	4.32	5.88	7.58	64.81	1.85	33.33	*Chthonomonas calidirosea*	Species	78.98	81.44
14	49.7	1.238	5.29	1.81	1.92	1.88	61.68	2.91	0	Crenarchaeota	Phylum	99.03	83.35
15	60.9	2.207	11.24	3.47	4.62	3.39	61.56	1.83	33.33	Chloroflexi	Phylum	N/A	
16	58.7	1.811	18.55	5.14	6.18	7.82	66.56	1.19	0	*Dehalococcoidia*	Class	N/A	
17	65.8	0.902	17.12	3.74	2.21	11.25	33.35	0.99	0	*Dehalococcoidia*	Class	N/A	
18	53.1	4.304	5.05	1.46	1.93	1.88	92.29	53.79	2.99	Bacterial Composite	Domain	N/A	79.66
21	60.9	6.856	4.72	1.42	1.33	2.08	80.49	101.35	0.54	Chloroflexi	Phylum	N/A	
22	49.8	0.277	14.71	5.24	4.94	5.97	11.68	0	0	*Chthonomonas calidirosea*	Species	N/A	
23	46.1	2.762	4.93	3.28	2.22	0.01	62.73	1.69	0	Bacteria	Domain	N/A	
25	70.4	1.279	6.52	2.27	0.64	3.48	56.44	2.71	37.5	*Deltaproteobacteria*	Class	N/A	
26	58.4	0.084	3.30	0.89	1.03	1.47	3.74	0	0	*Thermococcaceae*	Family	N/A	
27	61.0	0.652	4.01	1.54	1.00	1.52	17.4	0	0	*Chthonomonas calidirosea*	Species	N/A	
28	57.7	5.275	72.09	22.19	24.12	30.38	94.24	6.09	11.11	*Anaerolinea thermophila*	Species	99.32[e]	85.22
29	34.5	1.688	4.76	2.58	2.75	0.00	66.74	1.75	0	*Bacteroidales*	Order	100	87.6
31	65.8	2.005	4.24	1.32	0.61	2.27	34.94	5.13	0	*Acidobacteriaceae*	Family	N/A	
32	64.6	0.549	4.45	0.69	0.43	3.22	15.18	1.17	0	*Comamonadaceae*	Family	N/A	
33	62.9	0.792	5.46	1.38	0.98	3.13	50.79	0	0	Bacteria	Domain	N/A	
34	66.4	2.667	11.00	3.16	1.58	6.22	80.73	0.92	100	*Chloroflexi*	Phylum	99.09	84.78
36	45.3	0.268	3.57	1.61	1.09	1.19	20.06	0	0	*"Candidatus* Endomicrobium"	Genus	N/A	
37	60.7	2.176	4.41	1.25	1.12	2.08	33.01	5.26	0	*Chthonomonas*	Genus	99.54	82.86
38	53.2	1.339	22.26	6.62	8.69	8.30	76.31	0.97	0	Crenarchaeota	Phylum	100[e]	82.38
39	48.0	1.480	4.07	1.42	1.34	1.60	62.22	7.09	0	Crenarchaeota	Phylum	N/A	
40	57.4	1.804	9.17	2.59	3.08	3.77	77.59	0.31	50	Proteobacteria	Phylum	N/A	
42	66.6	3.430	14.59	6.38	2.27	6.02	83.64	0.91	0	Chloroflexi	Phylum	99.55	88.11
43	45.2	0.979	34.18	14.22	11.47	12.68	57.13	0	0	Crenarchaeota	Phylum	100	82.78
44	43.4	1.665	4.73	2.56	1.40	1.34	54.88	1.1	0	Firmicutes	Phylum	N/A	
46	63.2	4.996	8.10	2.60	1.84	3.71	94.83	48.65	3.12	Chloroflexi	Phylum	100	83.56
47	57.8	1.084	4.00	1.15	1.45	1.47	17.52	0	0	Candidate division Zixibacteria	Phylum	N/A	
48	59.5	2.568	6.09	1.49	2.51	2.15	63.72	1.39	100	*Chthonomonas calidirosea*	Species	N/A	
49	37.3	1.532	157.85	29.49	157.19	2.59	61.01	5.04	100	*Geobacter*	Genus	99.14	85.07
50	44.1	1.045	4.60	1.90	1.51	1.64	54.45	1.66	50	Euryarchaeota	Phylum	N/A	
51	30.3	2.019	6.70	5.26	2.17	0.37	75.63	0	0	*Thermoanaerobaculum*	Genus	N/A	
52	44.5	2.018	5.33	2.59	1.72	1.59	67.27	2.51	42.86	*Deltaproteobacteria*	Class	N/A	
53	45.3	3.682	16.33	6.95	5.96	4.90	95.88	3.28	14.29	*Ignavibacteriales*	Order	N/A	
54	62.1	1.173	5.17	1.45	1.00	2.73	62.61	0.06	0	Euryarchaeota	Phylum	N/A	
58	53.6	1.679	4.63	1.43	1.80	1.63	55.36	1.19	0	Crenarchaeota	Phylum	N/A	
60	50.1	1.396	10.74	3.89	3.92	3.69	64.34	0	0	Bacteria	Domain	99.55	82.42

62	36.2	1.112	45.83	27.54	21.84	5.19	53.73	0.55	0	*Ignavibacterium*	Genus	N/A	
63	56.8	4.414	8.96	3.02	4.83	1.53	89.5	54.2	29.17	Chloroflexi	Phylum	N/A	
64	55.2	0.777	41.27	14.31	18.93	12.28	16.02	0.92	100	Chloroflexi	Phylum	99.76	83.46
65	51.5	1.042	4.82	1.61	1.88	1.59	59.56	1.98	0	Chloroflexi	Phylum	N/A	
66	45.5	1.168	4.71	2.37	1.45	1.32	77.59	29.66	2.5	Parcubacteria	Phylum	N/A	82.96
67	54.5	3.352	10.59	3.28	4.41	3.33	76.41	2.84	20	*Pedosphaera parvula*	Species	N/A	
69	45.1	0.137	3.69	1.70	1.15	1.13	8.41	0	0	*Thermococcaceae*	Family	N/A	
70	47.4	2.654	22.32	7.93	7.57	9.15	77.18	26.62	51.16	Crenarchaeota	Phylum	100[e]	80.82
71	61.0	2.298	16.89	4.56	5.22	7.50	55.99	0	0	*Dehalococcoides*	Genus	N/A	
72	64.2	2.433	6.34	2.08	1.00	3.28	53.54	2.23	25	*Anaerolineaceae*	Family	N/A	
73	56.4	0.726	4.15	1.89	1.18	1.29	28.95	0	0	*Peptococcaceae*	Family	N/A	
74	59.9	0.443	4.43	1.22	1.60	1.68	4.7	0	0	*Chthonomonas*	Genus	N/A	
75	44.3	1.276	5.40	1.55	3.89	0.40	66.04	0.51	50	*Thermodesulfovibrio*	Genus	N/A	
76	31.4	2.301	11.22	9.59	2.53	1.02	89.09	3.3	13.33	Chlorobi	Phylum	100	84.04
78	56.0	0.331	3.21	0.68	0.92	1.65	9.74	0	0	*Desulfobacteraceae*	Family	N/A	
79	36.7	0.326	3.14	2.32	0.90	0.42	14.57	0	0	Acidobacteria	Phylum	N/A	
80	53.8	2.036	9.21	2.25	2.77	4.54	81.01	3.45	0	*"Candidatus* Methylomirabilis"	Genus	N/A	
81	36.1	0.395	3.44	2.10	1.43	0.42	46.08	2.85	0	Parcubacteria	Phylum	N/A	82.79
82	61.9	1.930	4.68	1.43	0.95	2.34	47.32	0.09	0	Acidobacteria	Phylum	N/A	
84	55.1	4.658	5.93	1.84	2.27	2.08	72.14	20.32	0	Chloroflexi	Phylum	N/A	
85a	27.9	0.607	8.20	4.86	4.39	0.07	73.96	2.3	100	Parcubacteria	Phylum	N/A	
85b	28.8	2.185	28.39	13.16	19.45	0.02	95.51	0	0	*Elusimicrobium*	Genus	99.55[e]	85.48
86	55.9	2.116	17.10	5.73	6.60	5.79	58.88	0.46	100	*Chthonomonas*	Genus	N/A	
87	38.5	0.720	12.53	8.65	4.27	1.61	27.46	0.05	100	Chlorobi	Phylum	N/A	
88	50.3	2.580	19.18	6.39	6.99	7.34	86.44	3.08	0	*"Candidatus* Acetothermum"	Genus	98.91	80.71
89	62.9	1.773	17.67	4.67	3.71	9.45	56.26	0	0	*Chthonomonas*	Genus	N/A	
91	63.6	2.135	28.65	6.63	5.26	17.05	67.67	2.1	28.57	*Rhodocyclaceae*	Family	N/A	
92	56.5	0.030	3.26	0.84	1.74	0.75	2.51	0	0	*Anaerolineaceae*	Family	N/A	
93	65.0	1.825	5.82	1.35	0.96	3.42	65.15	1.1	28.57	*Dehalococcoidia*	Class	100	81.63
94	60.6	3.065	7.78	2.60	2.11	3.24	80.32	3.95	16.67	Candidate division Zixibacteria	Phylum	N/A	
95	44.5	1.186	3.97	1.70	1.80	0.82	47.41	3.55	0	*Deltaproteobacteria*	Class	N/A	
96	62.6	2.562	14.30	14.15	1.41	0.06	95.74	1.29	100	*Geobacter*	Genus	N/A	
97	54.4	3.393	10.71	3.30	4.13	3.79	76.54	4.23	11.11	*Geobacter*	Genus	N/A	
98	62.5	2.943	5.25	1.86	0.94	2.47	59.23	0	0	*Haliangium*	Genus	N/A	87.43
99	63.5	0.591	4.75	2.01	1.07	2.13	16.93	1.82	50	*Anaerolinea thermophila*	Species	N/A	
100	60.5	1.173	4.89	1.44	2.00	1.51	36.97	0.91	0	Chloroflexi	Phylum	N/A	
101	46.6	1.124	5.18	2.26	2.56	0.81	70.87	0.66	100	Elusimicrobia	Phylum	N/A	
102	39.6	1.228	6.44	3.09	3.21	1.10	11.48	0.58	0	*Syntrophaceae*	Family	N/A	
104	53.3	0.275	4.26	0.89	1.30	2.25	10.69	0	0	*Clostridia*	Class	N/A	
106	62.9	1.151	4.41	1.21	1.23	1.97	41.05	0	0	*Chthonomonas calidirosea*	Species	N/A	
107	33.1	0.235	3.36	2.65	0.70	0.55	11.8	0	0	*Nitrosopumilaceae*	Family	N/A	
108	63.9	1.262	4.54	1.46	1.06	2.04	41.46	0	0	*Anaerolineaceae*	Family	N/A	
109	33.2	1.510	5.43	1.58	4.25	0.12	76.36	1.27	25	*Calditerrivibrio nitroreducens*	Species	N/A	
110	49.3	1.423	9.18	3.15	2.99	3.63	81.11	1.6	50	*Nitrospira*	Genus	N/A	
111	47.2	0.218	3.29	0.99	2.25	0.27	6.43	0	0	*Anaerolineaceae*	Family	N/A	
112	64.6	5.488	17.14	4.57	3.00	9.54	91.67	6.11	22.22	*Chthonomonas calidirosea*	Species	100	82.28
113	60.3	2.140	11.38	2.94	2.79	5.63	93.01	0.18	0	Candidate division Zixibacteria	Phylum	99.78	79.96
114	46.5	0.148	3.20	1.25	1.06	1.10	9.21	0	0	*Thermococcaceae*	Family	N/A	
115	57.8	1.496	3.97	1.09	1.43	1.55	35.12	0	0	*Chthonomonas*	Genus	N/A	
116	41.7	2.985	5.21	2.79	1.66	1.43	94.8	76.71	12.5	Crenarchaeota	Phylum	N/A	
117	63.8	8.101	17.10	4.46	4.55	7.99	93.52	3.89	0	*Chthonomonas calidirosea*	Species	98.5	84.89
118	63.2	3.330	150.28	49.24	32.65	74.95	83.18	2.94	0	*Anaerolineaceae*	Family	98.64	87.18
120	59.5	1.862	5.19	1.50	1.35	2.44	57.57	0.92	100	Chloroflexi	Phylum	100	87.68
121	67.6	1.261	8.09	2.63	1.09	4.44	50.64	0.85	0	*Thermoanaerobaculum*	Genus	99.57	98.69
122	56.1	1.983	5.70	1.84	2.51	1.58	73.39	2.27	0	*Anaerolineae*	Class	N/A	

123	48.3	2.400	41.00	17.03	18.93	10.01	74.02	1.71	0	*Geobacter*	Genus	N/A	
124	46.8	0.287	3.82	1.58	0.93	1.58	28.04	0	0	Elusimicrobia	Phylum	N/A	
125	54.2	1.752	10.23	3.55	3.90	3.96	0.86	0	0	Bacteria	Domain	97.93	89.08
127	41.6	0.851	3.93	2.23	1.12	1.04	38.28	0	0	Bacteria	Domain	N/A	
128	42.7	1.439	9.21	4.86	2.46	2.92	86.97	3.64	0	*Nitrospira*	Genus	N/A	
129	44.5	1.605	41.25	13.38	26.79	5.40	78.37	0.91	0	*Thermodesulfovibrio*	Genus	99.54[e]	89.87
130	65.8	1.588	14.19	3.66	2.41	8.17	64.51	1.2	0	Euryarchaeota	Phylum	100	86.85
131a	56.5	2.759	26.52	7.49	8.75	12.08	80.17	72.46	25.32	*"Candidatus* Acetothermum"	Genus	100	80.35

[a] No electron donor

[b] Taxonomy determined by a consensus between Phylosift, CheckM, and MEGAN

[c] Pairwise alignment used to calculate %identity between 16S rRNA sequences recovered from the metagenomic libraries and 16S rRNA gene amplicon libraries

[d] %Identity of 16S rRNA gene sequences recovered from the metagenomic libraries compared to the NCBI GenBank database

[e] N/A = not applicable. Either no significant match to amplicon library, or metagenomic 16S rRNA sequence assembled on contig <2500 bp and not binned

[f] OTU represents one of the 10 most dominant OTUs in the 16S library for at least one of the treatments, remaining represent <2% of total reads recovered.

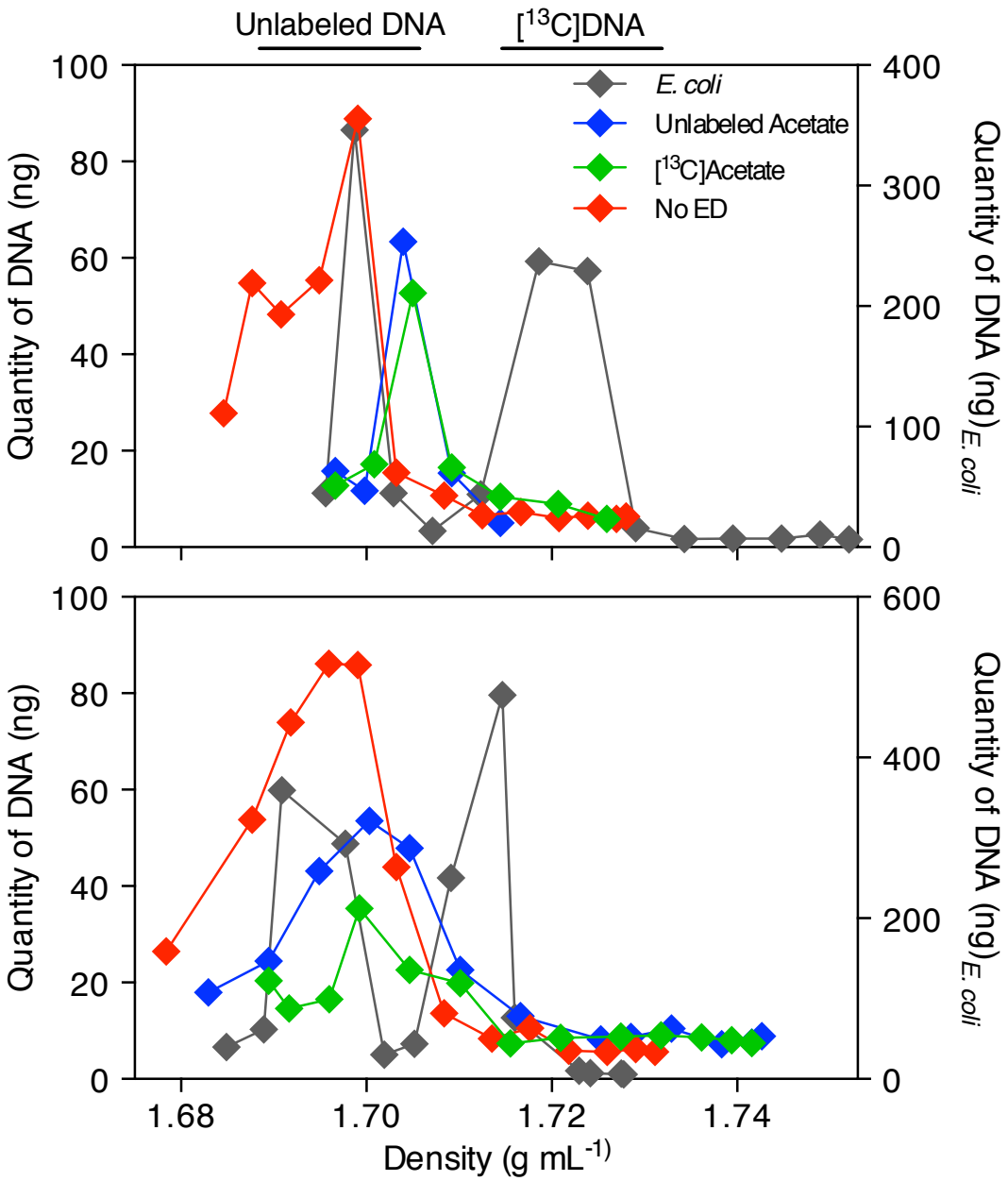

Figure A.1.1. Quantity of DNA collected from gradient fraction replicates A (top panel) and C (bottom panel) following isopycnic ultracentrifugation. Densities corresponding to the fractions of greatest DNA concentration in the high- and low-density *E. coli* DNA, labeled as Unlabeled DNA and [^{13}C]DNA, respectively, were used to identify high- and low-density fractions in the DNA samples from the Fe(III)-reducing incubations.. Note different scales for quantity of DNA measured in samples from the Fe(III)-reducing incubation (left Y-axis scale) and *E. coli* standard (right Y-axis scale). Abbreviations: No ED, No electron donor.

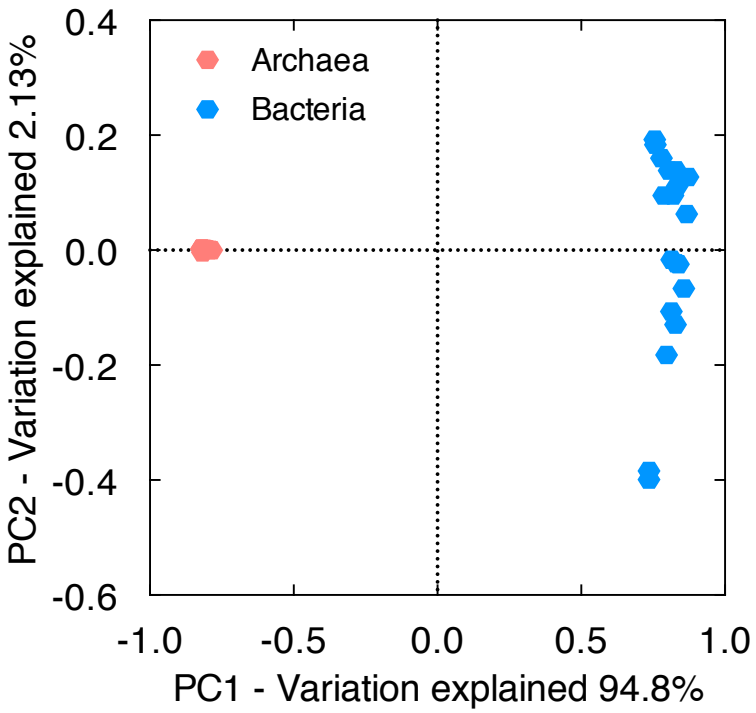

Figure A.1.2. Principal components analysis plot of pair-wise sample dissimilarity calculated using weighted UniFrac metrics of the microbial community from high- and low-density fractions (containing [^{13}C]DNA and unlabeled DNA, respectively), from all treatments of the Fe(III)-reducing SIP incubations based on 16S rRNA gene amplicon sequences. Principal Component 1 (PC1) is primarily separating archaeal and bacterial components of the community. Negligible variation in archaeal samples along PC2 suggests these members of the microbial community were unaffected by the Fe(III)-reducing and acetate-oxidizing conditions imposed on the incubations.

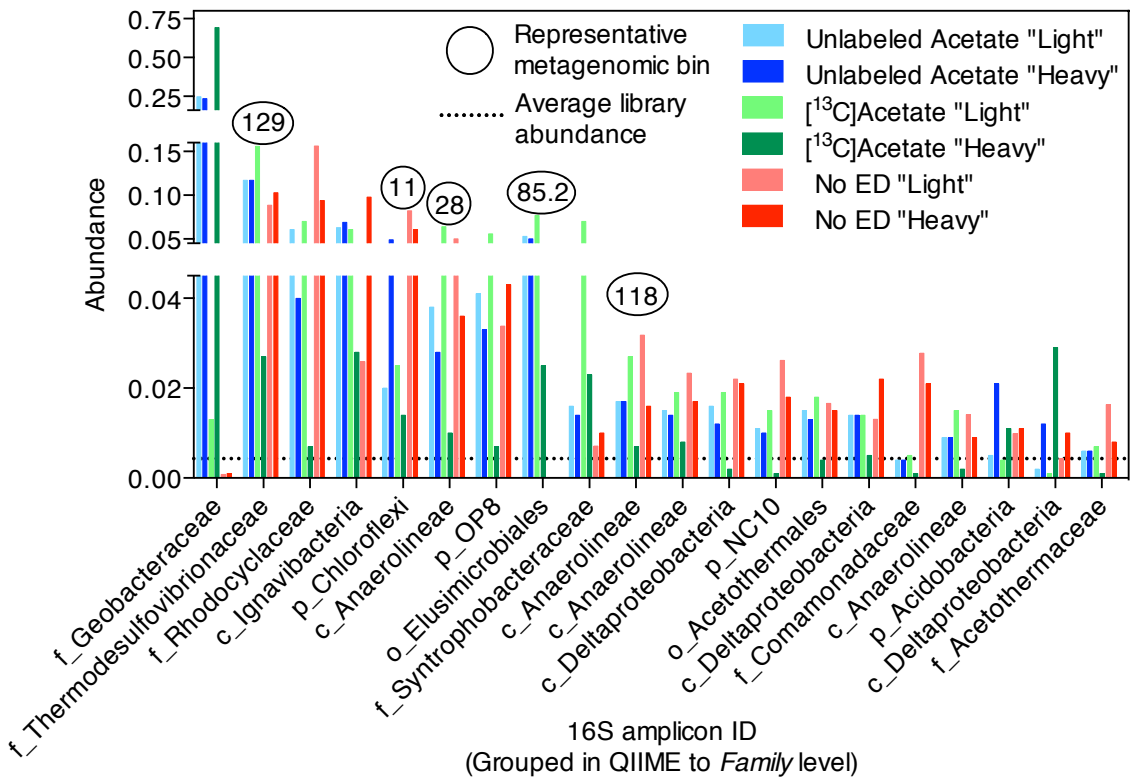

Figure A.1.3. Rank abundance plot of the 20 most dominant bacterial groups from the 16S rRNA gene amplicon libraries generated from high- and low-density fractions (containing [^{13}C]DNA and unlabeled DNA, respectively), from the Fe(III)-reducing SIP incubations. Groups were clustered to the taxonomic Family level using the QIIME `summarize_taxa.py` script. Correlation between 16S taxonomic groups and metagenomic bins was accomplished by searching 16S rRNA gene sequences recovered from the Fe(III)-reducing metagenomic assembly against a database generated from the 16S rRNA gene amplicon library using the `makeblastdb` and `blastn` functions of command-line NCBI BLAST. Abbreviations: No ED, No electron donor; Ac, acetate; f, family; o, order; c, class; p, phylum

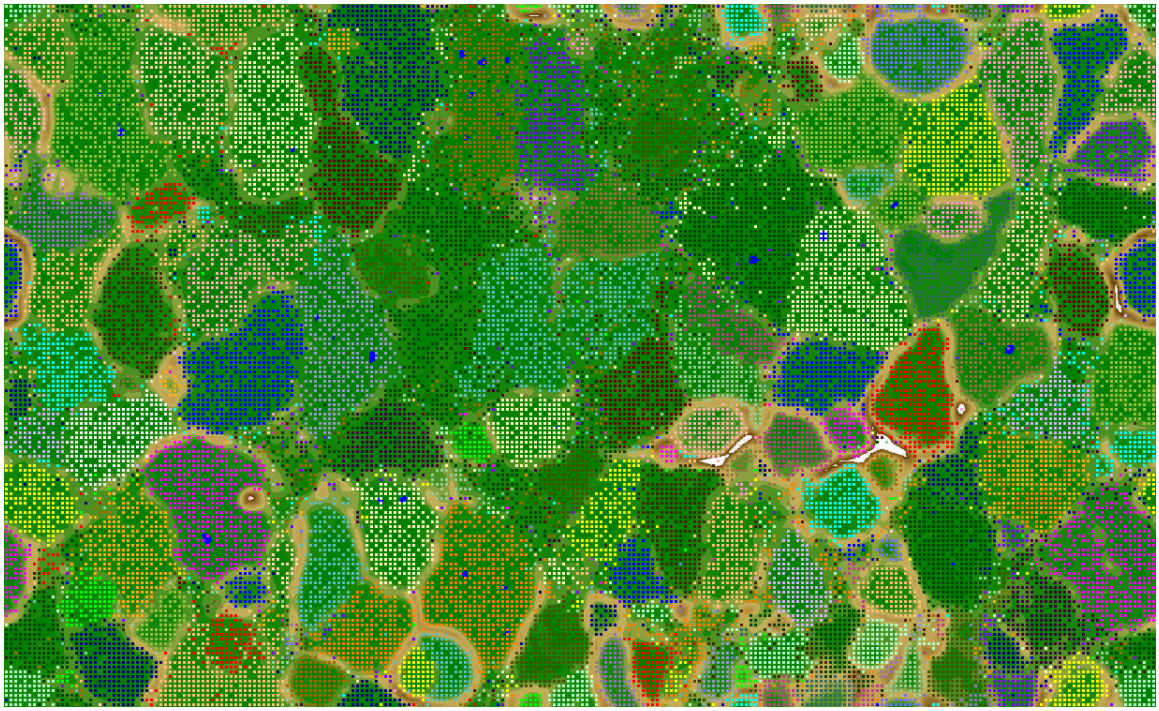

Figure A.1.4. Emergent Self Organizing Map (ESOM) visualization of metagenomic DNA fragments from the combined assembly of shotgun metagenomic sequence reads from the Fe(III)-reducing SIP incubation experiment. Each cluster represents one of the 133 metagenomic bins. Fragments were clustered according to CONCOCT binning approaches (5 kb window size, all contigs ≥2500 bp were considered).

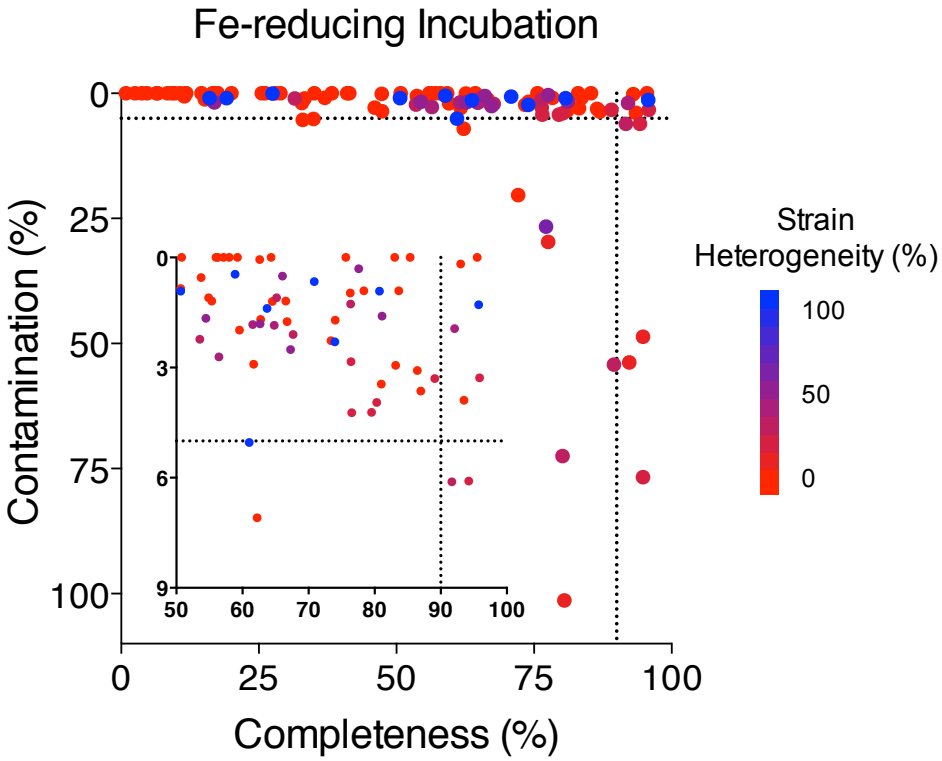

Figure A.1.5. Completeness, contamination and strain heterogeneity calculated using CheckM for each taxonomic bin clustered using CONCOCT for the Fe(III)-reducing metagenomic co-assembly from the SIP incubation experiments. Inset panel shows the bins with greater than 50% completeness and less than 10% contamination.

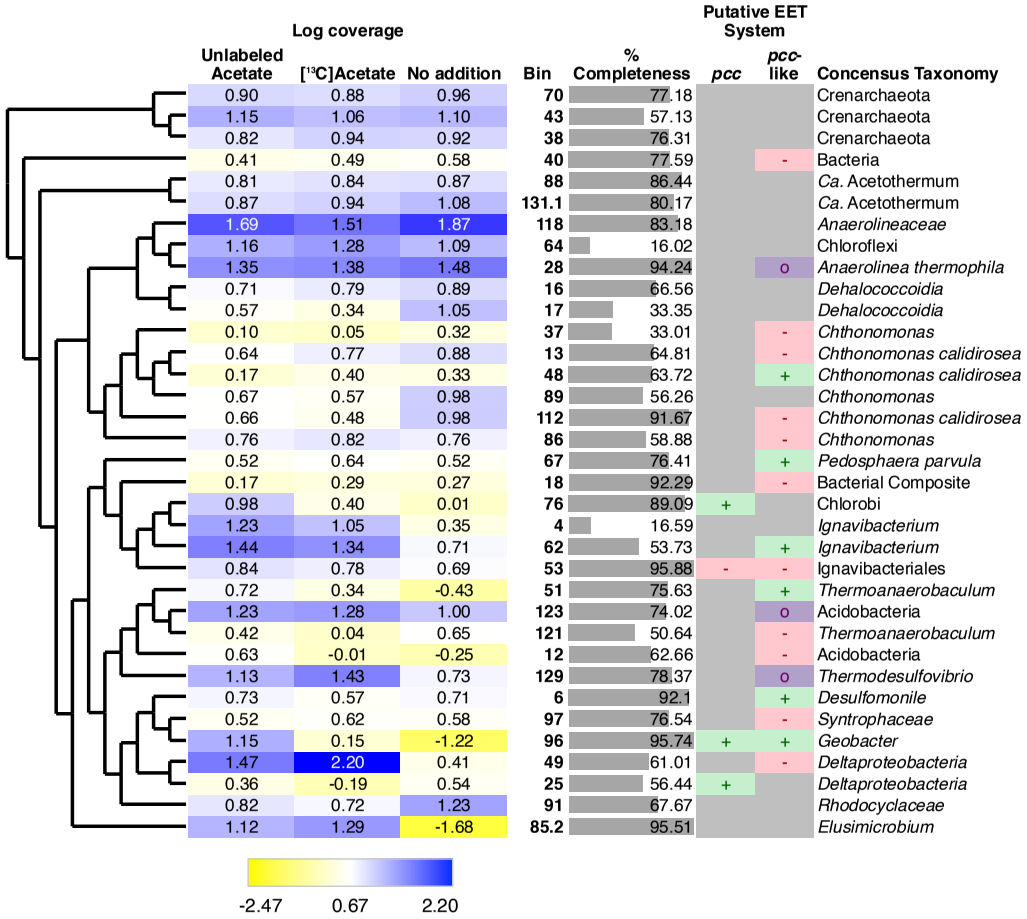

Figure A.1.6. Twenty highest-coverage metagenomic bins from the Fe(III)-reducing SIP incubations, and bins containing genes involved in EET. Reads from individual treatment groups were mapped against the entire co-assembly to visualize how coverage of taxonomic bins changed in response to acetate addition, with cells in blue representing high-coverage bins, and yellow representing low-coverage bins. Scale range was determined by calculating the log of the maximum, minimum, and average coverage for the entire co-assembly. Percent completeness of each bin was determined by the presence of single-copy housekeeping marker genes in CheckM. Phylogenetic identity of the bins was determined from a consensus between Phylosift, CheckM, and BLASTp. Phylogenetic tree was produced using the output from CheckM visualized in Dendroscope. EET (either *pcc*, or *pcc*-like) was positively identified (green +) in bins that contained a putative OM porin, extracellular and periplasmic *c*-cyts, and all supplemental EET-related genes (Table A.1.1). High-coverage bins that contained a partially complete (purple o) putative EET system may still be involved in EET. Bins that were missing several EET-related genes (red -) were too incomplete for further consideration. Remaining bins were abundant members of the microbial community under Fe(III)-reducing conditions, but were not obviously involved in EET. Abbreviations: No ED, No electron donor; *Ca., Candidatus*.

CHAPTER 2

Investigating the Composition and Metabolic Potential of Microbial Communities in Chocolate Pots Hot Springs

Nathaniel W. Fortney[1], Shaomei He[1,2], Brandon J. Converse[1], Eric S. Boyd[3], and Eric E. Roden[1]

[1]NASA Astrobiology Institute, Department of Geoscience, University of Wisconsin-Madison, Madison, WI, USA
[2]Department of Bacteriology, University of Wisconsin-Madison, Madison, WI, USA
[3] NASA Astrobiology Institute, Department of Microbiology and Immunology, Montana State University, Bozeman, MT, USA

Submitted to *Frontiers in Microbiology*

ABSTRACT

Iron (Fe) redox-based metabolisms likely supported life on early Earth and may support life on other Fe-rich rocky planets such as Mars. Modern systems that support active Fe redox cycling such as Chocolate Pots (CP) hot springs provide insight into how life could have functioned in such environments. Previous research demonstrated that Fe- and Si-rich and slightly acidic to circumneutral-pH springs at CP host active dissimilatory Fe(III) reducing microorganisms. However, the abundance and distribution of Fe(III)-reducing communities at CP is not well understood, especially as they exist *in situ*. In addition, the potential for direct Fe(II) oxidation by lithotrophs in CP springs is understudied, in particular when compared to indirect oxidation promoted by oxygen producing Cyanobacteria. Here, a culture-independent approach, including 16S rRNA gene amplicon and shotgun metagenomic sequencing, was used to determine the distribution of putative Fe cycling microorganisms in vent fluids and sediment cores collected along the outflow channel of CP. Metagenome-assembled genomes (MAGs) of organisms native to sediment and planktonic microbial communities were screened for extracellular electron transfer (EET) systems putatively involved in Fe redox cycling and for CO_2 fixation pathways. Abundant MAGs containing putative EET systems were identified as part of the sediment community at locations where Fe(III) reduction activity has previously been documented. MAGs encoding both putative EET systems and CO_2 fixation pathways, inferred to be FeOB, were also present, but were less abundant components of the communities. These results suggest that the majority of the Fe(III) oxides that support *in situ* Fe(III) reduction are derived from abiotic oxidation. This study provides new insights into the interplay between Fe redox cycling and CO_2 fixation in sustaining chemotrophic communities in CP with attendant implications for other neutral-pH hot springs.

KEYWORDS

Chocolate Pots, Yellowstone, iron(III)-reducing bacteria, iron(II)-oxidizing bacteria, metagenomics, extracellular electron transfer

Introduction

Environments containing high concentrations of redox active elements, such as iron (Fe), are important areas of study because of the potential for these elements support the energy metabolism of microbial cells. In its oxidized state [Fe(III)] Fe can serve as a terminal electron acceptor for dissimilatory iron reduction (DIR) by Fe(III)-reducing bacteria (FeRB) (Lovley et al., 2004). In its reduced form [Fe(II)] Fe can serve as an electron donor for lithoautotrophic Fe(II)-oxidizing bacteria (FeOB) (Emerson et al., 2010). Although less prominent in modern Earth environments, Fe(II) can also serve as an electron donor for photosynthetic reactions (Crowe et al., 2008;Llirós et al., 2015;Camacho et al., 2017). Fe is the most abundant redox-active element in the Earth's crust (Taylor and McLennan, 1985) and on astrobiologically relevant worlds, like Mars (Taylor and McLennan, 1985;Taylor and McLennan, 2009). Researchers have suggested that both Fe(II) oxidation and Fe(III) reduction have been active microbial metabolic processes since before the Great Oxidation Event (ca. 2.4 Ga) when Fe(II) concentrations in the Archean ocean were high (Hafenbradl et al., 1996;Vargas et al., 1998;Emerson, 2000). Additionally, it is hypothesized that DIR was one of the earliest forms of microbial respiration (Vargas et al., 1998).

Chocolate Pots (CP) is an Fe(II)- and Si-rich circumneutral-pH geothermal spring in the northwestern portion of Yellowstone National Park. The anoxic spring water issuing from the vent source at CP is of a similar composition to what is predicted for the Archean ocean (Canfield, 2005). Additionally, mineralogical analyses of the Martian surface have identified deposits indicative of circumneutral-pH (Arvidson et al., 2014), and relic hot spring environments (Squyres et al., 2008;Ruff and Farmer, 2016). Together, this makes CP a suitable

analog environment in terms of gaining insight into metabolic processes that could have supported life on early Earth and possibly Mars.

For the past two decades, investigators have used CP as a model environment to study ancient Fe deposition by focusing on the role the microbial community plays in the formation of Fe oxide deposits. In particular, significant attention has been placed on understanding the role of oxygen produced by photosynthetic microbial mat communities in promoting the indirect, abiotic oxidation of Fe(II) (Pierson et al., 1999;Pierson and Parenteau, 2000;Trouwborst et al., 2007;Parenteau and Cady, 2010;Parenteau et al., 2014). The potential for lithoautotrophic Fe(II) oxidation has been considered as well, however after unsuccessful culturing of putative FeOB (Emerson and Weiss, 2004) and little experimental evidence to support their activity in the microbial mats (Trouwborst et al., 2007), research has not been continued in this area.

The potential for DIR in redox transformation of Fe-Si oxides at CP was cited early on (Pierson et al., 1999), but in-depth studies of the anaerobic heterotrophic microbial community have been relatively recent. For example, natural amorphous Fe(III)-oxides from CP were shown to host communities containing known and putative FeRB (Fortney et al., 2016). Subsequent incubation experiments combined with stable isotope probing (SIP) experiments using ^{13}C-labeled acetate identified putative FeRB under acetate-stimulated and unamended incubation conditions (Fortney et al., 2018). However, constraints on the spatial distribution of FeRB within the sediment column of CP were not examined in detail.

In this study we used DNA sequencing to further investigate the spatial distribution of microorganisms involved in Fe cycling in CP vent waters, along the flow path of the outflow channel, and as a function of sediment column depth along the flow path. 16S rRNA gene amplicon sequencing was conducted on filtered spring water samples and sediment core samples

collected from the vent and further downstream with increasing distances from the vent pool. Shotgun metagenomic sequences were obtained from the top 1 cm of three of these sediment cores as well as filtered vent pool water biomass in order to identify abundant taxa containing genes involved in extracellular electron transfer (EET) and CO_2 fixation. Our results provide further support for an active FeRB community in the CP sediments, especially proximal to the vent pool. In contrast, although our genomic data supports the metabolic potential for lithoautotrophic FeOB, they do not appear to be prominent members of the microbial community.

MATERIALS AND METHODS

Sample collection and processing. A total of six small (ca. 1 x 10 cm) sediment cores were collected from the CP vent pool and along the flow path in August 2013 (Figure 2.1). Spring water was filtered from the hot spring source and the vent pool source in October 2015 using an in-line 0.2 μm polyethersulfone (PES) membrane and a peristaltic pump. In an anaerobic chamber, core samples were thawed, extruded, and sectioned into 1 cm intervals. Subsections were split for sequential HCl extraction for Fe geochemical and isotope analyses (Fortney et al., *in prep.*) and DNA extraction.

DNA extraction and sequencing. DNA was extracted according to previously described methods (Fortney et al., 2016). DNA extracts from the core samples were PCR amplified using the universal primer set 515f/806r (Caporaso et al., 2011) targeting 16S rRNA genes and were multiplexed using standard Roche MID primer tags. Amplicons were sequenced at the University of Wisconsin Biotech Center (UWBC, https://www.biotech.wisc.edu/) using the Roche 454 FLX+ pyrosequencing platform. DNA from the top 1 cm sample from cores 1, 2, and

3 was submitted to UWBC for paired-end 2x100 bp Illumina HiSeq 2000 shotgun metagenomic sequencing.

PES membrane filters were cut in half and sliced into strips using a sterile razor blade for use in DNA extraction. DNA from replicate extracts was pooled and submitted to UWBC for paired-end 2x250 bp Illumina HiSeq Rapid shotgun metagenomic sequencing. An additional DNA sample was submitted to Argonne National Labs for PCR amplification (using the universal primers 515f/806r) prior to paired-end 2x200 bp Illumina MiSeq 16S amplicon sequencing.

Analysis of 16S rRNA gene amplicon data. Raw sequences were processed using QIIME following the protocol for 454 pyrosequencing data or Illumina MiSeq 16S rRNA gene amplicon sequencing data, according to previously published methods (Fortney et al., 2016;Fortney et al., 2018).

Metagenome assembly, binning, and assessment of MAGs. Raw shotgun metagenomic sequence from the CP sediment core DNA samples was assembled using metaSPAdes 3.9 (Bankevich et al., 2012;Nurk et al., 2016). Binning was accomplished using CONCOCT 0.4.0 (Alneberg et al., 2014) along with some manual binning based on %GC and coverage to produce metagenome-assembled genomes (MAGs). Differential read coverage was obtained by mapping reads from each metagenome against the contigs from the combined metagenomic assembly (co-assembly) using SNAP 0.15.4 (Zaharia et al., 2011) with default settings, and Samtools 1.3.1 to obtain the coverage of each contig (http://samtools.sourceforge.net) (Li et al., 2009). MAG quality (i.e. completeness, contamination, and strain heterogeneity) was determined using CheckM 1.0.7 (Parks et al., 2015). Putative phylogenetic identities of each MAG were determined through a consensus between the identities provided by CheckM and the

classification based on the lowest common ancestor of essential housekeeping genes based on sequence homology. The CheckM algorithm infers phylogeny based on placement of the MAG within the reference genome tree constructed from 43 conserved phylogenetic marker genes. The 111 bacterial housekeeping genes expected to be encoded in each MAG were identified using previously described methods (Albertsen et al., 2013), including gene prediction by Prodigal (Hyatt et al., 2010) and essential housekeeping gene identification by HMMer search against HMM models (Finn et al., 2011); protein sequences of the detected essential housekeeping genes were aligned to the NCBI nr database (current as of June 8, 2016) using BLASTp. BLAST output was input into in MEGAN (Huson et al., 2007) to determine the lowest common ancestor of these genes to aid in taxonomic classification of each MAG. Dendroscope 3.5.9 (Huson and Scornavacca, 2012) was used to project phylogenetic trees using the CheckM output.

Metagenomic sequence data from the vent pool DNA sample was processed identically with the following exceptions: Raw reads were quality-trimmed, merged, and sequencing adapters were removed in CLC Genomic Workbench 7.5.1 (http://www.clcbio.com) at the UWBC computer center. Processed reads were assembled with raw reads in metaSPAdes 3.10 using the "trusted contigs" command in order to improve assembly quality (e.g. N50). Manual kmer sizes of 21, 33, 55, 77, 99, and 127 were used for assembly. Read mapping was unnecessary in the Vent metagenome because it was a single sample, and coverage for each contig is contained in the metaSPAdes output. Assembly, automated binning, read mapping, and BLAST for both the CP core and vent pool metagenomes were all run using the UW-Madison Center For High Throughput Computing (CHTC) in the Department of Computer Sciences (http://chtc.cs.wisc.edu/).

Inference of metabolic potential. Metagenomic assemblies were uploaded to IMG/M ER (http://img.jgi.doe.gov/mer) for gene annotation (Mavromatis et al., 2009). Metagenomes were screened for homologs of EET systems found in FeRB (e.g. the *Geobacter*-like *pcc* system (Liu et al., 2014;Shi et al., 2014)) using previously published methods (Fortney et al., 2016). Metagenomes were also screened for EET systems found in known FeRB (*Shewanella* spp.*, mtrABC* (Hartshorne et al., 2009)) and FeOB (*Acidithiobacillus ferrooxidans*, *cyc2*; *Sideroxydans* spp. *mtoABCD*; *Rhodobacter ferrooxidans*, *foxEZY*; and *Rhodopseudomonas palustris*, *pioABC* (Ilbert and Bonnefoy, 2013) and references therein) using command-line BLAST and the BLASTp function in IMG. Genes coding for putative EET systems, which are not homologous to known models, were identified according to previously published methods (Fortney et al., 2018). MAGs encoding putative outer-membrane porins, and multiheme *c*-type cytochromes (*c*-cyts) with predicted extracellular and periplasmic locations, as well as other supplemental genes predicted to be involved in Fe transformation pathways, are hereafter referred to as *pcc*-like EET systems. MAGs with genes fitting the above criteria but lacking extracellular *c*-cyts are hereafter referred to as *mto*-like EET systems.

Metagenomes were screened for four different CO_2 fixation pathways: the reductive pentose phosphate cycle [Calvin-Benson-Bassham (CBB)], reductive tricarboxylic acid cycle (rTCA), reductive acetyl-CoA pathway [Wood-Ljungdahl (WL)], and 3-hydroxypropionate (3HP) bicycle. Metagenomes were not screened for the 3-hydroxypropionate/4-hydroxybutyrate pathway or the dicarboxylate/4-hydroxybutyrate pathway because these systems are thus far restricted to thermophilic Archaea isolated from hydrothermal systems much hotter than CP (Hügler and Sievert, 2011). MAGs potentially involved in CO_2 fixation were positively

identified by the presence of all genes predicted to be in a given pathway. Details are provided in Supplementary Text A.2.1.1.

To determine whether CO_2 fixation pathways identified were associated with lithotrophs or phototrophs, MAGs related to known phototrophic organisms were screened for phototrophy-related genes. Firstly, MAGs were screened for genes coding for photoreaction centers and associated photosynthetic genes (e.g. photosystems II and I (PS-II and -I), *puhA* and *pufLM*) using queries from anoxygenic (*Chloroflexus aurantiacus* J-10-fl, *Rhodopseudomonas palustris* 42OL, *Blastochloris viridis* DSM 133, and *Roseiflexus castenholzii* HLO8) and oxygenic (*Cyanothece* sp. BH68, *Oscillatoria* sp. PCC 10802, *Pseudanabaena* sp. PCC 6802, and *Synechococcus* sp. JA-3-3Ab) phototrophs within the IMG database. Next, MAGs were screened for photosynthetic gene categories in annotations (e.g. pfam, COG, EC).

Linking 16S rRNA amplicon data to MAGs. 16S rRNA gene sequences were recovered from the metagenomic libraries using the CheckM algorithm and aligned to the respective 16S rRNA gene in the amplicon libraries by BLASTn search. This allowed for identification of a representative MAG for a given 16S rRNA sequence defined OTU, and vise-versa in order to correlate abundant MAGs and OTUs between sequence libraries.

Accession numbers and sequence files. All metagenomic contigs for the CP core metagenomic co-assemblies and the CP vent pool water column assembly are available through IMG/M ER under taxon identification numbers 3300010938 and 3300014149, respectively. Processed reads (FASTA files) from the 16S rRNA gene amplicon sequencing of the CP cores and CP vent pool water column, and raw OTU table text files are available as in the Supplementary Material of this paper.

RESULTS AND DISCUSSION

Description of Chocolate Pots hot springs. The Chocolate Pots are a series of vent features along and within the Gibbon River approximately 5 km south of the Norris Geyser Basin (Allen and Day, 1935;McCleskey et al., 2010). The hot spring studied here (Thermal ID: GCPNN002; 44.71008, -110.7413) is located along the southeastern bank of the Gibbon River and is comprised of a main hot spring vent and pool which flows over Fe(III) oxide deposits about 10 m down the bank to the river. The vent pool and flow path (see Figure 2.1) were the foci of this study. Two satellite vents located about half way down the bank were not sampled as part of this study.

The temperature of the core sampling site in the vent pool in 2013 was 50.7°C, and decreased to 40.8°C at the collection site of core 6. The temperature where the effluent from CP meets the Gibbon River was 38.1°C. The pH of the Vent coring site was 5.94, increasing to 7.90 at the site of core 6, and 8.25 upon entering the river. The concentration of aqueous Fe(II) was ca. 0.1 mmol L^{-1} at the Vent and decreased to <0.01 mmol L^{-1} by the site of core 4. Water was at a slightly higher temperature (ca. 51.4°C), and lower pH (ca. 5.79) at the vent source where water samples were collected in 2015 (see Table A.2.1 for details).

Composition of the CP sediment cores and vent pool microbial communities: 16S rRNA gene amplicon sequence analysis. *CP sediment cores.* A total of 370544 high-quality 16S rRNA gene amplicon sequences were obtained from 42 sediment core subsamples. Following quality trimming and processing through QIIME (e.g. OTU picking) a total of 18088 reads were distributed between 885 OTUs (excluding singletons) at 97% identity. Overall, the microbial community of the CP core samples is diverse with only 22 OTUs (out of 320 OTUs collapsed to the Family level) having greater than 1% read abundance in the 16S amplicon

library (Table 2.1). However, these few OTUs comprise 61% of all reads in the libraries. OTUs with unassigned taxa comprised 10-15% of the reads.

Principal coordinate analysis of the 16S rRNA gene libraries revealed a few major trends in microbial community structure within and among the cores. Broadly, microbial communities associated with core 1 were distinct from those associated with core 2, and both were distinct from communities from the distal cores (Figure 2.2). The variation in community dissimilarity captured by core 1 along the depth transect encompassed that associated with the other cores combined. Within core 1, the samples from the top two cm diverged considerably from the deeper samples. Likewise, the surface samples tended to be separate from samples deeper within each core, in particular in cores 2 and 5. This resulted in trajectories in community dissimilarity following a trend with increasing depth (at least as it relates to PC1 and PC2) for cores 1, 2, and 5.

The dominant OTUs across all libraries were related to a crenarchaeote (ca. 9% of total reads, 87% 16S rRNA gene identity (ID) to an anaerobic methanogenic archaeon (Chin et al., 1999)), and two Chlorobi (ca. 5% of total reads, each, 84% ID to *Ignavibacterium album* (Iino et al., 2010)) (Table 2.1). The abundant Crenarchaeota OTU was most prevalent in the lower depths of core 1 (below 2 cm) comprising 17.3-41.9% of the reads in the respective libraries; it was also present in the core 2 samples below 1 cm depth (3.4-13.2% read abundance). An additional abundant Crenarchaeota-related OTU was present in only the core 1 samples at all depth intervals at 7.3-12.2% read abundance (Table 2.1).

The role of Archaea in the CP community remains understudied at this time and requires further analysis in this environment. Several prominent OTUs and MAGs identified as archaeal relatives were identified in the 16S amplicon libraries and metagenomic libraries, respectively.

Although the Archaea undoubtedly contributed significantly to the distribution observed in the core samples from the amplicon library, the archaeal OTUs in this study were not related to organisms known to be involved in Fe redox metabolism or CO_2 fixation. Additionally, putative genes involved in these metabolic systems were not identified in the archaeal MAGs in our study. As such, the Archaea are not a focus for the remainder of this paper.

Although not extremely abundant in the CP community, when all sediment cores were considered together (ca. 0.8% read abundance), OTUs related to *Thermodesulfovibrio* (90% ID to *Thermodesulfovibrio yellowstonii* (Henry et al., 1994;Sekiguchi et al., 2008)) are particularly abundant in the topmost layers of core 1 (ca. 6-8% read abundance), less abundant at core 2 (ca. 1-2% read abundance), and absent from core 3 (Table 2.1) and the majority of the core samples from deeper and farther downstream (data not shown). The presence of abundant *Thermodesulfovibrio*-related OTUs in samples from core 1 (CP vent) is not surprising since members of this genus have been shown to reduce Fe(III) (Sekiguchi et al., 2008). Results from previous Fe(III) reducing incubations and recent SIP experiments have suggested that *Thermodesulfovibrio* relatives native to CP may contribute to Fe(III) reduction *in situ* (Fortney et al., 2016;Fortney et al., 2018). Additionally, these studies showed decreasing levels of Fe(III) reduction activity with increasing distance from the CP vent. The presence of *Thermodesulfovibrio*-related OTUs in samples from cores 1 and 2, and not in core samples further downstream from CP vent is consistent with results from these studies and together support the potential involvement of *Thermodesulfovibrio* in Fe(III) oxide reduction in CP. Additional abundant OTUs in the core library, including those related to *Acetothermales* (4.7% read abundance), *Nitrospirales* (3.8% read abundance), and Acidobacteria (3.5% read

abundance) tended to be present in greater abundance in the deeper and more distal core samples, and were largely absent from core 1 samples, especially the top few centimeters (Table 2.1).

Microbial communities in surface samples from cores 2-5 exhibited the greatest separation from deeper samples within those respective cores (Figure 2.2). Notably, these surface communities comprised abundant OTUs (ca. 4-14% read abundance, Table 2.1) affiliated with the lithoautotrophic Fe(II) oxidizing betaproteobacterium *Sideroxydans paludicola* (98% ID (Weiss et al., 2007). This OTU was largely absent from deeper samples from within the cores suggesting it was a likely driver of the overall separation of the surface and subsurface samples within these cores (Figure 2.2). The restricted distribution of this OTU in surface samples may be attributable to its dependence on microaerophilic conditions to catalyze Fe(II) dependent growth. The presence of abundant OTUs (4-14% read abundance) related to *Sideroxydans* lends support to the hypothesis that chemolithotrophic Fe(II) oxidation could contribute to Fe redox cycling at CP.

CP vent pool. A total of 20618 high-quality 16S rRNA gene amplicon sequences were obtained from the vent pool sample. Following processing though QIIME a total of 8587 reads were distributed across 675 OTUs (excluding singletons) at 97% identity. The vent pool was also a diverse microbial community with only 8 OTUs (out of 267 OTUs collapsed to the Family level) with greater than 1% read abundance (Table 2.2). Together, these OTUs accounted for 43% of all reads. OTUs with unassigned taxa made up 27% of the reads in the vent pool library.

Not surprisingly, the CP vent pool sample was distinct from the core samples (Figure 2.2). With the exception of relatives of *Sideroxydans* and *Thermodesulfovibrionaceae,* there was no overlap between the abundant OTUs in the CP sediment cores and CP vent pool libraries. A *Pseudanabaenaceae*-related OTU dominated the vent pool community and accounted for 20% of

the total reads in the library. The second most abundant OTU was affiliated with *Thermodesulfovibrionaceae* (90% ID to *Thermodesulfovibrio yellowstonii* (Henry et al., 1994;Sekiguchi et al., 2008)) at 10% read abundance. The remaining abundant OTUs each comprised about 2% of the total reads in the library and were related to the lithoautotrophic FeOB *Sideroxydans* (99% ID to *Sideroxydans paludicola* (Weiss et al., 2007)) and the anoxygenic phototroph *Roseiflexus* (99% ID to *Roseiflexus* sp. RS-1 (Klatt et al., 2007;van der Meer et al., 2010)).

Pseudanabaenaceae are cyanobacteria that have previously been identified as one of the primary microbial mat-forming species at CP where they form floating streamers at the highest temperature locations (e.g. near the vent, ca. 52°C) (Pierson et al., 1999;Pierson and Parenteau, 2000;Parenteau and Cady, 2010). Although less abundant in the amplicon library, *Chloroflexi*, including an OTU related to *Roseiflexus*, (2.6% read abundance, 99% ID to *Roseiflexus* sp. RS-1 (Klatt et al., 2007;van der Meer et al., 2010)) are also recognized as principal members of the CP mat community (Pierson et al., 1999;Pierson and Parenteau, 2000;Parenteau and Cady, 2010) and thus were also expected in the CP water column. Intriguingly, the presence of relatively abundant OTUs related to *Thermodesulfovibrio* as well as *Sideroxydans* and *Roseiflexus* in the vent pool water column (in addition to the presence of *Thermodesulfovibrio* relatives in the vent sediment) suggests that a coupled Fe redox cycle could be operative at the CP vent.

Composition of the CP sediment cores and vent pool microbial communities: metagenomic sequence analysis. *CP sediment cores.* The communities inhabiting the top 1 cm depth transects of cores 1, 2, and 3 contained a representative set of OTUs found in all other core libraries based on 16S rRNA gene amplicon analysis. Thus, shotgun metagenomic sequence libraries were obtained from DNA extracted from these three samples. Details on the assembly

statistics of the co-assembly can be found in Supplementary Text A.2.1.2. We obtained a total of 167 MAGs from the co-assembly, and the average read coverage of all MAGs in the co-assembly was 15.09. The assemblies were then screened for genes coding for putative EET systems and CO_2 fixation pathways to assess the possibility of Fe redox cycling and contribution to primary production in CP.

We defined "abundant" MAGs as those with higher than average read coverage, and focused on these for further analysis. From the co-assembly of the three metagenomes, eleven abundant MAGs were shown to encode putative EET systems (see Materials and Methods), four encoded putative CO_2 fixation pathways, and three MAGs encoded both. These 18 MAGs accounted for greater than 40% of total mapped reads, suggesting the high abundance of populations represented by these MAGs, and the importance of putative EET and CO_2 fixation processes in the environment. The remaining abundant MAGs (*n*=22, 27.9% mapped reads, Figure 2.3) did not contain either pathway and these organisms were not considered further in this study. MAGs with below average coverage (*n*=127, 30.1% mapped reads) were also not subjected to further analysis. The microbial community of each core was considered individually in addition to the co-assembly in order to determine how the metabolic potential changes with distance moving away from the hot spring vent (Figure 2.3). Core 1 contained 88 MAGs with an average normalized coverage of 7.94, core 2 contained 95 MAGs with an average normalized coverage of 9.75, and core 3 contained only 62 MAGs with an average normalized coverage of 11.27.

A separation of microbial communities from the three cores was evident both when considering the collection of MAGs as a whole (Figure 2.4) and in relation to MAGs containing either a putative EET system or CO_2 fixation pathway (Figures 2.3-2.5). The high-coverage

MAGs from the metagenomic libraries were representative of the abundant OTUs from the amplicon libraries (Table A.2.2). Core 1 was predominantly composed of Chloroflexi, *Ignavibacteriales*, *Thermodesulfovibrio*, Acidobacteria, and *Deferrisoma*. Chloroflexi are known members of the microbial mat community at CP and not unexpected in the core 1 sediment (Parenteau and Cady, 2010). *Thermodesulfovibrio*, Acidobacteria, and *Ignavibacteriales* have all been previously cited as principal members of the CP Community (Fortney et al., 2016;Fortney et al., 2018) (Figure 2.4, A.2.3 and A.2.4). Aside from the archaeal MAGs, core 2 also contained high-coverage *Ignavibacteriales* and *Sideroxydans* MAGs. Core 3 comprised a high-coverage *Caldithrix* MAG, two MAGs related to *Ignavibacteriales* and a *Deferrisoma* MAG. A number of high-coverage MAGs related to *Ignavibacteriales,* Acidobacteria, *Caldithrix* and *Deferrisoma* encoded putative EET systems and were distributed between different core samples. This observation, when coupled with the documented Fe(III) reduction activity at core sites 1 and 3 (see Fortney et al., 2018), suggests that the Fe(III) reducing community at CP is complex and diverse.

Cores 1 and 2 presented more similarity in terms of MAGs encoding putative EET systems than either individual community had with that of core 3 (Figure 2.4). While the overall number of MAGs encoding a particular EET system was similar between the cores (Figure 2.3), in core 3 over 50% of all assembled reads mapped to MAGs containing putative EET systems. In contrast, for cores 1 and 2, only 20% of the assembled reads were mapped to EET-containing MAGs. This is an interesting result considering the activity levels of Fe(III)-reduction observed in previous studies (Fortney et al., 2018). For example, Fe(III)-reduction is more active at the CP vent (i.e. core 1) whereas the genomic potential for Fe(III)-reduction (e.g. the presence of a putative EET system) is more evident at core 3. Not only was the overall read abundance of

EET-containing MAGs driving the separation between cores 1, 2, and 3 but the distribution of abundant MAGs, most of which contained putative EET systems, is also a likely driver.

CP vent pool water column. A shotgun metagenomic sequence library was obtained from DNA extracted from membrane filters collected from the vent pool at CP. The average adjusted coverage (see Supplementary Text A.2.1.2) of all MAGs in the metagenomic assembly was 28.61. The high-coverage MAGs from the metagenomic library were representative of the abundant OTUs from the 16S rRNA gene amplicon library (Table A.2.3). Eleven MAGs had an above-average coverage and comprised 79.2% of the mapped metagenomic reads. One MAG encoded a putative EET system and two MAGs encoded a putative CO_2 fixation pathway; these two MAGs comprised over 20% of the mapped reads in the entire metagenomic assembly. One MAG encoded both systems. The remaining high-coverage MAGs did not encode metabolic pathways directly relevant to Fe cycling and thus were not considered further in this study. The below-average coverage MAGs (*n*=32, 20.2% mapped reads) which did not encode putative EET systems or CO_2 fixation pathways are also not considered in the remainder of this study.

EET systems are much less prevalent in the CP vent pool water column metagenomic assembly than in the surface samples from sediment cores 1, 2, and 3. Less than 4% of the metagenomic reads mapped to MAGs containing these pathways, as compared to >30% in the CP core co-assembly (Figures 2.3 and 2.5). The type of putative EET system was also quite different between the metagenomic assemblies; in particular there was a lack of high-coverage MAGs encoding a *Geobacter*-like *pcc* system in the CP vent pool (Figure 2.6).

Carbon dioxide fixation was a prominent metabolic process in the water column vent pool metagenome. Approximately 24% of the metagenomic reads mapped to only 3 MAGs containing these putative metabolic systems (Figure 2.6). The highest read-coverage MAG was

related to the cyanobacterium *Pseudanabaena* and encoded a full CBB cycle. No MAGs encoded alternative archaeal pathways utilizing RuBisCO nor did any high-coverage MAGs encode a complete putative rTCA cycle. A partially complete 3HP bicycle was identified in one MAG related to *Roseiflexus* (Figure A.2.4). Putative CO_2 fixation pathways were identified in additional lower-coverage MAGs including a relative of *Sideroxydans*.

While *Pelodictyon* (now called *Chlorobium* (Imhoff, 2003)) and *Chloroherpeton* have not specifically been identified at CP before, anoxygenic phototrophic Chlorobi related to "*Candidatus* Thermochlorobacter aerophilum" have been previously described as part of the microbial mat community (Klatt et al., 2013). A high-coverage *Pseudanabaena* MAG was unsurprising given its abundance as part of the mat community at CP ((Parenteau and Cady, 2010) and references therein). As described above in reference to the OTU libraries, multiple MAGs related to Chloroflexi, *Thermodesulfovibrio*, and *Ignavibacteriales* were identified in the CP vent pool metagenomic library and are expected members of the microbial community. Although multiple MAGs of the aforementioned taxa were identified in the metagenome, only one particularly high-coverage representative MAG of each organism was present (Figure A.2.4, Table A.2.3).

One of the guiding hypotheses of this study was that putative lithoautotrophic FeOB are present and active at CP. Given that the *Sideroxydans* MAG in the CP vent pool metagenomic assembly had only slightly below-average read coverage, it would appear that this group of organisms may have a modest presence in CP vent pool microbial community. Metagenomic read coverage and inferred microbial abundance based on 16S rRNA gene amplicon OTU abundance track reasonable well (Tables 2.1, 2.2, A.2.3 and A.2.4). In previous Fe(III)-reducing incubation experiments a high abundance of putative FeRB correlated with high levels of Fe(III)

reduction activity(Fortney et al., 2016;Fortney et al., 2018). However, it is necessary to point out that in terms of the energetics of Fe-based microbial metabolisms, Fe(III) reduction yields greater free energy for cell processes, including cell division, than does Fe(II) oxidation (Neubauer et al., 2002;Bird et al., 2011). Even if FeRB and FeOB have equivalent levels of activity, e.g. the same number of moles of Fe metabolized, one would expect a lower cell density of FeOB simply because of the lower energy potential of the metabolic reaction. Nevertheless, as is detailed below, the metabolic potential of this MAG along with its inferred phylogeny supports the hypothesized presence of lithoautotrophic FeOB at CP.

Presence of putative EET systems at CP and the potential for Fe(III) reduction. It is important to acknowledge that although several MAGs in both metagenomic assemblies contain putative EET systems, the presence of these gene homologs does not in and of itself prove the existence of Fe(III) reduction activity (Shi et al., 2014). However, the previously documented Fe(III) reduction activity from materials collected from these locations at CP (Fortney et al., 2018), coupled with the genomic results identifying the metabolic potential for EET systems, support the hypothesis that these taxa are involved in Fe(III) reduction *in situ*. In contrast, experimental evidence for lithoautotrophic Fe(II) oxidation is currently not available and the operation of this metabolic pathway at CP is more speculative.

CP cores. Sequences homologous to the porin from the well characterized *Geobacter*-like *pcc* EET system were identified in several abundant MAGs in the metagenomic co-assembly, whereas homologs to the *Shewanella*-like *mtrABC* or any of the model Fe(II)-oxidizing EET systems were not identified in the metagenomic co-assembly of the cores. Searches for non-model EET systems identified *pcc*-like systems in abundant MAGs from all three cores and *mto*-like systems in abundant MAGs from all cores (Figures 2.3, 2.5, and A.2.3).

Homologs to the *Geobacter*-like *pcc* porin (Liu et al., 2014;Shi et al., 2014) were located in MAGs identified *Ignavibacteriales* (*n*=7) and *Deferrisoma camini* (*n*=2) (Figure A.2.3). The genome of *Ignavibacterium album* is known to encode a *Geobacter*-like *pcc*-porin (Shi et al., 2014); the same is true for the related *Ignavibacteriales* species, *Melioribacter roseus* (Fortney et al., 2016). The three *Ignavibacteriales* MAGs identified as having only a partially complete *Geobacter*-like *pcc* system are missing a homolog to *gsu1999*, an additional periplasmic *c*-cyt predicted to be in this EET system (Santos et al., 2015;Shi et al., 2016). It should be noted that while the *Ignavibacterium* genome is expected to encode this homolog, the *Melioribacter* genome is not known to encode this gene as part of its *Geobacter*-like *pcc* system, and *Melioribacter* is still capable of carrying out Fe(III) reduction (Podosokorskaya et al., 2013). *Deferrisoma* spp. are known to be FeRB (Slobodkina et al., 2012;Pérez-Rodríguez et al., 2016), and although the exact mechanism for Fe(III) reduction has not been described in this organism, the published genome for *Deferrisoma camini* S3R1 encodes a homolog of the *Geobacter*-like *pcc*-porin (IMG gene ID 2517273319) and accompanying *c*-cyts that were predicted in the EET system model (Shi et al., 2016). Although the *c*-cyts in *D. camini* were predicted to be only periplasmic, extracellular *c*-cyts were detected elsewhere in the genomes. Unexpectedly, we also identified the metabolic potential for autotrophic Fe(III) reduction in one *D. camini* MAG, that is, the presence of both a putative EET system and CO_2 fixation pathway (see "Presence of putative CO_2 fixation systems" section below, and Figure A.2.3). While not observed in *D. camini*, a related *Deferrisoma* sp. has previously demonstrated this capability (Pérez-Rodríguez et al., 2016).

Putative EET systems that were not homologous to the *Geobacter*-like *pcc*-system were detected in MAGs identified as "*Candidatus* Nitrospira defluvii", Acidobacteria (*n*=3), and

Desulfobacterium anilini. A *pcc*-like EET system was also detected in the *Caldithrix* MAG, and while *Caldithrix* spp. are not known to be FeRB (Miroshnichenko et al., 2003;Miroshnichenko et al., 2010;Kublanov et al., 2017), the ability to use Fe(III) as a terminal electron acceptor has not been explicitly tested in these organisms. In any case, the published genome for *Caldithrix abyssi* LF13 also encodes a homolog of the *Geobacter*-like *pcc* porin (IMG gene IDs 2720325731) as well as the predicted associated *c*-cyts. "*Ca.* N. defluvii" and *Desulfobacterium* spp. are known as nitrite oxidizing bacteria and sulfate reducing bacteria, respectively (Brysch et al., 1987;Lücker et al., 2010;Suzuki et al., 2014). *D. autotrophicum* is capable of reducing Fe(III), although not as a means of respiration (Lovley, 2006), and a similar process may be taking place here. The detection of putative EET systems in the Acidobacteria MAGs is consistent with previous data indicating that organisms within this lineage (e.g. *Geothrix fermentans* and *Thermoanaerobaculum aquaticum*) can reduce Fe(III) (Coates et al., 1999;Losey et al., 2013). Acidobacteria have also been identified in metagenomic assemblies of Fe(III) enrichment cultures (Fortney et al., 2016) and Fe(III) reducing incubations derived from CP (Fortney et al., 2018).

The MAG identified as *Gemmatimonas aurantiaca* encoded an *mto*-like EET system, although it is necessary to reiterate that our classification of "*mto*-like" simply refers to the lack of an identified extracellular *c*-cyt that is predicted for Fe(III) reducing EET systems as opposed to any specific knowledge about the metabolic potential of a particular MAG. The representative isolate *G. aurantiaca* T-27^{T} has not been specifically investigated for its ability to oxidize Fe(II) or reduce Fe(III) (Zhang et al., 2003). Curiously, the two *Thermodesulfovibrio* MAGs (although only one MAG was particularly abundant) also encoded putative "*mto*-like" EET systems. However, a possible explanation for the "missing" extracellular *c*-cyt, as is also potentially the

case for the *Gemmatimonas* MAG, could be due to the metagenomic assembly and binning process, which failed to generate contigs containing this gene. This is especially likely given the previous identification of the *Geobacter*-like *pcc* and *pcc*-like EET systems in MAGs related to *Thermodesulfovibrio* (Fortney et al., 2016;Fortney et al., 2018) and, as is discussed below, the identification of a complete *pcc*-like EET system in the CP vent pool *Thermodesulfovibrio*-like MAG (Figure A.2.4).

It was surprising to determine that the *Sideroxydans* MAG did not contain any evidence for an EET system. No 16S rRNA gene was recovered from this MAG so it cannot be specifically related back to the 16S rRNA gene amplicon library of the sediment core samples. However based on a similar change in relative abundance/coverage between the sediment cores and the phylogenetic identity of this MAG, we can reasonable conclude this MAG derives from the same organism. Given the close relatedness of the 16S rRNA gene amplicon to the known FeOB *S. paludicola*, we would expect the MAG to present the same putative metabolic potential. The lack of detection of an EET system in this MAG suggests that it may be differentiated from *S. paludicola* metabolically.

CP vent pool water column. Two above-average coverage MAGs from the vent pool metagenome encoded putative EET systems. An *mto*-like EET system was identified in a MAG belonging to the *Ignavibacteriales*, and a *pcc*-like EET system was identified in a *Thermodesulfovibrio* relative. The presence of putative EET systems in MAGs related to either of these taxa is consistent with our previous work (Fortney et al., 2016;Fortney et al., 2018). However, the putative EET system in the *Ignavibacteriales* MAG is identified as "*mto*-like." Although as discussed above, this classification refers to the lack of an extracellular *c*-cyt proximal to the putative porin and may simply represent an incomplete EET system.

It is interesting to note that several putative EET systems, both *Geobacter*-like *pcc* and *pcc*-like, were identified in low coverage MAGs including multiple *Thermodesulfovibrio*, *Ignavibacteriales*, and *Deferrisoma* MAGs, among others (Figure A.2.4). In contrast to the MAG from the CP sediment core metagenomic co-assembly, the *Sideroxydans* MAG from the CP vent pool metagenomic assembly encoded a putative EET system. However, it was identified as *pcc*-like and shared no homology to the *mtoABCD* system, which is expected for *Sideroxydans* spp. (Emerson et al., 2013). The potential metabolic differentiation between planktonic and sediment microbial communities at CP is consistent with the observations made at other hot springs in Yellowstone (Colman et al., 2016).

Presence of putative CO_2 fixation systems at CP and the potential for litho- or photoautotrophy. *CP cores.* Overall, MAGs encoding putative CO_2 fixation pathways were less abundant than those encoding putative EET systems (Figure A.2.3). CO_2 fixation appeared to be a less prevalent metabolic process in the CP sediment core system, especially in core 3, as compared to potential Fe-based metabolisms (i.e. MAGs containing an EET system) (Figure 2.5). Genes encoding the WL pathway were the most abundant in terms of both the number of MAGs encoding a complete CO_2 fixation pathway and the high percentage of metagenomic reads which mapped to these MAGs relative to other putative CO_2 fixation pathways. Genes encoding the WL pathway were detected in MAGs identified in core 1 (n=5) and core 2 (n=1) while genes encoding the CBB pathway were detected in one MAG identified in both sediment cores 2 and 3. Genes encoding for the rTCA pathway were detected in a single MAG in core 2 (Figure 2.3). One archaeal MAG encoded a homolog to thiazole-adenylate synthase, the alternate ribulose bisphosphate regenerating enzyme proposed by Finn and Tabita (2004); however this MAG was only partially complete as sedoheptulose-1,7-bisphosphatase, a key enzyme in the

pathway, was not detected. We were unable to identify a complete 3HP bicycle in any of the MAGs from the metagenomic co-assembly. Only one moderately abundant MAG identified as a relative of *Dehalococcoides* from core 3 coded for a partial 3HP pathway (Figure 2.3). However, this MAG did not code for a homolog of malonyl-CoA reductase (EC:1.2.1.17), a key marker gene predicted to be in the pathway. This apparent absence of a complete 3HP pathway in this MAG is consistent with the previous suggestion that members of this genus do not encode this pathway (Hügler and Sievert, 2011).

As expected based on the genome sequence of *Sideroxydans lithotrophicus* ES-1 available on IMG (genome ID 646564569) and previous studies of *Sideroxydans* spp. (Weiss et al., 2007;Emerson et al., 2013), the *Sideroxydans* MAG identified in the CP sediment cores encoded a full CBB cycle. However, the detection of a complete CBB pathway in one of the low-coverage *Thermodesulfovibrio* MAGs was unexpected since *Thermodesulfovibrio* spp. are not known to be autotrophic (Henry et al., 1994;Sekiguchi et al., 2008;Orcutt et al., 2015).

Genes encoding a full WL pathway were identified in five MAGs (Figure 2.5). Although one MAG was identified as *Desulfobacterium anilini*, it has since been reclassified as the genus *Desulfatiglans* (Suzuki et al., 2014). Its distant relative, *Desulfobacterium autotrophicum*, has been shown to use the WL pathway to fix CO_2 (Schauder et al., 1989). While the two genera are distinct (ca. 85% 16S rRNA gene sequence similarity) and *Desulfatiglans* are not known to be autotrophic (Suzuki et al., 2014), the evolutionary history of the two organisms may offer an explanation for why a putative WL pathway was detected in this MAG. Additionally, heterotrophic acetate assimilation has been shown to occur using the WL pathway run in reverse (oxidative acetyl-CoA pathway) (Schauder et al., 1989;Hattori et al., 2005;Can et al., 2014). This is a possible explanation for the detection of genes encoding the WL pathway in MAGs

identified as Chloroflexi and *Deltaproteobacteria*, both of which are known to encode the WL pathway (Can et al., 2014). Heterotrophic metabolism via the oxidative acetyl-CoA pathway additionally offers an explanation for the detection of genes encoding a full WL pathway in one of the MAGs identified as *Thermodesulfovibrio*. An incomplete WL pathway (lacking carbon monoxide dehydrogenase (CODH)) has been detected in other *Thermodesulfovibrio* spp. (Henry et al., 1994;Frank et al., 2016) and it is plausible that the *Thermodesulfovibrio*-relatives native to CP have acquired the missing CODH gene through horizontal gene transfer. Further investigation is required to fully resolve the metabolic capabilities of these organisms.

Genes encoding ATP-citrate lyase (*aclAB*) have been used previously as genetic markers of the rTCA cycle in microbial communities (Hügler et al., 2005). However, caution has been stressed in using *aclAB* alone as indication for the presence of rTCA (Williams et al., 2006). More recent studies have identified additional mechanisms that bacteria can use to cleave citrate (i.e. citryl-CoA synthase and citryl-CoA lyase, see Supplementary Text A.2.1.1 for details) along with other enzymes (i.e. 2-oxoglutarate synthase) that can catalyze the irreversible reactions unique to the pathway (Hügler and Sievert, 2011). For these reasons, we took a conservative approach when looking for the presence of the key marker genes along with all other genes predicted in the pathway as a positive indication for the rTCA cycle in a bin. As a result the high-coverage "*Ca.* Nitrospira defluvii" MAG was the only positive identification of a full rTCA cycle, which is consistent with previous reports of this pathway in "*Ca.* N. defluvii" (Lücker et al., 2010).

Definitive abundant phototrophic MAGs were not present in the CP sediment core metagenomic co-assembly. Genes encoding PS-II and -I were detected in cyanobacterial MAGs

(e.g. *Oscillatoriales*, *Pseudanabaena*, and *Synechococcus*). However, these MAGs had very low read-coverage (ca. 2-5x) and were not considered further in this study.

CP vent pool water column. The two cyanobacterial MAGs, *Synechococcus* and *Pseudanabaena* coded for full a CBB cycle and complete PS-II and -I gene complex. The *Sideroxydans* MAG also encoded a full CBB pathway (Figure 2.4), as expected based of previous genomic characterization of this genus (see above). A single abundant MAG, *Thermodesulfovibrio*, encoded a full WL pathway. As is described above in regard to the CP sediment core metagenomic co-assembly, this *Thermodesulfovibrio*-relative may have acquired CODH through horizontal gene transfer, although further phylogenetic analysis is needed to evaluate this possibility. Even though the *Pelodictyon* and *Chloroherpeton* MAGs only encoded partial rTCA cycles, they also encoded homologs of anoxygenic photoreaction centers (Figure 2.4); anoxygenic photoautotrophy via rTCA is expected for members of the *Chlorobiaceae* (Hügler and Sievert, 2011). The 3HP cycle was proposed for and characterized in *Chloroflexus aurantiacus* (Strauss and Fuchs, 1993;Zarzycki et al., 2009). Genes involved in this autotrophic pathway have since been identified in related Chloroflexi, i.e. *Roseiflexus* spp. (van der Meer et al., 2010), and stable isotope probing experiments have indicated the potential for CO_2 fixation via 3HP (Klatt et al., 2007). The putative 3HP bicycle in the *Roseiflexus* MAG is only partially complete, however given the aforementioned information; it is not unexpected for this organism.

Evidence for a coupled Fe redox cycling microbial community at CP. Although this study took a bioinformatics approach to probing the *in situ* microbial community for evidence for Fe redox cycling, it is important to recall that previous enrichment culturing (Fortney et al., 2016) and incubation studies (Fortney et al., 2018) have experimentally demonstrated the Fe(III) reducing capability of the CP microbial community. These observations, combined with the

genomic evidence for the metabolic potential for EET and Fe(III) reduction as presented here (Figures 2.5 and A.2.3), allows us to confidently assert that Fe redox cycling is an important process supporting microbial metabolism in CP.

As for the oxidative side of the Fe cycle, putative FeOB (i.e. *Sideroxydans* MAGs) were detected in both the sediment and planktonic components of the CP microbial community, and genomic evidence indicates their potential contribution to lithoautotrophic Fe(II) oxidation (Figures A.2.3 and A.2.4). The relatively low metagenomic coverage of these MAGs (at least in the CP vent pool water column) is reasonable given the expected lower energy yields of this Fe(II) oxidation (Bird et al., 2011). The *in situ* activity of putative FeOB warrants further direct investigation (e.g. transcriptomics), and despite the relatively low abundance these MAGs, it is possible that they have a nontrivial contribution to Fe(II) oxidation and CO_2 fixation *in situ*. *Sideroxydans* spp. are microaerophiles (Neubauer et al., 2002;Emerson and Weiss, 2004) and the low O_2 concentrations measured at the CP vent, ca. 0-5% air saturation (E. Roden, unpublished data)(Wu et al., 2013), are amenable to growth of these organisms. Dissolved oxygen never reaches supersaturation in the spring water in the CP flow path nor within the microbial mats (Pierson et al., 1999;Parenteau et al., 2014), however higher concentrations of O_2 have been measured in the vent pool, ca. 25% air saturation (Pierson et al., 1999), which could be toxic to these cells and may have an impact on their overall abundance. This information, combined with that from previous studies of the potential for lithoautotrophic Fe(II) oxidation activity at CP (Trouwborst et al., 2007) as well as unsuccessful attempts at culturing these organisms (Emerson and Weiss, 2004), suggests that the majority of Fe(II) oxidation at CP is due to abiotic oxidation by biogenic O_2 produced by Cyanobacteria. We thus conclude that the vast majority of Fe(II) oxidation occurs as an indirect result of the production of O_2 by Cyanobacteria in the

community, a conclusion that is consistent with those made previously (Pierson et al., 1999;Pierson and Parenteau, 2000;Emerson and Weiss, 2004;Trouwborst et al., 2007;Parenteau and Cady, 2010).

In addition to indirect Fe(II) oxidation, Cyanobacteria undoubtedly have the greatest impact on fixed carbon within the water column, mat, and sediment environments at CP. There is still some uncertainty as to the ability of *Roseiflexus* to fix CO_2 (Klatt et al., 2007;van der Meer et al., 2010;Tang et al., 2011;Tank et al., 2017), and while the abundant MAGs of other anoxygenic phototrophs, *Pelodictyon* and *Chloroherpeton,* encoded only partial putative CO_2 fixation pathways, the rTCA cycle is known to be operative in the Chlorobi (Frigaard and Bryant, 2008). Members of these photoautotrophic phyla have previously been identified at CP (Klatt et al., 2013;Fortney et al., 2018) and are all likely contributing substantially to the fixed carbon budget that is in turn supplying the heterotrophic FeRB community at CP.

It is entirely possible that *Sideroxydans*, as well as the rest of the CP community fluctuates temporally or spatially, however without more data we can merely speculate at this time. A protracted sampling campaign to assess diurnal and even seasonal cycles could illuminate whether the abundant organisms found in this study consistently dominate the microbial community, or if they are subject to significant temporal variations. Due to the unsuccessful attempts to study the FeOB community at CP using culturing (Emerson and Weiss, 2004) or stable isotope probing techniques (Fortney et al., unpublished results), future investigations will almost certainly require culture-independent techniques (e.g. transcriptomics) to measure levels of abundance and activity of the Fe cycling microbial community at CP.

Comparison of CP to other circumneutral Fe-rich seep/spring environments. In many ways CP resembles other circumneutral-pH Fe seep (Haaijer et al., 2008;Blöthe and

Roden, 2009;Roden et al., 2012) and Fe-rich spring-like environments (Hegler et al., 2012;Ward et al., 2017), where Fe(II)-rich subsurface fluids contact atmospheric oxygen, resulting in the accumulation of Fe(III) oxide deposits. The results of our incubation studies and metagenomic investigations are consistent with other studies that have demonstrated the potential for such oxide deposits to serve as electron acceptors for FeRB (Emerson and Revsbech, 1994;Haaijer et al., 2008;Blöthe and Roden, 2009;Hegler et al., 2012;Roden et al., 2012). However, a notable characteristic that sets CP apart from these other ecosystems is the absence of abundant putative FeOB in the spring water near the vent source. One might attribute this difference to the mildly thermophilic conditions at the CP vent (ca. 50°C), which is significantly warmer than canonical neutrophilic FeOB (e.g. *Sideroxydans*) habitats (Emerson et al., 2013). However, *Sideroxydans*-related sequences have been identified in a Japanese thermal spring (ca. 45°C) similar to CP (Ward et al., 2017). The extent to which these ecosystems are exposed to direct sunlight, and therefore the presence or absence of phototrophs (e.g. Cyanobacteria), may have a pronounced effect on the Fe-oxidizing microbial community. Cyanobacteria are absent from the Jackson Creek Fe seep environment in Indiana where tree canopy cover prevents abundant growth of phototrophic microorganisms, and the main O_2 input is from the atmosphere (Roden et al., 2012). In contrast, CP is fully exposed and hosts an abundant phototrophic community comprised of Cyanobacteria, Chlorobi and Chloroflexi in both microbial mats and planktonic phases (Parenteau and Cady, 2010)(Figure A.2.4). In this way CP is analogous to other Fe-rich spring systems in that the Cyanobacteria mat communities are spatially segregated to the margins of the vent pool (Hegler et al., 2012) and flow path further downstream (Ward et al., 2017).

Ultimately, it is a combination of factors (e.g. flow rate, insolation, temperature, oxygen saturation) in these circumneutral-pH Fe-rich ecosystems that control microbial community

composition, and therefore the Fe redox cycling metabolic pathways that are present and active in each of these environments. The reason for the diminished role of FeOB in the CP vent pool water column is not clear at this time. Further analysis of this hot spring and other Fe-rich seep/spring-like environments is needed to resolve these differences.

ACKNOWLEDGEMENTS

This research was supported by the NASA Astrobiology Institute award #NNA13AA94A.

REFERENCES

Albertsen, M., Hugenholtz, P., Skarshewski, A., Nielsen, K.R.L., Tyson, G.W., and Nielsen, P.H. (2013). Genome sequences of rare, uncultured bacteria obtained by differential coverage binning of multiple metagenomes. *Nat Biotechnol* 31**,** 533-538. doi: 10.1038/nbt.2579

Allen, E.T., and Day, A.L. (1935). *Hot Springs of the Yellowstone National Park.* Carnegie Institution of Washington.

Alneberg, J., Bjarnason, B.S.R., De Bruijn, I., Schirmer, M., Quick, J., Ijaz, U.Z., Lahti, L., Loman, N.J., Andersson, A.F., and Quince, C. (2014). Binning metagenomic contigs by coverage and composition. *Nat Methods* 11**,** 1144-1146. doi: 10.1038/nmeth.3103

Arvidson, R.E., Squyres, S.W., Bell, J.F., 3rd, Catalano, J.G., Clark, B.C., Crumpler, L.S., De Souza, P.A., Jr., Fairen, A.G., Farrand, W.H., Fox, V.K., Gellert, R., Ghosh, A., Golombek, M.P., Grotzinger, J.P., Guinness, E.A., Herkenhoff, K.E., Jolliff, B.L., Knoll, A.H., Li, R., Mclennan, S.M., Ming, D.W., Mittlefehldt, D.W., Moore, J.M., Morris, R.V., Murchie, S.L., Parker, T.J., Paulsen, G., Rice, J.W., Ruff, S.W., Smith, M.D., and Wolff, M.J. (2014). Ancient aqueous environments at Endeavour Crater, Mars. *Science* 343**,** 8. doi: 10.1126/science.1248097

Bankevich, A., Nurk, S., Antipov, D., Gurevich, A.A., Dvorkin, M., Kulikov, A.S., Lesin, V.M., Nikolenko, S.I., Pham, S., Prjibelski, A.D., Pyshkin, A.V., Sirotkin, A.V., Vyahhi, N., Tesler, G., Alekseyev, M.A., and Pevzner, P.A. (2012). SPAdes: a new genome assembly algorithm and its applications to single-cell sequencing. *J Comput Biol* 19**,** 455-477. doi: 10.1089/cmb.2012.0021

Bird, L.J., Bonnefoy, V., and Newman, D.K. (2011). Bioenergetic challenges of microbial iron metabolisms. *Trends Microbiol* 19**,** 330-340. doi: 10.1016/j.tim.2011.05.001

Blöthe, M., and Roden, E.E. (2009). Microbial iron redox cycling in a circumneutral-pH groundwater seep. *Appl Environ Microbiol* 75**,** 468-473. doi: 10.1128/AEM.01817-08

Brysch, K., Schneider, C., Fuchs, G., and Widdel, F. (1987). Lithoautotrophic growth of sulfate-reducing bacteria, and description of *Desulfobacterium autotrophicum* gen. nov., sp. nov. *Arch Microbiol* 148**,** 264-274. doi:

Camacho, A., Walter, X.A., Picazo, A., and Zopfi, J. (2017). Photoferrotrophy: Remains of an Ancient Photosynthesis in Modern Environments. *Front Microbiol* 8**,** 323. doi: 10.3389/fmicb.2017.00323

Can, M., Armstrong, F.A., and Ragsdale, S.W. (2014). Structure, function, and mechanism of the nickel metalloenzymes, CO dehydrogenase, and acetyl-CoA synthase. *Chem Rev* 114**,** 4149-4174. doi: 10.1021/cr400461p

Canfield, D.E. (2005). The early history of atmospheric oxygen: Homage to Robert M. Garrels. *Ann Rev Earth Planet Sci* 33**,** 1-36. doi: 10.1146/annurev.earth.33.092203.122711

Caporaso, J.G., Lauber, C.L., Walters, W.A., Berg-Lyons, D., Lozupone, C.A., Turnbaugh, P.J., Fierer, N., and Knight, R. (2011). Global patterns of 16S rRNA diversity at a depth of millions of sequences per sample. *Proc Natl Acad Sci U S A* 108 Suppl 1**,** 4516-4522. doi: 10.1073/pnas.1000080107

Chin, K.-J., Lukow, T., Stubner, S., and Conrad, R. (1999). Structure and function of the methanogenic archaeal community in stable cellulose-degrading enrichment cultures at two different temperatures (15 and 30°C). *FEMS Microbiol Ecol* 30**,** 313-326. doi:

Coates, J.D., Ellis, D.J., Gaw, C.V., and Lovley, D.R. (1999). *Geothrix fermentans* gen. nov., sp. nov., a novel Fe(III)-reducing bacterium from a hydrocarbon-contaminated aquifer. *Int J Syst Bacteriol* 49**,** 1615-1622. doi:

Colman, D.R., Feyhl-Buska, J., Robinson, K.J., Fecteau, K.M., Xu, H., Shock, E.L., and Boyd, E.S. (2016). Ecological differentiation in planktonic and sediment-associated chemotrophic microbial populations in Yellowstone hot springs. *FEMS Microbiol Ecol* 92. doi: 10.1093/femsec/fiw137

Crowe, S.A., Jones, C., Katsev, S., Magen, C., O'neill, A.H., Sturm, A., Canfield, D.E., Haffner, G.D., Mucci, A., Sundby, B., and Fowle, D.A. (2008). Photoferrotrophs thrive in an Archean Ocean analogue. *Proc Natl Acad Sci U S A* 105**,** 15938-15943. doi: 10.1073/pnas.0805313105

Emerson, D. (2000). "Microbial Oxidation of Fe(II) and Mn(II) at Circumneutral pH," in *Environmental Microbe-Metal Interactions,* ed. D.R. Lovley. (Washington, D.C.: ASM Press), 31-52.

Emerson, D., Field, E.K., Chertkov, O., Davenport, K.W., Goodwin, L., Munk, C., Nolan, M., and Woyke, T. (2013). Comparative genomics of freshwater Fe-oxidizing bacteria: implications for physiology, ecology, and systematics. *Front Microbiol* 4**,** 254. doi: 10.3389/fmicb.2013.00254

Emerson, D., Fleming, E.J., and Mcbeth, J.M. (2010). Iron-oxidizing bacteria: an environmental and genomic perspective. *Ann Rev Microbiol* 64**,** 561-583. doi: 10.1146/annurev.micro.112408.134208

Emerson, D., and Revsbech, N.P. (1994). Investigation of an Iron-Oxidizing Microbial Mat Community Located near Aarhus, Denmark: Laboratory Studies. *Appl Environ Microbiol* 60**,** 4032-4038. doi:

Emerson, D., and Weiss, J.V. (2004). Bacterial Iron Oxidation in Circumneutral Freshwater Habitats: Findings from the Field and the Laboratory. *Geomicrobiol J* 21**,** 405-414. doi: 10.1080/01490450490485881

Finn, M.W., and Tabita, F.R. (2004). Modified Pathway To Synthesize Ribulose 1,5-Bisphosphate in Methanogenic Archaea. *J Bacteriol* 186**,** 6360-6366. doi: 10.1128/JB.186.19.6360-6366.2004

Finn, R.D., Clements, J., and Eddy, S.R. (2011). HMMER web server: interactive sequence similarity searching. *Nucleic Acids Res* 39**,** W29-37. doi: 10.1093/nar/gkr367

Fortney, N.W., He, S., Converse, B.J., Beard, B.L., Johnson, C.M., Boyd, E.S., and Roden, E.E. (2016). Microbial Fe(III) oxide reduction potential in Chocolate Pots hot spring, Yellowstone National Park. *Geobiology* 14**,** 255-275. doi: 10.1111/gbi.12173

Fortney, N.W., He, S., Kulkarni, A., Friedrich, M.W., Holz, C., Boyd, E.S., and Roden, E.E. (2018). Stable isotope probing of microbial iron reduction in Chocolate Pots hot spring, Yellowstone National Park. *Appl Environ Microbiol* 84**,** 15. doi: 10.1128/AEM.02894-17

Frank, Y.A., Kadnikov, V.V., Lukina, A.P., Banks, D., Beletsky, A.V., Mardanov, A.V., Sen'kina, E.I., Avakyan, M.R., Karnachuk, O.V., and Ravin, N.V. (2016). Characterization and Genome Analysis of the First Facultatively Alkaliphilic *Thermodesulfovibrio* Isolated from the Deep Terrestrial Subsurface. *Front Microbiol* 7**,** 2000. doi: 10.3389/fmicb.2016.02000

Frigaard, N.-U., and Bryant, D.A. (2008). "Genomic and Evolutionary Perspectives on Sulfur Metabolism in Green Sulfur Bacteria," in *Microbial Sulfur Metabolism,* eds. C. Dahl & C.G. Friedrich. (Berlin: Springer-Verlag), 60-76.

Haaijer, S.C.M., Harhangi, H.R., Meijerink, B.B., Strous, M., Pol, A., Smolders, A.J., Verwegen, K., Jetten, M.S.M., and Op Den Camp, H.J.M. (2008). Bacteria associated with iron seeps in a sulfur-rich, neutral pH, freshwater ecosystem. *ISME J* 2**,** 1231-1242. doi: 10.1038/ismej.2008.75

Hafenbradl, D., Keller, M., Dirmeier, R., Rachel, R., Roßnagel, P., Burggraf, S., Huber, H., and Stetter, K.O. (1996). *Ferroglobus placidus* gen. nov., sp. nov., a novel hyperthermophilic archaeum that oxidizes Fe^{2+} at neutral pH under anoxic conditions. *Arch Microbiol* 16**,** 308-314. doi:

Hartshorne, R.S., Reardon, C.L., Ross, D., Nuester, J., Clarke, T.A., Gates, A.J., Mills, P.C., Fredrickson, J.K., Zachara, J.M., Shi, L., Beliaev, A.S., Marshall, M.J., Tien, M., Brantley, S., Butt, J.N., and Richardson, D.J. (2009). Characterization of an electron conduit between bacteria and the extracellular environment. *Proc Natl Acad Sci U S A* 106**,** 22169-22174. doi: 10.1073/pnas.0900086106

Hattori, S., Galushko, A.S., Kamagata, Y., and Schink, B. (2005). Operation of the CO dehydrogenase/acetyl coenzyme A pathway in both acetate oxidation and acetate formation by the syntrophically acetate-oxidizing bacterium *Thermacetogenium phaeum*. *J Bacteriol* 187**,** 3471-3476. doi: 10.1128/JB.187.10.3471-3476.2005

Hegler, F., Lösekann-Behrens, T., Hanselmann, K., Behrens, S., and Kappler, A. (2012). Influence of Seasonal and Geochemical Changes on the Geomicrobiology of an Iron Carbonate Mineral Water Spring. *Appl Environ Microbiol* 78**,** 7185-7196. doi: 10.1128/AEM.01440-12

Henry, E.A., Devereux, R., Maki, J.S., Gilmour, C.C., Woese, C.R., Mandelco, L., Schauder, R., Remen, C.C., and Mitchell, R. (1994). Characterization of a new thermophilic sulfate-reducing bacterium *Thermodesulfovibrio yellowstonii*, gen. nov. and sp. nov.: its phylogenetic relationship to *Thermodesulfobacterium commune* and their origins deep within the bacterial domain. *Arch Microbiol* 161**,** 62-69. doi:

Hügler, M., and Sievert, S.M. (2011). Beyond the Calvin Cycle: Autotrophic Carbon Fixation in the Ocean. *Annu Rev Mar Sci* 3. doi: 10.1146/annurev-marine-120709-142712

Hügler, M., Wirsen, C.O., Fuchs, G., Taylor, C.D., and Sievert, S.M. (2005). Evidence for Autotrophic CO_2 Fixation via the Reductive Tricarboxylic Acid Cycle by Members of the ε Subdivision of Proteobacteria. *J Bacteriol* 187**,** 3020-3027. doi: 10.1128/JB.187.9.3020-3027.2005

Huson, D.H., Auch, A.F., Qi, J., and Schuster, S.C. (2007). MEGAN analysis of metagenomic data. *Genome Res* 17**,** 377-386. doi: 10.1101/gr.5969107

Huson, D.H., and Scornavacca, C. (2012). Dendroscope 3: an interactive tool for rooted phylogenetic trees and networks. *Syst Biol* 61**,** 1061-1067. doi: 10.1093/sysbio/sys062

Hyatt, D., Chen, G.-L., Locascio, P.F., Land, M.L., Larimer, F.W., and Hauser, L.J. (2010). Prodigal: prokaryotic gene recognition and translation initiation site identification. *BMC bioinformatics* 11**,** 119. doi:

Iino, T., Mori, K., Uchino, Y., Nakagawa, T., Harayama, S., and Suzuki, K. (2010). *Ignavibacterium album* gen. nov., sp. nov., a moderately thermophilic anaerobic bacterium isolated from microbial mats at a terrestrial hot spring and proposal of *Ignavibacteria* classis nov., for a novel lineage at the periphery of green sulfur bacteria. *Int J Syst Evol Micr* 60**,** 1376-1382. doi: 10.1099/ijs.0.012484-0

Iino, T., Nakagawa, T., Mori, K., Harayama, S., and Suzuki, K.-I. (2008). Calditerrivibrio nitroreducens gen. nov., sp. nov., a thermophilic, nitrate-reducing bacterium isolated

from a terrestrial hot spring in Japan. *Int J Syst Evol Micr* 58**,** 1675-1679. doi: 10.1099/ijs.0.65714-0

Ilbert, M., and Bonnefoy, V. (2013). Insight into the evolution of the iron oxidation pathways. *Biochim Biophys Acta* 1827**,** 161-175. doi: 10.1016/j.bbabio.2012.10.001

Imhoff, J.F. (2003). Phylogenetic taxonomy of the family *Chlorobiaceae* on the basis of 16S rRNA and *fmo* (Fenna-Matthews-Olson protein) gene sequences. *Int J Syst Evol Micr* 53**,** 941-951. doi: 10.1099/ijs.0.02403-0

Klatt, C.G., Bryant, D.A., and Ward, D.M. (2007). Comparative genomics provides evidence for the 3-hydroxypropionate autotrophic pathway in filamentous anoxygenic phototrophic bacteria and in hot spring microbial mats. *Environ Microbiol* 9**,** 2067-2078. doi: 10.1111/j.1462-2920.2007.01323.x

Klatt, C.G., Inskeep, W.P., Herrgard, M.J., Jay, Z.J., Rusch, D.B., Tringe, S.G., Parenteau, M.N., Ward, D.M., Boomer, S.M., Bryant, D.A., and Miller, S.R. (2013). Community structure and function of high-temperature chlorophototrophic microbial mats inhabiting diverse geothermal environments. *Front Microbiol* 4**,** 106. doi: 10.3389/fmicb.2013.00106

Kublanov, I.V., Sigalova, O.M., Gavrilov, S.N., Lebedinsky, A.V., Rinke, C., Kovaleva, O., Chernyh, N.A., Ivanova, N., Daum, C., Reddy, T.B.K., Klenk, H.-P., Spring, S., Göker, M., Reva, O.N., Miroshnichenko, M.L., Kyrpides, N.C., Woyke, T., Gelfand, M.S., and Bonch-Osmolovskaya, E.A. (2017). Genomic Analysis of *Caldithrix abyssi*, the Thermophilic Anaerobic Bacterium of the Novel Bacterial Phylum *Calditrichaeota*. *Front Microbiol* 8**,** 195. doi: 10.3389/fmicb.2017.00195

Li, H., Handsaker, B., Wysoker, A., Fennell, T., Ruan, J., Homer, N., Marth, G., Abecasis, G., Durbin, R., and Genome Project Data Processing, S. (2009). The Sequence Alignment/Map format and SAMtools. *Bioinformatics* 25**,** 2078-2079. doi: 10.1093/bioinformatics/btp352

Liu, Y., Wang, Z., Liu, J., Levar, C., Edwards, M.J., Babauta, J.T., Kennedy, D.W., Shi, Z., Beyenal, H., Bond, D.R., Clarke, T.A., Butt, J.N., Richardson, D.J., Rosso, K.M., Zachara, J.M., Fredrickson, J.K., and Shi, L. (2014). A trans-outer membrane porin-cytochrome protein complex for extracellular electron transfer by *Geobacter sulfurreducens* PCA. *Environ Microbiol Rep* 6**,** 776-785. doi: 10.1111/1758-2229.12204

Liu, Z., Frigaard, N.-U., Vogl, K., Iino, T., Ohkuma, M., Overmann, J.R., and Bryant, D.A. (2012). Complete Genome of Ignavibacterium album, a Metabolically Versatile, Flagellated, Facultative Anaerobe from the Phylum Chlorobi. *Front Microbiol* 3**,** 1-15. doi: 10.3389/fmicb.2012.00185

Llirós, M., García-Armisen, T., Darchambeau, F., Morana, C., Triadó-Margarit, X., Inceoğlu, Ö., Borrego, C.M., Bouillon, S., Servais, P., Borges, A.V., Descy, J.-P., Canfield, D.E., and Crowe, S.A. (2015). Pelagic photoferrotrophy and iron cycling in a modern ferruginous basin. *Sci Rep* 5. doi: 10.1038/srep13803

Losey, N.A., Stevenson, B.S., Busse, H.-J., Sinninghé Damste, J.S., Rijpstra, W.I.C., Rudd, S., and Lawson, P.A. (2013). *Thermoanaerobaculum aquaticum* gen. nov., sp. nov., the first cultivated member of *Acidobacteria* subdivision 23, isolated from a hot spring. *Int J Syst Evol Micr* 63**,** 4149-4157. doi: 10.1099/ijs.0.051425-0

Lovley, D. (2006). "Dissimilatory Fe(III)- and Mn(IV)-Reducing Prokaryotes," in *The Prokaryotes,* eds. M. Dworkin, S. Falkow, E. Rosenberg, K.H. Schleifer & E. Stackebrandt. (New York, NY: Springer), 635-658.

Lovley, D.R., Holmes, D.E., and Nevin, K.P. (2004). Dissimilatory Fe(III) and Mn(IV) Reduction. *Adv Microb Physiol* 49**,** 219-286. doi: 10.1016/s0065-2911(04)49005-5

Lücker, S., Wagner, M., Maixner, F., Pelletier, E., Koch, H., Vacherie, B., Rattei, T., Sinninghe Damsté, J.S., Spieck, E., Le Paslier, D., and Daims, H. (2010). A *Nitrospira* metagenome illuminates the physiology and evolution of globally important nitrite-oxidizing bacteria. *Proc Natl Acad Sci USA* 107**,** 13479-13484. doi: 10.1073/pnas.1003860107

Mavromatis, K., Ivanova, N.N., Chen, I.M., Szeto, E., Markowitz, V.M., and Kyrpides, N.C. (2009). The DOE-JGI Standard Operating Procedure for the Annotations of Microbial Genomes. *Stand Genomic Sci* 1**,** 63-67. doi: 10.4056/sigs.632

McCleskey, R.B., Nordstrom, D.K., Susong, D.D., Ball, J.W., and Holloway, J.M. (2010). Source and fate of inorganic solutes in the Gibbon River, Yellowstone National Park, Wyoming, USA. *J Volcanol Geoth Res* 193**,** 189-202. doi: 10.1016/j.jvolgeores.2010.03.014

Miroshnichenko, M.L., Kolganova, T.V., Spring, S., Chernyh, N., and Bonch-Osmolovskaya, E.A. (2010). Caldithrix palaeochoryensis sp. nov., a thermophilic, anaerobic, chemo-organotrophic bacterium from a geothermally heated sediment, and emended description of the genus Caldithrix. *Int J Syst Evol Micr* 60**,** 2120-2123. doi: 10.1099/ijs.0.016667-0

Miroshnichenko, M.L., Kostrikina, N.A., Chernyh, N.A., Pimenov, N.V., Tourova, T.P., Antipov, A.N., Spring, S., Stackebrandt, E., and Bonch-Osmolovskaya, E.A. (2003). *Caldithrix abyssi* gen. nov., sp. nov., a nitrate-reducing, thermophilic, anaerobic bacterium isolated from a Mid-Atlantic Ridge hydrothermal vent, represents a novel bacterial lineage. *Int J Syst Evol Micr* 53**,** 323-329. doi: 10.1099/ijs.0.02390-0

Neubauer, S.C., Emerson, D., and Megonigal, J.P. (2002). Life at the Energetic Edge: Kinetics of Circumneutral Iron Oxidation by Lithotrophic Iron-Oxidizing Bacteria Isolated from the Wetland-Plant Rhizosphere. *Appl Environ Microbiol* 68**,** 3988-3995. doi: 10.1128/aem.68.8.3988-3995.2002

Nunoura, T., Hirai, M., Miyazaki, M., Kazama, H., Makita, H., Hirayama, H., Furushima, Y., Yamamoto, H., Imachi, H., and Takai, K. (2013). Isolation and Characterization of a Thermophilic, Obligately Anaerobic and Heterotrophic Marine *Chloroflexi* Bacterium from a *Chloroflexi*-dominated Microbial Community Associated with a Japanese Shallow Hydrothermal System, and Proposal for *Thermomarinilinea lacunofontalis* gen. nov., sp. nov. *Microbes Environ* 28**,** 228-235. doi: 10.1264/jsme2.ME12193

Nunoura, T., Hirayama, H., Takami, H., Oida, H., Nishi, S., Shimamura, S., Suzuki, Y., Inagaki, F., Takai, K., Nealson, K.H., and Horikoshi, K. (2005). Genetic and functional properties of uncultivated thermophilic crenarchaeotes from a subsurface gold mine as revealed by analysis of genome fragments. *Environ Microbiol* 7**,** 1967-1984. doi: 10.1111/j.1462-2920.2005.00881.x

Nunoura, T., Takaki, Y., Kakuta, J., Nishi, S., Sugahara, J., Kazama, H., Chee, G.-J., Hattori, M., Kanai, A., Atomi, H., Takai, K., and Takami, H. (2011). Insights into the evolution of Archaea and eukaryotic protein modifier systems revealed by the genome of a novel archaeal group. *Nucleic Acids Res* 39**,** 3204-3223. doi: 10.1093/nar/gkq1228

Nurk, S., Meleshko, D., Korobeynikov, A., and Pevzner, P. (2016). metaSPAdes: a new versatile de novo metagenomics assembler. *arXiv* q-Bio.GN. doi: arXiv:1604.03071v2

Orcutt, B.N., Sylvan, J.B., Rogers, D.R., Delaney, J., Lee, R.W., and Girguis, P.R. (2015). Carbon fixation by basalt-hosted microbial communities. *Front Microbiol* 6**,** 904. doi: 10.3389/fmicb.2015.00904

Parenteau, M.N., and Cady, S.L. (2010). Microbial Biosignatures in Iron-Mineralized Phototrophic Mats at Chocolate Pots Hot Springs, Yellowstone National Park, United States. *Palaios* 25**,** 97-111. doi: 10.2110/palo.2008.p08-133r

Parenteau, M.N., Jahnke, L.L., Farmer, J.D., and Cady, S.L. (2014). Production and Early Preservation of Lipid Biomarkers in Iron Hot Springs. *Astrobiology* 14**,** 502-521. doi: 10.1089/ast.2013.1122

Parks, D.H., Imelfort, M., Skennerton, C.T., Hugenholtz, P., and Tyson, G.W. (2015). CheckM: assessing the quality of microbial genomes recovered from isolates, single cells, and metagenomes. *Genome Res* 25**,** 1043-1055. doi: 10.1101/gr.186072.114

Pérez-Rodríguez, I., Rawls, M., Coykendall, D.K., and Foustoukos, D.I. (2016). Deferrisoma palaeochoriense sp. nov., a thermophilic, iron(III)-reducing bacterium from a shallow-water hydrothermal vent in the Mediterranean Sea. *Int J Syst Evol Micr* 66**,** 830-836. doi: 10.1099/ijsem.0.000798

Pierson, B.K., and Parenteau, M.N. (2000). Phototrophs in high iron microbial mats: microstructure of mats in iron-depositing hot springs. *FEMS Microbiol Ecol* 32**,** 181-196. doi:

Pierson, B.K., Parenteau, M.N., and Griffin, B.M. (1999). Phototrophs in High-Iron-Concentration Microbial Mats: Physiological Ecology of Phototrophs in an Iron-Depositing Hot Spring. *Appl Environ Microbiol* 65**,** 5474-5483. doi:

Podosokorskaya, O.A., Kadnikov, V.V., Gavrilov, S.N., Mardanov, A.V., Merkel, A.Y., Karnachuk, O.V., Ravin, N.V., Bonch-Osmolovskaya, E.A., and Kublanov, I.V. (2013). Characterization of *Melioribacter roseus* gen. nov., sp. nov., a novel facultatively anaerobic thermophilic cellulolytic bacterium from the class *Ignavibacteria*, and a proposal of a novel bacterial phylum *Ignavibacteriae*. *Environ Microbiol* 15**,** 1759-1771. doi: 10.1111/1462-2920.12067

Roden, E.E., Mcbeth, J.M., Blothe, M., Percak-Dennett, E.M., Fleming, E.J., Holyoke, R.R., Luther, G.W., 3rd, Emerson, D., and Schieber, J. (2012). The Microbial Ferrous Wheel in a Neutral pH Groundwater Seep. *Front Microbiol* 3**,** 172. doi: 10.3389/fmicb.2012.00172

Ruff, S.W., and Farmer, J.D. (2016). Silica deposits on Mars with features resembling hot spring biosignatures at El Tatio in Chile. *Nat Commun* 7**,** 13554. doi: 10.1038/ncomms13554

Santos, T.C., Silva, M.A., Morgado, L., Dantas, J.M., and Salgueiro, C.A. (2015). Diving into the redox properties of Geobacter sulfurreducens cytochromes: a model for extracellular electron transfer. *Dalton Trans* 44**,** 9335-9344. doi: 10.1039/c5dt00556f

Schauder, R., Preuß, A., Jetten, M., and Fuchs, G. (1989). Oxidative and reductive acetyl CoA/carbon monoxide dehydrogenase pathway in *Desulfohacterium autotrophicum*. *Arch Microbiol* 151**,** 84-89. doi:

Sekiguchi, Y., Muramatsu, M., Imachi, H., Narihiro, T., Ohashi, A., Harada, H., Hanada, S., and Kamagata, Y. (2008). *Thermodesulfovibrio aggregans* sp. nov. and *Thermodesulfovibrio thiophilus* sp. nov., anaerobic, thermophilic, sulfate-reducing bacteria isolated from thermophilic methanogenic sludge, and emended description of the genus *Thermodesulfovibrio*. *Int J Syst Evol Micr* 58**,** 2541-2548. doi: 10.1099/ijs.0.2008/000893-0

Shi, L., Dong, H., Reguera, G., Beyenal, H., Lu, A., Liu, J., Yu, H.-Q., and Fredrickson, J.K. (2016). Extracellular electron transfer mechanisms between microorganisms and minerals. *Nat Rev Microbiol* 14**,** 651-662. doi: 10.1038/nrmicro.2016.93

Shi, L., Fredrickson, J.K., and Zachara, J.M. (2014). Genomic analyses of bacterial porin-cytochrome gene clusters. *Front Microbiol* 5**,** 657. doi: 10.3389/fmicb.2014.00657

Slobodkina, G.B., Reysenbach, A.L., Panteleeva, A.N., Kostrikina, N.A., Wagner, I.D., Bonch-Osmolovskaya, E.A., and Slobodkin, A.I. (2012). *Deferrisoma camini* gen. nov., sp. nov., a moderately thermophilic, dissimilatory iron(III)-reducing bacterium from a deep-sea hydrothermal vent that forms a distinct phylogenetic branch in the *Deltaproteobacteria*. *Int J Syst Evol Micr* 62**,** 2463-2468. doi: 10.1099/ijs.0.038372-0

Squyres, S.W., Arvidson, R.E., Ruff, S., Gellert, R., Morris, R.V., Ming, D.W., Crumpler, L., Farmer, J.D., Des Marais, D.J., Yen, A., Mclennan, S.M., Calvin, W., Bell, J.F., 3rd, Clark, B.C., Wang, A., Mccoy, T.J., Schmidt, M.E., and De Souza, P.A., Jr. (2008). Detection of Silica-Rich Deposits on Mars. *Science* 320**,** 1063-1067. doi:

Strauss, G., and Fuchs, G. (1993). Enzymes of a novel autotrophic CO_2 fixation pathway in the phototrophic bacterium *Chloroflexus aurantiacus*, the 3-hydroxypropionate cycle. *Eur J Biochem* 215**,** 633-643. doi:

Suzuki, D., Li, Z., Cui, X., Zhang, C., and Katayama, A. (2014). Reclassification of *Desulfobacterium anilini* as *Desulfatiglans anilini* comb. nov. within *Desulfatiglans* gen. nov., and description of a 4-chlorophenol-degrading sulfate-reducing bacterium, *Desulfatiglans parachlorophenolica* sp. nov. *Int J Syst Evol Micr* 64**,** 3081-3086. doi: 10.1099/ijs.0.064360-0

Takami, H., Noguchi, H., Takaki, Y., Uchiyama, I., Toyada, A., Nishi, S., Chee, G.-J., Arai, W., Nunoura, T., Itoh, T., Hattori, M., and Takai, K. (2012). A Deeply Branching Thermophilic Bacterium with an Ancient Acetyl-CoA Pathway Dominates a Subsurface Ecosystem. *PLoS One* 7**,** e30559. doi: 10.1371/journal.pone.0030559.t001

Tang, K.-H., Tang, Y.J., and Blankenship, R.E. (2011). Carbon metabolic pathways in phototrophic bacteria and their broader evolutionary implications. *Front Microbiol* 2**,** 165. doi: 10.3389/fmicb.2011.00165

Tank, M., Thiel, V., Ward, D.M., and Bryant, D.A. (2017). "A Panoply of Phototrophs: An Overview of the Thermophilic Chlorophototrophs of the Microbial Mats of Alkaline Siliceous Hot Springs in Yellowstone National Park, WY, USA," in *Modern Topics in the Phototrophic Prokaryotes,* ed. P.C. Hallenbeck. (Switzerland: Springer International), 87-137.

Taylor, S.R., and Mclennan, S.M. (1985). "The continental crust: its composition and evolution." (Oxford: Blackwell Scientific Publications).

Taylor, S.R., and Mclennan, S.M. (2009). "Mars: crustal composition and evolution," in *Planetary Crusts: Their Composition, Origin, and Evolution*. (Cambridge, UK: Cambridge University Press), 141-180.

Trouwborst, R.E., Johnston, A., Koch, G., Luther, G.W., and Pierson, B.K. (2007). Biogeochemistry of Fe(II) oxidation in a photosynthetic microbial mat: Implications for Precambrian Fe(II) oxidation. *Geochim Cosmochim Ac* 71**,** 4629-4643. doi: 10.1016/j.gca.2007.07.018

Van Der Meer, M.T.J., Klatt, C.G., Wood, J., Bryant, D.A., Bateson, M.M., Lammerts, L., Schouten, S., Sinninghe Damsté, J.S., Madigan, M.T., and Ward, D.M. (2010). Cultivation and genomic, nutritional, and lipid biomarker characterization of *Roseiflexus* strains closely related to predominant *in situ* populations inhabiting Yellowstone hot spring microbial mats. *J Bacteriol* 192**,** 3033-3042. doi: 10.1128/JB.01610-09

Vargas, M., Kashefi, K., Blunt-Harris, E.L., and Lovley, D.R. (1998). Microbiological evidence for Fe(III) reduction on early Earth. *Nature* 395**,** 65-67. doi:

Ward, L.M., Idei, A., Terajima, S., Kakegawa, T., Fischer, W.W., and Mcglynn, S.E. (2017). Microbial diversity and iron oxidation at Okuoku-hachikurou Onsen, a Japanese hot spring analog of Precambrian iron formations. *Geobiology* 15**,** 817-835. doi: 10.1111/gbi.12266

Weiss, J.V., Rentz, J.A., Plaia, T., Neubauer, S.C., Merrill-Floyd, M., Lilburn, T., Bradburne, C., Megonigal, J.P., and Emerson, D. (2007). Characterization of Neutrophilic Fe(II)-Oxidizing Bacteria Isolated from the Rhizosphere of Wetland Plants and Description of *Ferritrophicum radicicolagen*. nov. sp. nov., and *Sideroxydans paludicola* sp. nov. *Geomicrobiol J* 24**,** 559-570. doi: 10.1080/01490450701670152

Williams, T.J., Zhang, C.L., Scott, J.H., and Bazylinski, D.A. (2006). Evidence for Autotrophy via the Reverse Tricarboxylic Acid Cycle in the Marine Magnetotactic Coccus Strain MC-1. *Appl Environ Microbiol* 72**,** 1322-1329. doi: 10.1128/AEM.72.2.1322-1329.2006

Wu, L., Brucker, R.P., Beard, B.L., Roden, E.E., and Johnson, C.M. (2013). Iron Isotope Characteristics of Hot Springs at Chocolate Pots, Yellowstone National Park. *Astrobiology* 13**,** 1091-1101. doi: 10.1089/ast.2013.0996

Yergeau, E., Newsham, K.K., Pearce, D.A., and Kowalchuk, G.A. (2007). Patterns of bacterial diversity across a range of Antarctic terrestrial habitats. *Environ Microbiol* 9**,** 2670-2682. doi: 10.1111/j.1462-2920.2007.01379.x

Zaharia, M., Bolonsky, W.J., Curtis, K., Fox, A., Patterson, D., Shenker, S., Stoica, I., Karp, R.M., and Sittler, T. (2011). Faster and More Accurate Sequence Alignment with SNAP. *arXiv* cs.DS. doi: arXiv:1111.5572v1

Zarzycki, J., Brecht, V., Müller, M., and Fuchs, G. (2009). Identifying the missing steps of the autotrophic 3-hydroxypropionate CO_2 fixation cycle in *Chloroflexus aurantiacus*. *Proc Natl Acad Sci USA* 106**,** 21317-21322. doi: 10.1073/pnas.0908356106

Zhang, H., Sekiguchi, Y., Hanada, S., Hugenholtz, P., Kim, H., Kamagata, Y., and Nakamura, K. (2003). *Gemmatimonas aurantiaca* gen. nov., sp. nov., a gram-negative, aerobic, polyphosphate-accumulating micro-organism, the first cultured representative of the new bacterial phylum *Gemmatimonadetes* phyl. nov. *Int J Syst Evol Micr* 53**,** 1155-1163. doi: 10.1099/ijs.0.02520-0

Table 2.1. Microbial community composition of Chocolate Pots core samples.

Sample	Greengenes Taxonomic Assignment[a]	% Total[b]	Representative Species Match[d]	Accession Number	Identity (%)	Inferred Physiology	Reference	Representative MAG[e]	Similarity (%)
Combined core libraries (*n*=42)	Crenarchaeota (p)	9.0	Anaerobic methanogenic archaeon ET1-8	AJ244284.1	87	Methanogenic cellulolytic archaeon	(Chin et al., 1999)	N/A[f]	
	Chlorobi (p)	5.0	*Ignavibacterium album* strain JCM 16511	NR_074698.1	83	Facultative anaerobic heterotroph	(Iino et al., 2008;Liu et al., 2012)	39	99.3
	Chlorobi (p)	4.7	*I. album* strain JCM 16511	NR_074698.1	84	Facultative anaerobic heterotroph	(Iino et al., 2008;Liu et al., 2012)	N/A	
	Acetothermales (o)	4.7	"*Candidatus* Acetothermus autotrophicum"	AP011801.1	83	Lithoautotrophic acetogen	(Nunoura et al., 2005;Takami et al., 2012)	N/A	
	Nitrospirales (o)	3.8	Uncultured bacterium clone Fl-1F_E11	EF220517.1	92	Uncharacterized	(Yergeau et al., 2007)	N/A	
	GAL15 (p)	3.6	*Thermovenabulum ferriorganovorum* strain Z-9801	NR_042719.1	86	Fe(III) reducer	(Zavarzina et al., 2002)	N/A	
	Acidobacteria (p)	3.5	*Thermanaerovibrio* sp. R101	FN556061.1	87	Uncharacterized thermophile	R. Sayeh, J. Birrien, M. Hamdi, et al., direct submission	N/A	
	Crenarchaeota (p)	3.1	Anaerobic methanogenic archaeon ET1-8	AJ244284.1	91	Methanogenic cellulolytic archaeon	(Chin et al., 1999)	N/A	
	Anaerolineae (c)	2.5	Chloroflexi bacterium SCGC AAA240-O05	HQ675640.1	88	Uncharacterized	(Swan et al., 2011)	N/A	
	Cenarchaeaceae (f)	2.2	"*Ca*. Nitrosotenuis sp. AQ6f"	CP024808.1	97	Ammonia oxidizer	L. Sauder, P. Chain, J. Neufeld, et al., unpublished data	N/A	
	Thaumarchaeota (c)	2.1	*Nitrososphaera viennensis* strain EN76	NR_134097.1	93	Ammonia oxidizer	(Stieglmeier et al., 2014)	N/A	
	Syntrophobacteraceae (f)	2.1	*Thermodesulforhabdus* sp. nov. M40/2 CIV-3.2	AF170420.1	87	Thermophilic sulfate oxidizer	(Beeder et al., 1995;Sievert and Kuever, 2000)	N/A	
	NC10 (p)	2.1	"*Ca*. Methylomirabilis oxyfera"	FP565575.1	89	Methane oxidizer, nitrate reducer	(Ettwig et al., 2010)	N/A	
	Methylomirabiliaceae (f)	1.9	"*Ca*. M. oxyfera"	FP565575.1	93	Methane oxidizer, nitrate reducer	(Ettwig et al., 2010)	N/A	
	Chloroflexi (p)	1.7	Chloroflexi bacterium SCGC AAA240-C09	HQ675555.1	88	Uncharacterized	(Swan et al., 2011)	N/A	
	Aigarchaeota (c)	1.7	"*Ca*. Caldiarchaeum subterraneum"	AP011878.1	85	Chemolithotroph	(Nunoura et al., 2011)	N/A	
	Betaproteobacteria (c)	1.4	*Sideroxydans paludicola* strain BrT	DQ386858.1	98	Lithoautotrophic Fe(II) oxidizer	(Weiss et al., 2007)	N/A	
	SBR1093 (p)	1.4	Bacterium Kaz2	AB491166.1	90	Uncharacterized	K. Sueoka, H. Satoh, M. Onuki et al., unpublished data	N/A	
	NC10 (p)	1.3	"*Ca*. Methylomirabilis sp. RS3"	KU891932.1	88	Denitrifying methanotroph	Z. He, & B. Hu, unpublished data	N/A	
	Methanomassiliicoccaceae (f)	1.2	*Methanomassiliicoccus* sp. N89-2	LN827539.1	92	Methanogen	(Huynh et al., 2016)	1	99.3
	Acetothermaceae (f)	1.0	"*Ca*. A. autotrophicum"	AP011801.1	97	Lithoautotrophic acetogen	(Nunoura et al., 2005;Takami et al., 2012)	N/A	
	Acidobacteria (p)	1.0	Bacterium Ellin7505	HM748715.1	85	Uncharacterized	(Davis et al., 2011)	N/A	
		61.2[c]							
Core 1 surface	Crenarchaeota (p)	8.5	Anaerobic methanogenic archaeon ET1-8	AJ244284.1	87	Methanogenic cellulolytic archaeon	(Chin et al., 1999)	N/A[f]	
	Thermodesulfovibrionaceae (f)	8.1	*Thermodesulfovibrio yellowstonii* DSM 11347	CP001147.1	90	Fe(III), sulfate reduction	(Henry et al., 1994;Sekiguchi et al., 2008)	N/A	
	Anaerolineae (c)	7.3	*Dehalococcoides* sp. BHI80-15	AJ431246.1	87	Uncharacterized thermophile	M. Cambon-Bonavita, V. Riou, K. Alain, et al., unpublished data	N/A	
	Armatimonadetes (p)	6.0	*Dictyoglomus turgidum* DSM 6724	NR_043385.1	88	Uncharacterized thermophile	S. Lucas, A. Copeland, A. Lapidus, et al., unpublished data	N/A	
	Anaerolineae (c)	5.3	Chloroflexi bacterium SCGC AAA240-O05	HQ675640.1	88	Uncharacterized	(Swan et al., 2011)	N/A	
	Crenarchaeota (p)	3.6	Anaerobic methanogenic archaeon ET1-8	AJ244284.1	87	Methanogenic cellulose degrader	(Chin et al., 1999)	N/A	
	Chlorobi (p)	3.0	*I. album* strain JCM 16511	NR_074698.1	83	Facultative anaerobic heterotroph	(Iino et al., 2008;Liu et al., 2012)	39	99.3
	Chthonomonadetes (c)	2.8	Armatimonadetes bacterium JGI 0000077-K19	KJ535399.1	97	Uncharacterized	(Nobu et al., 2015)	N/A	
	Acetothermaceae (f)	2.4	"Ca. A. autotrophicum"	AP011801.1	97	Lithoautotrophic acetogen	(Nunoura et al., 2005;Takami et al., 2012)	N/A	
	Chlorobi (p)	2.4	*Rhodothermus profundi* strain PRI 2902	NR_116762.1	87	Thermophilic aerobic heterotroph	(Marteinsson et al., 2010)	N/A	
	Deltaproteobacteria (c)	2.4	*Desulfomonile limimaris* DCB-M	NR_025079.1	92	Reductive dechlorinating bacterium	(Sun et al., 2001)	146	99.3
	Anaerolineae (c)	2.4	"*Ca*. Roseilinea gracile" clone JGI24185J35167_1001(	KY937207.1	89	Thermophilic phototroph	(Tank et al., 2017)	N/A	
	Anaerolineae (c)	2.1	*Litorilinea aerophila* strain PRI-4131	NR_132330.1	88	Thermophilic heterotroph	(Kale et al., 2013)	N/A	
	Chlorobi (p)	1.9	Unidentified bacterium clone K2-30-37	AY344403.2	89	Uncharacterized	S. Donachie, S. Hou, K. Lee, et al., unpublished data	N/A	
	Syntrophobacteraceae (f)	1.7	*Thermodesulforhabdus* sp. nov. M40/2 CIV-3.2	AF170420.1	87	Thermophilic sulfate oxidizer	(Beeder et al., 1995;Sievert and Kuever, 2000)	N/A	
	AC1 (p)	1.3	Unidentified eubacterium from the Amazon	U68651.1	86	Uncharacterized soil bacterium	(Borneman and Triplett, 1997)	N/A	
		61.1[c]							

Core 2 surface	*Betaproteobacteria* (c)	11.1	*S. paludicola* strain BrT	DQ386858.1	98	Lithoautotrophic Fe(II) oxidizer	(Weiss et al., 2007)	N/A[f]	
	Chlorobi (p)	9.6	*I. album* strain JCM 16511	NR_074698.1	84	Facultative anaerobic heterotroph	(Iino et al., 2008;Liu et al., 2012)	N/A	
	Thaumarchaeota (c)	6.8	"*Ca.* Nitrosocosmicus sp. Kfb"	KX863712.1	88	Ammonia oxidizer	R. Alves, S. Abby, A. Zappe, et al., unpublished data	194	99.6
	Acetothermales (o)	5.1	"*Ca.* A. autotrophicum"	AP011801.1	83	Lithoautotrophic acetogen	(Nunoura et al., 2005;Takami et al., 2012)	N/A	
	Anaerolineae (c)	3.4	Chloroflexi bacterium SCGC AAA240-O05	HQ675640.1	88	Uncharacterized	(Swan et al., 2011)	N/A	
	GAL15 (p)	3.2	*T. ferriorganovorum* strain Z-9801	NR_042719.1	86	Fe(III) reducer	(Zavarzina et al., 2002)	N/A	
	Nitrospirales (o)	3.2	sulfate-reducing bacterium R-PropA1	AJ012591.1	88	Sulfate reducer	T. Wind, S. Stubner & R. Conrad, unpublished data	N/A	
	Chlorobi (p)	2.1	*I. album* strain JCM 16511	NR_074698.1	83	Facultative anaerobic heterotroph	(Iino et al., 2008;Liu et al., 2012)	39	99.3
	Acetothermaceae (f)	2.1	"*Ca.* A. autotrophicum"	AP011801.1	97	Lithoautotrophic acetogen	(Nunoura et al., 2005;Takami et al., 2012)	N/A	
	Acidobacteria (p)	2.1	*Thermanaerovibrio* sp. R101	FN556061.1	87	Uncharacterized thermophile	R. Sayeh, J. Birrien, M. Hamdi, et al., direct submission	N/A	
	Methanomassiliicoccaceae (f)	2.1	*Methanomassiliicoccus* sp. N89-2	LN827539.1	92	Methanogen	(Huynh et al., 2016)	1	99.3
	Chloroflexi (p)	1.9	Chloroflexi bacterium SCGC AAA240-C09	HQ675555.1	88	Uncharacterized	(Swan et al., 2011)	N/A	
	NC10 (p)	1.7	"*Ca.* Methylomirabilis sp. RS3"	KU891932.1	88	Denitrifying methanotroph	Z. He & B. Hu, unpublished data	N/A	
	Anaerolineae (c)	1.7	*Thermanaerothrix daxensis* strain GNS-1	NR_117865.1	89	Thermophilic anaerobic fermenter	(Grégoire et al., 2011)	N/A	
	Chthonomonadetes (c)	1.5	Armatimonadetes bacterium JGI 0000077-K19	KJ535399.1	97	Uncharacterized	(Nobu et al., 2015)	N/A	
	Anaerolineae (c)	1.5	*Thermomarinilinea lacunifontana* strain SW7	NR_132293.1	91	Thermophilic anaerobic fermenter	(Nunoura et al., 2013)	N/A	
	Rhodocyclaceae (f)	1.3	*Thauera* sp. strain DK5	MF155554.1	95	Denitrifying bacterium	Q. Wang, unpublished data	N/A	
	Methylomirabiliaceae (f)	1.3	"*Ca.* M. oxyfera"	FP565575.1	93	Methane oxidizer, nitrate reducer	(Ettwig et al., 2010)	N/A	
	Acidobacteria (p)	1.3	*Holophaga* sp. WY42	KC921174.1	89	Uncharacterized	T. Chen, direct submission	N/A	
	Thermodesulfovibrionaceae (f)	1.1	*T. yellowstonii* DSM 11347	CP001147.1	90	Fe(III), sulfate reduction	(Henry et al., 1994;Sekiguchi et al., 2008)	N/A	
		64.3[c]							
Core 3 surface	*Cenarchaeaceae* (f)	16.5	*"Ca.* Nitrosotenuis sp. AQ6f"	CP024808.1	97	Ammonia oxidizer	L. Sauder, P. Chain, J. Neufeld, et al., unpublished data	N/A[f]	
	Syntrophobacteraceae (f)	10.7	*Thermodesulforhabdus* sp. nov. M40/2 CIV-3.2	AF170420.1	87	Thermophilic sulfate oxidizer	(Beeder et al., 1995;Sievert and Kuever, 2000)	N/A	
	Chlorobi (p)	9.2	*I. album* strain JCM 16511	NR_074698.1	83	Facultative anaerobic heterotroph	(Iino et al., 2008;Liu et al., 2012)	39	99.3
	Chlorobi (p)	5.6	*I. album* strain JCM 16511	NR_074698.1	84	Facultative anaerobic heterotroph	(Iino et al., 2008;Liu et al., 2012)	N/A	
	Calditrichaceae (f)	4.1	*Caldithrix abyssi* DSM 13497	CP018099.1	87	Thermophilic anaerobic mixotroph	(Miroshnichenko et al., 2003); I. Kublanov, O. Sigalova, S. Gavrilov, et al., direct submission	197.1	99.6
	Betaproteobacteria (c)	3.8	*S. paludicola* strain BrT	DQ386858.1	98	Lithoautotrophic Fe(II) oxidizer	(Weiss et al., 2007)	N/A	
	Nitrospirales (o)	3.0	Bacterium strain CS35	MG271829.1	87	Uncharacterized	K. Das & S. Kerkar, direct submission	N/A	
	Pirellulaceae (f)	2.4	*Thermogutta terrifontis* strain R1	CP018477.1	91	Thermophilic polysaccharolytic bacterium	(Elcheninov et al., 2017)	35.2	99.6
	Acidobacteria (p)	2.1	*Stenotrophobacter terrae* strain Ac_28_D10	NR_146023.1	96	Aerobic heterotroph	(Pascual et al., 2015)	N/A	
	Chitinophagaceae (f)	1.9	*Cnuella* sp. strain N24	MF797952.1	90	Aerobic heterotroph	(Zhao et al., 2014); C. Wang & Z.-J. Du, direct submission	N/A	
	Chlorobi (p)	1.7	Unidentified bacterium clone TK-NH7	DQ463733.2	88	Uncharacterized	A. De Wever, K. Van der Gucht, K. Muylaert, et al., unpublished data	N/A	
	Chthonomonadetes (c)	1.5	Armatimonadetes bacterium JGI 0000077-K19	KJ535399.1	97	Uncharacterized	(Nobu et al., 2015)	N/A	
	Anaerolineae (c)	1.5	*T. daxensis* strain GNS-1	NR_117865.1	86	Thermophilic anaerobic fermenter	(Grégoire et al., 2011)	N/A	
	Chloroflexi (p)	1.3	Chloroflexi bacterium SCGC AAA240-C09	HQ675555.1	88	Uncharacterized	(Swan et al., 2011)	N/A	
	Pseudanabaenaceae (f)	1.3	*Pseudanabaena limnetica* PUPCCC 106.2	KM376980.1	95	Thermophilic cyanobacterium	Y. Singh, A. Gulati, J. Khattar, et al., unpublished data	N/A	
	Nitrospiraceae (f)	1.3	*Nitrospira* cf. *moscoviensis* SBR2046	AF155155.1	99	Thermophilic nitrite oxidizer	(Ehrich et al., 1995); P. Burrell, J. Keller & L. Blackall, unpublished data	128.2	98.9
	Rhabdochlamydiaceae (f)	1.3	*Rhabdochlamydia crassificans* strain CRIB01	AY928092.1	93	Intracellular pathogen	(Corsaro et al., 2007)	N/A	
	Hyphomicrobiaceae (f)	1.1	*Rhodoplanes* sp. Z2-YC6860	CP007440.1	96	Anoxygenic phototroph	J. Lee, E. Chung, J. Lim, et al., direct submission	N/A	
	Phycisphaerae (c)	1.1	Phycisphaerae bacterium ST-NAGAB-D1	CP019791.1	84	Uncharacterized anaerobe	S. Spring, B. Bunk & C. Sproer, unpublished data	N/A	
		71.2[c]							

[a] Letters in parentheses indicate taxonomic level: k, kingdom; p, phylum; c, class; o, order; f, family; g, genus.
[b] Average percent read abundance across all CP core libraries (*n*=42)
[c] Total percent of reads comprising OTUs with >1% average read abundance
[d] As determined by NCBI BLASTn
[e] 16S rRNA gene sequences recovered from MAGs using CheckM, and aligned to amplicon sequences using BLASTn
[f] Not applicable; no 16S rRNA gene sequences from MAGs aligned to this OTU

Table 2.2. Microbial community composition of Chocolate Pots vent pool water column.

SILVA Taxonomic Assignment[a]	% Total	Representative Species Match[c]	Accession Number	Similarity (%)	Inferred Physiology	Reference	Representative MAG[d]	Similarity (%)
Pseudanabaenaceae (f)	20.1	*Pseudanabaena* sp. 1a-03	FR798944.1	89	Oxygenic photoautotroph	(Cuzman et al., 2010)	64	100
Thermodesulfovibrionaceae (f)	10.3	*Thermodesulfovibrio yellowstonii* DSM 11347	CP001147.1	90	Fe(III), sulfate reduction	(Henry et al., 1994;Sekiguchi et al., 2008)	74	98.8
Roseiflexaceae (f)	2.6	*Roseiflexus* sp. RS-1	CP000686.1	99	Anoxygenic photo(auto)troph	(Klatt et al., 2007;van der Meer et al., 2010)	N/A[e]	
Betaproteobacteria (c)	2.6	*Sideroxydans paludicola* strain BrT	DQ386858.1	99	Lithoautotrophic Fe(II) oxidizer	(Weiss et al., 2007)	17	100
Chlorobi (p)	2.2	*Rhodothermus profundi* strain PRI 2902	NR_116762.1	87	Thermophilic aerobic heterotroph	(Marteinsson et al., 2010)	16	100
Rhodocyclaceae (f)	2.2	*Thauera* sp. strain DK5	MF155554.1	96	Denitrifying bacterium	Q. Wang, direct submission	79	100
Chloroherpetales (o)	2.1	*Chloroherpeton thalassium* ATCC 35110	NR_074270.1	89	Anoxygenic photoautotroph	(Gibson et al., 1984)	54	100
Anaerolineae (c)	1.3	*Dehalococcoides* sp. BHI80-15	AJ431246.1	88	Hydrogen oxidizer	(Vander Roost et al., 2017)	59	100
	43.4[b]							

[a] Letters in parentheses indicate taxonomic level: k, kingdom; p, phylum; c, class; o, order; f, family; g, genus.

[b] Total percent of reads comprising OTUs with >1% average read abundance

[c] As determined by NCBI BLASTn

[d] 16S rRNA gene sequences recovered from MAGs using CheckM, and aligned to amplicon sequences using BLASTn

[e] Not applicable; no 16S rRNA gene sequences from MAGs aligned to this OTU

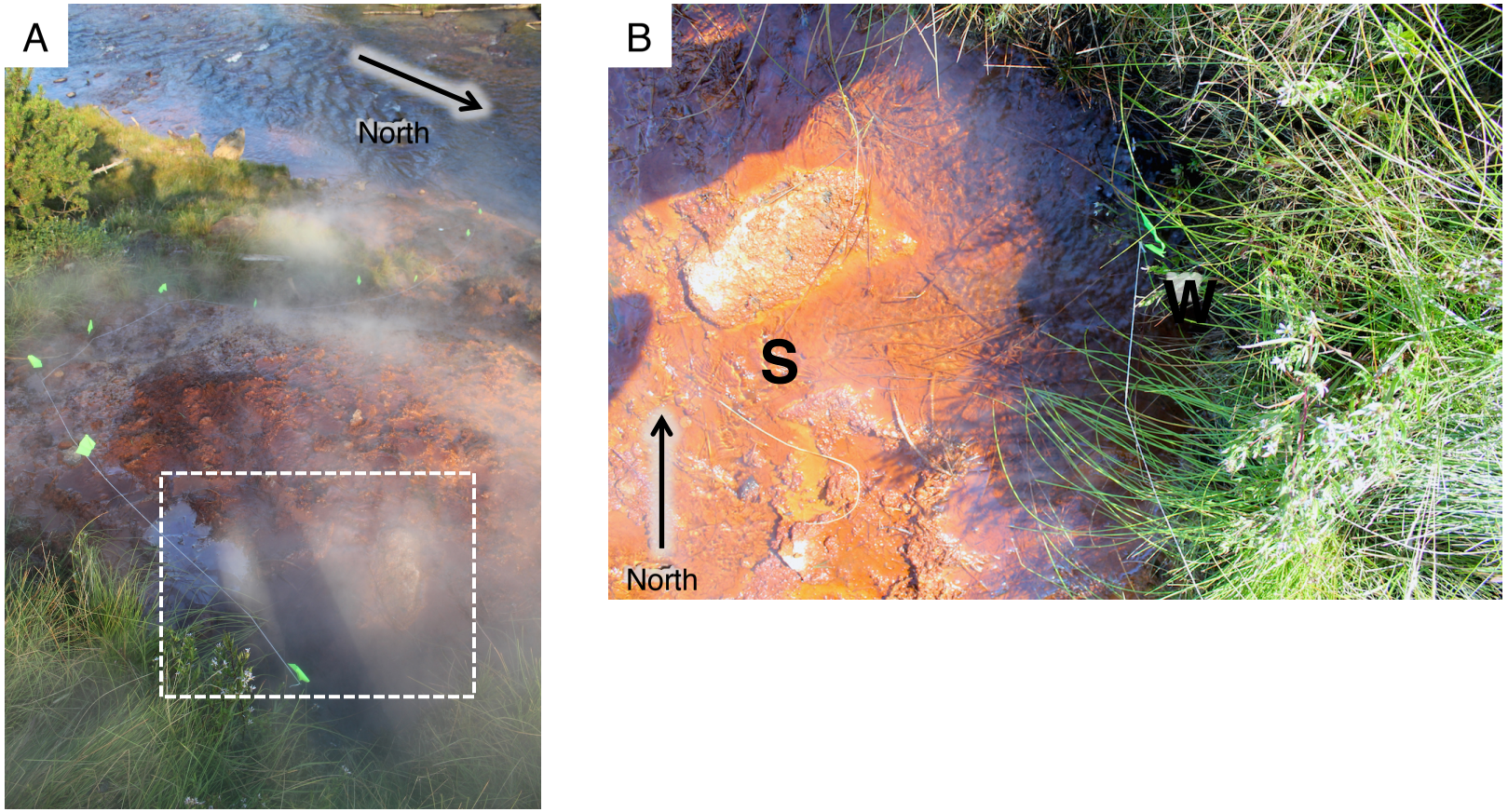

Figure 2.1. (A) View from the top of the main hot spring mound looking toward the Gibbon River. The flow path is marked with neon-green flags. The approximate area of the vent pool is marked with a white dotted line. (B) Top-down view of the pool at the main hot spring vent pool at Chocolate Pots. The site for the sediment core collection in 2013 is indicated with an S. The vent source (partially obscured by grasses) where spring water was collected in 2015 is indicated with a W.

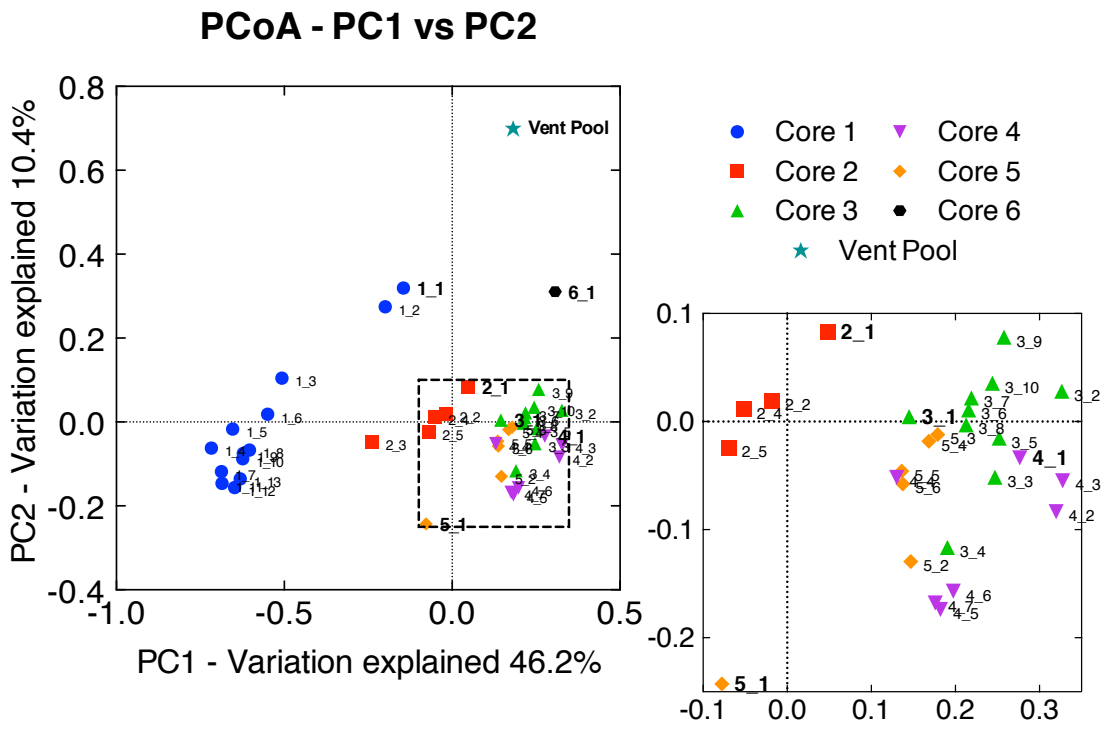

Figure 2.2. Principal coordinate analysis (PCoA) ordination of pair-wise sample dissimilarity using weighted UniFrac metrics comparing samples from the 16S rRNA gene amplicon library of all CP cores and depth intervals. Zoomed-in panel highlights the less pronounced distribution of samples from cores 3, 4, and 5. Surface sample from each core is labeled in bold, and subsections are labeled with increasing depth. The 16S rRNA gene amplicon library from the CP vent pool water column sample was aligned and normalized to the CP core libraries in order to plot along with the core samples.

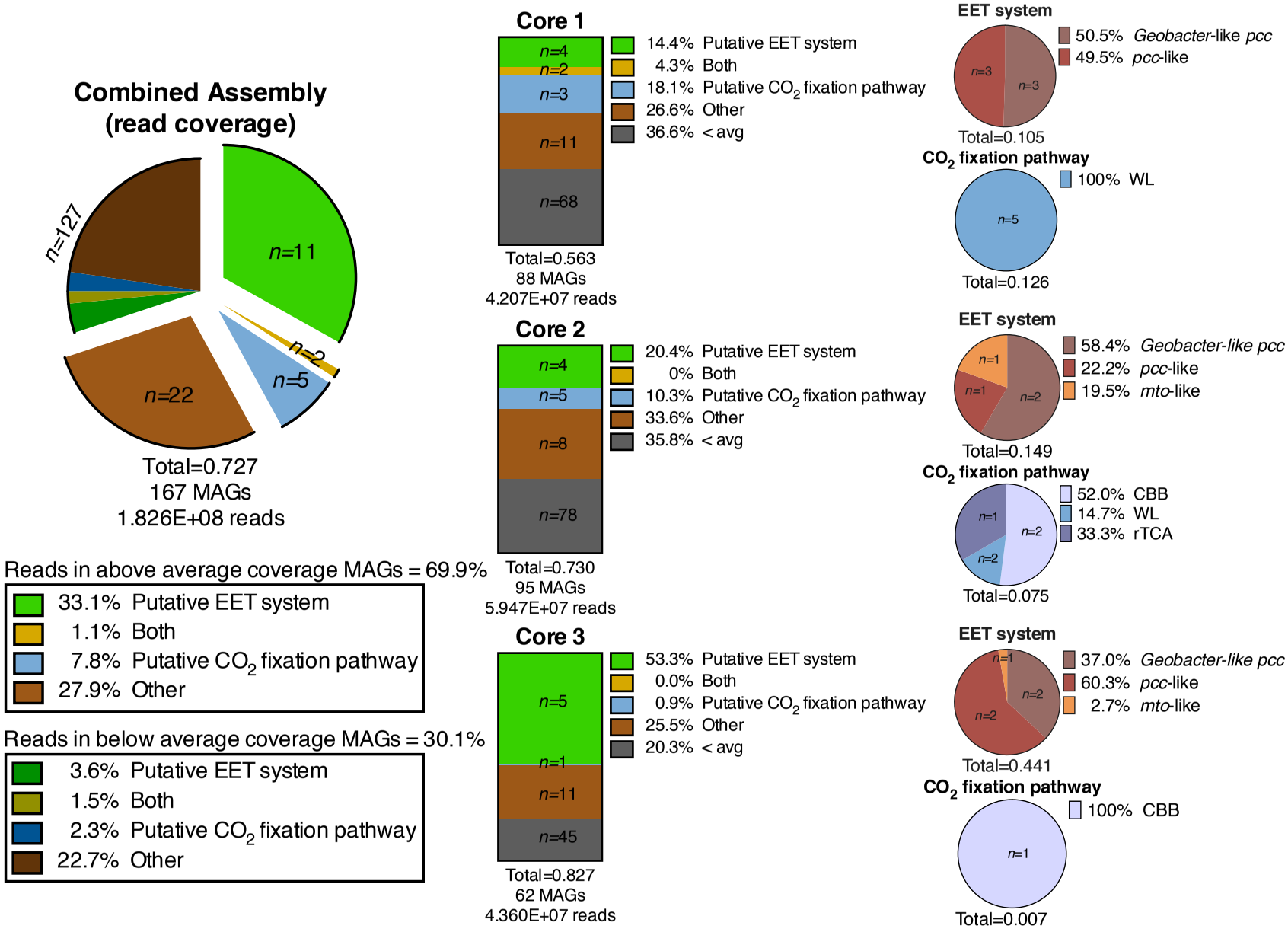
Combined Assembly
(read coverage)
n=11
n=2
n=5
n=22
n=127
Total=0.727
167 MAGs
1.826E+08 reads
Reads in above average coverage MAGs = 69.9%
33.1% Putative EET system
1.1% Both
7.8% Putative CO2 fixation pathway
27.9% Other
Reads in below average coverage MAGs = 30.1%
3.6% Putative EET system
1.5% Both
2.3% Putative CO2 fixation pathway
22.7% Other
Core 1
n=4
n=2
n=3
n=11
n=68
14.4% Putative EET system
4.3% Both
18.1% Putative CO2 fixation pathway
26.6% Other
36.6% < avg
Total=0.563
88 MAGs
4.207E+07 reads
EET system
n=3
n=3
50.5% Geobacter-like pcc
49.5% pcc-like
Total=0.105
CO2 fixation pathway
n=5
100% WL
Total=0.126
Core 2
n=4
n=5
n=8
n=78
20.4% Putative EET system
0% Both
10.3% Putative CO2 fixation pathway
33.6% Other
35.8% < avg
Total=0.730
95 MAGs
5.947E+07 reads
EET system
n=1
n=1
n=2
58.4% Geobacter-like pcc
22.2% pcc-like
19.5% mto-like
Total=0.149
CO2 fixation pathway
n=1
n=2
n=2
52.0% CBB
14.7% WL
33.3% rTCA
Total=0.075
Core 3
n=5
n=1
n=11
n=45
53.3% Putative EET system
0.0% Both
0.9% Putative CO2 fixation pathway
25.5% Other
20.3% < avg
Total=0.827
62 MAGs
4.360E+07 reads
EET system
n=1
n=2
n=2
37.0% Geobacter-like pcc
60.3% pcc-like
2.7% mto-like
Total=0.441
CO2 fixation pathway
n=1
100% CBB
Total=0.007

Figure 2.3. Distribution of MAGs from the metagenomic co-assembly of the CP cores containing putative metabolic pathways of interest, and percentage of metagenomic reads mapped to those MAGs. Exploded pie chard on the left shows a distribution of MAGs and percentage of metagenomic sequence reads mapped to MAGs containing metabolic pathways of interest. Middle bars represent the MAGs identified in the three individual core metagenomes and the numbers of MAGs containing pathways of interest and percentage of reads mapped to those MAGs. Pie charts on the right show break down of specific EET systems or CO_2 fixation pathways present in each core sample. Total listed below each pie and bar chart represents the ratio of mapped reads in a given metagenomic assembly or pathway to the total number of mapped reads for that assembly. Abbreviation: EET, extracellular electron transfer; CBB, Calvin-Benson-Bassham cycle; WL, Wood-Ljungdahl pathway; rTCA, reductive tricarboxylic acid cycle; 3HP, 3-hydroxypropionate bicycle.

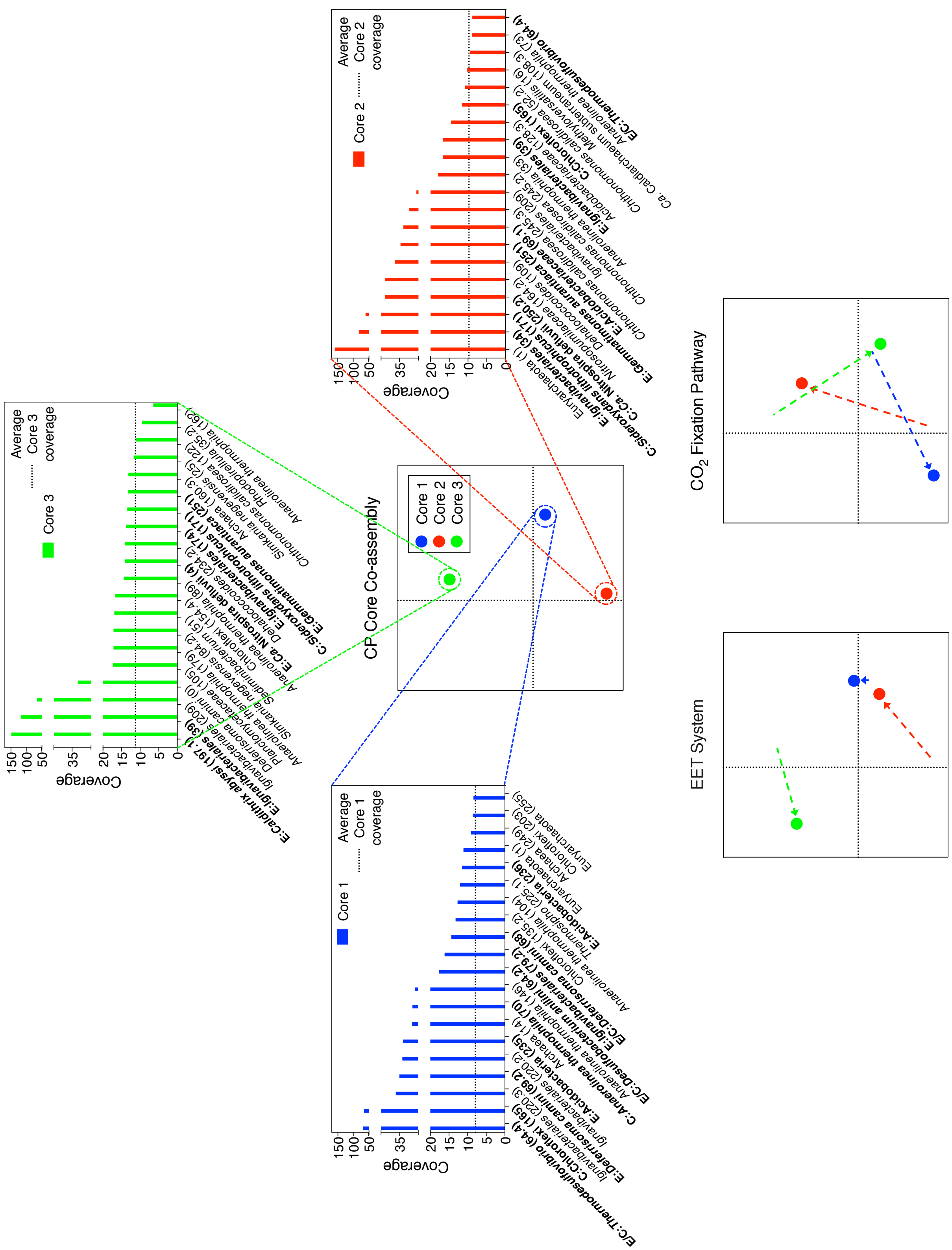
CP Core Co-assembly
Core 1
Core 2
Core 3
EET System
CO_2 Fixation Pathway
Coverage
Average Core 1 coverage
Average Core 2 coverage
Average Core 3 coverage

Figure 2.4. Nonmetric multidimensional scaling (NMDS) plots using Euclidean distance metrics comparing the microbial community between CP cores 1, 2, and 3 using shotgun metagenomic sequencing data, based on the abundance of MAGs within the cores. Proximity of two points is related to the similarity of the microbial community between those two samples based on normalized read coverage. Top NMDS plot is a comparison of the community as a whole. Bottom left NMDS plot shows a comparison of only the community containing putative EET systems. Bottom right NMDS plot shows a comparison of only the community containing putative CO_2 fixation pathways. Dotted lines represent how the EET-containing or CO_2 fixing communities differ from the microbial community of the respective core sample as a whole community. Rank-abundance plots of cores 1, 2, and 3 highlight the 20 most abundant taxa within each core sample, the presence or absence of which is controlling the differences and similarities represented in the NMDS plots. An average normalized read coverage of 7.94, 9.75, and 11.27 for MAGs in cores 1, 2, and 3, respectively, is marked with a horizontal dotted line. MAGs containing putative EET systems or CO_2 fixation pathways are bolded and labeled with “E” or “C”, respectively, or “E/C” for MAGs containing both putative metabolisms. MAG IDs are listed in parentheses.

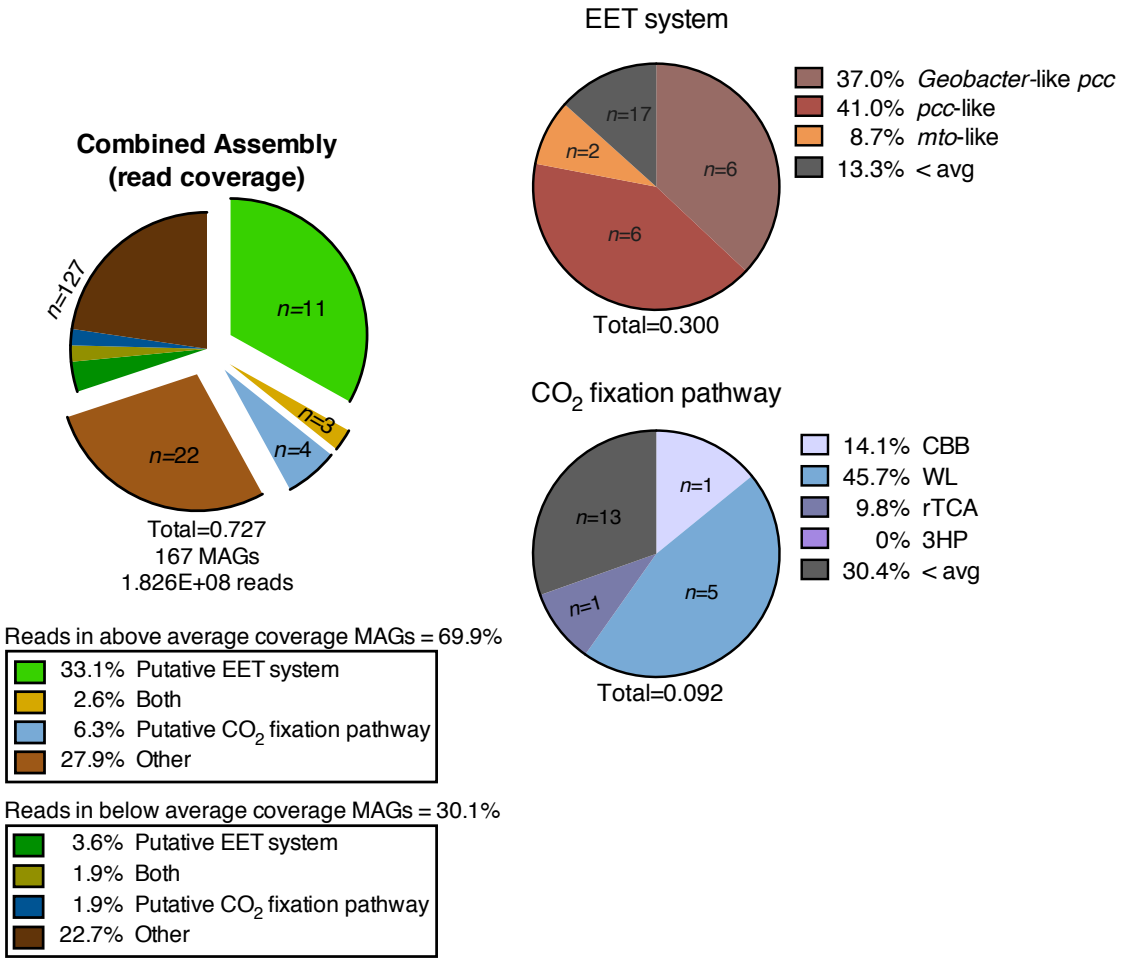

Figure 2.5. Distribution of MAGs from the metagenomic co-assembly of the CP cores containing putative metabolic pathways of interest, and percentage of metagenomic reads mapped to those MAGs. Abbreviations: EET, extracellular electron transfer; CBB, Calvin-Benson-Bassham cycle; WL, Wood-Ljungdahl pathway; rTCA, reductive tricarboxylic acid cycle; 3HP, 3-hydroxypropionate bicycle.

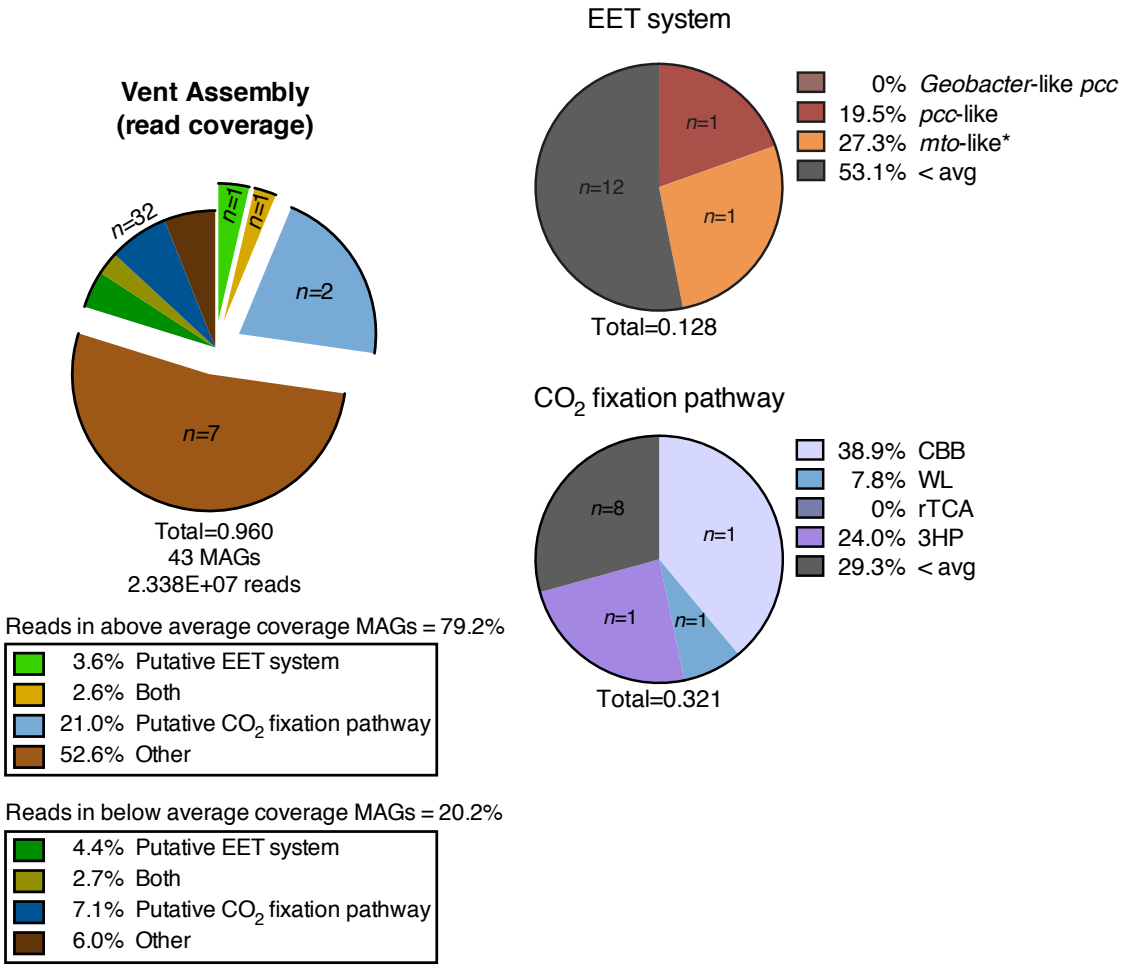

Figure 2.6. Distribution of MAGs from the metagenomic assembly of the CP vent pool water column containing putative metabolic pathways of interest, and percentage of metagenomic reads mapped to those MAGs. Abbreviation: EET, extracellular electron transfer; CBB, Calvin-Benson-Bassham cycle; WL, Wood-Ljungdahl pathway; rTCA, reductive tricarboxylic acid cycle; 3HP, 3-hydroxypropionate bicycle.

A.2.1. SUPPLEMENTARY TEXT

A.2.1.1 SUPPLEMENTARY MATERIALS AND METHODS

The four CO_2 fixation pathways searched for within the metagenomic assemblies were positively identified within a metagenome-assembled genome (MAG) if it encoded all genes predicted to be involved in the pathway. The four CO_2 fixation pathways investigated were: the reductive pentose phosphate cycle [Calvin-Benson-Bassham (CBB)], reductive tricarboxylic acid cycle (rTCA), reductive acetyl-CoA pathway [Wood-Ljungdahl (WL)], and 3-hydroxypropionate (3HP) bicycle.

Calvin-Benson-Bassham cycle. CBB genes in either metagenomic assembly were identified using the Function Search option in IMG/M ER using Enzyme Commission (EC, http://enzyme.expasy.org/) numbers for each enzyme involved in the pathway. The enzyme ribulose bisphosphate carboxylase/oxidase (RuBisCO) is involved in the first step of the CBB cycle and was the basis for determining whether or not a member of the microbial community, represented by a metagenomic MAG, was putatively capable of carbon fixation via the CBB pathway. Putative RuBisCO-encoding archaeal MAGs were investigated for an alternative enzyme for regenerating ribulose 1,5-bisphosphate (RuBP): thiazole-adenylate synthase (TAS) (Finn and Tabita, 2004;Tabita et al., 2008). Additionally, some Archaea can use RuBisCO as part of the ribulose monophosphate (RuMP) pathway (Kono et al., 2017). Key enzymes in this pathway, D-arabino-3-hexulose-6-phosphate synthase and phospho-3-hexuloisomerase, were searched for in RuBisCO-containing archaeal MAGs also. MAGs which did not encode proteins identified as sedoheptulose-1,7-bisphosphatase (SBPase, EC:3.1.3.37) were investigated for the presence of genes encoding potential bifunctional fructose-1,6-bisphosphatase (FBPase, EC:3.1.3.11) (Jiang et al., 2012), or fructose-1,6-bisphosphate aldolase (FBP aldolase,

EC:4.1.2.13) (Say and Fuchs, 2010;Du et al., 2011). MAGs were only considered to encode a full CBB pathway if genes encoding all enzymes (or bifunctional variants) were identified. If all key enzymes (e.g. RuBisCO) were coded for in a MAG, and no more than one gene predicted in the pathway was undetected, these were considered partially complete. Despite coding for essential proteins (i.e. RuBisCO) MAGs that did not encode two or more proteins in the CBB pathway were considered too incomplete for further study.

Wood-Ljungdahl pathway. Genes involved in the WL pathway were identified in the metagenomic assemblies using the EC numbers for each enzyme involved in the pathway. There are two key enzymes in the pathway, carbon monoxide dehydrogenase (EC:1.2.7.4, and EC:1.2.99.2) and CO-methylating acetyl-CoA synthase (EC:2.3.1.169). MAGs that did not encode either of these key enzymes were considered too incomplete to investigate further. Despite prior identification of organisms capable of utilizing the WL pathway for CO_2 fixation that do not encode a complete set of proteins, as identified by KEGG (Matschiavelli et al., 2012), in this study MAGs were only considered to encode a complete WL pathway if all of the predicted protein coding genes were present.

Reductive tricarboxylic acid cycle. Genes coding for enzymes involved in the rTCA pathway were identified in the metagenomic assemblies using the EC numbers for each enzyme involved in the pathway. There are three enzymes unique to this pathway that differentiate it from the TCA cycle: fumarate reductase (EC:1.3.5.4), 2-oxoglutarate synthase (EC:1.2.7.3), and the citrate-cleaving reaction which can occur as a one- or two-step reaction (Hügler and Sievert, 2011). Citrate can be cleaved into oxaloacetate and acetyl-CoA by ATP citrate lyase (EC:2.3.3.8), or citryl-CoA synthetase (CCS, EC:6.2.1.18) and citryl-CoA lyase (CCL, EC:4.1.3.34) with citryl-CoA as an intermediate (Aoshima et al., 2004;Aoshima, 2007). MAGs

were only considered to contain a complete rTCA cycle if genes encoding the aforementioned unidirectional enzymes were detected, as well as the genes encoding enzymes that catalyze the reversible reactions in the pathway.

3-hydroxypropionate bicycle. Genes encoding proteins involved in the 3HP pathway were identified in the metagenomic assemblies using EC numbers for each enzyme involved in the pathway. The three key marker proteins from the 3HP pathway, first identified in *Chloroflexus aurantiacus*, are propionyl-CoA/3-hydroxypropionyl-CoA synthetase (EC:6.2.1.17/EC:6.2.1.36), malyl-CoA/mesaconyl-C1-CoA/citramalyl-CoA (MMC) lyase (EC:4.2.3.25/EC:4.2.3.24/EC:4.2.1.148), and malonyl-CoA reductase (EC:1.2.1.75) (Strauss and Fuchs, 1993;Alber and Fuchs, 2002;Hügler et al., 2002;Zarzycki et al., 2008). MAGs were considered to contain a full 3HP pathway if all marker genes were identified. MAGs that did not encode any of the key marker genes were considered too incomplete for further study.

A.2.1.2 SUPPLEMENTARY RESULTS AND DISCUSSION

Statistics of CP sediment core metagenomes and MAGs. Paired-end 2x100 bp Illumina HiSeq 2000 shotgun metagenomic sequencing produced a total of 103840982, 110482524, and 116861176 reads for cores 1, 2, and 3, respectively. The combined metagenomic assembly (co-assembly) of the cores contained 331184682 reads assembled into 1712324 contigs with an N50 of 3198 bp, and an average length of 938 bp. The CONCOCT binning algorithm identified 256 MAGs; 37 of these were composite MAGs which were manually split based on %GC and coverage into 82 MAGs (Figure A.2.1). MAGs that were only partially complete (<50% completeness) or very highly contaminated (>15% contamination) were removed before further analysis (n=134). The remaining 167 high-quality MAGs contained 72.7% of all reads mapped

to the metagenomic co-assembly. MAGs had an average completeness of 86.2% ± 12.5%, and an average contamination of 2.4% ± 2.8% (Table A.2.2).

Statistics of CP vent pool water column metagenome and MAGs. Paired-end 2x250 Illumina HiSeq 2500 Rapid shotgun metagenomic sequencing produced a total of 48106126 reads assembled into 281407 contigs with an N50 of 1361 bp, and an average length of 1107 bp. The CONCOCT binning algorithm identified 82 MAGs (Figure A.2.2); one composite MAG was split in two. MAGs that were only partially complete (<50% completeness) or very highly contaminated (>15% contamination) were removed before further analysis (n=40). The remaining 43 high-quality MAGs contained 96.0% of all reads mapped to the metagenomic assembly. MAGs had an average completeness of 84.8% ± 14.4%, and an average contamination of 2.7% ± 4.1% (Table A.2.3). The coverage of the two extremely high-coverage MAGs (ca. 1093x and 493x coverage for *Thermococcaceae* and Archaea, respectively) was not included in the calculation of average coverage for the metagenomic assembly, due to their extremely high coverage.

A.2.1.3 SUPPLEMENTARY REFERENCES

Alber, B.E., and Fuchs, G. (2002). Propionyl-Coenzyme A Synthase from *Chloroflexus aurantiacus*, a Key Enzyme of the 3-Hydroxypropionate Cycle for Autotrophic CO_2 Fixation. *J Biol Chem* 277**,** 12137-12143. doi: 10.1074/jbc.M110802200

Albertsen, M., Hugenholtz, P., Skarshewski, A., Nielsen, K.R.L., Tyson, G.W., and Nielsen, P.H. (2013). Genome sequences of rare, uncultured bacteria obtained by differential coverage binning of multiple metagenomes. *Nat Biotechnol* 31**,** 533-538. doi: 10.1038/nbt.2579

Allen, E.T., and Day, A.L. (1935). *Hot Springs of the Yellowstone National Park.* Carnegie Institution of Washington.

Alneberg, J., Bjarnason, B.S.R., De Bruijn, I., Schirmer, M., Quick, J., Ijaz, U.Z., Lahti, L., Loman, N.J., Andersson, A.F., and Quince, C. (2014). Binning metagenomic contigs by coverage and composition. *Nat Methods* 11**,** 1144-1146. doi: 10.1038/nmeth.3103

Aoshima, M. (2007). Novel enzyme reactions related to the tricarboxylic acid cycle: phylogenetic/functional implications and biotechnological applications. *Appl Microbiol Biotechnol* 75**,** 249-255. doi: 10.1007/s00253-007-0893-0

Aoshima, M., Ishii, M., and Igarashi, Y. (2004). A novel enzyme, citryl-CoA lyase, catalysing the second step of the citrate cleavage reaction in *Hydrogenobacter thermophilus* TK-6. *Mol Microbiol* 52**,** 763-770. doi: 10.1111/j.1365-2958.2004.04010.x

Arvidson, R.E., Squyres, S.W., Bell, J.F., 3rd, Catalano, J.G., Clark, B.C., Crumpler, L.S., De Souza, P.A., Jr., Fairen, A.G., Farrand, W.H., Fox, V.K., Gellert, R., Ghosh, A., Golombek, M.P., Grotzinger, J.P., Guinness, E.A., Herkenhoff, K.E., Jolliff, B.L., Knoll, A.H., Li, R., Mclennan, S.M., Ming, D.W., Mittlefehldt, D.W., Moore, J.M., Morris, R.V., Murchie, S.L., Parker, T.J., Paulsen, G., Rice, J.W., Ruff, S.W., Smith, M.D., and Wolff, M.J. (2014). Ancient aqueous environments at Endeavour Crater, Mars. *Science* 343**,** 8. doi: 10.1126/science.1248097

Bankevich, A., Nurk, S., Antipov, D., Gurevich, A.A., Dvorkin, M., Kulikov, A.S., Lesin, V.M., Nikolenko, S.I., Pham, S., Prjibelski, A.D., Pyshkin, A.V., Sirotkin, A.V., Vyahhi, N., Tesler, G., Alekseyev, M.A., and Pevzner, P.A. (2012). SPAdes: a new genome assembly algorithm and its applications to single-cell sequencing. *J Comput Biol* 19**,** 455-477. doi: 10.1089/cmb.2012.0021

Blöthe, M., and Roden, E.E. (2009). Microbial iron redox cycling in a circumneutral-pH groundwater seep. *Appl Environ Microbiol* 75**,** 468-473. doi: 10.1128/AEM.01817-08

Brysch, K., Schneider, C., Fuchs, G., and Widdel, F. (1987). Lithoautotrophic growth of sulfate-reducing bacteria, and description of *Desulfobacterium autotrophicum* gen. nov., sp. nov. *Arch Microbiol* 148**,** 264-274. doi:

Camacho, A., Walter, X.A., Picazo, A., and Zopfi, J. (2017). Photoferrotrophy: Remains of an Ancient Photosynthesis in Modern Environments. *Front Microbiol* 8**,** 323. doi: 10.3389/fmicb.2017.00323

Can, M., Armstrong, F.A., and Ragsdale, S.W. (2014). Structure, function, and mechanism of the nickel metalloenzymes, CO dehydrogenase, and acetyl-CoA synthase. *Chem Rev* 114**,** 4149-4174. doi: 10.1021/cr400461p

Canfield, D.E. (2005). The early history of atmospheric oxygen: Homage to Robert M. Garrels. *Ann Rev Earth Planet Sci* 33**,** 1-36. doi: 10.1146/annurev.earth.33.092203.122711

Caporaso, J.G., Lauber, C.L., Walters, W.A., Berg-Lyons, D., Lozupone, C.A., Turnbaugh, P.J., Fierer, N., and Knight, R. (2011). Global patterns of 16S rRNA diversity at a depth of

millions of sequences per sample. *Proc Natl Acad Sci U S A* 108 Suppl 1**,** 4516-4522. doi: 10.1073/pnas.1000080107

Chin, K.-J., Lukow, T., Stubner, S., and Conrad, R. (1999). Structure and function of the methanogenic archaeal community in stable cellulose-degrading enrichment cultures at two different temperatures (15 and 30°C). *FEMS Microbiol Ecol* 30**,** 313-326. doi:

Coates, J.D., Ellis, D.J., Gaw, C.V., and Lovley, D.R. (1999). *Geothrix fermentans* gen. nov., sp. nov., a novel Fe(III)-reducing bacterium from a hydrocarbon-contaminated aquifer. *Int J Syst Bacteriol* 49**,** 1615-1622. doi:

Colman, D.R., Feyhl-Buska, J., Robinson, K.J., Fecteau, K.M., Xu, H., Shock, E.L., and Boyd, E.S. (2016). Ecological differentiation in planktonic and sediment-associated chemotrophic microbial populations in Yellowstone hot springs. *FEMS Microbiol Ecol* 92. doi: 10.1093/femsec/fiw137

Crowe, S.A., Jones, C., Katsev, S., Magen, C., O'neill, A.H., Sturm, A., Canfield, D.E., Haffner, G.D., Mucci, A., Sundby, B., and Fowle, D.A. (2008). Photoferrotrophs thrive in an Archean Ocean analogue. *Proc Natl Acad Sci U S A* 105**,** 15938-15943. doi: 10.1073/pnas.0805313105

Du, J., Say, R.F., Lü, W., Fuchs, G., and Einsle, O. (2011). Active-site remodelling in the bifunctional fructose-1,6-bisphosphate aldolase/phosphatase. *Nature* 478**,** 534-537. doi: 10.1038/nature10458

Emerson, D. (2000). "Microbial Oxidation of Fe(II) and Mn(II) at Circumneutral pH," in *Environmental Microbe-Metal Interactions,* ed. D.R. Lovley. (Washington, D.C.: ASM Press), 31-52.

Emerson, D., Field, E.K., Chertkov, O., Davenport, K.W., Goodwin, L., Munk, C., Nolan, M., and Woyke, T. (2013). Comparative genomics of freshwater Fe-oxidizing bacteria: implications for physiology, ecology, and systematics. *Front Microbiol* 4**,** 254. doi: 10.3389/fmicb.2013.00254

Emerson, D., Fleming, E.J., and Mcbeth, J.M. (2010). Iron-oxidizing bacteria: an environmental and genomic perspective. *Ann Rev Microbiol* 64**,** 561-583. doi: 10.1146/annurev.micro.112408.134208

Emerson, D., and Revsbech, N.P. (1994). Investigation of an Iron-Oxidizing Microbial Mat Community Located near Aarhus, Denmark: Laboratory Studies. *Appl Environ Microbiol* 60**,** 4032-4038. doi:

Emerson, D., and Weiss, J.V. (2004). Bacterial Iron Oxidation in Circumneutral Freshwater Habitats: Findings from the Field and the Laboratory. *Geomicrobiol J* 21**,** 405-414. doi: 10.1080/01490450490485881

Finn, M.W., and Tabita, F.R. (2004). Modified Pathway To Synthesize Ribulose 1,5-Bisphosphate in Methanogenic Archaea. *J Bacteriol* 186**,** 6360-6366. doi: 10.1128/JB.186.19.6360-6366.2004

Finn, R.D., Clements, J., and Eddy, S.R. (2011). HMMER web server: interactive sequence similarity searching. *Nucleic Acids Res* 39**,** W29-37. doi: 10.1093/nar/gkr367

Fortney, N.W., He, S., Converse, B.J., Beard, B.L., Johnson, C.M., Boyd, E.S., and Roden, E.E. (2016). Microbial Fe(III) oxide reduction potential in Chocolate Pots hot spring, Yellowstone National Park. *Geobiology* 14**,** 255-275. doi: 10.1111/gbi.12173

Fortney, N.W., He, S., Kulkarni, A., Friedrich, M.W., Holz, C., Boyd, E.S., and Roden, E.E. (2018). Stable isotope probing of microbial iron reduction in Chocolate Pots hot spring, Yellowstone National Park. *Appl Environ Microbiol*. doi: 10.1128/AEM.02894-17

Frank, Y.A., Kadnikov, V.V., Lukina, A.P., Banks, D., Beletsky, A.V., Mardanov, A.V., Sen'kina, E.I., Avakyan, M.R., Karnachuk, O.V., and Ravin, N.V. (2016). Characterization and Genome Analysis of the First Facultatively Alkaliphilic *Thermodesulfovibrio* Isolated from the Deep Terrestrial Subsurface. *Front Microbiol* 7**,** 2000. doi: 10.3389/fmicb.2016.02000

Frigaard, N.-U., and Bryant, D.A. (2008). "Genomic and Evolutionary Perspectives on Sulfur Metabolism in Green Sulfur Bacteria," in *Microbial Sulfur Metabolism,* eds. C. Dahl & C.G. Friedrich. (Berlin: Springer-Verlag), 60-76.

Haaijer, S.C.M., Harhangi, H.R., Meijerink, B.B., Strous, M., Pol, A., Smolders, A.J., Verwegen, K., Jetten, M.S.M., and Op Den Camp, H.J.M. (2008). Bacteria associated with iron seeps in a sulfur-rich, neutral pH, freshwater ecosystem. *ISME J* 2**,** 1231-1242. doi: 10.1038/ismej.2008.75

Hafenbradl, D., Keller, M., Dirmeier, R., Rachel, R., Roßnagel, P., Burggraf, S., Huber, H., and Stetter, K.O. (1996). *Ferroglobus placidus* gen. nov., sp. nov., a novel hyperthermophilic archaeum that oxidizes Fe^{2+} at neutral pH under anoxic conditions. *Arch Microbiol* 16**,** 308-314. doi:

Hartshorne, R.S., Reardon, C.L., Ross, D., Nuester, J., Clarke, T.A., Gates, A.J., Mills, P.C., Fredrickson, J.K., Zachara, J.M., Shi, L., Beliaev, A.S., Marshall, M.J., Tien, M., Brantley, S., Butt, J.N., and Richardson, D.J. (2009). Characterization of an electron conduit between bacteria and the extracellular environment. *Proc Natl Acad Sci U S A* 106**,** 22169-22174. doi: 10.1073/pnas.0900086106

Hattori, S., Galushko, A.S., Kamagata, Y., and Schink, B. (2005). Operation of the CO dehydrogenase/acetyl coenzyme A pathway in both acetate oxidation and acetate formation by the syntrophically acetate-oxidizing bacterium *Thermacetogenium phaeum*. *J Bacteriol* 187**,** 3471-3476. doi: 10.1128/JB.187.10.3471-3476.2005

Hegler, F., Lösekann-Behrens, T., Hanselmann, K., Behrens, S., and Kappler, A. (2012). Influence of Seasonal and Geochemical Changes on the Geomicrobiology of an Iron Carbonate Mineral Water Spring. *Appl Environ Microbiol* 78**,** 7185-7196. doi: 10.1128/AEM.01440-12

Henry, E.A., Devereux, R., Maki, J.S., Gilmour, C.C., Woese, C.R., Mandelco, L., Schauder, R., Remen, C.C., and Mitchell, R. (1994). Characterization of a new thermophilic sulfate-reducing bacterium *Thermodesulfovibrio yellowstonii*, gen. nov. and sp. nov.: its phylogenetic relationship to *Thermodesulfobacterium commune* and their origins deep within the bacterial domain. *Arch Microbiol* 161**,** 62-69. doi:

Hügler, M., Menendez, C., Schägger, H., and Fuchs, G. (2002). Malonyl-Coenzyme A Reductase from *Chloroflexus aurantiacus*, a Key Enzyme of the 3-Hydroxypropionate Cycle for Autotrophic CO_2 Fixation. *J Bacteriol* 184**,** 2404-2410. doi: 10.1128/jb.184.9.2404-2410.2002

Hügler, M., and Sievert, S.M. (2011). Beyond the Calvin Cycle: Autotrophic Carbon Fixation in the Ocean. *Annu Rev Mar Sci* 3. doi: 10.1146/annurev-marine-120709-142712

Hügler, M., Wirsen, C.O., Fuchs, G., Taylor, C.D., and Sievert, S.M. (2005). Evidence for Autotrophic CO_2 Fixation via the Reductive Tricarboxylic Acid Cycle by Members of the ε Subdivision of Proteobacteria. *J Bacteriol* 187**,** 3020-3027. doi: 10.1128/JB.187.9.3020-3027.2005

Huson, D.H., Auch, A.F., Qi, J., and Schuster, S.C. (2007). MEGAN analysis of metagenomic data. *Genome Res* 17**,** 377-386. doi: 10.1101/gr.5969107

Huson, D.H., and Scornavacca, C. (2012). Dendroscope 3: an interactive tool for rooted phylogenetic trees and networks. *Syst Biol* 61**,** 1061-1067. doi: 10.1093/sysbio/sys062

Hyatt, D., Chen, G.-L., Locascio, P.F., Land, M.L., Larimer, F.W., and Hauser, L.J. (2010). Prodigal: prokaryotic gene recognition and translation initiation site identification. *BMC bioinformatics* 11**,** 119. doi:

Iino, T., Mori, K., Uchino, Y., Nakagawa, T., Harayama, S., and Suzuki, K. (2010). *Ignavibacterium album* gen. nov., sp. nov., a moderately thermophilic anaerobic bacterium isolated from microbial mats at a terrestrial hot spring and proposal of *Ignavibacteria* classis nov., for a novel lineage at the periphery of green sulfur bacteria. *Int J Syst Evol Micr* 60**,** 1376-1382. doi: 10.1099/ijs.0.012484-0

Ilbert, M., and Bonnefoy, V. (2013). Insight into the evolution of the iron oxidation pathways. *Biochim Biophys Acta* 1827**,** 161-175. doi: 10.1016/j.bbabio.2012.10.001

Imhoff, J.F. (2003). Phylogenetic taxonomy of the family *Chlorobiaceae* on the basis of 16S rRNA and *fmo* (Fenna-Matthews-Olson protein) gene sequences. *Int J Syst Evol Micr* 53**,** 941-951. doi: 10.1099/ijs.0.02403-0

Jiang, Y.-H., Wang, D.-Y., and Wen, J.-F. (2012). The independent prokaryotic origins of eukaryotic fructose-1, 6-bisphosphatase and sedoheptulose-1, 7-bisphosphatase and the implications of their origins for the evolution of eukaryotic Calvin cycle. *BMC Evol Biol* 12**,** 208. doi:

Klatt, C.G., Bryant, D.A., and Ward, D.M. (2007). Comparative genomics provides evidence for the 3-hydroxypropionate autotrophic pathway in filamentous anoxygenic phototrophic bacteria and in hot spring microbial mats. *Environ Microbiol* 9**,** 2067-2078. doi: 10.1111/j.1462-2920.2007.01323.x

Klatt, C.G., Inskeep, W.P., Herrgard, M.J., Jay, Z.J., Rusch, D.B., Tringe, S.G., Parenteau, M.N., Ward, D.M., Boomer, S.M., Bryant, D.A., and Miller, S.R. (2013). Community structure and function of high-temperature chlorophototrophic microbial mats inhabiting diverse geothermal environments. *Front Microbiol* 4**,** 106. doi: 10.3389/fmicb.2013.00106

Kono, T., Mehrotra, S., Endo, C., Kizu, N., Matusda, M., Kimura, H., Mizohata, E., Inoue, T., Hasunuma, T., Yokota, A., Matsumura, H., and Ashida, H. (2017). A RuBisCO-mediated carbon metabolic pathway in methanogenic archaea. *Nat Commun* 8**,** 14007. doi: 10.1038/ncomms14007

Kublanov, I.V., Sigalova, O.M., Gavrilov, S.N., Lebedinsky, A.V., Rinke, C., Kovaleva, O., Chernyh, N.A., Ivanova, N., Daum, C., Reddy, T.B.K., Klenk, H.-P., Spring, S., Göker, M., Reva, O.N., Miroshnichenko, M.L., Kyrpides, N.C., Woyke, T., Gelfand, M.S., and Bonch-Osmolovskaya, E.A. (2017). Genomic Analysis of *Caldithrix abyssi*, the Thermophilic Anaerobic Bacterium of the Novel Bacterial Phylum *Calditrichaeota*. *Front Microbiol* 8**,** 195. doi: 10.3389/fmicb.2017.00195

Li, H., Handsaker, B., Wysoker, A., Fennell, T., Ruan, J., Homer, N., Marth, G., Abecasis, G., Durbin, R., and Genome Project Data Processing, S. (2009). The Sequence Alignment/Map format and SAMtools. *Bioinformatics* 25**,** 2078-2079. doi: 10.1093/bioinformatics/btp352

Liu, Y., Wang, Z., Liu, J., Levar, C., Edwards, M.J., Babauta, J.T., Kennedy, D.W., Shi, Z., Beyenal, H., Bond, D.R., Clarke, T.A., Butt, J.N., Richardson, D.J., Rosso, K.M., Zachara, J.M., Fredrickson, J.K., and Shi, L. (2014). A trans-outer membrane porin-cytochrome protein complex for extracellular electron transfer by *Geobacter sulfurreducens* PCA. *Environ Microbiol Rep* 6**,** 776-785. doi: 10.1111/1758-2229.12204

Llirós, M., García-Armisen, T., Darchambeau, F., Morana, C., Triadó-Margarit, X., Inceoğlu, Ö., Borrego, C.M., Bouillon, S., Servais, P., Borges, A.V., Descy, J.-P., Canfield, D.E., and Crowe, S.A. (2015). Pelagic photoferrotrophy and iron cycling in a modern ferruginous basin. *Sci Rep* 5. doi: 10.1038/srep13803

Losey, N.A., Stevenson, B.S., Busse, H.-J., Sinninghé Damste, J.S., Rijpstra, W.I.C., Rudd, S., and Lawson, P.A. (2013). *Thermoanaerobaculum aquaticum* gen. nov., sp. nov., the first cultivated member of *Acidobacteria* subdivision 23, isolated from a hot spring. *Int J Syst Evol Micr* 63**,** 4149-4157. doi: 10.1099/ijs.0.051425-0

Lovley, D. (2006). "Dissimilatory Fe(III)- and Mn(IV)-Reducing Prokaryotes," in *The Prokaryotes,* eds. M. Dworkin, S. Falkow, E. Rosenberg, K.H. Schleifer & E. Stackebrandt. (New York, NY: Springer), 635-658.

Lovley, D.R., Holmes, D.E., and Nevin, K.P. (2004). Dissimilatory Fe(III) and Mn(IV) Reduction. *Adv Microb Physiol* 49**,** 219-286. doi: 10.1016/s0065-2911(04)49005-5

Lücker, S., Wagner, M., Maixner, F., Pelletier, E., Koch, H., Vacherie, B., Rattei, T., Sinninghe Damsté, J.S., Spieck, E., Le Paslier, D., and Daims, H. (2010). A *Nitrospira* metagenome illuminates the physiology and evolution of globally important nitrite-oxidizing bacteria. *Proc Natl Acad Sci USA* 107**,** 13479-13484. doi: 10.1073/pnas.1003860107

Matschiavelli, N., Oelgeschläger, E., Cocchiararo, B., Finke, J., and Rother, M. (2012). Function and Regulation of Isoforms of Carbon Monoxide Dehydrogenase/Acetyl Coenzyme A Synthase in *Methanosarcina Acetivorans*. *J Bacteriol* 194**,** 5377-5387. doi: 10.1128/JB.00881-12

Mavromatis, K., Ivanova, N.N., Chen, I.M., Szeto, E., Markowitz, V.M., and Kyrpides, N.C. (2009). The DOE-JGI Standard Operating Procedure for the Annotations of Microbial Genomes. *Stand Genomic Sci* 1**,** 63-67. doi: 10.4056/sigs.632

McCleskey, R.B., Nordstrom, D.K., Susong, D.D., Ball, J.W., and Holloway, J.M. (2010). Source and fate of inorganic solutes in the Gibbon River, Yellowstone National Park, Wyoming, USA. *J Volcanol Geoth Res* 193**,** 189-202. doi: 10.1016/j.jvolgeores.2010.03.014

Miroshnichenko, M.L., Kolganova, T.V., Spring, S., Chernyh, N., and Bonch-Osmolovskaya, E.A. (2010). Caldithrix palaeochoryensis sp. nov., a thermophilic, anaerobic, chemo-organotrophic bacterium from a geothermally heated sediment, and emended description of the genus Caldithrix. *Int J Syst Evol Micr* 60**,** 2120-2123. doi: 10.1099/ijs.0.016667-0

Miroshnichenko, M.L., Kostrikina, N.A., Chernyh, N.A., Pimenov, N.V., Tourova, T.P., Antipov, A.N., Spring, S., Stackebrandt, E., and Bonch-Osmolovskaya, E.A. (2003). *Caldithrix abyssi* gen. nov., sp. nov., a nitrate-reducing, thermophilic, anaerobic bacterium isolated from a Mid-Atlantic Ridge hydrothermal vent, represents a novel bacterial lineage. *Int J Syst Evol Micr* 53**,** 323-329. doi: 10.1099/ijs.0.02390-0

Neubauer, S.C., Emerson, D., and Megonigal, J.P. (2002). Life at the Energetic Edge: Kinetics of Circumneutral Iron Oxidation by Lithotrophic Iron-Oxidizing Bacteria Isolated from the Wetland-Plant Rhizosphere. *Appl Environ Microbiol* 68**,** 3988-3995. doi: 10.1128/aem.68.8.3988-3995.2002

Nurk, S., Meleshko, D., Korobeynikov, A., and Pevzner, P. (2016). metaSPAdes: a new versatile de novo metagenomics assembler. *arXiv* q-Bio.GN. doi: arXiv:1604.03071v2

Orcutt, B.N., Sylvan, J.B., Rogers, D.R., Delaney, J., Lee, R.W., and Girguis, P.R. (2015). Carbon fixation by basalt-hosted microbial communities. *Front Microbiol* 6**,** 904. doi: 10.3389/fmicb.2015.00904

Parenteau, M.N., and Cady, S.L. (2010). Microbial Biosignatures in Iron-Mineralized Phototrophic Mats at Chocolate Pots Hot Springs, Yellowstone National Park, United States. *Palaios* 25**,** 97-111. doi: 10.2110/palo.2008.p08-133r

Parenteau, M.N., Jahnke, L.L., Farmer, J.D., and Cady, S.L. (2014). Production and Early Preservation of Lipid Biomarkers in Iron Hot Springs. *Astrobiology* 14**,** 502-521. doi: 10.1089/ast.2013.1122

Parks, D.H., Imelfort, M., Skennerton, C.T., Hugenholtz, P., and Tyson, G.W. (2015). CheckM: assessing the quality of microbial genomes recovered from isolates, single cells, and metagenomes. *Genome Res* 25**,** 1043-1055. doi: 10.1101/gr.186072.114

Pérez-Rodríguez, I., Rawls, M., Coykendall, D.K., and Foustoukos, D.I. (2016). Deferrisoma palaeochoriense sp. nov., a thermophilic, iron(III)-reducing bacterium from a shallow-water hydrothermal vent in the Mediterranean Sea. *Int J Syst Evol Micr* 66**,** 830-836. doi: 10.1099/ijsem.0.000798

Pierson, B.K., and Parenteau, M.N. (2000). Phototrophs in high iron microbial mats: microstructure of mats in iron-depositing hot springs. *FEMS Microbiol Ecol* 32**,** 181-196. doi:

Pierson, B.K., Parenteau, M.N., and Griffin, B.M. (1999). Phototrophs in High-Iron-Concentration Microbial Mats: Physiological Ecology of Phototrophs in an Iron-Depositing Hot Spring. *Appl Environ Microbiol* 65**,** 5474-5483. doi:

Podosokorskaya, O.A., Kadnikov, V.V., Gavrilov, S.N., Mardanov, A.V., Merkel, A.Y., Karnachuk, O.V., Ravin, N.V., Bonch-Osmolovskaya, E.A., and Kublanov, I.V. (2013). Characterization of *Melioribacter roseus* gen. nov., sp. nov., a novel facultatively anaerobic thermophilic cellulolytic bacterium from the class *Ignavibacteria*, and a proposal of a novel bacterial phylum *Ignavibacteriae*. *Environ Microbiol* 15**,** 1759-1771. doi: 10.1111/1462-2920.12067

Roden, E.E., Mcbeth, J.M., Blothe, M., Percak-Dennett, E.M., Fleming, E.J., Holyoke, R.R., Luther, G.W., 3rd, Emerson, D., and Schieber, J. (2012). The Microbial Ferrous Wheel in a Neutral pH Groundwater Seep. *Front Microbiol* 3**,** 172. doi: 10.3389/fmicb.2012.00172

Ruff, S.W., and Farmer, J.D. (2016). Silica deposits on Mars with features resembling hot spring biosignatures at El Tatio in Chile. *Nat Commun* 7**,** 13554. doi: 10.1038/ncomms13554

Santos, T.C., Silva, M.A., Morgado, L., Dantas, J.M., and Salgueiro, C.A. (2015). Diving into the redox properties of Geobacter sulfurreducens cytochromes: a model for extracellular electron transfer. *Dalton Trans* 44**,** 9335-9344. doi: 10.1039/c5dt00556f

Say, R.F., and Fuchs, G. (2010). Fructose 1,6-bisphosphate aldolase/phosphatase may be an ancestral gluconeogenic enzyme. *Nature* 464**,** 1077-1081. doi: 10.1038/nature08884

Schauder, R., Preuß, A., Jetten, M., and Fuchs, G. (1989). Oxidative and reductive acetyl CoA/carbon monoxide dehydrogenase pathway in *Desulfohacterium autotrophicum*. *Arch Microbiol* 151**,** 84-89. doi:

Sekiguchi, Y., Muramatsu, M., Imachi, H., Narihiro, T., Ohashi, A., Harada, H., Hanada, S., and Kamagata, Y. (2008). *Thermodesulfovibrio aggregans* sp. nov. and *Thermodesulfovibrio thiophilus* sp. nov., anaerobic, thermophilic, sulfate-reducing bacteria isolated from thermophilic methanogenic sludge, and emended description of the genus *Thermodesulfovibrio*. *Int J Syst Evol Micr* 58**,** 2541-2548. doi: 10.1099/ijs.0.2008/000893-0

Shi, L., Dong, H., Reguera, G., Beyenal, H., Lu, A., Liu, J., Yu, H.-Q., and Fredrickson, J.K. (2016). Extracellular electron transfer mechanisms between microorganisms and minerals. *Nat Rev Microbiol* 14**,** 651-662. doi: 10.1038/nrmicro.2016.93

Shi, L., Fredrickson, J.K., and Zachara, J.M. (2014). Genomic analyses of bacterial porin-cytochrome gene clusters. *Front Microbiol* 5**,** 657. doi: 10.3389/fmicb.2014.00657

Slobodkina, G.B., Reysenbach, A.L., Panteleeva, A.N., Kostrikina, N.A., Wagner, I.D., Bonch-Osmolovskaya, E.A., and Slobodkin, A.I. (2012). *Deferrisoma camini* gen. nov., sp. nov., a moderately thermophilic, dissimilatory iron(III)-reducing bacterium from a deep-sea hydrothermal vent that forms a distinct phylogenetic branch in the *Deltaproteobacteria*. *Int J Syst Evol Micr* 62**,** 2463-2468. doi: 10.1099/ijs.0.038372-0

Squyres, S.W., Arvidson, R.E., Ruff, S., Gellert, R., Morris, R.V., Ming, D.W., Crumpler, L., Farmer, J.D., Des Marais, D.J., Yen, A., Mclennan, S.M., Calvin, W., Bell, J.F., 3rd, Clark, B.C., Wang, A., Mccoy, T.J., Schmidt, M.E., and De Souza, P.A., Jr. (2008). Detection of Silica-Rich Deposits on Mars. *Science* 320**,** 1063-1067. doi:

Strauss, G., and Fuchs, G. (1993). Enzymes of a novel autotrophic CO_2 fixation pathway in the phototrophic bacterium *Chloroflexus aurantiacus*, the 3-hydroxypropionate cycle. *Eur J Biochem* 215**,** 633-643. doi:

Suzuki, D., Li, Z., Cui, X., Zhang, C., and Katayama, A. (2014). Reclassification of *Desulfobacterium anilini* as *Desulfatiglans anilini* comb. nov. within *Desulfatiglans* gen. nov., and description of a 4-chlorophenol-degrading sulfate-reducing bacterium, *Desulfatiglans parachlorophenolica* sp. nov. *Int J Syst Evol Micr* 64**,** 3081-3086. doi: 10.1099/ijs.0.064360-0

Tabita, F.R., Satagopan, S., Hanson, T.E., Kreel, N.E., and Scott, S.S. (2008). Distinct form I, II, III, and IV Rubisco proteins from the three kingdoms of life provide clues about Rubisco evolution and structure/function relationships. *J Exp Bot* 59**,** 1515-1524. doi: 10.1093/jxb/erm361

Tang, K.-H., Tang, Y.J., and Blankenship, R.E. (2011). Carbon metabolic pathways in phototrophic bacteria and their broader evolutionary implications. *Front Microbiol* 2**,** 165. doi: 10.3389/fmicb.2011.00165

Tank, M., Thiel, V., Ward, D.M., and Bryant, D.A. (2017). "A Panoply of Phototrophs: An Overview of the Thermophilic Chlorophototrophs of the Microbial Mats of Alkaline Siliceous Hot Springs in Yellowstone National Park, WY, USA," in *Modern Topics in the Phototrophic Prokaryotes,* ed. P.C. Hallenbeck. (Switzerland: Springer International), 87-137.

Taylor, S.R., and Mclennan, S.M. (1985). "The continental crust: its composition and evolution." (Oxford: Blackwell Scientific Publications).

Taylor, S.R., and Mclennan, S.M. (2009). "Mars: crustal composition and evolution," in *Planetary Crusts: Their Composition, Origin, and Evolution*. (Cambridge, UK: Cambridge University Press), 141-180.

Trouwborst, R.E., Johnston, A., Koch, G., Luther, G.W., and Pierson, B.K. (2007). Biogeochemistry of Fe(II) oxidation in a photosynthetic microbial mat: Implications for Precambrian Fe(II) oxidation. *Geochim Cosmochim Ac* 71**,** 4629-4643. doi: 10.1016/j.gca.2007.07.018

Van Der Meer, M.T.J., Klatt, C.G., Wood, J., Bryant, D.A., Bateson, M.M., Lammerts, L., Schouten, S., Sinninghe Damsté, J.S., Madigan, M.T., and Ward, D.M. (2010). Cultivation and genomic, nutritional, and lipid biomarker characterization of *Roseiflexus*

strains closely related to predominant *in situ* populations inhabiting Yellowstone hot spring microbial mats. *J Bacteriol* 192**,** 3033-3042. doi: 10.1128/JB.01610-09

Vargas, M., Kashefi, K., Blunt-Harris, E.L., and Lovley, D.R. (1998). Microbiological evidence for Fe(III) reduction on early Earth. *Nature* 395**,** 65-67. doi:

Ward, L.M., Idei, A., Terajima, S., Kakegawa, T., Fischer, W.W., and Mcglynn, S.E. (2017). Microbial diversity and iron oxidation at Okuoku-hachikurou Onsen, a Japanese hot spring analog of Precambrian iron formations. *Geobiology* 15**,** 817-835. doi: 10.1111/gbi.12266

Weiss, J.V., Rentz, J.A., Plaia, T., Neubauer, S.C., Merrill-Floyd, M., Lilburn, T., Bradburne, C., Megonigal, J.P., and Emerson, D. (2007). Characterization of Neutrophilic Fe(II)-Oxidizing Bacteria Isolated from the Rhizosphere of Wetland Plants and Description of *Ferritrophicum radicicolagen*. nov. sp. nov., and *Sideroxydans paludicola* sp. nov. *Geomicrobiol J* 24**,** 559-570. doi: 10.1080/01490450701670152

Williams, T.J., Zhang, C.L., Scott, J.H., and Bazylinski, D.A. (2006). Evidence for Autotrophy via the Reverse Tricarboxylic Acid Cycle in the Marine Magnetotactic Coccus Strain MC-1. *Appl Environ Microbiol* 72**,** 1322-1329. doi: 10.1128/AEM.72.2.1322-1329.2006

Zaharia, M., Bolonsky, W.J., Curtis, K., Fox, A., Patterson, D., Shenker, S., Stoica, I., Karp, R.M., and Sittler, T. (2011). Faster and More Accurate Sequence Alignment with SNAP. *arXiv* cs.DS. doi: arXiv:1111.5572v1

Zarzycki, J., Brecht, V., Müller, M., and Fuchs, G. (2009). Identifying the missing steps of the autotrophic 3-hydroxypropionate CO_2 fixation cycle in *Chloroflexus aurantiacus*. *Proc Natl Acad Sci USA* 106**,** 21317-21322. doi: 10.1073/pnas.0908356106

Zarzycki, J., Schlichting, A., Strychalsky, N., Müller, M., Alber, B.E., and Fuchs, G. (2008). Mesaconyl-coenzyme A hydratase, a new enzyme of two central carbon metabolic pathways in bacteria. *J Bacteriol* 190**,** 1366-1374. doi: 10.1128/JB.01621-07

Zhang, H., Sekiguchi, Y., Hanada, S., Hugenholtz, P., Kim, H., Kamagata, Y., and Nakamura, K. (2003). *Gemmatimonas aurantiaca* gen. nov., sp. nov., a gram-negative, aerobic, polyphosphate-accumulating micro-organism, the first cultured representative of the new bacterial phylum *Gemmatimonadetes* phyl. nov. *Int J Syst Evol Micr* 53**,** 1155-1163. doi: 10.1099/ijs.0.02520-0

Table A.2.1.
Properties of Chocolate Pots spring water at sampling sites along the flow path.

Sampling Date	Sample Site	Distance from Vent (m)	Temperature (°C)	pH	Fe(II) (mmol L^{-1})[a]
Aug-13	Core 1	0	50.7	5.94	0.103
Aug-13	Core 2	1.0	49.9	6.06	0.090
Aug-13	Core 3	2.1	48.4	6.51	0.052
Aug-13	Core 4	4.1	42.8	7.77	0.006
Aug-13	Core 5	6.8	42.7	7.76	0.008
Aug-13	Core 6	8.2	40.8	7.90	0.004
Aug-13	Entry to Gibbon River	~13	38.1	8.25	0.003
Oct-15	Core 1	0	50.6	5.83	nd[b]
Oct-15	Core 2	1.0	50.2	5.90	nd
Oct-15	Core 3	2.1	47.3	6.46	nd
Oct-15	Core 4	4.1	46.2	6.88	nd
Oct-15	Core 5	6.8	41.9	7.38	nd
Oct-15	Core 6	8.2	40.1	7.56	nd
Oct-15	Vent source	0	51.3	5.76	0.029

[a] *In situ* Fe(II) concentration from the core sampling sites was only measured in 2013. Concentration at the vent source in 2015 was measured at t_0 of the incubation experiments.
[b] Not determined

Table A.2.2.
Phylogenetic assignment and statistics of metagenomic co-assembly of the Chocolate Pots cores.

			Co-assmebly		Core 1		Core 2		Core 3							
MAG#	GC%	MAG size (Mbp)	% Total Reads	Average assembly coverage	% Total Reads[c]	Average normalized coverage[d]	% Total Reads	Average normalized coverage	% Total Reads	Average normalized coverage	% Completeness	% Contamination	% Strain heterogeneity	Concensus Phylogeny	Taxonomic Rank	% Similarity to 16S amplicon library[e]	% Identity to GenBank[f]
0	56.4	6.590	2.32	40.08	0.09	1.10	0.48	4.34	6.04	30.57	96.59	4.2	0	*Deferrisoma camini*	Species	N/A[d]	
1	66.1	2.148	4.08	180.42	0.87	11.10	10.89	159.47			97.47	1.6	0	Euryarchaeota	Phylum	99.3[g]	85.6
2	45.8	3.387	0.08	2.69					0.23	2.26	89.64	4.37	0	*Deferrisoma camini*	Species	N/A	
4	56.1	4.107	0.59	15.96					1.68	14.11	94.94	5.45	0	*Ca.* Nitrospira defluvii	Species	N/A	
6	66.0	4.771	0.19	3.70					0.40	2.08	85.54	8.05	52.63	*Acidobacteriales*	Order	N/A	
7	52.0	2.090	0.07	3.53			0.11	1.67	0.08	1.16	96.45	0	0	*Pelodictyon*	Genus	N/A	
10	57.6	1.183	0.03	2.35					0.06	1.53	55.62	0	0	Acidobacteria	Phylum	N/A	
11	63.1	3.495	0.20	5.64	0.58	4.86					92.59	0.93	0	*Chthonomonas calidirosea*	Species	N/A	
13.2	66.2	5.307	0.40	7.43	0.28	1.61	0.58	3.51	0.31	1.88	95.27	3.51	0	*Ca.* Solibacter usitatus	Species	98.9	87.6
13.3	68.2	4.292	0.39	8.98	0.54	3.64	0.66	4.93			92.05	2.26	27.27	*Ca.* Solibacter	Genus	N/A	
14	27.2	0.880	0.20	25.31	0.66	25.16					89.72	0	0	Archaea	Kingdom	98.9	75.7
15.1	59.7	5.460	0.22	4.25			0.60	3.75			90.61	3.82	20	*Anaerolinea thermophila*	Species	N/A	
15.2	57.6	3.838	0.20	5.89	0.59	4.44	0.07	1.32			99.09	5.64	0	*Anaerolinea thermophila*	Species	N/A	
16	63.7	2.534	0.33	13.60	0.18	2.08	0.76	10.19			89.73	1.56	35.71	*Methyloversatilis*	Genus	N/A	
20	38.3	3.982	0.10	2.61	0.33	2.60					83.44	9.84	0	*Haliangium ochraceum*	Species	N/A	
22	69.7	3.254	0.11	3.41			0.31	3.10			85.54	2.97	0	*Dehalococcoides*	Genus	N/A	
25	53.7	1.754	0.20	13.28					0.57	11.71	93.24	1.35	0	*Simkania negevensis*	Species	N/A	
26	69.7	2.547	0.06	2.36			0.13	1.75			54.92	0.92	0	*Thermomicrobia*	Class	N/A	
27	51.0	1.493	0.03	2.24			0.08	1.83			69.95	8.25	7.14	*Ca.* Caldiarchaeum subterraneum	Species	N/A	
28	60.5	2.665	0.05	2.17			0.14	1.88			63.32	4.39	0	*Nitrospina gracilis*	Species	N/A	
29	58.5	1.715	0.04	2.41	0.13	2.32					71.35	0	0	*Dehalococcoides*	Genus	N/A	
33	55.5	2.631	0.45	20.48	0.12	1.88	1.12	16.74			88.64	2.91	10	*Anaerolinea thermophila*	Species	N/A	
34	52.7	3.054	2.62	93.04	0.18	2.05	7.07	81.33	0.24	4.40	93.97	1.37	0	*Ignavibacteriales*	Order	98.5	84.4
35.1	66.4	4.848	0.28	5.52					0.78	4.85	94.83	0.1	0	*Pirellula staleyi*	Species	99.3	90.2
35.2	65.8	6.133	0.61	10.77					1.74	9.44	99.37	0	0	*Rhodopirellula*	Genus	99.6[g]	88.2
38	45.8	2.948	0.07	2.41	0.22	2.04					83.94	12.99	11.76	*Anaerolinea thermophila*	Species	N/A	
39	55.3	3.982	5.98	153.76	0.49	3.86	1.68	16.74	14.90	117.50	96.17	2.73	0	*Ignavibacteriales*	Order	99.3[g]	82.0
45	33.5	3.122	0.13	5.37	0.44	5.30					91.88	1.71	0	Acidobacteria	Phylum	N/A	
47	53.4	3.003	0.07	2.57					0.20	2.25	74.70	0.93	0	*Chthonomonas calidirosea*	Species	N/A	
48	58.6	1.143	0.04	3.31	0.12	3.19					90.89	0	0	Archaea	Kingdom	N/A	
51	48.0	4.392	0.73	19.90					2.04	16.92	98.52	1.31	0	*Sediminibacterium*	Genus	N/A	
52.2	73.1	1.942	0.24	11.86			0.66	10.82			87.04	1.23	0	*Chthonomonas calidirosea*	Species	N/A	
54	58.5	5.419	0.31	6.21			0.79	5.16			94.44	0.93	0	*Chthonomonas calidirosea*	Species	N/A	
56	60.5	2.851	0.06	2.21			0.13	1.50			50.43	0.91	0	*Anaerolinea thermophila*	Species	N/A	
57.2	42.0	0.670	0.03	4.04	0.08	3.41					52.78	0	0	*Chthonomonas calidirosea*	Species	N/A	
58	59.8	2.700	0.07	2.70	0.12	1.33	0.10	1.28			87.19	0	0	*Dehalococcoides*	Genus	N/A	
59.2	45.0	1.007	0.05	5.86	0.02	1.16			0.11	3.29	74.42	0	0	*Dehalococcoides*	Genus	100.0	94.9
60	62.9	3.820	0.11	3.10					0.28	2.39	78.64	1.92	0	*Anaerolinea thermophila*	Species	N/A	
61	39.9	1.340	0.06	3.45			0.13	2.03			72.06	2.04	0	Bacteria	Kingdom	N/A	
64.1	43.7	1.760	0.10	6.50	0.34	6.42					94.09	1.82	0	*Thermodesulfovibrio*	Genus	N/A	
64.2	45.0	2.728	0.41	18.20	1.36	17.58					94.84	3.55	0	*Desulfobacterium anilini*	Species	N/A	
64.4	44.8	1.613	1.07	78.42	3.10	67.66	0.37	8.83	0.06	1.26	90.91	0	0	*Thermodesulfovibrio*	Genus	N/A	
65.1	48.6	2.440	0.10	4.21	0.15	1.77	0.15	1.93			94.22	0.71	0	*Pseudanabaena*	Genus	N/A	
65.2	47.4	5.389	0.29	6.24					0.80	5.08	98.58	1.18	0	*Oscillatoriales*	Order	98.9	89.5
66	64.5	5.853	0.34	5.87	1.09	5.62					93.52	4.26	0	*Chthonomonas calidirosea*	Species	N/A	
67	58.5	2.322	0.25	11.31	0.23	3.10	0.50	7.66			89.09	1.36	0	*Anaerolinea thermophila*	Species	N/A	
68	37.4	2.768	0.36	16.11	1.05	14.33	0.09	1.03			95.80	2.52	0	*Deferrisoma camini*	Species	N/A	
69.1	68.8	3.161	1.23	38.53	0.20	4.61	3.33	31.94			94.87	2.56	0	*Acidobacteriaceae*	Family	N/A	
69.2	71.2	2.024	0.81	38.41	2.46	34.84	0.20	3.21			95.80	0.42	100	*Deferrisoma camini*	Species	N/A	
70	64.4	3.457	0.79	25.26	2.62	24.92					82.00	0	0	*Anaerolinea thermophila*	Species	N/A	
73	64.0	3.702	0.45	11.88	0.25	2.03	1.01	8.89			96.36	2.27	0	*Anaerolinea thermophila*	Species	N/A	

75	62.3	4.018	0.14	3.52	0.43	3.20					84.91	1.82	0	*Caldilinea aerophila*	Species	N/A		
76	46.4	0.886	0.02	2.39	0.07	2.29					90.51	4.67	0	Archaea	Kingdom	N/A		
79.1	45.1	2.593	0.16	6.97	0.04	1.05	0.35	4.52	0.07	1.02	92.24	2.75	0	*Ignavibacteriales*	Order	99.3	83.4	
79.2	45.2	3.662	0.67	20.32	1.79	16.14	0.38	3.82			95.34	2.46	0	*Ignavibacteriales*	Order	N/A		
81	58.1	2.443	0.06	2.48			0.15	2.17			79.68	3.64	12.5	*Thermodesulfovibrio*	Genus	N/A		
84.2	38.8	2.171	0.36	19.96					1.03	17.12	95.10	2.25	0	*Simkania negevensis*	Species	N/A		
87	61.2	2.668	0.07	2.84	0.21	2.59					54.15	1.82	0	*Anaerolinea thermophila*	Species	N/A		
88	66.0	2.945	0.08	2.75			0.22	2.45			77.32	0.84	0	*Deferrisoma camini*	Species	N/A		
89	56.3	3.104	0.54	21.17	0.11	1.27	0.26	3.48	1.18	14.41	86.55	1.82	0	*Anaerolinea thermophila*	Species	N/A		
90.1	70.2	3.122	0.13	4.02					0.32	2.98	80.67	5.91	4	*Frankia*	Genus	N/A		
90.2	72.2	4.251	0.40	9.02			0.23	1.71	0.91	6.33	77.11	5.13	0	*Acidobacteriaceae*	Family	N/A		
94	64.3	2.568	0.09	3.58			0.23	3.13			66.17	2.69	18.18	*Bradyrhizobiaceae*	Family	N/A		
96	36.0	2.017	0.06	3.10	0.19	3.03					89.25	0	0	Bacteria	Kingdom	N/A		
97	72.6	2.385	0.16	6.10			0.35	4.42	0.09	1.09	70.83	0	0	*Dehalococcoides*	Genus	N/A		
98	44.9	1.944	0.04	2.30					0.10	1.70	66.25	1.64	0	*Ignavibacteriales*	Order	N/A		
101.1	42.6	2.987	0.09	3.41					0.26	3.02	98.77	1.97	0	*Chitinophagaceae*	Family	N/A		
101.2	48.1	2.916	0.12	4.25					0.33	3.77	97.62	2.68	0	*Fulvivirga imtechensis*	Species	N/A		
104	66.5	4.007	0.60	15.03	1.70	12.66	0.25	2.12			95.91	3.52	0	*Anaerolinea thermophila*	Species	99.3	87.3	
105	72.1	2.990	0.62	19.66					1.75	17.36	90.34	0	0	*Planctomycetaceae*	Family	98.5	82.2	
106	60.8	4.418	0.18	3.95	0.59	3.82					95.27	4.84	11.11	*Deltaproteobacteria*	Class	N/A		
108.2	57.0	2.117	0.12	5.77			0.32	4.79			99.07	4.67	0	*Nitrosopumilaceae*	Family	N/A		
108.3	54.7	1.802	0.18	10.86			0.50	9.42			94.82	0	0	*Ca.* Caldiarchaeum subterraneum	Species	100.0	79.9	
109	65.9	2.261	1.07	48.61	0.35	5.36	2.59	38.35	0.16	2.39	95.71	0.99	0	*Dehalococcoides*	Genus	N/A		
111	62.9	4.216	0.24	6.34	0.66	4.87	0.12	1.31			90.00	6.09	0	*Anaerolinea thermophila*	Species	N/A		
114	39.0	2.508	0.16	6.70			0.20	2.73	0.21	2.72	95.71	0.24	0	Bacteroidetes	Phylum	N/A		
115	55.2	3.519	0.13	3.86			0.29	2.54			99.80	1.12	0	*Ca.* Endomicrobium	Genus	100.0	85.4	
116	60.9	4.803	0.13	2.88					0.36	2.49	79.79	3.36	0	*Deferrisoma camini*	Species	N/A		
119	55.7	4.534	0.43	9.83	0.49	3.28	0.81	6.17			93.52	1.11	0	*Chthonomonas calidirosea*	Species	100.0	81.7	
122	64.1	4.634	0.65	12.92					1.83	11.08	93.77	0.93	0	*Chthonomonas calidirosea*	Species	98.2	83.4	
123	30.8	2.195	0.05	2.44			0.11	1.70			75.49	1.4	0	*Melioribacter roseus*	Species	N/A		
125	59.7	5.698	0.34	6.98			0.84	5.67			89.81	2.04	0	*Chthonomonas calidirosea*	Species	N/A		
127	72.7	2.103	0.17	7.47			0.34	4.95	0.08	1.12	85.19	1.52	0	*Acidimicrobium ferrooxidans*	Species	N/A		
128.1	59.1	3.395	0.26	7.98			0.03	1.29	0.72	5.84	95.55	8.18	0	*Ca.* Nitrospira defluvii	Species	N/A		
128.2	61.3	3.001	0.32	11.39			0.42	4.98	0.49	5.35	93.18	2.73	0	*Ca.* Nitrospira defluvii	Species	98.9[g]	98.0	
128.3	59.7	3.870	0.62	17.05			1.60	14.50	0.15	1.41	94.02	2.56	0	*Acidobacteriaceae*	Family	N/A		
129	61.4	3.394	0.09	2.84			0.24	2.39			93.93	3.23	0	*Planctomycetaceae*	Family	N/A		
133	31.8	3.057	0.23	8.32	0.63	6.72	0.13	1.49			92.31	3.42	0	Acidobacteria	Phylum	N/A		
134	67.7	3.852	0.24	6.71			0.66	6.10			85.51	1.94	0	*Anaeromyxobacter*	Genus	N/A		
135.1	56.9	2.926	0.14	5.14	0.39	3.93	0.08	1.10			69.57	5.54	20	Chloroflexi	Phylum	N/A		
135.2	56.4	4.197	0.53	15.13	1.62	13.19	0.14	1.76			89.60	17.19	29.17	Chloroflexi	Phylum	N/A		
136	65.0	4.506	0.16	3.57	0.39	2.51					90.26	1.55	0	*Caldilinea aerophila*	Species	N/A		
139	41.6	1.681	0.06	4.05			0.16	3.55			95.64	0	0	*Actinobacteria*	Class	N/A		
140	56.2	3.413	0.20	6.29			0.52	5.35			90.91	4.73	0	*Anaerolinea thermophila*	Species	N/A		
141	57.4	1.810	0.05	2.47	0.09	1.48					73.28	0	0	Bacteria	Kingdom	N/A		
145.1	51.1	3.368	0.09	2.76			0.23	2.28			88.58	1.91	25	*Ignavibacteriales*	Order	N/A		
145.2	50.7	2.996	0.18	3.39			0.03	1.20	0.48	4.60	97.52	1.91	0	*Ignavibacteriales*	Order	N/A		
146	65.0	3.501	0.74	23.21	2.46	23.01					87.73	2.73	0	*Anaerolinea thermophila*	Species	99.3[g]	89.7	
150	62.3	3.557	0.13	3.46	0.41	3.23					93.52	0	0	*Chthonomonas calidirosea*	Species	N/A		
153	61.2	2.382	0.05	2.21			0.11	1.47			63.96	3.9	0	Chloroflexi	Phylum	N/A		
154.4	38.0	0.826	0.15	20.25			0.00	1.38	0.44	16.64	62.50	0.93	0	Chloroflexi	Phylum	100.0	78.4	
157.1	48.6	0.658	0.03	4.48			0.09	4.04			62.16	2.78	0	*Chthonomonas calidirosea*	Species	N/A		
157.2	46.8	0.899	0.05	6.85					0.15	5.51	60.65	0.93	0	*Chthonomonas calidirosea*	Species	99.6	79.0	
158.1	63.8	4.390	0.12	2.92					0.33	2.36	89.00	5.11	0	*Planctomycetaceae*	Family	N/A		
158.2	64.5	4.213	0.20	4.80			0.54	3.87			94.59	1.75	0	*Ca.* Solibacter usitatus	Species	N/A		
159	61.9	3.854	0.11	3.01	0.35	2.95					88.06	0.43	100	*Desulfomonile tiedjei*	Species	N/A		
160.2	51.7	0.729	0.02	3.39			0.05	2.43			78.83	1.01	0	*Nitrosopumilaceae*	Family	N/A		
160.3	40.9	0.896	0.12	14.80					0.34	13.13	75.93	0	0	Archaea	Kingdom	N/A		

161	66.0	3.519	0.08	2.33					0.22	2.05	52.92	0	0	*Planctomyces*	Genus	N/A		
162	65.2	4.734	0.46	10.38	0.07	2.36			1.23	6.43	97.27	6.36	0	*Anaerolinea thermophila*	Species	N/A		
163	56.6	1.878	0.05	2.86	0.16	2.74					89.57	0	0	*Dehalococcoides*	Genus	N/A		
164.1	52.6	6.212	0.61	7.84			1.61	6.58			98.22	11.33	0	*Nitrosopumilaceae*	Family	N/A		
164.2	53.5	2.221	1.15	53.68	0.27	3.85	3.03	45.98	0.02	1.05	94.01	1.29	0	*Nitrosopumilaceae*	Family	N/A		
165	55.1	2.411	1.57	77.71	4.45	65.37	0.71	11.55			71.59	0.31	33.33	Chloroflexi	Phylum	97.1	86.9	
167	69.7	3.232	0.16	4.99					0.47	4.40	64.80	0.43	0	*Rhodospirillaceae*	Family	N/A		
168	31.9	2.263	0.11	5.33			0.27	4.23			94.76	0.48	0	Bacteroidetes	Phylum	N/A		
171	61.6	1.805	1.34	79.39	0.06	1.07	3.06	59.75	0.70	13.43	95.24	0	0	*Sideroxydans lithotrophicus*	Species	N/A		
172	61.1	2.553	0.08	3.35	0.25	3.06					79.60	0	0	*Anaerolinea thermophila*	Species	N/A		
174	54.3	3.260	0.66	22.86	0.06	1.07	0.44	6.01	1.37	13.72	97.81	0.82	0	*Ignavibacteriales*	Order	N/A		
179	57.1	2.994	0.54	19.64					1.51	17.14	88.18	3.31	0	*Anaerolinea thermophila*	Species	N/A		
181	50.1	2.095	0.12	5.66	0.33	4.47	0.07	1.13			96.55	0	0	Bacteria	Kingdom	N/A		
184	59.3	3.961	0.29	6.87	0.83	5.81					95.29	0	0	*Chthonomonas calidirosea*	Species	99.6	83.8	
185	54.5	0.970	0.03	2.77	0.08	2.48					78.89	1.87	0	Archaea	Kingdom	N/A		
186	67.4	4.670	0.55	11.80	0.21	1.32	0.99	7.08	0.39	2.66	94.59	5.07	0	*Pedosphaera parvula*	Species	99.3	91.5	
187	60.3	2.243	0.08	3.78	0.26	3.57					94.38	1.12	0	*Ca.* Endomicrobium	Genus	N/A		
189.2	48.0	0.530	0.02	4.12			0.05	3.12			60.53	0	0	*Dehalococcoides*	Genus	N/A		
190	60.5	3.561	0.30	8.65	0.17	1.80	0.62	5.17	0.08	1.23	94.55	7.61	0	*Anaerolinea thermophila*	Species	N/A		
191	60.1	4.924	0.15	3.16	0.17	1.12	0.25	1.82			93.08	0.73	33.33	*Roseiflexus*	Genus	N/A		
194	29.3	2.867	0.50	9.16			1.23	5.96	0.17	1.95	98.54	5.1	0	*Nitrosopumilaceae*	Family	99.6[g]	90.0	
196	53.3	2.412	0.10	4.54			0.26	3.38			91.53	0	0	*Thermosipho*	Genus	N/A		
197.1	58.4	5.905	8.78	168.63					24.96	148.24	95.54	1.1	0	*Caldithrix abyssi*	Species	99.6[g]	83.0	
200	48.8	2.477	0.07	2.90	0.16	1.96					90.38	0.79	20	*Synechococcus*	Genus	N/A		
202	51.0	2.125	0.27	11.70	0.44	5.70	0.39	5.64			93.10	1.72	0	Bacteria	Kingdom	99.6	81.0	
203	64.2	3.665	0.29	8.79	0.96	8.61					85.78	0	0	Chloroflexi	Phylum	99.3	85.0	
208	56.4	4.014	0.30	7.87	0.84	6.50	0.13	1.27			96.77	1.29	0	*Desulfomonile tiedjei*	Species	99.6	88.6	
209	51.7	2.584	2.33	96.53			1.55	21.99	5.06	64.97	93.72	0.55	0	*Ignavibacteriales*	Order	N/A		
214	68.8	1.851	0.05	2.88	0.14	2.26					64.75	0.85	0	Acidobacteria	Phylum	N/A		
216	64.2	3.319	0.08	2.36			0.15	1.30			65.67	14.21	2.44	*Pedosphaera parvula*	Species	N/A		
220.2	31.2	2.602	0.82	35.05	2.64	32.57	0.10	2.20			93.44	5.19	0	*Ignavibacteriales*	Order	N/A		
220.3	32.9	2.477	1.00	46.41	2.73	37.62	0.51	7.89			88.51	1.09	0	*Ignavibacteriales*	Order	N/A		
221	66.4	2.926	0.18	6.09	0.58	5.94					88.53	0.18	0	*Chloroflexaceae*	Family	100.0	83.0	
225.1	56.1	1.643	0.28	19.24	0.60	11.97	0.23	6.32			64.79	0	0	*Thermosipho*	Genus	N/A		
226	54.5	3.835	0.11	2.82	0.18	1.36	0.16	1.37			92.91	3.38	0	*Pedosphaera parvula*	Species	N/A		
227	62.3	3.279	0.33	10.57	0.11	1.38	0.83	8.68			93.97	3.56	0	*Thermodesulfovibrio*	Genus	N/A		
228.1	36.2	0.572	0.04	7.62	0.13	7.41					50.00	7.27	0	*Ca.* Endomicrobium	Genus	78.3	79.3	
230.1	36.5	2.814	0.07	2.96	0.19	2.28					87.18	1.4	0	*Thermodesulfovibrio*	Genus	N/A		
232	70.3	2.287	0.12	4.94					0.31	4.10	51.47	0.29	0	*Thermomicrobia*	Class	N/A		
234.2	66.4	2.360	0.43	18.81			0.09	2.69	1.11	14.10	93.73	1.98	0	*Dehalococcoides*	Genus	N/A		
235	30.6	2.766	0.80	32.54	2.66	32.15					95.73	0	0	Acidobacteria	Phylum	N/A		
236	67.6	2.715	0.46	15.67	1.14	11.47	0.35	3.96			94.44	2.14	33.33	Acidobacteria	Phylum	98.9	98.3	
237	43.5	3.870	0.22	5.96	0.72	5.85					96.13	3.55	0	*Desulfomonile tiedjei*	Species	N/A		
238	48.0	3.249	0.20	6.72	0.68	6.62					91.97	3.42	0	Acidobacteria	Phylum	N/A		
241	61.5	3.660	0.16	4.12			0.23	1.97	0.14	1.17	93.28	3.36	0	*Deferrisoma camini*	Species	N/A		
244	60.7	2.139	0.04	2.22					0.08	1.21	59.13	0.19	0	*Dehalococcoides*	Genus	N/A		
245.1	70.1	3.183	0.27	8.53			0.68	7.24			81.77	0.93	0	*Chthonomonas calidirosea*	Species	N/A		
245.2	69.9	2.805	0.57	20.44			1.50	18.00	0.11	1.18	93.10	8.15	31.25	*Chthonomonas calidirosea*	Species	N/A		
245.3	68.1	2.502	0.73	30.55			2.01	27.49	0.05	1.04	92.59	0.93	0	*Chthonomonas calidirosea*	Species	99.3	83.0	
246	66.5	4.489	0.16	3.63					0.43	2.95	73.64	5.91	8.33	*Bradyrhizobiaceae*	Family	N/A		
247	61.6	4.322	0.12	2.80	0.37	2.60					82.65	2.93	0	*Deltaproteobacteria*	Class	N/A		
249	43.1	1.122	0.10	9.54	0.33	9.06					74.46	5.61	57.14	Archaea	Kingdom	99.6	76.6	
250.1	48.6	1.951	0.15	8.68	0.31	5.44	0.13	2.66			94.55	1.82	0	*Thermodesulfovibrio*	Genus	N/A		
250.2	49.3	2.026	0.90	49.53			2.54	45.99			95.85	1.82	0	*Ca.* Nitrospira defluvii	Species	N/A		
251	68.7	2.744	1.47	52.80	0.17	1.88	2.85	34.07	1.18	13.23	98.90	1.1	0	*Gemmatimonas aurantiaca*	Species	N/A		
252.1	30.7	1.759	0.05	3.30	0.18	3.21					91.61	0	0	*Ca. Cloacamonas acidaminovorans*	Species	99.4	79.6	
252.2	36.8	2.347	0.08	3.30	0.26	3.40					91.28	2.33	0	Acidobacteria	Phylum	N/A		

254	68.5	3.539	0.39	10.32			0.27	2.44	0.76	6.33	90.43	1.75	0 *Sutterella wadsworthensis*	Species	97.4	93.6
255	62.1	1.920	0.16	8.50	0.53	8.39					98.40	0.8	0 Euryarchaeota	Phylum	99.6	87.8
sum[a]			72.72		56.29		73.03		82.66							
avg[b]				*15.09*		*7.94*		*9.75*		*11.27*						

[a] Total percentage of reads mapping to MAGs in a given metagenomic assembly

[b] Average read coverage of the contigs in each MAG

[c] Calculated as the percent of reads mapped to a given MAG out of the total number of normalized reads for an individual core library

[d] MAGs with a calculated coverage of <1.0 are considered to be absent from a metagenomic library for an individual core, and not listed

[e] Alignment between 16S rRNA gene sequences from the metagenomic co-assembly and the 16S rRNA gene amplicon library

[f] %Identity of 16S rRNA gene sequences from the metagenomic library aligned to the NCBI GenBank database

[g] Not applicable; no significant alignment to 16S rRNA gene amplicon library, or metagenomic 16S rRNA gene sequence on unbinned condig

[h] >1% OTU read abundance in 16S rRNA gene amplicon library

Table A.2.3.

Phylogenetic assignment and statistics of metagenomic assembly of the Chocolate Pots vent pool water column.

MAG#	GC%	MAG size (Mbp)	% Total Reads[c]	Average assembly coverage	% Completeness	% Contamination	% Strain heterogeneity	Concensus Phylogeny	Taxonomic rank	% Similarity to 16S amplicon library[d]	% Identity to GenBank[e]
2	43.7	1.217	0.16	5.53	87.20	3.2	50	*Methanobacteriaceae*	Family	N/A[f]	
3	70.8	2.374	0.67	8.56	96.64	2.1	0	*Deferrisoma camini*	Species	100	87.0
7	31.2	2.388	0.87	15.88	92.90	0.55	0	*Ignavibacteriales*	Order	100	85.5
9	68.1	1.955	0.22	4.25	56.01	6.27	0	*Chthonomonas calidirosea*	Species	N/A	
11	66.3	4.226	1.11	8.75	97.27	3.36	0	*Anaerolinea thermophila*	Species	100	88.4
12	36.2	2.670	0.68	9.81	96.72	4.37	44.44	*Ignavibacteriales*	Order	100	86.8
13	68.0	1.910	0.37	6.23	79.72	2.14	33.33	*Thermoanaerobaculum*	Genus	100	99.0
14	33.3	2.007	0.48	11.97	98.19	0.88	0	*Calditerrivibrio nitroreducens*	Species	N/A	
16	38.7	2.507	3.49	60.66	95.79	0.55	0	*Ignavibacteriales*	Order	100[g]	84.4
17	60.0	2.869	1.53	20.17	98.10	1.71	0	*Sideroxydans lithotrophicus*	Species	100[g]	95.2
20	32.3	2.163	0.29	6.04	50.68	12.93	0	*Ca.* Endomicrobium	Genus	N/A	
21	38.0	1.188	0.14	5.13	75.62	1.7	50	*Planctomycetaceae*	Family	98.8	78.1
22	49.0	3.076	10.41	148.08	98.36	1.91	0	*Pelodictyon*	Genus	100	86.3
25	55.2	0.791	0.10	4.99	61.41	0.56	0	*Ca.* Endomicrobium	Genus	100	84.4
31	39.2	1.234	0.18	6.08	60.34	7.08	0	*Deinococci*	Class	100	92.5
33	63.8	2.709	1.54	19.42	93.47	1.39	66.67	*Methyloversatilis*	Genus	N/A	
34	60.3	5.659	7.71	59.16	99.69	2.36	75	*Roseiflexus*	Genus	N/A	
36	37.3	2.058	0.34	7.18	94.91	3.36	25	*Deferrisoma camini*	Species	100	85.0
37	69.8	2.211	0.34	5.60	80.46	4.68	42.86	*Dehalococcoides*	Genus	99.6	85.4
38	30.5	2.019	0.24	5.15	70.59	0	0	*Leptonema illini*	Species	N/A	
42	34.1	0.583	1.51	120.02	63.92	0	0	Bacteria	Kingdom	100	76.8
46	58.3	2.555	1.30	20.85	95.45	0.91	0	*Anaerolinea thermophila*	Species	N/A	
49	31.8	1.419	2.04	127.06	82.10	3.96	12.5	*Thermococcaceae*	Family	N/A	
51	39.7	1.559	0.18	5.18	71.13	1.04	100	*Thermodesulfovibrio*	Genus	100	85.6
52	37.7	1.328	0.23	7.38	92.37	0	0	*Caldisericum exile*	Species	83.1	98.3
53	42.8	1.760	0.48	11.64	97.27	0.91	0	*Thermodesulfovibrio*	Genus	N/A	
54	47.4	3.227	3.26	49.63	98.91	1.91	0	*Chloroherpeton thalassium*	Species	100[g]	86.6
56	36.6	1.883	0.68	15.21	89.33	2.25	50	*Ca.* Endomicrobium	Genus	100	80.3
59	54.9	4.124	2.64	24.71	87.46	4.62	33.33	*Anaerolineaceae*	Family	100[g]	87.2
63	29.5	0.758	0.11	6.08	85.59	0.93	100	Archaea	Kingdom	82.4	77.7
64	48.3	2.661	12.48	177.95	96.58	0.24	0	*Pseudanabaena*	Genus	100[g]	90.3
67	42.0	1.986	0.70	15.41	95.61	23.44	52.38	*Thermodesulfovibrio*	Genus	N/A	
69	58.8	2.774	0.42	6.82	99.12	0	0	*Synechococcus*	Genus	N/A	
70	34.5	0.599	0.34	24.44	71.84	0	0	*Bacteria*	Kingdom	N/A	
73	39.5	1.557	0.96	29.22	93.75	0	0	*Ca. Endomicrobium*	Genus	100	83.2

74	45.9	3.179	2.14	26.58	97.27	6.36	25	*Thermodesulfovibrio*	Genus	98.8[g]	88.9
75	56.8	1.891	0.21	4.78	76.03	1.46	60	Bacteroidetes	Phylum	100	80.8
77	33.0	1.875	0.27	5.56	65.43	1.73	50	*Ignavibacteriales*	Order	N/A	
78	44.7	1.767	2.47	65.80	94.55	0.91	0	*Thermodesulfovibrio*	Genus	N/A	
79	60.9	1.152	0.11	4.19	54.57	0.03	100	*Uliginosibacterium gangwonense*	Species	100	95.5
80	44.8	2.417	0.30	5.65	91.39	0.88	33.33	*Desulfobacteraceae*	Family	N/A	
81.1	29.9	0.991	10.46	493.44	89.10	3.74	0	Archaea	Kingdom	100	76.5
81.2	31.7	0.928	21.87	1092.94	73.49	1.49	0	*Thermococcaceae*	Family	100	76.6
sum[a]			95.99								
avg[b]				*28.61*							

[a] Total percentage of reads mapping to MAGs in the metagenomic assembly

[b] Average read coverage of the contigs in each MAG

[c] Calculated as the percent of reads mapped to a given MAG out of the total number reads for the metagenomic library

[d] Alignment between 16S rRNA gene sequences from the metagenomic assembly and the 16S rRNA gene amplicon library

[e] %Identity of 16S rRNA gene sequences from the metagenomic library aligned to the NCBI GenBank database

[f] Not applicable; no significant alignment to 16S rRNA gene amplicon library, or metagenomic 16S rRNA gene sequence on unbinned condig

[g] >1% OTU read abundance in 16S rRNA gene amplicon library

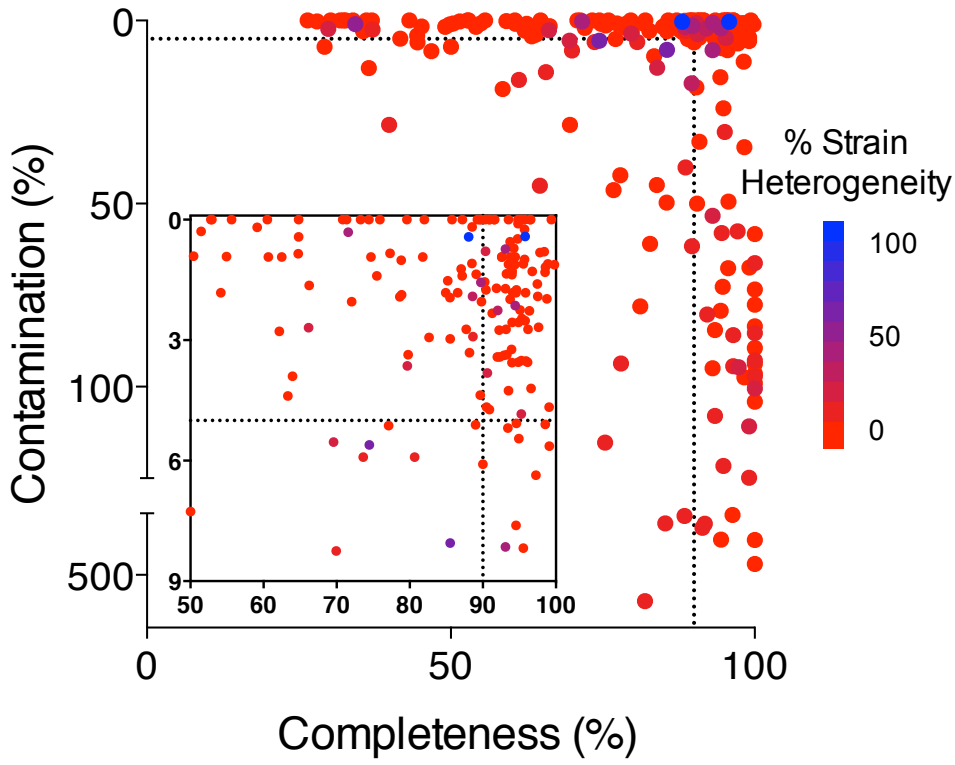

Figure A.2.1. Completeness, contamination, and strain heterogeneity calculated using CheckM for each MAG binned in CONCOCT for the CP core metagenomic co-assembly, following manual splitting of composite bins, and before removal of partially complete and very contaminated MAGs. Inset panel shows the MAGs with greater than 50% completeness and less than 10% contamination. The "contamination" statistic calculated in CheckM is a measurement of redundant marker and the additional measurement of "strain heterogeneity" is used to determine the similarity of the phylogeny of the redundant marker genes. MAGs with high contamination, along with high strain heterogeneity, represent very closely related organisms that the binning algorithm was unable to parse out (e.g. strains of the same species).

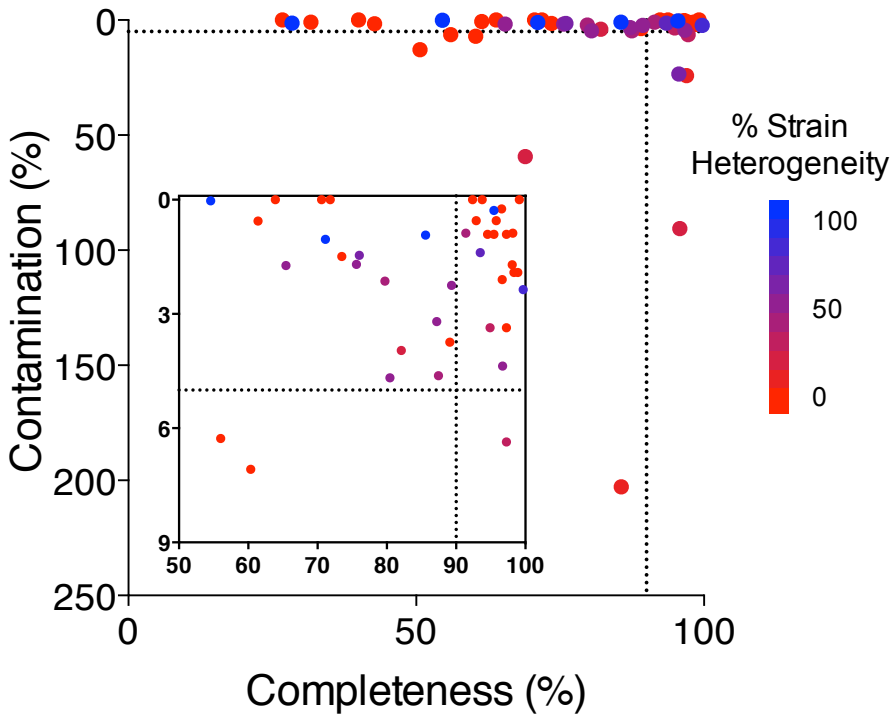

Figure A.2.2. Completeness, contamination and strain heterogeneity calculated using CheckM for each MAG clustered using CONCOCT for the CP vent pool metagenomic assembly. Inset panel shows the MAGs with greater than 50% completeness and less than 10% contamination.

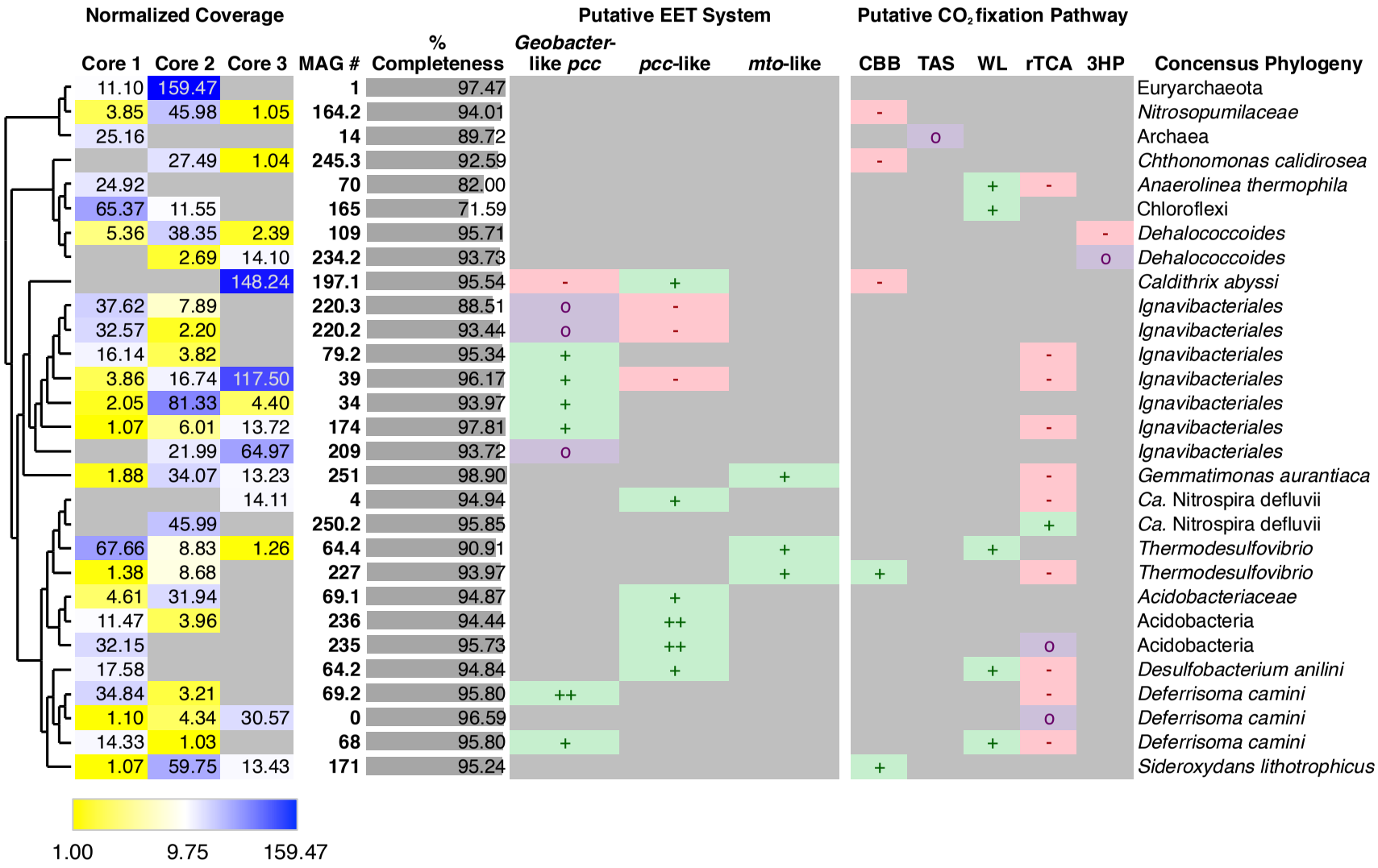
Normalized Coverage
Putative EET System
Putative CO_2 fixation Pathway
Core 1
Core 2
Core 3
MAG #
% Completeness
Geobacter-like pcc
pcc-like
mto-like
CBB
TAS
WL
rTCA
3HP
Concensus Phylogeny
11.10 159.47 1 97.47 Euryarchaeota
3.85 45.98 1.05 164.2 94.01 - Nitrosopumilaceae
25.16 14 89.72 o Archaea
27.49 1.04 245.3 92.59 - Chthonomonas calidirosea
24.92 70 82.00 + - Anaerolinea thermophila
65.37 11.55 165 71.59 + Chloroflexi
5.36 38.35 2.39 109 95.71 - Dehalococcoides
2.69 14.10 234.2 93.73 o Dehalococcoides
148.24 197.1 95.54 - + - Caldithrix abyssi
37.62 7.89 220.3 88.51 o - Ignavibacteriales
32.57 2.20 220.2 93.44 o - Ignavibacteriales
16.14 3.82 79.2 95.34 + - Ignavibacteriales
3.86 16.74 117.50 39 96.17 + - - Ignavibacteriales
2.05 81.33 4.40 34 93.97 + Ignavibacteriales
1.07 6.01 13.72 174 97.81 + - Ignavibacteriales
21.99 64.97 209 93.72 o Ignavibacteriales
1.88 34.07 13.23 251 98.90 + - Gemmatimonas aurantiaca
14.11 4 94.94 + - Ca. Nitrospira defluvii
45.99 250.2 95.85 + Ca. Nitrospira defluvii
67.66 8.83 1.26 64.4 90.91 + + Thermodesulfovibrio
1.38 8.68 227 93.97 + + - Thermodesulfovibrio
4.61 31.94 69.1 94.87 + Acidobacteriaceae
11.47 3.96 236 94.44 ++ Acidobacteria
32.15 235 95.73 ++ o Acidobacteria
17.58 64.2 94.84 + + - Desulfobacterium anilini
34.84 3.21 69.2 95.80 ++ - Deferrisoma camini
1.10 4.34 30.57 0 96.59 o Deferrisoma camini
14.33 1.03 68 95.80 + + - Deferrisoma camini
1.07 59.75 13.43 171 95.24 + Sideroxydans lithotrophicus
1.00
9.75
159.47

Figure A.2.3. The twenty highest coverage MAGs from the entire CP core co-assembly, and abundant MAGs from individual cores that encoded putative metabolic processes of interest, e.g. EET and CO_2 fixation. Metagenomic reads from individual core samples were mapped against the co-assembly to visualize how the abundance of certain MAGs changes with distance from the vent source. High-coverage (abundant) MAGs are highlighted in blue, low-coverage MAGs are in yellow, and MAGs that were below detection in a core sample (average coverage of mapped reads <1.0) are grayed out. Percent completeness of each MAG was calculated based on the presence of single-copy marker genes in CheckM. Putative phylogenetic identity of MAGs was determined by a consensus between CheckM and BLAST/MEGAN. The phylogenetic tree was produced in Dendroscope using output from CheckM. Putative EET systems were positively detected (green +) in MAGs encoding an OM porin, associated *c*-cyts, and all supplemental genes. MAGs that code for multiple sets of EET genes are indicated (green ++). MAGs encoding a homolog to the *Geobacter*-like *pcc* porin, and if no more than one of the predicted associated *c*-cyts was undetected, were considered partially complete (purple o). MAGs encoding an incomplete set of genes were considered too incomplete for further analysis (red -). For carbon fixation, MAGs that encoded a complete set of genes involved in the CBB, WL, or rTCA pathways are indicated (green +). MAGs that encoded all key marker genes, and if no more than one of the additional genes predicted for a given pathway was undetected, were classified as partially complete, and were considered to be potentially involved in CO_2 fixation (purple o). MAGs that did not encode any key marker genes were considered too incomplete for further analysis (red -). Remaining MAGs were abundant in the metagenomic co-assembly but had no obvious involvement in Fe transformation or carbon fixation. Abbreviation: *Ca*., *Candidatus*; CBB, Calvin-Benson-Bassham cycle; TAS, thiazole adenylate synthase; WL, Wood-Ljungdahl pathway; rTCA, reductive tricarboxylic acid cycle; 3HP, 3-hydroxypropionate cycle.

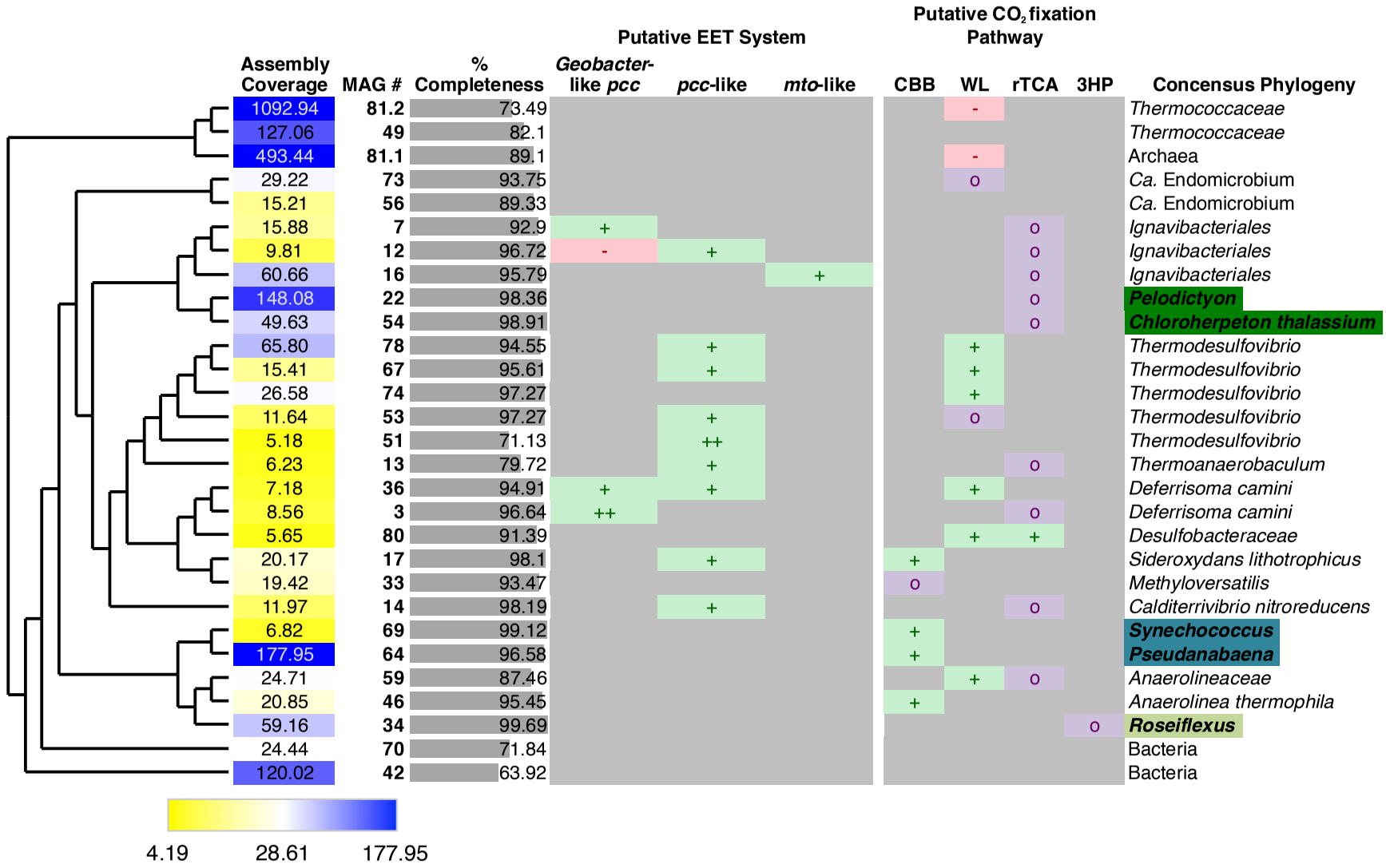
Putative EET System
Putative CO_2 fixation Pathway
Assembly Coverage
MAG #
% Completeness
Geobacter-like pcc
pcc-like
mto-like
CBB
WL
rTCA
3HP
Concensus Phylogeny
1092.94 81.2 73.49 - Thermococcaceae
127.06 49 82.1 Thermococcaceae
493.44 81.1 89.1 - Archaea
29.22 73 93.75 o Ca. Endomicrobium
15.21 56 89.33 Ca. Endomicrobium
15.88 7 92.9 + o Ignavibacteriales
9.81 12 96.72 - + o Ignavibacteriales
60.66 16 95.79 + o Ignavibacteriales
148.08 22 98.36 o Pelodictyon
49.63 54 98.91 o Chloroherpeton thalassium
65.80 78 94.55 + + Thermodesulfovibrio
15.41 67 95.61 + + Thermodesulfovibrio
26.58 74 97.27 + Thermodesulfovibrio
11.64 53 97.27 + o Thermodesulfovibrio
5.18 51 71.13 ++ Thermodesulfovibrio
6.23 13 79.72 + o Thermoanaerobaculum
7.18 36 94.91 + + + Deferrisoma camini
8.56 3 96.64 ++ o Deferrisoma camini
5.65 80 91.39 + + Desulfobacteraceae
20.17 17 98.1 + + Sideroxydans lithotrophicus
19.42 33 93.47 o Methyloversatilis
11.97 14 98.19 + o Calditerrivibrio nitroreducens
6.82 69 99.12 + Synechococcus
177.95 64 96.58 + Pseudanabaena
24.71 59 87.46 + o Anaerolineaceae
20.85 46 95.45 + Anaerolinea thermophila
59.16 34 99.69 o Roseiflexus
24.44 70 71.84 Bacteria
120.02 42 63.92 Bacteria
4.19
28.61
177.95

Figure A.2.4. The Eleven above-average coverage (28.61) MAGs from the CP vent pool assembly, and all MAGs containing putative metabolic processes of interest. High-coverage (abundant) MAGs are highlighted in blue and low-coverage bins are in yellow. The percent completeness of each MAG was calculated based on the presence of single-copy marker genes in CheckM. Putative phylogenetic identity of MAGs was determined by a consensus between CheckM and BLAST/MEGAN. The phylogenetic tree was produced in Dendroscope using output from CheckM. Putative EET systems were positively detected (green +) in MAGs containing an OM porin, associated *c*-cyts, and all supplemental genes. MAGs encoding multiple sets of EET genes are indicated (green ++). MAGs encoding an incomplete set of genes were considered too incomplete for further analysis (red -). MAGs that encoded a complete set of genes involved in the CBB or WL pathways are indicated (green +). MAGs encoding all key marker genes, and if no more than one of the additional genes predicted for a given pathway was undetected, were classified as partially complete and were considered to be potentially involved in CO_2 fixation (purple o). MAGs that did not encode any key marker genes were considered too incomplete for further analysis (red -). Putative photosynthetic MAGs are highlighted to indicate oxygenic (cyan) and anoxygenic (green sulfur bacteria, dark green; green non-sulfur bacteria, light green) phototrophs. The remaining MAGs were abundant in the metagenomic assembly but had no obvious involvement in Fe transformation or carbon fixation. Abbreviation: *Ca*., *Candidatus*; CBB, Calvin-Benson-Bassham cycle; WL, Wood-Ljungdahl pathway; rTCA, reductive tricarboxylic acid cycle; 3HP, 3-hydroxypropionate cycle.

CHAPTER 3

Geochemical and stable Fe isotopic analysis of dissimilatory microbial iron reduction in Chocolate Pots hot springs, Yellowstone National Park

Nathaniel W. Fortney[1], Brian L. Beard[1], Jack A. Hutchings[2], Michael R. Shields[2], Thomas S. Bianchi[2], Eric S. Boyd[3], Clark M. Johnson[1], and Eric E. Roden[1]

[1]Department of Geoscience, NASA Astrobiology Institute, University of Wisconsin-Madison, Madison, WI 53706
[2]Department of Geological Sciences, University of Florida, Gainsville, FL 32611
[3]Department of Microbiology and Immunology, NASA Astrobiology Institute, Montana State University, Bozeman, MT 59717

Planned submission to *Astrobiology*

ABSTRACT

Chocolate Pots hot springs (CP) is an iron (Fe)-rich, circumneutral-pH geothermal spring in Yellowstone National Park. Relic hydrothermal systems have been identified on Mars, and modern hydrothermal environments such CP are useful for gaining insight into potential pathways for and biosignatures of ancient microbial life on Earth and Mars. Fe isotope fractionation linked to dissimilatory microbial iron oxide reduction (DIR) is recognized as an indicator of microbial activity in both the rock record and modern Fe redox cycling environments. DIR produces Fe(II) which undergoes equilibrium electron and atom exchange with residual solid phase Fe(III), resulting in isotopically light Fe(II) relative to Fe(III). Previous studies in CP have demonstrated the presence of active DIR in vent pool deposits, and documented aqueous/solid-phase Fe isotope variations along the hot spring flow path that could be linked to this process. In this study we examined the Fe geochemistry and stable Fe isotopic composition of spring water and sediment core samples collected from the vent pool and along the flow path. The aim was to gain insight into whether Fe isotope ratios can inform us about microbial activity, with the ultimate goal of evaluating whether Fe isotopes can serve as a biomarker of past or present microbial activity in astrobiologically relevant hydrothermal vent systems. Despite the presence of Fe oxides along the outflow channel of CP and our previous detection of abundant putative Fe reducing bacteria along the outflow channel, our results indicate that DIR is active within but not beyond the hot spring vent pool, as revealed by the relative abundance of dilute HCl-extractable Fe(II). Fe isotope fractionation between Fe(II) and Fe(III) in the vent pool deposits was lower than in previous DIR-driven Fe isotope exchange studies and the reflects non-equilibrium conditions at CP due to high silica, rapid Fe(II) oxidation, and a high degree of microbial Fe(III) reduction. No systematic redox-associated

fractionation was observed in the more distal core samples. These findings suggest that under a modern oxygen-rich atmosphere, Fe isotope fractionation may only be a useful biosignature for active but not relic near-surface Fe cycling environments, because re-oxidation of microbially produced Fe(II) would be expected to erase any record of fractionation after cessation of DIR activity. The possibility exists, however, for preservation of Fe isotope biosignatures of DIR in vent systems like CP under conditions of low or zero atmospheric oxygen.

INTRODUCTION

Hydrothermal vent systems, both terrestrial and subaqueous, have been of astrobiological interest to researchers for the past several decades. Coinciding with the formal recognition of the domain Archaea, scientists identified hyperthermophilic Archaea and Bacteria near the branch point at the root of the phylogenetic tree of life, leading to the hypothesis that the universal common ancestor of all life was hyperthermophilic (Woese *et al.* 1990). There is still much debate over the likelihood of a high-temperature origin of life, however hydrothermal systems are regarded as being highly biologically productive environments due to the redox gradient formed between reduced hydrothermal fluids and surrounding oxidized ocean or atmosphere (Butterfield *et al.* 1997; Shock 1996; Wade *et al.* 1999). Opposing redox gradients are driver of microbial metabolism (Bird *et al.* 2011; Canfield *et al.* 2006) as either an electron donor in the case of Fe(II) oxidation (Emerson 2000; Emerson *et al.* 2010; Emerson and Moyer 1997; López-Archilla *et al.* 2001) or electron acceptor for Fe(III) reduction (Lovley 2006; Lovley 1991; Lovley *et al.* 2004; Tor *et al.* 2013). The fact that many of the aforementioned deeply rooted hyperthermophilic Archaea and Bacteria contain Fe redox based metabolic pathways suggests that Fe(III) reduction (Vargas *et al.* 1998) and Fe(II) oxidation (Hafenbradl *et al.* 1996) are ancient metabolic processes.

The history of Fe-based metabolic processes on Earth and the presumably early evolution of these pathways along with the presence of redox gradient in the Martian surface created by the presence of both oxidized and reduced Fe mineral species make Fe-based microbial life a reasonable candidate when looking for life in astrobiologically relevant settings, e.g. Mars. Furthermore, the discovery of opaline silica deposits have been at Gusev Crater by the *Spirit* rover (Squyres *et al.* 2008) and Vernal Crater by the Mars Reconnaissance Orbiter (Allen and

Oehler 2008) has been interpreted to suggest relic hydrothermal activity on the Martian surface. The surface conditions of modern Mars (low pressure, high radiation, low water activity) are not amenable to extant life and as such may necessitate a means of identifying evidence of ancient microbial activity, such as Fe isotope geochemistry.

There are four stable isotopes of Fe with an estimated percentage of occurrence in the Earth's crust at ^{54}Fe 5.84%, ^{56}Fe 91.76%, ^{57}Fe 2.12% and ^{58}Fe 0.28% and isotopic compositions are typically reported in δ^{56}Fe notation, which is the parts-per-thousand (per mil, ‰) variation of the isotope ratio ^{56}Fe/^{54}Fe (Beard and Johnson 1999; Beard *et al.* 2003). The average isotopic composition of igneous rocks has been well constrained to $\delta^{56}Fe = 0.00 \pm 0.05$‰ (Beard *et al.* 2003). Deviation from the bulk crustal isotopic values can occur when Fe undergoes redox transformations as either abiological or biological processes (Johnson *et al.* 2008b). However, processes resulting in partial redox transformation, e.g. microbial dissimilatory iron reduction (DIR), can result in a substantial isotope fractionation (Beard *et al.* 1999; Beard *et al.* 2003). The use of stable iron isotope compositions can be used to better understand the redox history of many environments and to assess the potential for relic or extant microbial activity (Beard *et al.* 1999; Dauphas *et al.* 2009; Johnson *et al.* 2008b).

Studies of modern systems where active Fe redox cycling is occurring can provide insight into how such processes could have occurred in similar environments on early Earth or Mars. High-temperature, low-pH hydrothermal systems (Kozubal *et al.* 2012) and low-temperature, neutral-pH Fe seeps (Blöthe and Roden 2009; Haaijer *et al.* 2008; Roden *et al.* 2012) have been well studied in terms of Fe geochemistry and metabolic processes occurring in the microbial community (i.e. Fe redox cycling). However, the microbial community and geochemistry of higher temperature, neutral-pH systems is understudied. These systems are of particular interest

in astrobiology research because of the potential energy source for microbial life and conditions may be more favorable for the evolution of life as compared to higher temperature and lower pH systems.

Chocolate Pots hot springs (CP) are a collection of Fe- and Si-rich circumneutral-pH thermal springs located in northwestern Yellowstone National Park. One of the prominent and well-studied features (Fig. 3.1) has been studied since the early twentieth century (Allen and Day 1935). For over a decade researchers have studied CP with an interest in indirect Fe(II) oxidation by biogenic oxygen (i.e. cyanobacterially derived) as a model system for the deposition of Archean banded iron formations (BIFs) (Pierson and Parenteau 2000; Pierson *et al.* 1999) and biosignature preservation (e.g. microfossils and lipids) (Parenteau and Cady 2010; Parenteau *et al.* 2014).

Previous studies in CP have demonstrated the presence of active dissimilatory microbial iron reduction (DIR) in the vent deposits (Fortney *et al.* 2016; Fortney *et al.* 2018a; Fortney *et al.* 2018b), and documented aqueous/solid-phase Fe isotope variations along the hot spring flow path (Wu *et al.* 2013) that could be linked to DIR. Here we expand upon these studies by exploring the bulk Fe geochemistry and Fe isotopic composition of aqueous and solid-phase materials collected from core samples taken along a transect moving away from the main hot spring vent. Additional incubations of native Fe(III) oxides were conducted to constrain expected Fe isotope fraction linked to DIR with the goal of understanding how the potential preservation of biosignatures (i.e. Fe isotope ratios) can inform on past ecosystems on Earth or Mars. Our results suggest that DIR is active near the vent outlet, and that this process generates a substantial pool of isotopically light solid-phase Fe(II) (relative to the residual Fe(III) pool) that is retained in the vent deposits. However, our findings do not support the previous hypothesis (Wu *et al.*

2013) that DIR provides an internal source of isotopically light Fe(II) along the main flow path of the hot spring.

MATRIALS AND METHODS

Sample collection. Six sediment cores were collected in August 2013 starting at approximately halfway down the flow path and every 1-2 m toward the vent pool (Fig. 3.1). Cores were collected in acrylic plastic tubes and both ends were sealed with butyl rubber stoppers immediately upon removal to prevent atmospheric oxidation of Fe(II) phases within the core samples. Sealed core tubes were then placed on dry ice. Prior to core collection, temperature and pH were measured, and spring water was collected at each sampling site and acidified to 0.5 M HCl to stabilize aqueous Fe(II). An aliquot of acid-stabilized spring water was used to determine the Fe(II) concentration at each sampling site using the *Ferrozine* (Fz) method (Stookey 1970).

Sample processing. Core samples were thawed in an anaerobic chamber, then extruded and sectioned into 1 cm depth intervals. Subsections were divided in half and a portion was frozen at -80°C for DNA extraction (Fortney *et al.* 2018a). The remaining material was subjected to a sequential HCl extraction according to previously published methods (Fortney *et al.* 2016), with the following exceptions. 1) Due to the low volume of pore fluid in the core samples, separation of the aqueous Fe phase by centrifugation was not feasible. Samples were therefore mixed with an equal mass of artificial spring water (ASW) (Fortney *et al.* 2016) followed by centrifugation and acidification of the supernatant to a final concentration of 0.5 M HCl. The Fe content of this phase (referred to hereafter as ASW-extractable Fe) was assumed to be equivalent to the aqueous Fe content *in situ*. 2) Following sequential Fe extraction using 0.01 M HCl and

0.5 M HCl, a final 24 hr 6 M HCl extraction was conducted on the residual material in order to analyze the total HCl-extractable Fe pool, including potential crystalline phases (Fig. A.3.1). Fe concentration for all phases was determined using Fz.

Incubation experiment. A Fe(III)-reducing incubation experiment was conducted to provide constraints on interpretations of *in situ* Fe isotope compositions. Duplicate serum bottles were prepared with a slurry of native CP Fe/Si oxides collected from the bottom of the CP vent pool in October 2014 and incubated as described previously (Fortney *et al.* 2018b). Incubations were sampled periodically for up to 72 d. Immediately following sample collection, a sequential HCl extraction was conducted on these samples as described above, except here aqueous Fe(II) was recoverable by centrifugation prior to the dilute HCl extraction, and the samples were extracted for 1 hr in 0.01 M HCl rather than 15 min.

Stable Fe isotope analysis. Sequential extraction of samples from the CP cores and Fe(III)-reducing incubation experiment was used to measure the isotopic composition of four pools of Fe. Aqueous dissolved Fe(II) was separated by centrifugation or extracted with ASW, 0.01 M HCl was used to remove the sorbed Fe(II) component, 0.5 M HCl was used to remove the outer layer of Fe(III) which represented the reactive Fe layer, that is, the portion of the Fe oxide that undergoes isotopic exchange with the sorbed Fe pool, and finally 6 M HCl was used to dissolve the remaining Fe oxide for the isotopic composition of the bulk substrate.

Fe isotope compositions are reported in standard δ notation:

$$\delta^{56}\text{Fe}\ (‰) = [(^{56}\text{Fe}/^{54}\text{Fe})_{\text{sample}} / (^{56}\text{Fe}/^{54}\text{Fe})_{\text{standard}} - 1] * 10^{3} \qquad (1)$$

where the $^{56}Fe/^{54}Fe_{standard}$ is the average isotopic composition for igneous rocks, $\delta^{56}Fe = 0.00 \pm 0.05‰$ (Beard *et al.* 2003).

The isotopic composition of the system, that is, the isotopic composition of all phases extracted from a given sample can be represented by a simple mixing model defined by the sum of the mole fraction of the isotopic composition for all phases extracted from a single sample as described by (Welch *et al.* 2003):

$$\delta^{56}Fe_{system} = (X_{Aq})(\delta^{56}Fe_{Aq}) + (X_{0.01\ M\ HCl})(\delta^{56}Fe_{0.01\ M\ HCl}) + (X_{0.5\ M\ HCl})(\delta^{56}Fe_{0.5\ M\ HCl}) + (X_{6\ M\ HCl})(\delta^{56}Fe_{6\ M\ HCl}) \quad (2)$$

Note that in Equation 2 "Aq" can represent either the true aqueous Fe(II), as is the case in the incubation study, or the ASW-extracted Fe phase from the core samples.

Approximately 100 μg Fe from each phase of the sequential HCl extraction of the core samples was processed through two rounds of anion-exchange chromatography (Beard *et al.* 2003). Processed samples were analyzed at a total Fe concentration of 600 ppb Fe by MC-ICP-MS using either a Micromass *IsoProbe* or a Nu Instruments *Nu Plasma II*, according to previously published methods (Beard *et al.* 2003; Reddy *et al.* 2015). Based on the results of Fe isotope analyses on ultrapure Fe standards, there is no difference between the isotope compositions measured using either instrument. The following Fe isotope compositions of the ultrapure standards analyzed using the *IsoProbe* were obtained: IRMM-014: $\delta^{56}Fe = -0.06 \pm 0.06‰$ (2σ; $n = 28$), J-M Fe: $\delta^{56}Fe = 0.26 \pm 0.08‰$ (2σ; $n = 28$), and HPS-II: $\delta^{56}Fe = 0.51 \pm 0.08‰$ (2σ; n=19). Fe isotope compositions of ultrapure standards analyzed using the *Nu Plasma II* were: IRMM-014: $\delta^{56}Fe = -0.08 \pm 0.07‰$ (2σ; $n = 28$), J-M Fe: $\delta^{56}Fe = 0.23 \pm 0.06‰$ (2σ; n =

29), and HPS-II: $\delta^{56}Fe = 0.46 \pm 0.07‰$ (2σ; $n = 11$). Accuracy of the measured Fe isotopic ratios was determined using matrix-matched test solutions of a known isotopic composition. Briefly, effluent from the first round of anion-exchange chromatography of an experimental sample was spiked with 100 μg HPS-II, and processed through the entire analytical process as with the rest of the experimental samples, and isotopic composition of the test solution was compared to that of the pure standard. Fe isotopic composition of the test solutions analyzed on the *IsoProbe* was: $\delta^{56}Fe = 0.46 \pm 0.07‰$ (2σ; $n = 19$), which is identical to the measured isotope composition of the standard, within error. Fe isotopic composition of the test solutions analyzed on the *Nu Plasma II* was $\delta^{56}Fe = 0.48 \pm 0.10‰$ (2σ; $n = 16$) which is also identical, within error, to the measured composition of the pure standard. External precision was estimated by the average standard deviation of replicate samples run through the entire analytical process. Three numbers are reported here because several samples were reprocessed and analyzed on the *Nu Plasma II* after previously having been analyzed on the *IsoProbe*. Estimates of precision are as follows: *Isoprobe*: ± 0.06‰ (2σ; $n = 5$), *Nu Plasma II*: ± 0.11‰ (2σ; $n = 7$), both: ± 0.13‰ (2σ: $n = 2$). In total, 179 Fe isotope ratios were measured on the *Isoprobe*, and 39 were measured on the *Nu Plasma II*, yielding an average reproducibility of replicate analyses on both instruments of ± 0.09‰ (2σ; *Isoprobe* $n = 61$; *Nu plasma II* $n = 32$).

Sequentially extracted Fe from the Fe(III)-reducing incubation study was purified through two rounds of anion exchange chromatography (Beard *et al.* 2003). Processed samples were analyzed at 600 ppb or 1000 ppb Fe by MC-ICP-MS using a Nu Instruments *Nu Plasma II*, according to previously published methods (Reddy *et al.* 2015). The following Fe isotope compositions of ultrapure standards were obtained: IRMM-014: $\delta^{56}Fe = -0.08 \pm 0.07‰$ (2σ; $n = 50$), J-M Fe: $\delta^{56}Fe = 0.23 \pm 0.09‰$ (2σ; $n = 52$), HPS-I: $\delta^{56}Fe = 0.45 \pm 0.13‰$ (2σ; $n = 6$), and

HPS-II: $\delta^{56}Fe = 0.48 \pm 0.07‰$ (2σ; n = 50). Due to the exceedingly low quantity of Fe in the aqueous Fe phase (4.3 ± 2.2 μg), accuracy of the measured Fe isotopic ratios was determined using matrix-matched test solutions containing 2-100 μg Fe of a known isotopic composition. Effluent from the first round of anion-exchange chromatography of an experimental sample, or artificial spring water was spiked with HPS-I, -II, or IRMM-014. Isotopic composition of the test solutions was determined separately for "low Fe" (≤10 μg Fe), and "high Fe" (>10 μg Fe) samples. Low Fe HPS-I: $\delta^{56}Fe = 0.58 \pm 0.20‰$ (2σ; n = 6), high Fe HPS-I: $\delta^{56}Fe = 0.48 \pm 0.15‰$ (2σ; n = 51), low Fe HPS-II: $\delta^{56}Fe = 0.41 \pm 0.21‰$ (2σ; n = 14), high Fe HPS-II: $\delta^{56}Fe = 0.44 \pm 0.08‰$ (2σ; n = 8), low Fe IRMM-014: $\delta^{56}Fe = 0.02 \pm 0.10‰$ (2σ; n = 2), and high Fe IRMM-014: $\delta^{56}Fe = -0.10 \pm 0.08‰$ (2σ; n = 12). External precision was determined separately for low and high concentration Fe samples, and overall precision for all samples. Precision estimates are as follows: low Fe: ± 0.18‰ (2σ; n = 30), high Fe: ± 0.14‰ (2σ; n = 90), overall: ± 0.14‰ (2σ; n = 120). The Fe isotope ratio was measured on a total of 95 sequentially extracted Fe samples, yielding an average reproducibility on replicate analyses of ± 0.08‰ (2σ; n = 91).

X-ray diffraction analysis. Samples for X-ray diffraction (XRD) were prepared from an aliquot of Fe/Si oxide sediment retained from the material preserved for DNA extraction. Samples (n =18) were chosen from the top, bottom, and a middle subsection from all cores and dried at 80°C under an oxic atmosphere for 2 hr, powdered and mounted in thin-walled capillary tubes. Spectra were collected using a Rigaku D/Max Rapid II diffractometer (Rigaku Americas, The Woodlands, TX, USA) with a two-dimensional imaging plate operating at 50 keV and 50 mA with a Mo Kα X-ray source. Scans were integrated over 15 minutes. Diffraction patterns were converted to conventional intensity patterns using the Rigaku 2DP software, and peaks were identified using the Jade 9 software package (KS Analytical Systems, Aubrey, TX, USA).

Organic carbon analysis. A small sediment core (ca. 1 x 10 cm) was collected from the vicinity of the CP vent in October 2015 using the same techniques as described previously. Additional samples of sediment were collected along the hot spring flow path from previous core sampling sites. Headspace on the sediment collection jars was degassed with N_2 and frozen on dry ice along with the core sample. Spring water was collected from the CP vent pool using a peristaltic pump while bubbling the sample jar with N_2 to maintain anoxia. Samples of plant biomass (e.g. grasses, pine needles) were collected from the area immediately surrounding the CP vent pool for comparison to lipid biomarkers present in the CP sediment.

The core sample from the CP vent was thawed, extruded and divided into four equal subsections. CP vent core subsamples, sediment from the flow path, and plant biomass was frozen on dry ice and sent to University of Florida. CP sediment was freeze-dried prior to elemental analysis (carbon and nitrogen), lipid, lignin and pigment analyses. A portion of the CP Fe oxide sediment from the vent and flow path (ca. 20-50 mg) was analyzed for total nitrogen (TN), total carbon (TC) and total inorganic carbon (TIC). Total organic carbon (TOC) in the CP sediment was calculated by the difference between TC and TIC. Carbon isotope ratios of the CP sediment sample was determined using isotope ratio mass spectrometry (IRMS).

Lipids were extracted from CP sediments using multiple rounds of liquid-liquid extractions using aqueous and organic solvents to isolate alkanoic (fatty) acids and polar fractions. Briefly, fatty acids were saponified by base hydrolysis using 0.5 M KOH in methanol, followed by the addition of a 5% w/v NaCl solution in H_2O, and liquid-liquid extraction using hexane. Hexane extraction was repeated three times, followed by acidification to pH 1-2 using HCl, and another liquid-liquid extraction using 4:1 hexane:dichloromethane to isolate the isolate the saponified fatty acid phase. Resultant phases were analyzed and characterized using GC-MS.

Quantification of lignin monomers (vanillyl, syringyl, and cinnamyl [VSC]) by GC-MS was used to measure the concentration of lignin in the CP core and sediment samples. A qualitative estimate of the degree of degradation of the lignin was determined by the ratio of carboxylic acid (Ad) functional groups relative to aldehyde (Al). A higher ratio (AdAl value) is indicative of a greater amount of lignin degradation.

Spring water from the CP vent pool was passed through a 0.2 μm polyether sulfone filter to remove any solid-phase Fe or particulate organic matter. TOC concentration in the filtrate was measured at the University of Wisconsin Water Science and Engineering Laboratory using a General Electric Sievers M5310C Laboratory TOC analyzer.

RESULTS AND DISCUSSION

Description of Chocolate Pots hot springs. CP is located about 5 km southwest of the Norris Geyser Basin and is comprised of a number of features along both sides of the Gibbon River. The focus of this study is limited to one prominent feature along the southern bank of the river (Thermal ID: GCPNN002; 44.71008, -110.7413). Source waters emanating from the spring are ~50°C and slightly acidic, ca. pH 6. Spring water decreases in temperature and increases in alkalinity as it flows down the mound toward the river (Table 3.1). The spring water is anoxic at the vent source and contains high concentrations of dissolved Fe and Si at approximately 0.1 mM and 2.5 mM, respectively, (Parenteau and Cady 2010). The source of Fe and Si in the spring water is thought to be from leached bedrock as oxidized meteoric water mixes with reduced sulfide rich volcanic gases at depth, which allows for oxidation of the sulfide and generation of slightly acidic conditions before emerging from the hot spring vent (Colman *et al.* 2018;

McCleskey *et al.* 2010). The composition of the spring water has remained fairly consistent over the past several decades since CP was first described (Allen and Day 1935).

Aqueous and solid-phase chemistry of the cores. *Visual assessment of CP core samples.* Visual observations were made of the six thawed CP core samples during sectioning in an anaerobic chamber. Core 1 was sampled at the hot spring vent and sample collection extended away down the outflow channel (cores 2 through 6). Core descriptions were supplemented with observations made of a subset of core samples dried for XRD analysis.

Core 1) Overall core was dark brown with a fine sandy consistency. Visible organic matter (e.g. pine needles and twigs) was present in the top 2 cm of the core along with much darker coloration, possibly due to high organic carbon content. Core material transitioned to a lighter, green-brown color about halfway down. Core consistency immediately below was much coarser, where approximately 50% of the core material consisted of sand-sized, light-colored grains, ca. 1-2 mm, and some fine gravel sized clasts ≤ 5 mm surrounded by dark material. The bottom few centimeters of the core contained more dark clay-like material, but was also intermixed with a few larger black, and white/gray grains 2-4 mm in size making up about 25% of the core material.

Core 2) Core material was red-brown in color with a clay-like consistency. A few coarse sand-sized clasts were intermixed throughout. Core material became drier with increased depth.

Core 3) Core had a predominantly clay-like consistency throughout, and no grains larger than fine sand-sized grains (ca. 250 μm) were observed.

Core 4) Core contained a large amount of pore fluid throughout its depth with the consistency of wet mud. Core material was bright orange in color throughout and no grains larger than fine sand-sized were observed.

Core 5) Overall core was dry and did not slice easily into subsections, but rather flaked and crumbled apart. Core material was darker in color than cores more proximal to the Vent, with the exception of core 1. The bottom 2 cm of the core contained <10% dark brown fine gravel-sized grains.

Core 6) Core contained a relatively high amount of pore fluid and had the consistency of wet clay when slicing and sub-sectioning. Starting about halfway down the core, fine sand-sized white flakey grains made up about 5% of the core material. Grains increased to coarse sand-sized at the bottom of the core and comprised about 10% of the core material, and reflects the interface between the Fe(III) oxides and underlying Lava Creek Tuff.

Organic carbon analysis. Organic carbon concentration in the CP spring water ranged from 3-33 mg L^{-1} with an average of 13.0 mg L^{-1}. Organic carbon content of the CP core and sediment ranged from ca. 0.4-1.0 wt% TOC with an average of 0.56 wt% TOC. Total inorganic carbon was not measureable in the CP core or at core site 3. Total inorganic carbon concentrations at the remaining core sites ranged from 0.14-0.47 wt% TIC. Total nitrogen averaged 0.06±0.03 wt% TN for all core and sediment samples. Detailed results are presented in Table A.3.1 and A.3.2.

Carbon isotope composition of the sediment collected from the CP vent and along the flow path was relatively constant, $\delta^{13}C$ = -24.5‰ to -26.4‰, V-PDB. This was well within the expected range of carbon isotope ratios for photosynthetic biomass from C3 plants ((Kohn 2010) and references therein) (e.g. trees and temperate grasses) and cyanobacteria (Estep 1984). The liquid-liquid extractions used to isolate fatty acid lipids resulted in an interfacial layer between the organic and aqueous layers (Fig. A.3.2), indicating a potential iron-organic complex.

The core sample collected from the CP vent pool in 2015 contained relatively low concentrations of total VSC lignin, suggesting an overall low input of plant detritus. Concentration did not vary with depth in the core. VSC lignin concentrations were comparable in sediment collected from core sites 4-6, enriched at core site 2, and essentially absent at core site 3. Sediment samples from the flow path (core sites 2-6) were enriched in the vanillyl lignin monomer relative to the CP core sample, suggesting a greater degree of lignin degradation further downstream.

The concentrations and range of grade from fresh (AdAl value = ca. 0.3) to relatively degraded (AdAl value = ca. 0.6) of VSC lignin in the CP core and sediment samples suggests a variable amounts of input and lignin degradation at CP, and is potentially controlled by the geometry and other properties (e.g. temperature) of the hot spring. One can imagine that the depth of the CP vent pool and turbulence from upwelling spring water does not allow for plant matter detritus to settle to the bottom of the pool, and any influx of lignin-bearing biomass is flushed out of the vent pool. Downstream, the depth of the flow path channel is greatly reduced thus allowing for plant detritus to become “stuck” in the sediment (Fig. A.3.3). The greater degree of lignin degradation observed in sediment from core sites 4-6 may in part be due to the temperature decrease with distance from the CP vent. While thermophilic lignin degrading fungi have been identified (Salar and Aneja 2007), the relatively cooler temperatures of the distal CP flow path (ca. 42-48°C) may be more amenable to the growth of these organisms rather than locations proximal to the vent (ca. 50-52°C). The fungal community native to CP is understudied, and more thorough investigation is required to identify which organisms are present and what role they may have in providing carbon for the heterorophic prokaryotic community at CP.

Mineralogical analysis of Fe/Si oxide sediment. The top and bottom of each core along with a sample corresponding to the approximate transition zone in the middle of the core were analyzed by XRD for changes in mineralogy along the depth profile. This transition is most likely due to dewatering, compaction and maturation of the Fe/Si oxides. Offering further support to this explanation, the majority of the core samples (e.g. cores 2-5) only contained amorphous Fe oxides, with no obvious change in mineralogy in the middle of the core where the consistency change was observed (Fig. 3.2). While more crystalline phases (e.g. quartz, goethite, and magnetite) were identified in the sediment core samples (primarily cores 1 and 6, Fig. 3.3), we propose the origins of these minerals are as follows.

1) Maturation of the amorphous Fe oxide to the more stable phase goethite with depth (Blesa and Matijević 1989; Scheinost 2005). Although researchers have demonstrated that high silica concentrations reduces the transformation of amorphous Fe(III) oxides to more crystalline phases ((Jones *et al.* 2009) and references therein), this offers a reasonable explanation for the overall low goethite signal in the cores.

2) Incorporation of material from the underlying Lava Creek Tuff when the coring tubes reached refusal depth on the bedrock, hence presence of the coarse sand/fine gravel sized grains that were observed during core processing. The presence of magnetite in soils is interpreted as being inherited from the parent material (Scheinost 2005) and is a reasonable expectation in CP. Phenocrysts of quartz, and to a lesser extent, Fe-rich hornblende, and magnetite have been identified in the silica-rich rhyolitic tuff (Christiansen 2001; Christiansen and Blank Jr. 1972).

3) The presence of magnetite and quartz grains in the middle sections of cores 1 and 5 is potentially explained by eroded material entering the CP vent pool via rainwater runoff, followed by burial in precipitated amorphous Fe/Si oxides.

Although microbial activity (e.g. DIR) is present at the CP vent (Fortney *et al.* 2018a; Fortney *et al.* 2018b), and although magnetite formation by dissimilatory iron-reducing bacteria (DIRB) is well documented in laboratory experiments (Lovley *et al.* 1993; Lovley *et al.* 2004; Lovley *et al.* 1987; Roden and Lovley 1993), the formation of magnetite via DIR is less well characterized *in situ* (Gibbs-Eggar *et al.* 1999; Percak-Dennett *et al.* 2013), and the distribution of magnetite throughout the CP environment is not reflective of the distribution of microbial activity (Fig. 3.3), i.e. the highest magnetite signal was at the bottom of core 6 where there is no microbial activity (described in more detail below), and no magnetite was identified at the surface of core 1 where the highest microbial activity has been documented (Fortney *et al.* 2018b).

Core 1 bulk Fe geochemistry. The properties of core 1 collected from the hot spring vent stand apart from the more distal core samples from along the CP flow path. This has been demonstrated previously in the context of microbial community composition and putative metabolic processes occurring *in situ* (Fortney *et al.* 2018a; Fortney *et al.* 2018b). Here we have observed striking differences in the bulk Fe geochemistry and isotopic composition of samples derived from core 1 and therefore discuss it separately from the rest of the CP cores.

One of the geochemical hallmarks of DIR is the production of high concentrations of Fe(II) which can be separated into sorbed and aqueous phases. Qualitatively, the volume of pore fluid varied considerably between the different sediment core samples and with respect to depth, however it was not sufficient to be isolated by centrifugation. The ASW extracted Fe phase was thus taken to represent aqueous Fe in the pore fluid. The ASW phase contained relatively high Fe(II)/Fe total ratios (ca. 0.5) although only down to 3 cm depth, and in deeper samples the ratio decreased to ca. 0.1 (Fig. 3.4). Interestingly, this depth also corresponds to the depth past which

Thermodesulfovibrio-related bacteria, one of the hypothesized active DIRB, is no longer present as part of the microbial community (see Supplemental Material in (Fortney *et al.* 2018a)). The apparent correlation of Fe concentration and DIRB may be an indication of the depth to which the active microbial community extends into the CP mound. The sorbed Fe phase (0.01 M HCl extracted) was constant with respect to depth and predominantly comprised of Fe(II), with Fe(II)/Fe total ratios of ca. 0.75, and the concentrations (ca. 10 mmol L^{-1}, Fig. 3.5) were comparable to concentrations of sorbed Fe(II) measured in previous Fe(III)-reducing incubation experiments (Fortney *et al.* 2016)). Total Fe concentration in core 1 gradually decreased with depth, and overall contained the least amount of Fe out of all core samples (Fig. 3.6).

Bulk Fe geochemistry of other CP sediment cores and fluid. Fe(II) oxidizes and precipitates out of the CP spring water quickly within a few meters of the spring vent (i.e. core site 3) and is essentially nonexistent in the surface fluid beyond this point along the flow path (Fig. 3.7). Overall the Fe geochemistry of the core samples downstream of the vent does not support the presence of active Fe(III) reduction activity. For example, compared to core 1, the concentration of Fe(II) extracted from the all phases from the more distal core samples was low (<1 mmol L^{-1}) (Fig. 3.5) and Fe(II)/Fe total ratios were effectively zero. DIR is expected to produce high quantities of aqueous and 0.01 M HCl-extractable Fe(II), and the lack of Fe(II) in these phases extracted from the more distal core samples provides evidence that this process is not occurring. Of further note, the constancy of the Fe pools with respect to depth suggests Fe(III) reduction is not occurring deeper within the Fe/Si oxide sediments of the CP mound either (Fig. 3.4-3.6), as had previously been hypothesized (Wu *et al.* 2013).

While the geochemistry of core 6 at depth was quite distinct from the deeper subsections of the upstream core samples, we suggest that this is not a reflection of DIR, but rather reveals a

composite mixture of the Fe/Si-oxides precipitated from the CP spring water and the underlying Lava Creek Tuff. Although higher concentrations of Fe(II) were observed (ca. 100 mmol L^{-1}), this was limited to the 0.5 M HCl-extracted Fe phase in bottom of core 6 and not the ASW or 0.01M HCl-extracted phases where we would expect to see an increase in Fe(II) concentration as a signal of DIR (Crosby *et al.* 2005; Crosby *et al.* 2007; Fortney *et al.* 2016; Johnson *et al.* 2008b; Percak-Dennett *et al.* 2011; Tangalos *et al.* 2010). As described above, this transition from CP oxide to tuff was observed visually at mid depth with an increasing amount of clastic material. This was apparent geochemically by an increase in Fe(II)/Fe tot ratio and Fe(II) concentration (Fig. 3.4 and 3.5), and this transition region was reflected in the XRD spectra, and Fe isotope composition (see below).

Isotopic analysis of CP sediment cores and incubation. *Fe(III)-reducing incubation experiment.* We conducted an incubation experiment with a slurry of CP Fe/Si oxides inoculated with a small quantity of the CP vent sediment hosting the native microbial community in order to provide constraint on our interpretation of the Fe isotopic composition of the sediment cores. Fe(II) content in the aqueous phase increased quickly with the onset of DIR (Fig. 3.9). Fe extracted using 0.5 M HCl was a mixture of Fe(II) and Fe(III), with the Fe(II)/Fe total ratio increasing from ca. 0.25, to ca. 0.75 by the time microbial activity ceased.

The isotopic composition of Fe(II) in the aqueous and 0.01 M HCl extractable pools was ca. 1.5-2‰ lighter than the bulk residual Fe (Fig. 3.10A). Raw isotopic data for samples from the Fe(III)-reducing experiment are available in Table A.3.3. A mass balance approach was taken to calculate the isotopic composition of the pure Fe(III) component of the 0.5 M HCl extracted Fe which represents the reactive Fe(III) pool following the work of other researchers, e.g. (Crosby

et al. 2007; Percak-Dennett *et al.* 2011). The mass balance of the measured isotopic composition of total Fe in the 0.5 M HCl extracted phase can be represented by the following equation:

$$\delta^{56}Fe_{Fe0.5\ M\ HCl} = (X_{Fe(II)0.5\ M\ HCl})(\delta^{56}Fe_{Fe(II)0.5\ M\ HCl}) + (X_{Fe(III)0.5\ M\ HCl})(\delta^{56}Fe_{Fe(III)0.5\ M\ HCl}) \quad (3)$$

Using the $\delta^{56}Fe_{Fe(II)}$ value measured in the 0.01 M HCl extracted phase as the assumed isotopic composition for $\delta^{56}Fe_{Fe(II)}$ in the 0.5 M HCl extracted phase, the isotopic value of the pure Fe(III) component can be calculated by rearranging the equation thus:

$$\delta^{56}Fe_{Fe(III)0.5\ M\ HCl} = (\delta^{56}Fe_{Fe0.5\ M\ HCl}-(X_{Fe(II)0.5\ M\ HCl})(\delta^{56}Fe_{Fe(II)0.01\ M\ HCl}))/(1-X_{Fe(II)0.5\ M\ HCl}) \quad (4)$$

Using these equations, fractionation between $Fe(II)_{aq}$ and $Fe(III)_{0.5\ M\ HCl}$ phases was ca. -1.5 to -2.5‰ (Fig. 3.10B) and decreased to close to 0‰ by day 20, corresponding the cessation of DIR (Fig. 3.9). Fractionation between the aqueous Fe(II) pool and sorbed Fe(II) pool was calculated to be approximately 0‰ for the duration of the experiment. Calculated isotopic composition of the pure Fe(III) component of the 0.5 M HCl extracted Fe phase is presented in Table A.3.4 and the calculated $\delta^{56}Fe_{system}$ (Eqn. 2) for the Fe(III) reducing incubation is presented in Table A.3.5.

The substrates used in the Fe(III)-reducing incubation from Fortney *et al.* (2016) and the current study were fundamentally different and may have had a profound effect on the observed isotopic composition of the Fe phases and therefore the isotopic fractionation. Fortney *et al.* (2016) collected Fe/Si oxides from one of the satellite vents at CP and crushed, sieved and

resuspended the material in DI H_2O to produce a slurry of fully oxidized Fe(III) for the incubation experiment. Because of the substrate preparation method, no Fe(II) was present at the beginning of the incubation. All subsequent aqueous and sorbed Fe(II) phases produced as a result of DIR are in equilibrium as they form, and are in free isotopic exchange with each other as well as the Fe(III) substrate. Whereas in the current study, Fe/Si oxides were collected from the main vent at CP and diluted with two volumes of additional CP fluid from which the fine-grain material was collected via syringe and needle, this whole process was conducted under anoxic conditions (see Fortney *et al.* (2018b) for detailed methods). As such, preexisting Fe(II) was present in the system prior to the onset of DIR (Fig. 3.9). The isotopic composition of these preexisting Fe phases may be distinct from the composition of the Fe phases produced as a result of DIR and whether or not these phases are in isotopic communication with the rest of the system the physical or isotopic mixing of these phases could potentially produce an intermediary isotopic composition, resulting in the apparent lesser degree of fractionation at the early time points in the current study (Fig. 3.10B) as compared to previous Fe(III)-reducing experiments (Fortney *et al.* 2016).

It is important to note that the high proportion of Fe(II) relative to Fe(III) in the 0.5 M HCl extracted Fe phase in the current Fe(III)-reducing incubation study (Fig. 3.9) resulted in very high uncertainties (ca. ±1‰) in the calculated isotopic composition of the pure Fe(III) component of the 0.5 M HCl extracted Fe phase (Fig. 3.10A), and therefore the fractionation factors between the $Fe(III)_{0.5\ M\ HCl}$ and either $Fe(II)_{aq}$ or $Fe(II)_{0.01\ M\ HCl}$ (Fig. 3.10B). In incubation conditions with a relatively low extent of DIR (e.g. Fe(II)/Fe tot <0.2, (Fortney *et al.* 2016)) where the 0.5 M HCl extracted Fe phase is primarily Fe(III), the small amount of Fe(II) can be corrected for in this phase, and the extrapolated errors on the calculated $Fe(III)_{0.5\ M\ HCl}$ and

fractionation factors are relatively small (ca. ±0.25‰, see Fig. 3.4 in Fortney *et al.* (2016)). However in the current study, an alternative solution is required to estimate the fractionation between the Fe(II) and Fe(III) components. A plot of the $\delta^{56}Fe$ ratio of the $Fe(II)_{aq}$ and $Fe(II)_{0.01\ M\ HCl}$ phases relative to proportion of Fe(III) in the 0.5 M HCl extracted Fe phase illustrates the change in isotopic composition of the Fe phases from isotopically light Fe(II) at the onset of DIR, and approaching the composition of the starting material (ca. 0.7‰) as reduction approaches 100% (Fig. 3.11). The slope of the line of a linear regression of the data from either data set produces the change in isotopic composition of the phase from 0-100% Fe(III). This is equivalent to the fractionation between the Fe(II) phase and $Fe(III)_{0.5\ M\ HCl}$., where fractionation estimates are $\Delta^{56}Fe_{Fe(II)aq\text{-}Fe(III)0.5\ M\ HCl} = -3.2‰$ and $\Delta^{56}Fe_{Fe(II)0.01\ M\ HCl\text{-}Fe(III)0.5\ M\ HCl} = -3.5‰$. Furthermore, the difference between the two fractionation estimates can be used to infer the fractionation between the two Fe(II) phases, $\Delta^{56}Fe_{Fe(II)aq\text{-}Fe(II)0.01\ M\ HCl} = 0.3\ ‰$. The estimated $Fe(II)_{aq}$-$Fe(III)_{0.5\ M\ HCl}$ fractionation is more consistent with the fractionation calculated in Fortney *et al.* (2016) of ca. -2.5‰ to -3.5‰, and other equilibrium isotope exchange experiments ($\Delta^{56}Fe_{Fe(II)aq\text{-}amorphous\ Fe(III)} = \sim$-2‰ (Tangalos *et al.* 2010), $\Delta^{56}Fe_{Fe(II)aq\text{-}Fe/Si}$ = ca. -2.5‰ to -4‰ (Wu *et al.* 2012)). However, the $Fe(II)_{aq}$-$Fe(II)_{0.01\ M\ HCl}$ fractionation estimate is slightly positive, as opposed to the calculated fractionation in the previous experiment of ca. -0.9‰ to -1.7‰. This difference is likely due to preexisting of Fe(II) in the 0.01 M HCl extractable Fe phase resulting in a different measured isotopic ratio, and therefore fractionation. Interestingly, the $Fe(II)_{aq}$-$Fe(II)_{0.01\ M\ HCl}$ fractionation estimate of 0.3‰ from the Fe(III) reducing incubation experiment is consistent with the ASW-$Fe(II)_{0.01\ M\ HCl}$ fractionation calculated in the surficial layers of core 1 where DIR is most likely to be occurring *in situ* (ca. 0‰ to 0.5‰, Fig. 3.13B).

Fe isotope composition of the CP fluid. The $\delta^{56}Fe$ value of the CP spring water collected at the surface of each of the core sampling sites was a constant ca. -1‰ along the length of the flow path (Fig. 3.7, Table A.3.6). There was no correlation with the decreased Fe budget or the decreasing Fe(II)/Fe total ratio that occurred with distance from the hot spring vent pool. The calculated $\delta^{56}Fe_{system}$ value for the top centimeter of the cores was used to estimate the isotope composition of the corresponding solids to the surface fluids that were collected (Table A.3.7), equivalent to the $\delta^{56}Fe(III)_{am}$ measured along the CP flow path by Wu *et al.* (2013). Data between the two experiments are consistent from the proximal sampling location (Fig. 3.8) where the proportion of precipitation <0.5. Isotopic compositions deviated at more distal locations where $\delta^{56}Fe$ values for the fluid and solids measured in Wu *et al.* (2013) were isotopically lighter than measurements in the current study (Fig. 3.8). One possible explanation is the different sampling techniques used to collect the CP fluid along the flow path. Wu *et al.* (2013) passed the spring water through an in-line 0.2 μm filter and removed any suspended solid Fe(III) in the CP fluid. The filter and sample tubing were flushed with several volumes of spring water prior to sample collected in order to maintain anoxic conditions. Whereas, in the current study, samples were collected via syringe and immediately added to an acidified sample container, and the small amount of presumably colloidal Fe(III) was thereby dissolved (Fig. 3.7) and analyzed resulting in a slightly elevated isotopic composition of the fluid (Fig. 3.8). An alternate explanation is that the Fe(III) measured in the CP fluid in the current study was an artifact of the sampling process where dissolved Fe(II) in the spring water was slightly oxidized when removed via syringe or added to the sample container. Nevertheless, the difference in the isotopic composition of the two Fe phases from either experiment (i.e. $Fe(II)_{aq}$-$Fe(III)_{solid}$ fractionation) of ca. -0.25‰ to -0.5‰ (Fig. 3.8) was less than what is expected for typical

equilibrium exchange as a result of DIR in Fe/Si bearing systems of ca. -2.8‰ (Percak-Dennett *et al.* 2011) and may reflect sorption and subsequent oxidation of isotopically light Fe(II) from the CP fluid as was proposed by Wu *et al.* (2013).

Fe isotope composition of the CP sediment cores. Broadly, there was an overall decrease in the $\delta^{56}Fe_{system}$ from about 0.5‰ at the CP vent pool down to about -0.5‰ by core 3 beyond which it remained steady (Fig. 3.12). Between the top and bottom of core 6 the system isotopic composition increased by about 0.5‰ correlating with the anomalously high Fe(II) concentrations at these depths (Fig. 3.4 and 3.5). We were unable to determine the isotopic fractionation between different Fe pools from the distal core samples due to the absence of measurable Fe(II) in the ASW and 0.01M HCl-extracted phases. Thus, we focused on the isotopic composition of core 1 as a potential biomarker for DIR activity. Raw isotopic data of all CP sediment core samples is presented in Table A.3.8.

Fe extracted from core 1 using ASW and 0.01 M HCl was primarily Fe(II), however the isotopic composition of the ASW phase approached that of the system with increasing depth as the Fe(III) concentration increased in this phase (Fig. 3.4 and 3.12). As with the Fe(III)-reducing incubation experiment in the current study, the 0.5 M HCl-extracted Fe phase from core 1 was a mixture of Fe(II) and Fe(III). The isotopic composition of the pure Fe(III) component was calculated using a mass balance approach and the isotopic composition of the 0.01 M HCl-extracted Fe phase from core 1 as the assumed isotopic composition of the Fe(II) component of the 0.5 M HCl-extracted Fe (Eqn. 4, Fig. 3.13A, Table A.3.9). However, as was the case for the Fe(III)-reducing incubation, the extrapolated errors on the calculated isotopic compositions as well as fractionation factors were large, ca. ±1‰, due to the large proportion of Fe(II) relative to Fe(III) in the 0.5 M HCl extracted Fe phase. It should be noted that the Fe isotope results for the

3-6 cm depth range in core 1 were not considered in these calculations due to the anomalously low isotopic ratios measured in the 0.5 M HCl-extracted Fe pool from this interval (Fig. 3.12). These values resulted in uncharacteristically low (ca. 0 to -20‰) δ^{56}Fe values for $Fe(III)_{0.5\ M\ HCl}$ relative to the calculated isotope ratios for the rest of core 1 (Fig. 3.13). The anomalous δ^{56}Fe values were associated with exceptionally high Fe(II)/Fe total ratios (ca. 0.7-0.9; see Fig. 3.4) that were in some cases greater than Fe(II)/Fe total ratios for the 0.01 M HCl-extracted Fe phase. Although we do not know the origin of these errant values, it seems likely that the materials in question were deposited to the vent pool during a storm or other physical disturbance separate from the normal Fe/S-oxide formation and deposition process. Additionally, the 0.01 M HCl extracted Fe was a mixture of Fe(II) and Fe(III) itself (Fe(II)/Fe tot ≈ 0.75, Fig. 3.4), thereby introducing more error when this value was used to calculate the composition of $Fe(III)_{0.5\ M\ HCl}$. When the isotopic composition of the ASW and 0.01 M HCl extracted Fe versus the proportion of Fe(III) in the 0.5 M HCl Fe phase was plotted, the data did not fit a trend (Fig. A.3.4). Thus, the method for estimating the fractionation between the Fe(II) and Fe(III) phases in core 1 by the slope of the line of a linear regression of the data that was used in the Fe(III)-reducing experiment was not possible for core 1.

The calculated error was low in the ASW and 0.01 HCl extracted Fe phases, and the fractionation between these phases at the shallowest depths in core 1 (1-4 cm) was consistent with the fractionation estimated in the Fe(III)-reducing incubation (Fig. 3.11). A Fe isotope signal was present in the samples collected from core 1, however as is discussed above, the highly variable proportions of Fe(II) and Fe(III) in the Fe phases resulted in no systematic trends in the data (Fig. A.3.4), and high errors in the calculated fractionation (Fig. 3.13). Bearing this in mind, the projected uncertainties in the calculation fractionation were less in the top two cm of

core 1 (Fig. 3.13), and therefore a more reasonable representation of the Fe isotope exchange process that is taking place *in situ.* Previous microbial community analyses have suggested that putative FeRB are present and active in the surficial layers of core 1 (Fortney *et al.* 2018a; Fortney *et al.* 2018b). If we assume the *in situ* Fe(III) reduction and isotope exchange processes are equivalent to what took place in the incubation experiment, one would expect more similar trends in isotope composition. The fact that the isotopic compositions and fractionations were not the same between the CP core and incubation experiment can possibly be explained by the differences between the extents of reduction that have taken place, and the presence or absence of oxygen in the system. While the CP spring water is essentially anoxic when it exits the vent source and the Fe/Si sediments are anoxic, however CP is an open system the rapidity in which Fe(II) oxidizes and precipitation in a high Si environment has been hypothesized to prevent isotopic equilibrium from being reached, producing lower than expected isotopic fractionation (Wu *et al.* 2013). The greatest degree of fractionation can be observed at the earliest stages of DIR, and as Fe(III) reduction proceeds the fractionation between Fe(II) and Fe(III) approaches zero. Despite the uncertainties in the calculated fractionation factors, this trend was apparent in the Fe(III)-reducing incubation (Fig. 3.10). Consistent with previous incubation experiments (Fortney *et al.* 2018b), a high level of DIR activity was measurable in core 1 by the high concentration of Fe(II) relative to Fe(III) in the 0.5 M HCl extracted Fe phase (Fig. 3.4), which in turn was likely responsible for the decreased fractionation factor.

Evidence for iron isotope biosignatures at CP. The greatest fractionation between two phases is expected to be measured between $Fe(II)_{aq}$ and $Fe(III)_{reac}$, where $Fe(II)_{aq}$ is isotopically lighter and $Fe(III)_{reac}$ is the isotopically heavier "reactive" phase (relative to the Fe_{system} isotope composition) that satisfies isotope mass balance (Crosby *et al.* 2005; Crosby *et al.* 2007). Core 1

was the only location at CP where a substantial amount of Fe(II) was measured in the ASW and 0.01 M HCl-extracted Fe phases (Fig. 3.4 and 3.5), and thus, the only sediment core where the fractionation between Fe(II) and residual Fe(III) phases could be calculated (Fig. 3.13). The isotopic compositions of the Fe phases at core 1 and the fractionations between Fe(II) and Fe(III) phases were obscured (i.e associated with high uncertainties) by the high Fe(II) concentrations in the 0.5 M HCl extracted Fe phase. However an overall fractionation between Fe(II) and Fe(III) on the order of -0.5‰ to -1.5‰ is apparent in the upper few centimeters of core 1. While this is less than what has been calculated in previous microbial Fe(III)-reducing experiments (Beard *et al.* 1999; Tangalos *et al.* 2010), its interpretation as a positive biosignature is corroborated by documented microbial activity in the vicinity of core 1 (Fortney *et al.* 2018b).

The absence of Fe(II) downstream of the CP vent does not allow for the calculation of isotope fractionation between different Fe phases and therefore the isotopic composition of the more distal core sections does not support the presence of microbial activity. The progressive isotopic lightening of Fe/Si oxide sediments between cores 1 and 3 most likely reflects the sorption and precipitation of isotopically light Fe(II) derived from the spring water (Wu *et al.* 2013). The isotopic composition of cores 4 and 5 is homogenous with respect to depth as well as to the surface of core 6. This along with the continued absence of Fe(II) in the ASW and 0.01 M HCl-extracted phases does not support internal regeneration (and stepwise oxidation along the flow path) of isotopically light Fe(II) by DIR proposed by as an alternative explanation for the presence of isotopically-light solids downstream of the vent pool (Wu *et al.* 2013).

Our results indicate that under the oxidizing atmosphere on modern Earth, stable Fe isotopic biosignatures appear to be transient and highly localized to zones of active Fe(III) reduction. In contrast, BIFs deposited in the late Archean and early Proterozoic formed under

very low oxygen or anoxic conditions (Klein 2005). The alternating layers of siderite and magnetite are hypothesized to be microbial in origin (e.g. as a result of DIR) (Johnson *et al.* 2008a; Johnson *et al.* 2004; Nealson and Myers 1990), and the Fe isotope fractionation preserved in the layers is only possible because of the low oxygen environment in which BIFs formed. However, in the case of CP, our results suggest Fe isotope fractionation, and therefore a biosignature of microbial activity, may only present at the sediment surface of vent pool and to a relatively shallow depth because there is an active DIRB community that is constantly cycling Fe and constantly regenerating isotopically light Fe(II). The subsequent rapid oxidation of Fe(II) produced by DIRB prevents the formation of crystalline minerals with longer term stability like siderite and magnetite, effectively erasing a more permanent isotopic biosignature. These results contrast with findings for a variety of marine sedimentary environments, where burial of isotopically-light Fe(II)-bearing phases to depths below the surface aerobic layer has been well documented (see (Wu *et al.* 2012) for review and discussion).

In conclusion, CP hot spring has provided a useful natural environment to investigate the connection between microbial Fe redox cycling and the potential preservation of stable Fe isotopes ratios as a biosignature. Further investigation of other Fe redox cycling hydrothermal vent environments, including those that may have existed under a low-oxygen atmosphere, is warranted in order to further constrain whether the transient biosignature observed at CP is unique to this hot spring, or if it is more ubiquitous a result of the oxidizing conditions of the modern Earth surface.

ACKNOWLEDGEMENTS

This research was supported by the NASA Astrobiology Institute award #NNA13AA94A.

REFERENCES

Allen C. C., and Oehler D. Z. (2008) A case for ancient springs in Arabia Terra, Mars. *Astrobiology*, 8: 1093-1112.

Allen E. T., and Day A. L. (1935) Hot Springs of the Yellowstone National Park. Carnegie Institution of Washington.

Beard B. L., and Johnson C. M. (1999) High precision iron isotope measurements of terrestrial and lunar materials. *Geochimica et Cosmochimica Acta*, 63: 1653-1660.

Beard B. L., Johnson C. M., Cox L., Sun H., Nealson K. H., and Aguilar C. (1999) Iron isotope biosignatures. *Science*, 285: 1889-1892.

Beard B. L., Johnson C. M., Skulan J. L., Nealson K. H., Cox L., and Sun H. (2003) Application of Fe isotopes to tracing the geochemical and biological cycling of Fe. *Chemical Geology*, 195: 87-117.

Bird L. J., Bonnefoy V., and Newman D. K. (2011) Bioenergetic challenges of microbial iron metabolisms. *Trends in Microbiology*, 19: 330-40.

Blesa M. A., and Matijević E. (1989) Phase transformations of iron oxides, oxohydroxides, and hydrous oxides in aqueous media. *Advances in Colloid and Interface Science*, 29: 173-221.

Blöthe M., and Roden E. E. (2009) Microbial iron redox cycling in a circumneutral-pH groundwater seep. *Applied and Environmental Microbiology*, 75: 468-73.

Butterfield D. A., Jonasson I. R., Massoth G. J., Feely R. A., Roe K. K., Embley R. E., Holden J. F., McDuff R. E., Lilley M. D., Delaney J. R. and others. (1997) Seafloor Eruptions and Evolution of Hydrothermal Fluid Chemistry. *Philosophical Transactions of the Royal Society of London. Series A: Mathematical, Physical, and Engineering Sciences*, 355: 369-386.

Canfield D. E., Rosing M. T., and Bjerrum C. (2006) Early anaerobic metabolisms. *Philos Trans R Soc Lond B Biol Sci*, 361: 1819-34; discussion 1835-6.

Christiansen R. L. (2001) The Quaternary and Pliocene Yellowstone Plateau Volcanic Field of Wyoming, Idaho, and Montana. *US Geological Survey Professional Paper*, 729-G: 146.

Christiansen R. L., and Blank Jr. H. R. (1972) Volcanic Stratigraphy of the Quaternary Rhyolite Plateau in Yellowstone National Park. *US Geological Survey Professional Paper*, 729-B: 18.

Colman D. R., Poudel S., Hamilton T. L., Havig J. R., Selensky M. J., Shock E. L., and Boyd E. S. (2018) Geobiological feedbacks and the evolution of thermoacidophiles. *ISME J*, 12: 225-236.

Crosby H. A., Johnson C. M., Roden E. E., and Beard B. L. (2005) Coupled Fe(II)−Fe(III) Electron and Atom Exchange as a Mechanism for Fe Isotope Fractionation during Dissimilatory Iron Oxide Reduction. *Environmental Science & Technology*, 39: 6698-6704.

Crosby H. A., Roden E. E., Johnson C. M., and Beard B. L. (2007) The mechanisms of iron isotope fractionation produced during dissimilatory Fe(III) reduction by Shewanella putrefaciens and Geobacter sulfurreducens. *Geobiology*, 5: 169-189.

Dauphas N., Craddock P. R., Asimow P. D., Bennett V. C., Nutman A. P., and Ohnenstetter D. (2009) Iron isotopes may reveal the redox conditions of mantle melting from Archean to Present. *Earth and Planetary Science Letters*, 288: 255-267.

Emerson D. (2000) Microbial Oxidation of Fe(II) and Mn(II) at Circumneutral pH. In: *Environmental Microbe-Metal Interactions*. edited by DR Lovleys, ASM Press, Washington, D.C., pp 31-52.

Emerson D., Fleming E. J., and McBeth J. M. (2010) Iron-oxidizing bacteria: an environmental and genomic perspective. *Annual Review of Microbiology*, 64: 561-83.

Emerson D., and Moyer C. (1997) Isolation and Characterization of Novel Iron-Oxidizing Bacteria That Grow at Circumneutral pH. *Applied and Environmental Microbiology*, 63: 4784-4792.

Estep M. L. F. (1984) Carbon and hydrogen isotopic compositions of algae and bacteria from hydrothermal environments, Yellowstone National Park. *Geochimica et Cosmochimica Acta*, 48: 591-599.

Fortney N. W., He S., Converse B. J., Beard B. L., Johnson C. M., Boyd E. S., and Roden E. E. (2016) Microbial Fe(III) oxide reduction potential in Chocolate Pots hot spring, Yellowstone National Park. *Geobiology*, 14: 255-75.

Fortney N. W., He S., Converse B. J., Boyd E. S., and Roden E. E. (2018a) Investigating the composition and metabolic potential of microbial communities in Chocolate Pots hot springs. *Submitted to Front Microbiol*.

Fortney N. W., He S., Kulkarni A., Friedrich M. W., Holz C., Boyd E. S., and Roden E. E. (2018b) Stable isotope probing of microbial iron reduction in Chocolate Pots hot spring, Yellowstone National Park. *Applied and Environmental Microbiology*, 84: 15.

Gibbs-Eggar Z., Jude B., Dominik J., Loizeau J.-L., and Oldfield F. (1999) Possible evidence for dissimilatory bacterial magnetite dominating the magnetic properties of recent lake sediments. *Earth and Planetary Science Letters*, 168: 1-6.

Haaijer S. C. M., Harhangi H. R., Meijerink B. B., Strous M., Pol A., Smolders A. J., Verwegen K., Jetten M. S. M., and Op den Camp H. J. M. (2008) Bacteria associated with iron seeps in a sulfur-rich, neutral pH, freshwater ecosystem. *ISME J*, 2: 1231-42.

Hafenbradl D., Keller M., Dirmeier R., Rachel R., Roßnagel P., Burggraf S., Huber H., and Stetter K. O. (1996) *Ferroglobus placidus* gen. nov., sp. nov., a novel hyperthermophilic archaeum that oxidizes Fe^{2+} at neutral pH under anoxic conditions. *Archives of Microbiology*, 16: 308-314.

Johnson C. M., Beard B. L., Klein C., Beukes N. J., and Roden E. E. (2008a) Iron isotopes constrain biologic and abiologic processes in banded iron formation genesis. *Geochimica et Cosmochimica Acta*, 72: 151-169.

Johnson C. M., Beard B. L., and Roden E. E. (2008b) The Iron Isotope Fingerprints of Redox and Biogeochemical Cycling in Modern and Ancient Earth. *Annual Review of Earth and Planetary Sciences*, 36: 457-493.

Johnson C. M., Beard B. L., Roden E. E., Newman D. K., and Nealson K. H. (2004) Isotopic constraints on biogeochemical cycling of Fe. *Reviews in Mineralogy & Geochemistry*, 55: 359-408.

Jones A. M., Collins R. N., Rose J., and Waite T. D. (2009) The effect of silica and natural organic matter on the Fe(II)-catalysed transformation and reactivity of Fe(III) minerals. *Geochimica et Cosmochimica Acta*, 73: 4409-4422.

Klein C. (2005) Some Precambrian banded iron-formations (BIFs) from around the world: Their age, geologic setting, mineralogy, metamorphism, geochemistry, and origin. *American Mineralogist*, 90: 1473-1499.

Kohn M. J. (2010) Carbon isotope compositions of terrestrial C3 plants as indicators of (paleo)ecology and (paleo)climate. *Proceedings of the National Academy of Sciences of the United States of America*, 107: 19691-19695.

Kozubal M. A., Macur R. E., Jay Z. J., Beam J. P., Malfatti S. A., Tringe S. G., Kocar B. D., Borch T., and Inskeep W. P. (2012) Microbial iron cycling in acidic geothermal springs of Yellowstone National Park: integrating molecular surveys, geochemical processes, and isolation of novel Fe-active microorganisms. *Frontiers in Microbiology*, 3: 109.

López-Archilla A. I., Marin I., and Amils R. (2001) Microbial Community Composition and Ecology of an Acidic Aquatic Environment: The Tinto River, Spain. *Microb Ecol*, 41: 20-35.

Lovley D. (2006) Dissimilatory Fe(III)- and Mn(IV)-Reducing Prokaryotes. In: *The Prokaryotes*. edited by M Dworkin, S Falkow, E Rosenberg, KH Schleifer and E Stackebrandts, Springer, New York, NY, pp 635-658.

Lovley D. R. (1991) Dissimilatory Fe(III) and Mn(IV) Reduction. *Microbiological Reviews*, 55: 259-287.

Lovley D. R., Giovannoni S. J., White D. C., Champine J. E., Phillips E. J. P., Gorby Y. A., and Goodwin S. (1993) *Geobacter metallireducens* gen. nov. sp. nov., a microorganism capable of coupling the complete oxidation of organic compounds to the reduction of iron and other metals. *Archives of Microbiology*, 159: 336-344.

Lovley D. R., Holmes D. E., and Nevin K. P. (2004) Dissimilatory Fe(III) and Mn(IV) Reduction. *Advances in Microbial Physiology*, 49: 219-286.

Lovley D. R., Stolz J. F., Nord G. L. J., and Phillips E. J. P. (1987) Anaeroblc production of magnetite by a dissimilatory iron-reducing microorganism. *Nature*, 330: 252-254.

McCleskey R. B., Nordstrom D. K., Susong D. D., Ball J. W., and Holloway J. M. (2010) Source and fate of inorganic solutes in the Gibbon River, Yellowstone National Park, Wyoming, USA. *J Volcanol Geoth Res*, 193: 189-202.

Nealson K. H., and Myers C. R. (1990) Iron reduction by bacteria: a potenetial role in the genesis of banded iron formations. *American Journal of Science*, 290-A: 35-45.

Parenteau M. N., and Cady S. L. (2010) Microbial Biosignatures in Iron-Mineralized Phototrophic Mats at Chocolate Pots Hot Springs, Yellowstone National Park, United States. *Palaios*, 25: 97-111.

Parenteau M. N., Jahnke L. L., Farmer J. D., and Cady S. L. (2014) Production and Early Preservation of Lipid Biomarkers in Iron Hot Springs. *Astrobiology*, 14: 502-521.

Percak-Dennett E. M., Beard B. L., Xu H., Konishi H., Johnson C. M., and Roden E. E. (2011) Iron isotope fractionation during microbial dissimilatory iron oxide reduction in simulated Archaean seawater. *Geobiology*, 9: 205-20.

Percak-Dennett E. M., Loizeau J.-L., Beard B. L., Johnson C. M., and Roden E. E. (2013) Iron isotope geochemistry of biogenic magnetite-bearing sediments from the Bay of Vidy, Lake Geneva. *Chemical Geology*, 360-361: 32-40.

Pierson B. K., and Parenteau M. N. (2000) Phototrophs in high iron microbial mats: microstructure of mats in iron-depositing hot springs. *FEMS Microbiology Ecology*, 32: 181-196.

Pierson B. K., Parenteau M. N., and Griffin B. M. (1999) Phototrophs in High-Iron-Concentration Microbial Mats: Physiological Ecology of Phototrophs in an Iron-Depositing Hot Spring. *Applied and Environmental Microbiology*, 65: 5474-5483.

Reddy T. R., Frierdich A. J., Beard B. L., and Johnson C. M. (2015) The effect of pH on stable iron isotope exchange and fractionation between aqueous Fe(II) and goethite. *Chemical Geology*, 397: 118-127.

Roden E. E., and Lovley D. R. (1993) Dissimilatory Fe(III) Reduction by the Marine Microorganism *Desulfuromonas acetoxidans*. *Applied and Environmental Microbiology*, 59: 734-742.

Roden E. E., McBeth J. M., Blothe M., Percak-Dennett E. M., Fleming E. J., Holyoke R. R., Luther G. W., 3rd, Emerson D., and Schieber J. (2012) The Microbial Ferrous Wheel in a Neutral pH Groundwater Seep. *Front Microbiol*, 3: 172.

Salar R. K., and Aneja K. R. (2007) Thermophilic Fungi: Taxonomy and Biogeography. *International Journal of Agricultural Technology*, 3: 77-107.

Scheinost A. C. (2005) Metal oxides. In: *Encyclopedia of Soils in the Environment*. edited by D Hillel, JL Hatfield, KM Scow, DS Powlson, MJ Singer, C Rosenzweig and DL Sparkss, Academic Press, Cambridge, MA, pp 428-438.

Shock E. L. (1996) Hydrothermal systems as environments for the emergence of life. In: *Evolution of hydrothermal ecosytems on Earth (and Mars?)*. edited by GR Bock and JA Goodes, John Wiley & Sons, Ltd., Chichester, UK, pp 40-60.

Squyres S. W., Arvidson R. E., Ruff S., Gellert R., Morris R. V., Ming D. W., Crumpler L., Farmer J. D., Des Marais D. J., Yen A. and others. (2008) Detection of Silica-Rich Deposits on Mars. *Science*, 320: 1063-1067.

Stookey L. L. (1970) Ferrozine - a new spectrophotometric reagent for iron. *Analytical Chemistry*, 42: 779-781.

Tangalos G. E., Beard B. L., Johnson C. M., Alpers C. N., Shelobolina E. S., Xu H., Konishi H., and Roden E. E. (2010) Microbial production of isotopically light iron(II) in a modern chemically precipitated sediment and implications for isotopic variations in ancient rocks. *Geobiology*, 8: 197-208.

Tor J. M., Kashefi K., Holmes D. E., and Lovley D. R. (2013) Potential Importance of Dissimilatory Fe(III)-Reducing Microorganisms in Hot Sedimentary Environments. In: *The Subseafloor Biosphere at Mid-Ocean Ridges*. edited by WSD Wilcock, EF Delong, DS Kelley, JA Baross and SC Carys, American Geophysical Union, pp 199-211.

Vargas M., Kashefi K., Blunt-Harris E. L., and Lovley D. R. (1998) Microbiological evidence for Fe(III) reduction on early Earth. *Nature*, 395: 65-67.

Wade M. L., Agresti D. G., Wdowiak T. J., Armendarez L. P., and Farmer J. D. (1999) A Mossbauer investigation of iron-rich terrestrial hydrothermal vent systems: Lessons for Mars exploration. *Journal of Geophysical Research*, 104: 8489-8507.

Welch S. A., Beard B. L., Johnson C. M., and Braterman P. S. (2003) Kinetic and equilibrium Fe isotope fractionation between aqueous Fe(II) and Fe(III). *Geochimica et Cosmochimica Acta*, 67: 4231-4250.

Woese C. R., Kandler O., and Wheelis M. L. (1990) Towards a natural system of organisms: Proposal for the domains Archaea, Bacteria, and Eucarya. *Proceedings of the National Academy of Sciences of the United States of America*, 87: 4576-4579.

Wu L., Brucker R. P., Beard B. L., Roden E. E., and Johnson C. M. (2013) Iron Isotope Characteristics of Hot Springs at Chocolate Pots, Yellowstone National Park. *Astrobiology*, 13: 1091-101.

Wu L., Percak-Dennett E. M., Beard B. L., Roden E. E., and Johnson C. M. (2012) Stable iron isotope fractionation between aqueous Fe(II) and model Archean ocean Fe–Si

coprecipitates and implications for iron isotope variations in the ancient rock record. *Geochimica et Cosmochimica Acta*, 84: 14-28.

Table 3.1. Geochemical and isotopic properties of CP hot spring water and surface solids at core collection sites along the flow path.

Experiment[a]	Sample Site	Distance from Vent (m)	Temperature (°C)	pH	Fe(II) (mM)	Proportion of precipitation[b]	δ^{56}Fe aqueous (‰)	δ^{56}Fe solids[c] (‰)
(current study)	Core 1 (Vent)	0	50.7	5.94	0.083	0.00	-0.90	0.88
	Core 2	1.0	49.9	6.06	0.073	0.12	-0.97	0.74
	Core 3	2.1	48.4	6.51	0.040	0.52	-1.02	-0.65
	Core 4	4.1	42.8	7.77	0.004	0.95	-0.97	-0.56
	Core 5	6.8	42.7	7.76	0.007	0.92	-0.84	-0.64
	Core 6	8.2	40.8	7.90	0.005	0.94	-0.89	-0.32
	Entry to Gibbon River	~13	38.1	8.25	0.003	0.96	nd[d]	nd
(Wu *et al.* 2013)	MM0 (Vent)	0.0	51.8	5.58	0.104	0.00	-0.81	0.7
	MM1	0.6	52.1	nd	nd	0.04	nd	0.81
	MM2	1.8	51.7	5.70	0.096	0.08	-1.08	nd
	MM3	3.8	47.1	nd	nd	0.46	nd	-0.89
	MM4	6.0	43.0	7.50	0.016	0.85	nd	nd
	MM5	7.2	41.0	7.37	0.012	0.88	-1.28	nd
	MM6	9.0	40.7	7.47	0.007	0.93	-1.33	-0.85
	MM7	14.0	35.9	nd	nd	nd	nd	-1.17

[a] Comparison between Fe geochemistry and isotope composition of the CP spring water and solids in the current study to previous analyses conducted by Wu *et al.* (2013).

[b] Proportion of precipitation calculated by the difference between the sample [Fe(II)] and vent [Fe(II)], relative to the vent [Fe(II)].

[c] Surface samples of Fe oxides were not collected in the current study. The number reported here is the calculated $\delta^{56}Fe_{system}$ value (see Equation2) of the top cm of the core samples collected from each site.

[d] Not determined.

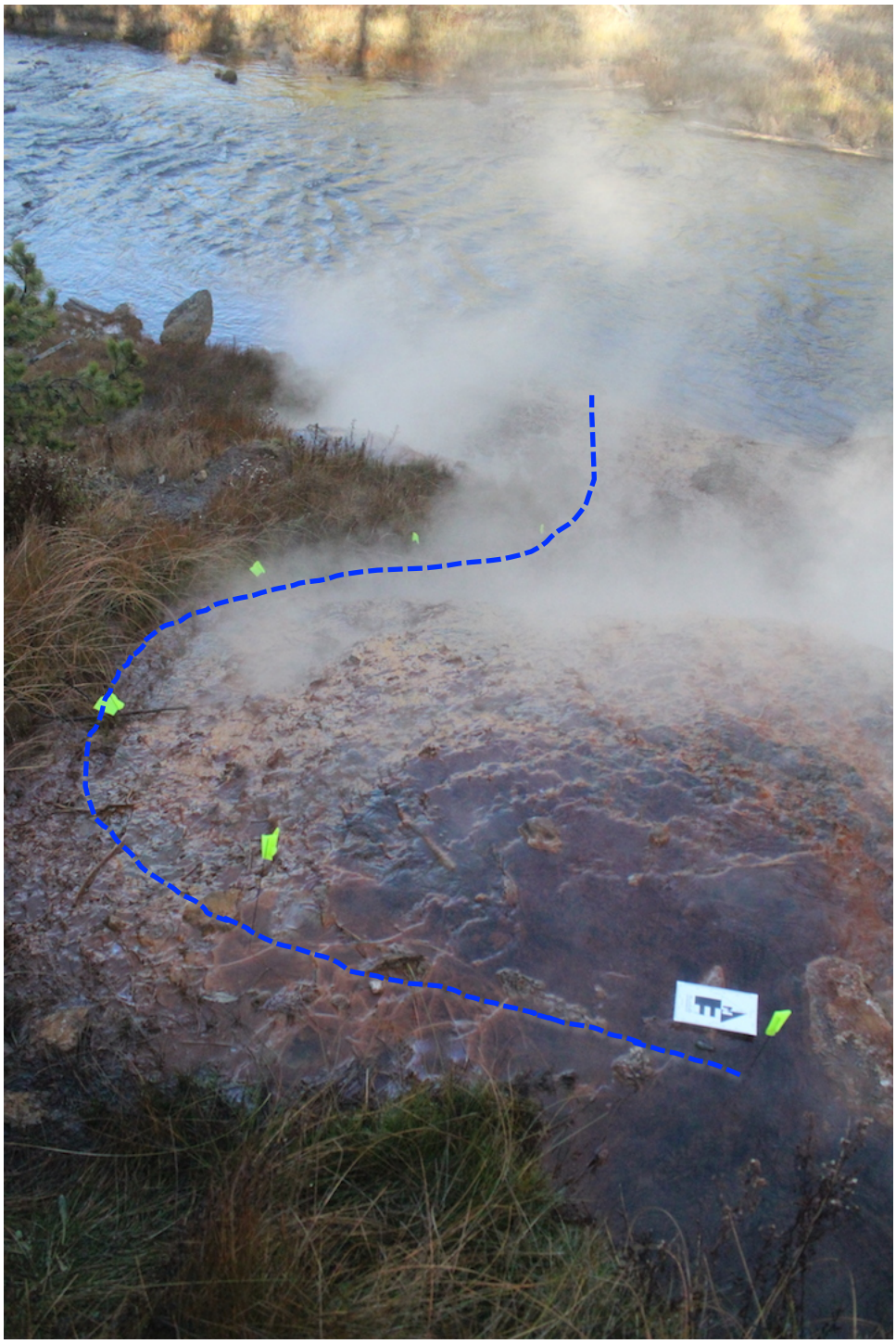

Figure 3.1. View from the top of Chocolate Pots looking west toward the Gibbon River. Blue dotted line marks the approximate flow path from the vent to the river. Locations where sediment cores and surface water were collected are marked by fluorescent green flags.

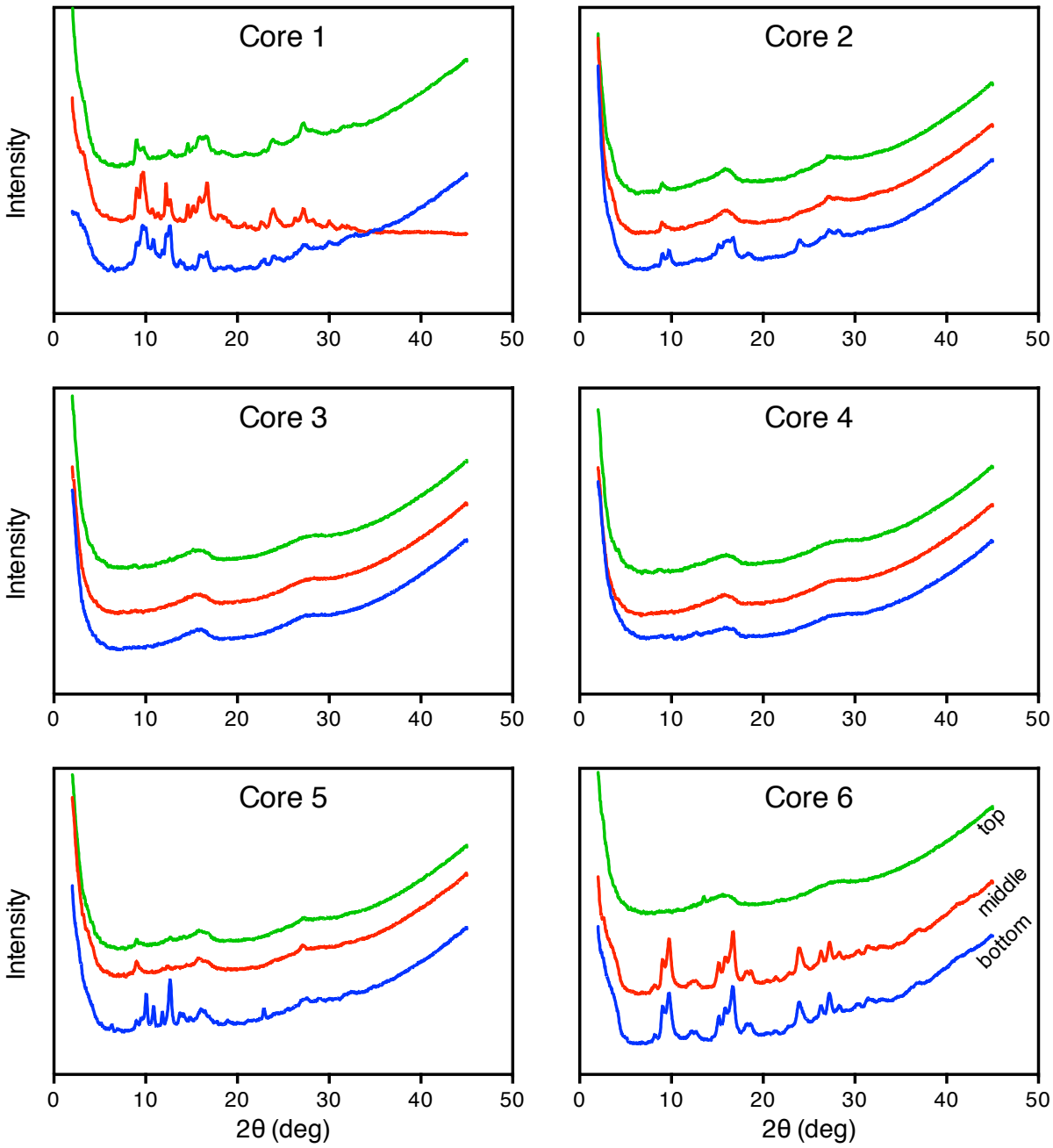

Figure 3.2. Comparison of Fe/Si oxide sediment from the top (green), middle (red), and bottom (blue) sections of CP cores collected at the hot spring vent pool (core 1) and along the flow path.

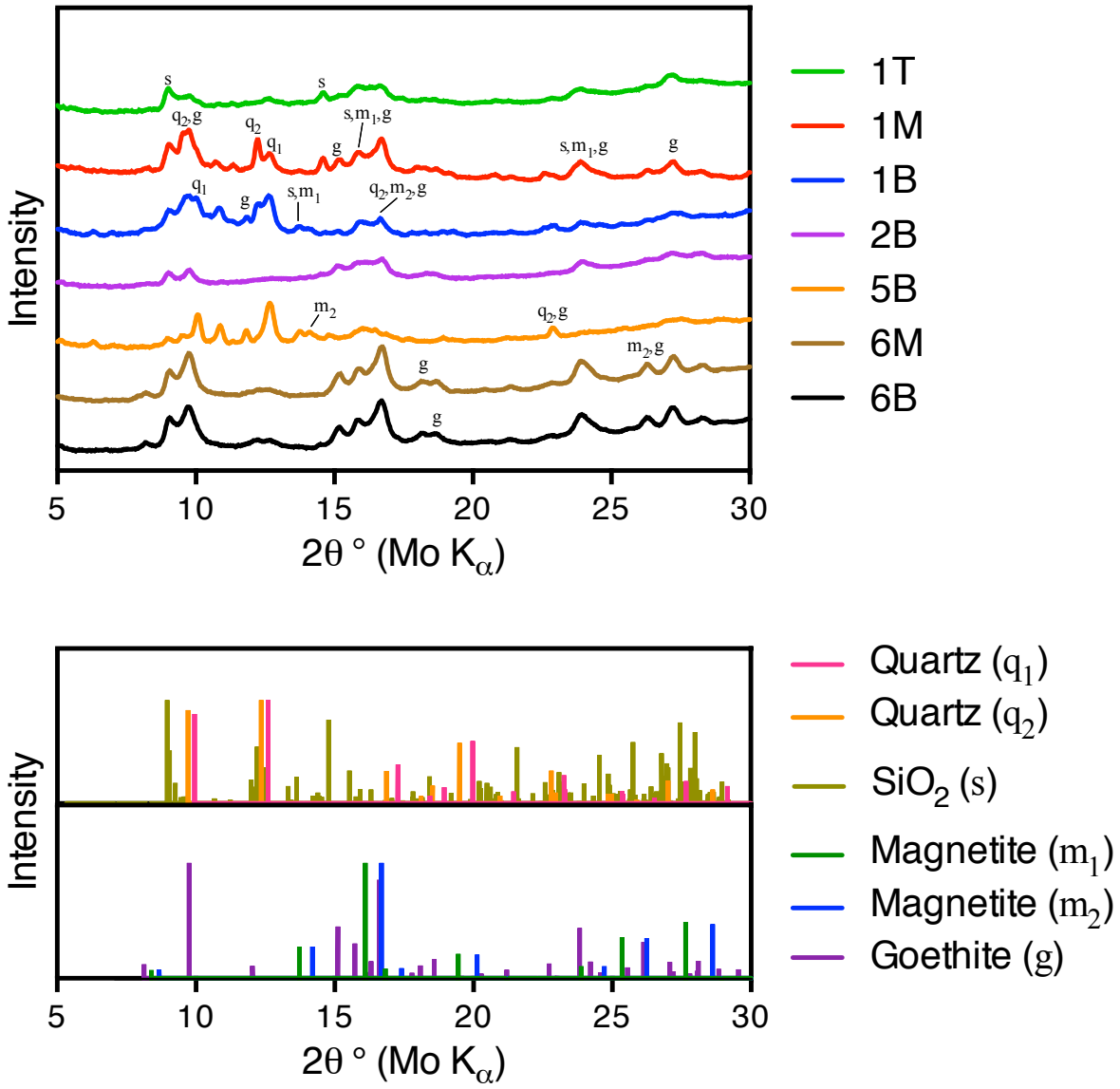

Figure 3.3. Powder XRD spectra of CP core samples containing crystalline minerals (top). Diffraction peaks matching known minerals (bottom) are labeled.

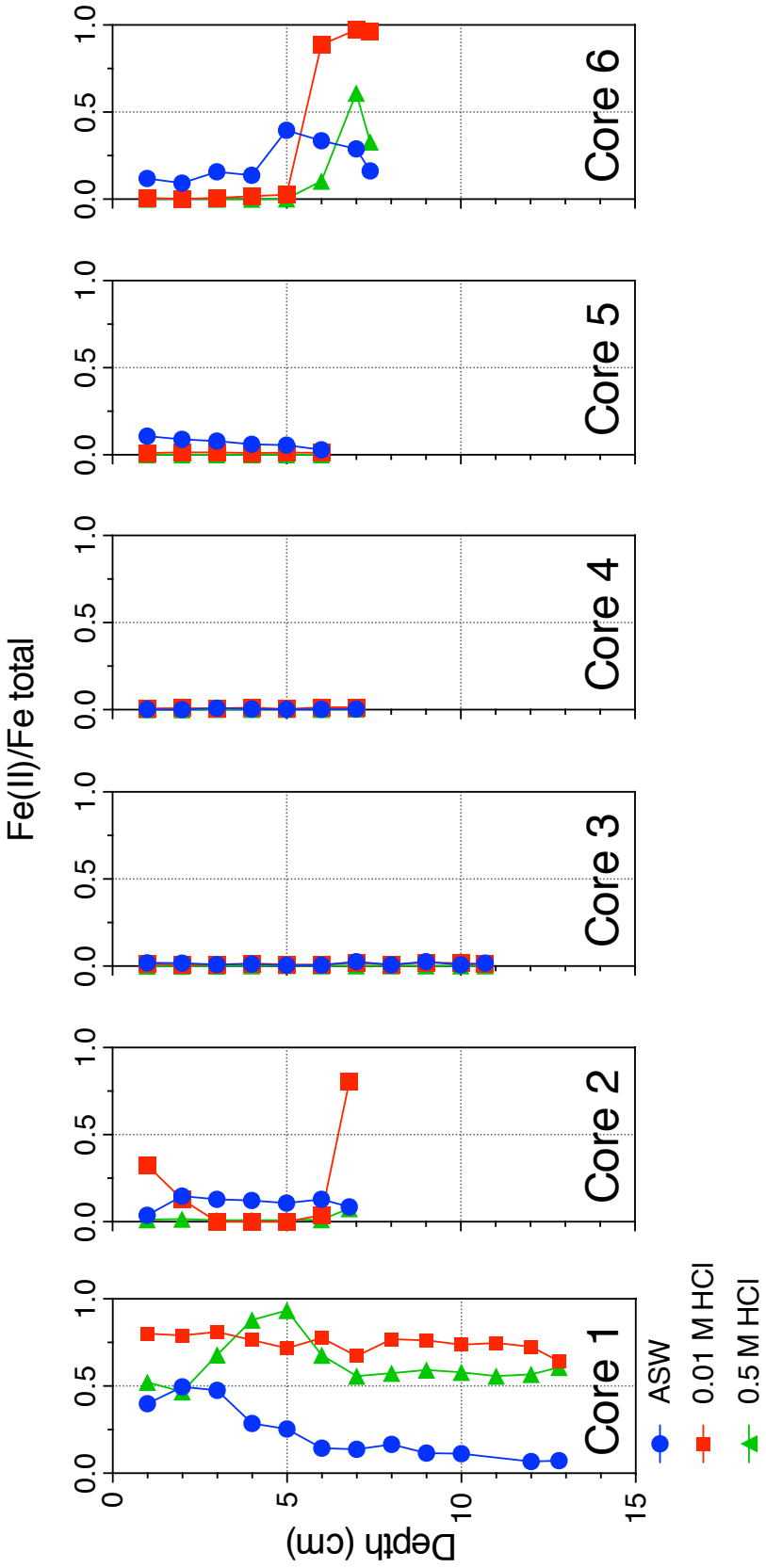

Figure 3.4. Variation in ASW and HCl-extractable Fe(II)/Fe total ratio in CP cores by depth.

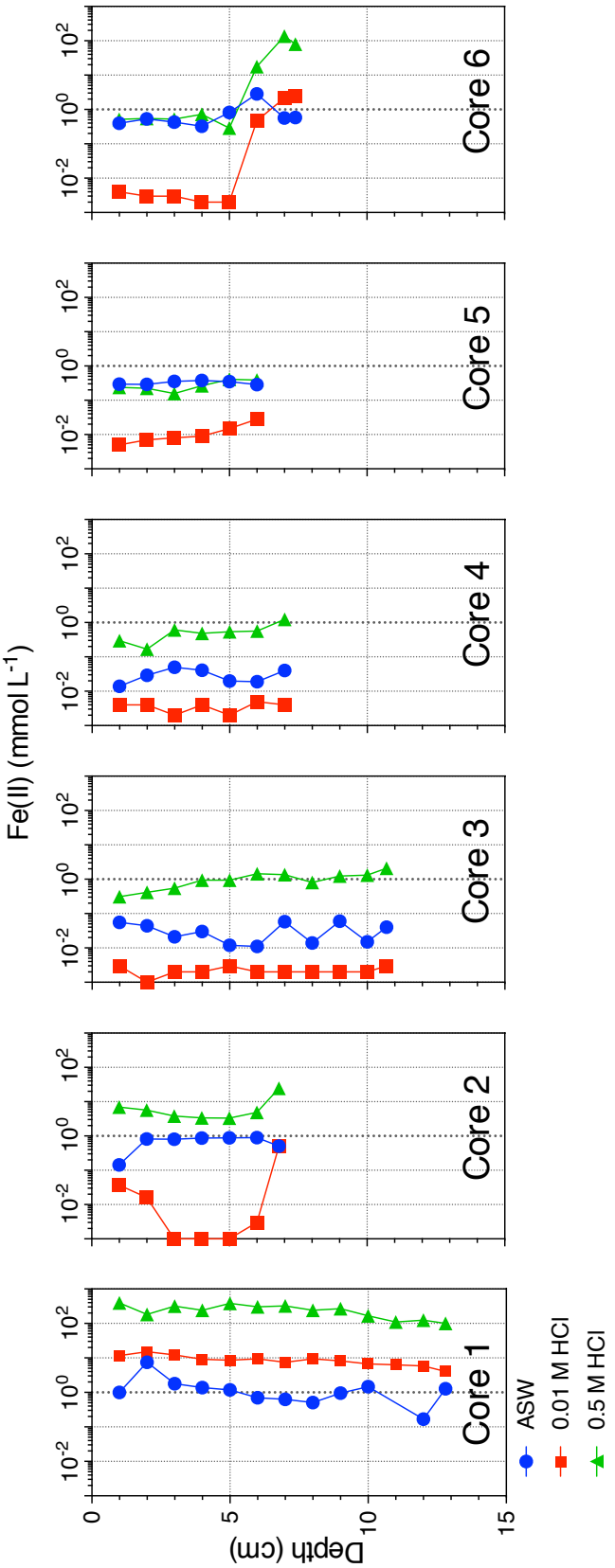

Figure 3.5. Variation in ASW and HCl-extractable Fe(II) content in CP cores by depth.

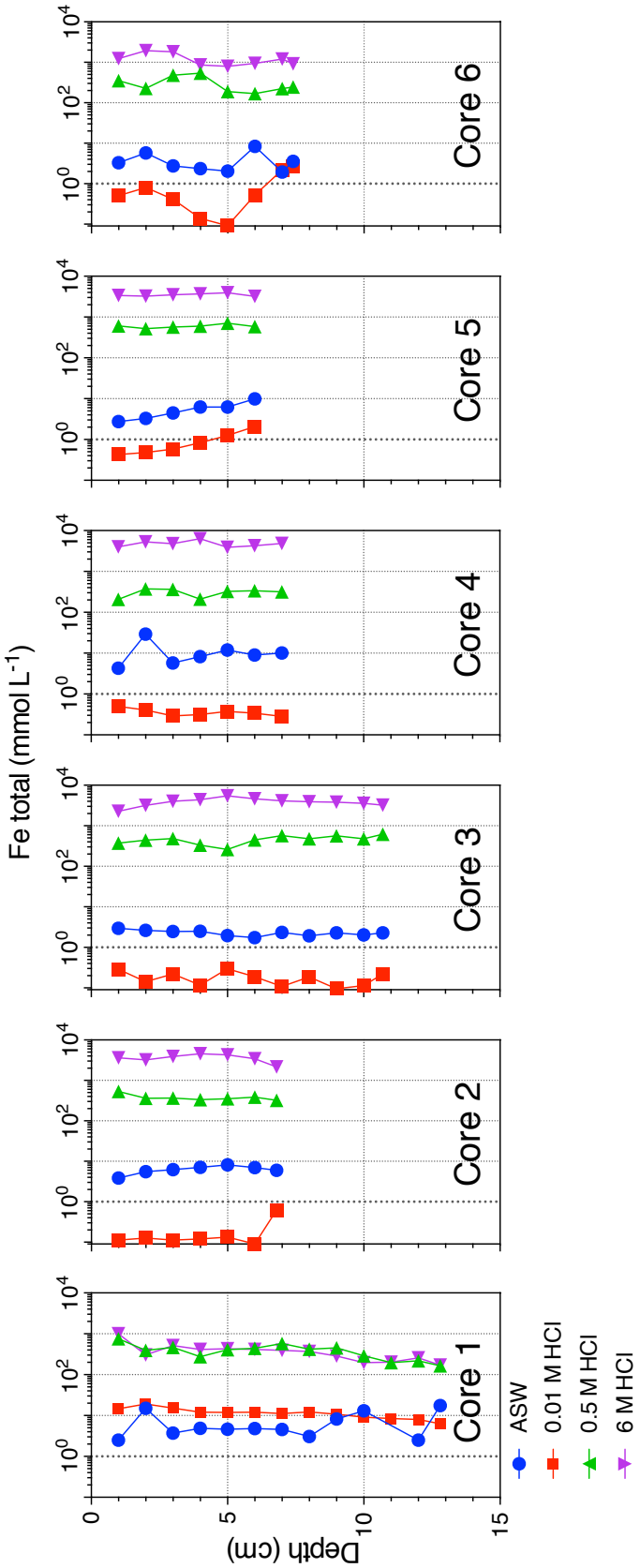

Figure 3.6. Variation in ASW and HCl-extractable total Fe content in CP cores by depth.

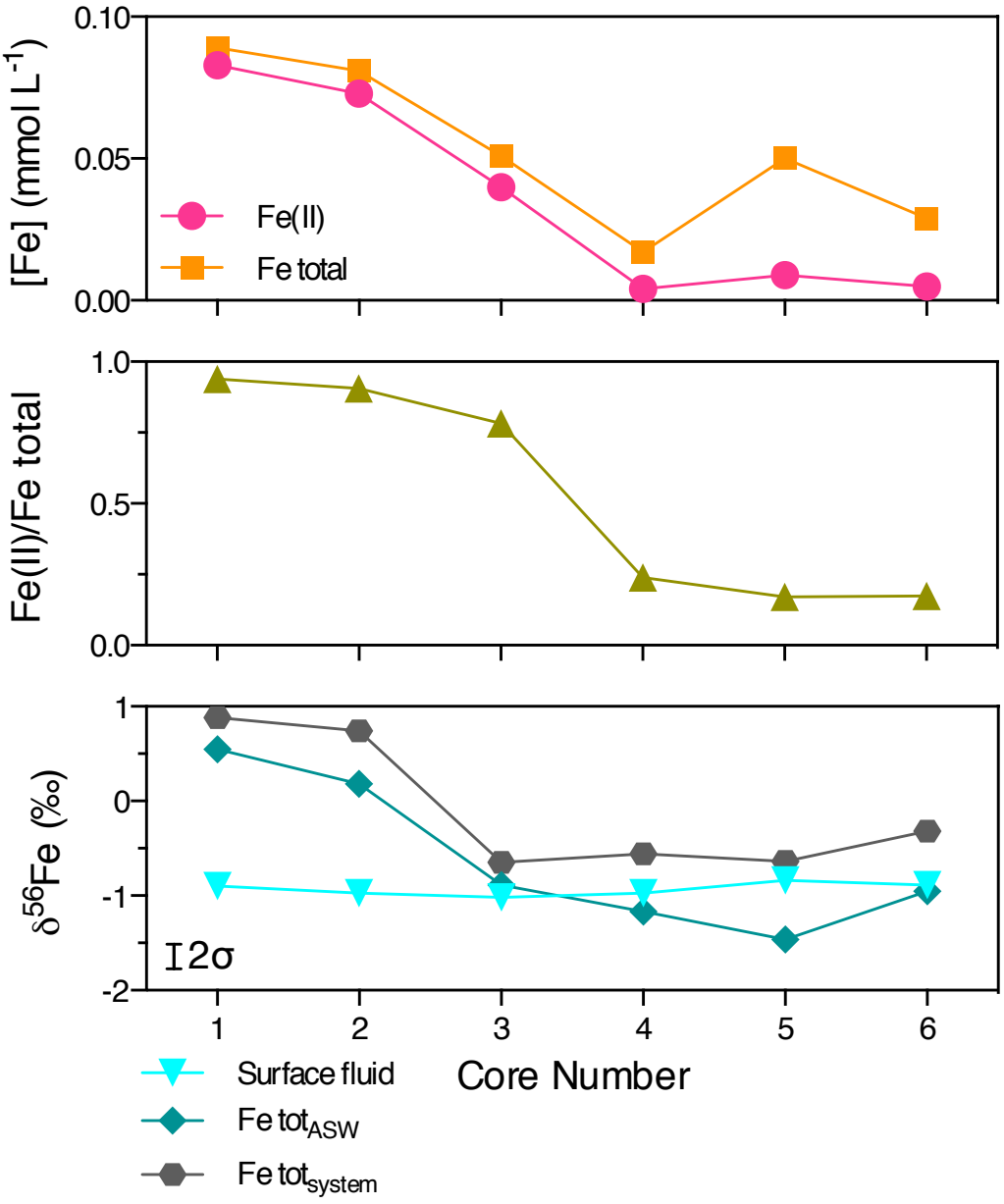

Figure 3.7. Fe concentrations, Fe(II)/Fe total ratio, and Fe isotope composition of total Fe in surface spring water at each core site. System Fe isotope composition calculated using Eqn 2 and measured isotopic composition of the ASW phase Fe from the top 1 cm of each core site are plotted for comparison. Error bar in the bottom panel represents a 2σ uncertainty of ± 0.13‰ in measured δ^{56}Fe values.

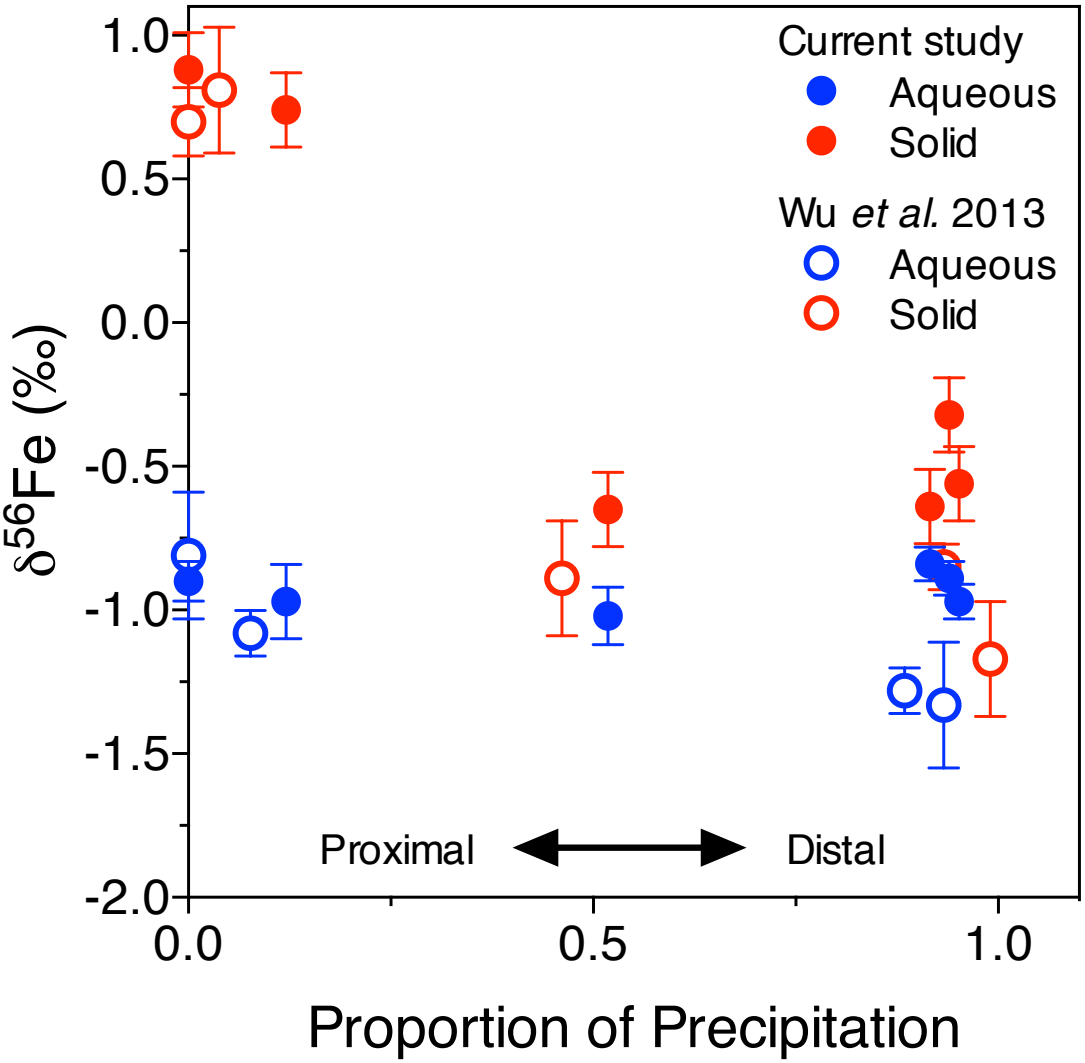

Figure 3.8. Isotope composition of the aqueous-phase Fe from the CP spring water collected at each core site and solid-phase Fe from the surface of each core versus the proportion of precipitation. Note that surface samples of Fe oxides were not collected in the current study. The number reported here is the calculated $\delta^{56}Fe_{system}$ value (see Equation2) of the top cm of the core samples collected from each site. Proportion of precipitation was calculated by the difference between the concentration of Fe(II) in a sample and the concentration of Fe(II) at the vent, relative to the concentration of Fe(II) at the vent. Samples collected from more distal locations experienced a greater degree of oxidation and precipitation as opposed to samples collected proximal to the vent.

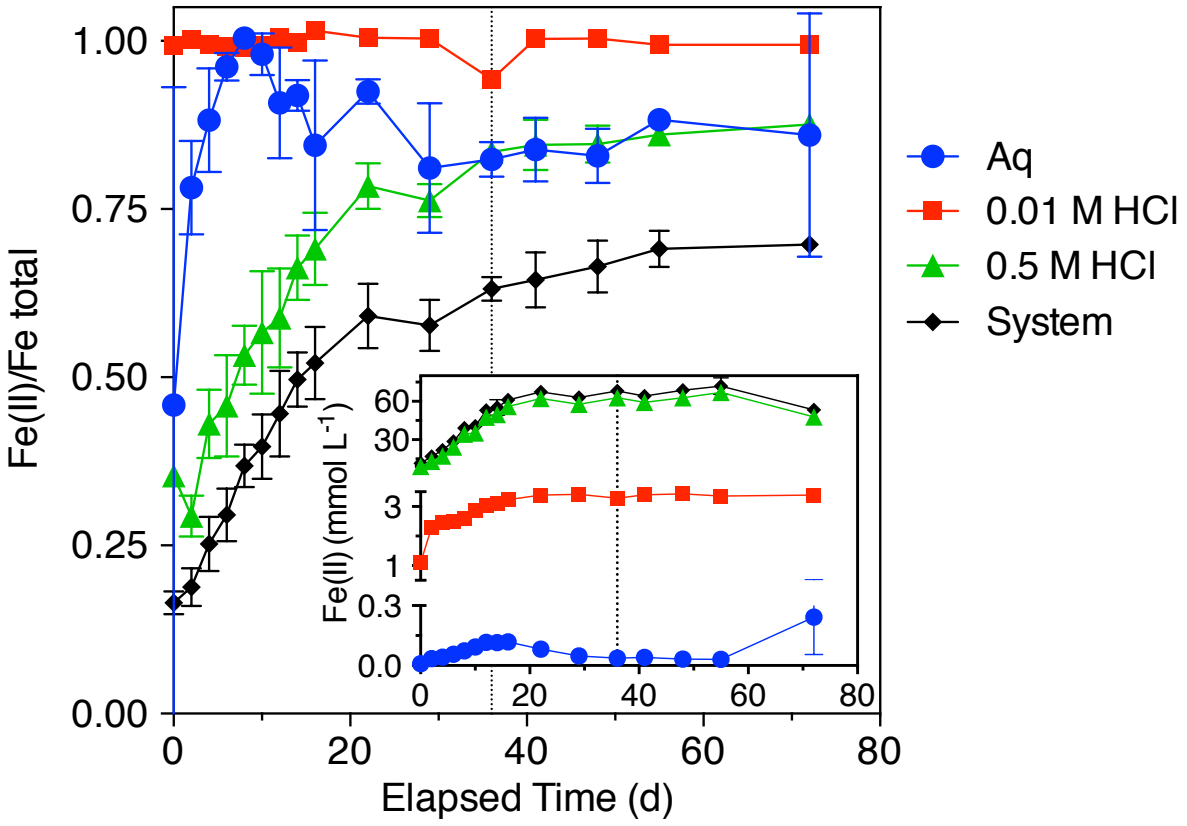

Figure 3.9. Plot of the ratio of Fe(II)/Fe total as a function of time in the Fe(III)-reducing incubation using native CP Fe oxide sediments and microbial community. A positive slope and high Fe(II) relative to total Fe is an indication of FeRB actively carrying out reduction of Fe/Si oxides in the CP slurry. Inset panel shows the accumulation of Fe(II) in the incubation. Values represent the average of a single measurement of two replicate incubations. Error bars represent 1σ variability in the measurements; error bars not shown are smaller than the size of the symbol. Microbial activity plateaued around 20 d and no isotope ratios were measured beyond 36 d, denoted by a vertical dotted line. System Fe(II)/Fe total represents the ratio of the sum of Fe(II) from all sequentially extracted phases to the sum of total Fe for all phases. System Fe(II) in the inset panel represents the sum of Fe(II) from all Fe phases. Abbreviations: Aq, aqueous phase Fe.

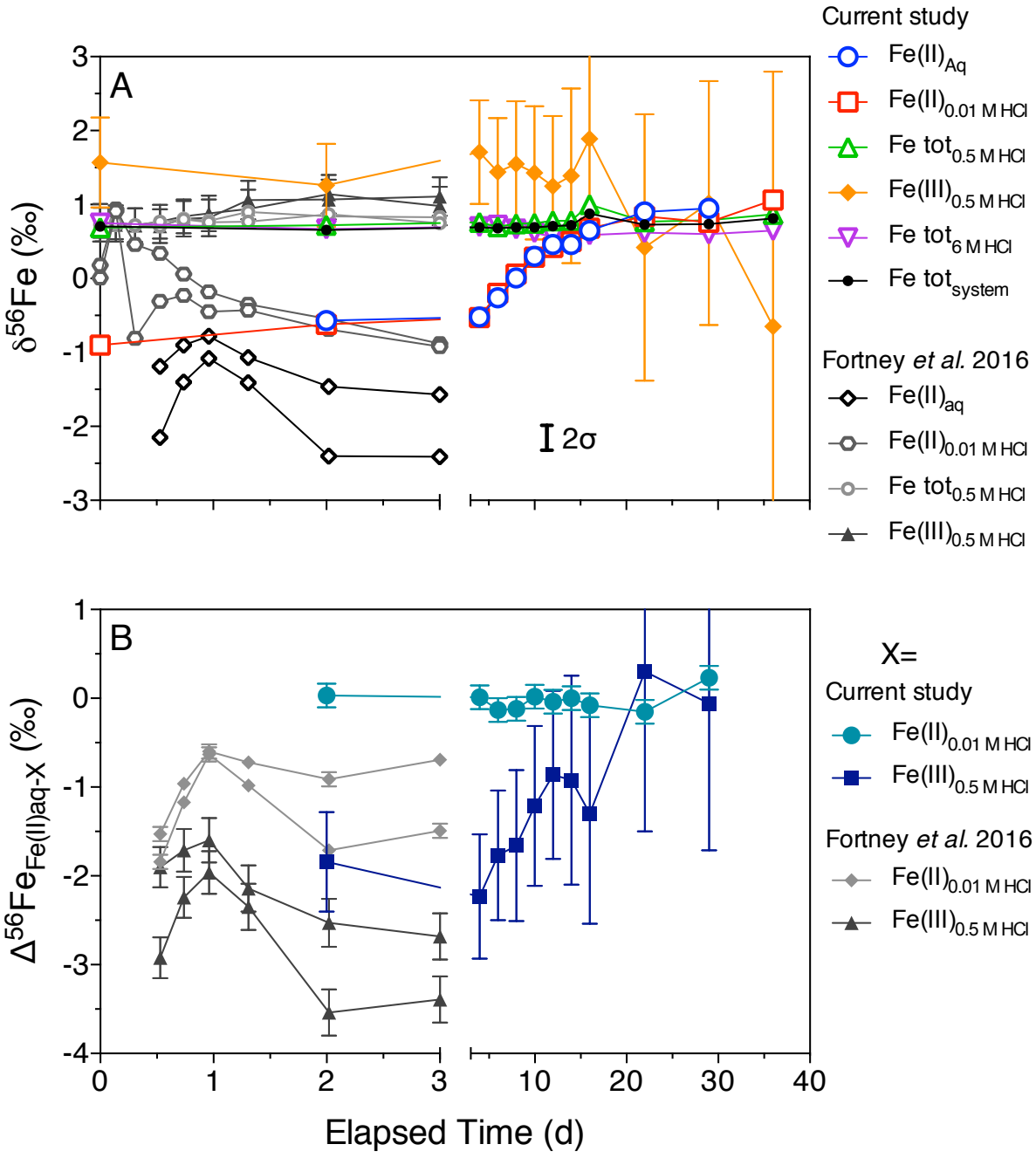
A
B
δ56Fe (‰)
Δ56FeFe(II)aq-X (‰)
Elapsed Time (d)
2σ
Current study
Fe(II)Aq
Fe(II)0.01 M HCl
Fe tot0.5 M HCl
Fe(III)0.5 M HCl
Fe tot6 M HCl
Fe tot system
Fortney et al. 2016
Fe(II)aq
Fe(II)0.01 M HCl
Fe tot0.5 M HCl
Fe(III)0.5 M HCl
X=
Current study
Fe(II)0.01 M HCl
Fe(III)0.5 M HCl
Fortney et al. 2016
Fe(II)0.01 M HCl
Fe(III)0.5 M HCl

Figure 3.10. (A) Measured (open symbols) and calculated (closed symbols) isotopic composition for each sequentially extracted phase of the Fe(III)-reducing incubation experiment. Aqueous Fe was predominantly comprised of Fe(II) and the 0.01 M HCl-extracted Fe was entirely Fe(II). Fe extracted in the 0.5 M HCl phase was a mixture of Fe(II) and Fe(III). Isotopic composition of the pure Fe(III) component was calculated assuming an isotopic composition of the Fe(II) component equivalent to that measured in the 0.01 M HCl extracted phase. Error bar represents a 2σ uncertainty of ± 0.14‰ in measured $\delta^{56}Fe$ values. Error bars on the $Fe(III)_{0.5\ M\ HCl}$ phase represents the extrapolated uncertainty for this calculation. Uncertainties in the isotope compositions of the calculated components were greatest when the Fe(II) component was relatively high in these samples. The isotopic composition of Fe tot_{system} represents the sum mole fraction of the isotopic composition of each phase from a given time point, defined by Eqn 2. Values of the isotopic ratios are represented by measurements on a single sample from duplicate incubations. (B) Fe isotope fractionation factor between the aqueous Fe(II) component and sequentially extracted phases representing the sorbed Fe(II) (0.01 M HCl extracted) and calculated reactive Fe(III) (0.5 M HCl extracted). Error bars in the $\Delta^{56}Fe_{Fe(II)aq\text{-}Fe(II)0.01M\ HCl}$ represents a 2σ uncertainty of ± 0.14‰. Uncertainty in the $\Delta^{56}Fe_{Fe(II)aq\text{-}Fe(III)0.5M\ HCl}$ fractionation factor was extrapolates from the calculated pure Fe(III) isotopic composition of the 0.5 M HCl extracted phase. Gray scale symbols in both plots represent imported data from Fortney *et al.* (2016) for comparison to earlier time points in the incubations when Fe(III) had undergone a lesser extent of reduction (e.g. Fe(II)/Fe tot < 0.2). Data from incubations inoculated with material from the CP vent or midway down the flow path are not differentiated in order to represent a range of expected results during this time period. Note that the starting Fe/Si oxide sediment was different in these two experiments. The current study was conducted using the unaltered fine-grain sediment collected directly from the CP vent pool, whereas the previous incubation was conducted using Fe/Si oxide sediments collected from a satellite vent and processed (crushed and sieved) under a fully oxic atmosphere. As a result, initial Fe isotope composition of the Fe/Si oxide was different between the two studies, $\delta^{56}Fe$ = 0.78‰ in the current study versus $\delta^{56}Fe$ = -0.71‰ in Fortney *et al.* (2016). Fe isotope ratios from the previous Fe(III)-reducing incubation was increased by 1.49‰ for the purpose of comparing trends in the datasets.

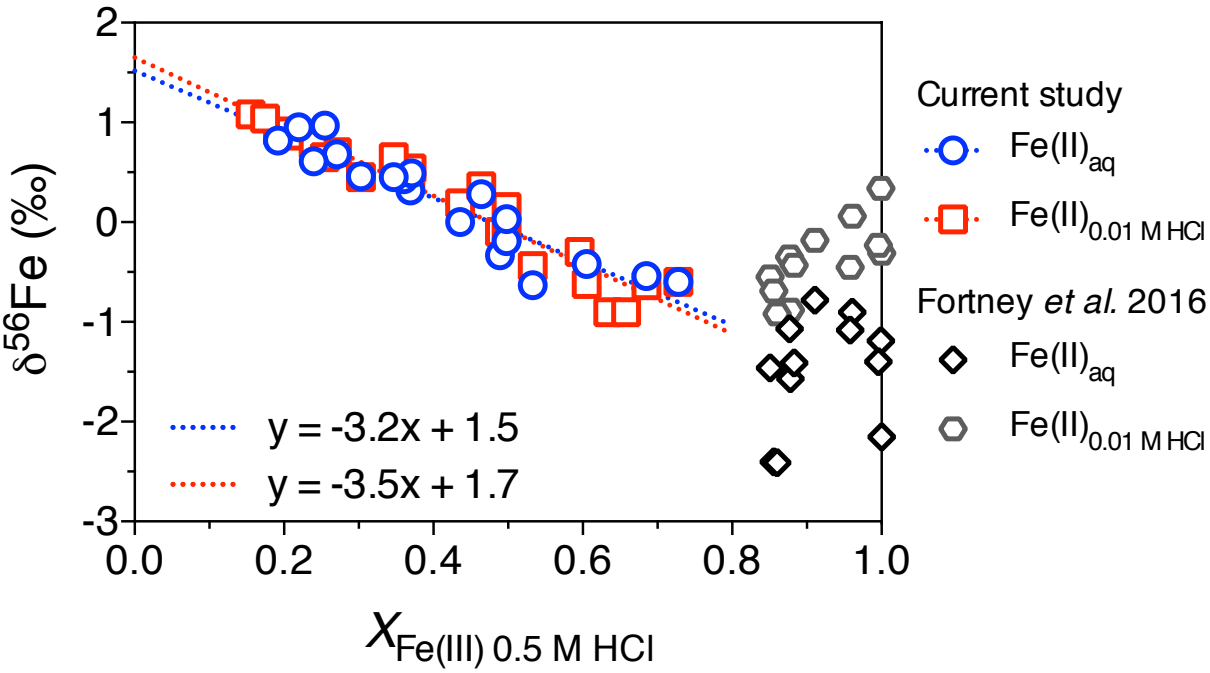

Figure 3.11. Isotope composition of the aqueous Fe(II) and 0.01 M HCl extracted Fe(II) versus the proportion of Fe(III) in the 0.5 M HCl extracted Fe phase from the same time series sample for the Fe(III)-reducing incubation experiment in the current study compared to results from Fortney *et al.* (2016) where a shorter duration incubation resulted in a lesser degree of Fe(III) reduction. A linear regression was calculated for the $Fe(II)_{aq}$ and $Fe(II)_{0.01\ M\ HCl}$ phases where the slope can be used to estimate isotopic fractionation between the Fe(II) phases and $Fe(III)_{0.5\ M\ HCl}$, e.g. -3.2‰ ≈ $\Delta^{56}Fe_{Fe(II)aq\text{-}Fe(III)0.5\ M\ HCl}$ and -3.5‰ ≈ $\Delta^{56}Fe_{Fe(II)0.01\ M\ HCl\text{-}Fe(III)0.5\ M\ HCl}$. Data fit the regression with R square values of 0.88 and 0.93 for the $Fe(II)_{aq}$ and $Fe(II)_{0.01\ M\ HCl}$, respectively. Fractionation between the two Fe(II) phases can be estimated by the difference in the slope of the regression lines, e.g. -3.2‰ – -3.5‰ = 0.3‰ = $\Delta^{56}Fe_{Fe(II)aq\text{-}Fe(II)0.01\ M\ HCl}$.

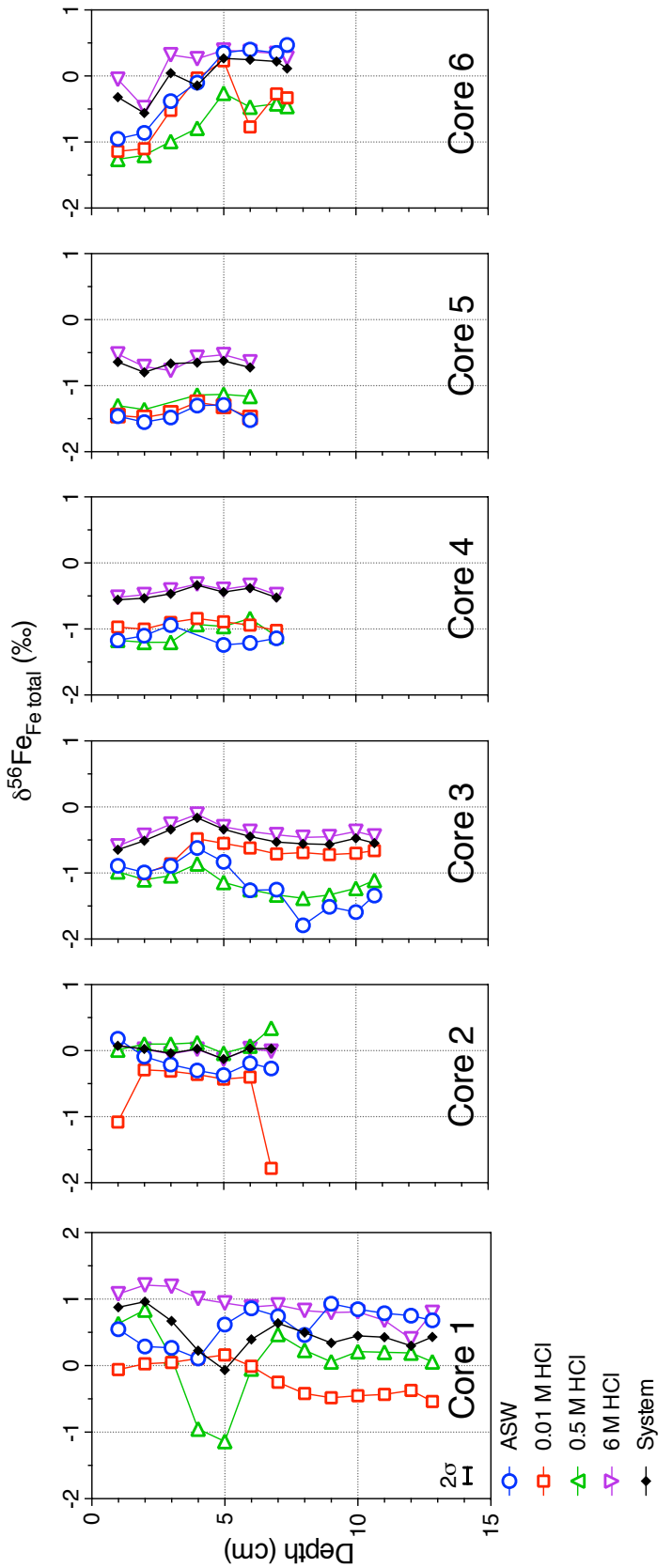

Figure 3.12. Variation in Fe isotope composition of total Fe in ASW and HCl-extracted phases in the CP cores by depth. Error bar in core 1 panel represents a 2σ uncertainty of ± 0.13‰ in measured δ^{56}Fe values.

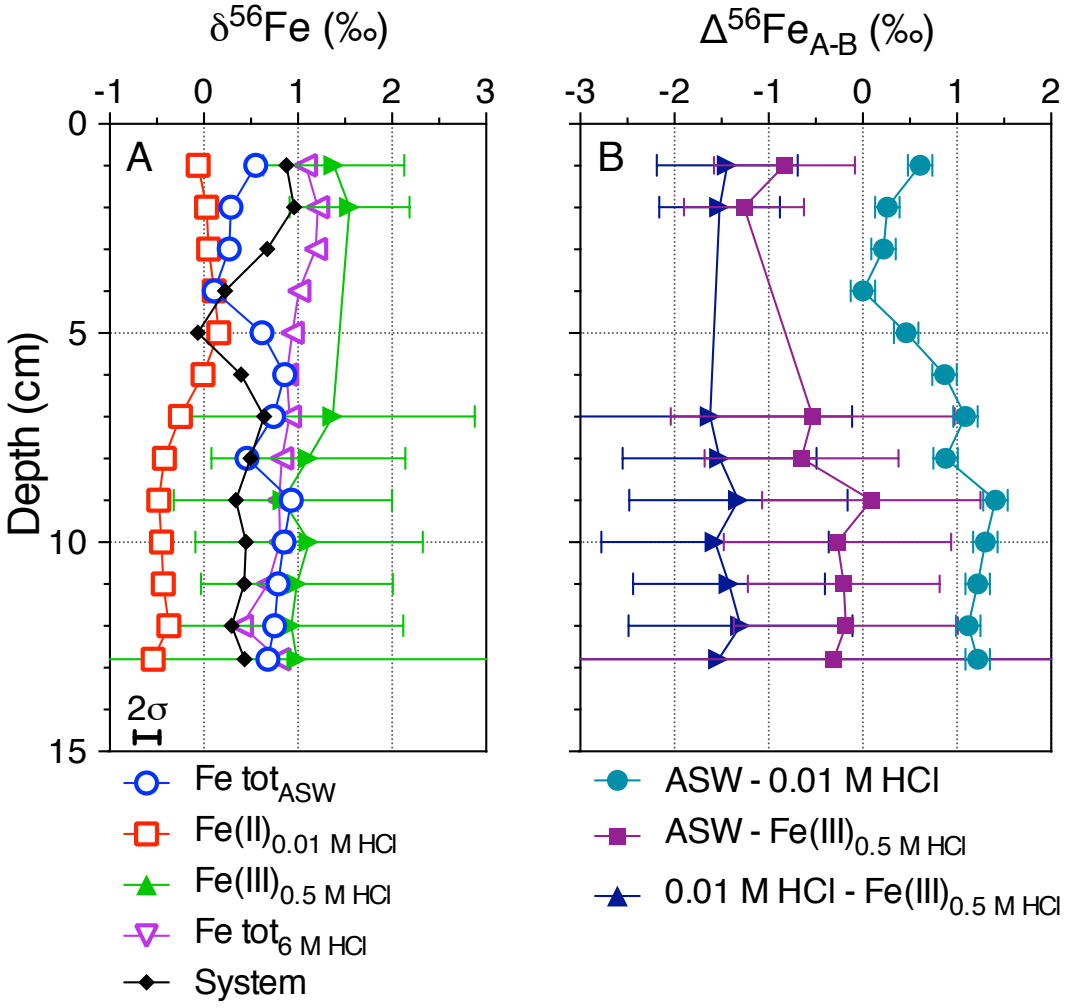

Figure 3.13. Measured (open symbols) and calculated (closed symbols) isotopic composition of Fe phases in core 1 (A) and fractionation between phases (B). Isotopic composition for the pure Fe(III) component of the 0.5 M HCl extracted phase was calculated assuming an isotopic value for the Fe(II) component equivalent to that of the predominantly Fe(II)-containing 0.01 M HCl extracted phase. Fractionation was calculated between $Fe(II)_{0.01M\ HCl}$ and $Fe(III)_{0.5\ M\ HCl}$ because of the 0‰ fractionation calculated between $Fe(II)_{aq}$ and $Fe(II)_{0.01\ M\ HCl}$ in the Fe(III)-reducing experiment, fractionation between ASW and 0.01 M HCl-extracted Fe in core 1 can also be assumed to be ca. 0‰. Fractionation was not calculated for the 3-6 cm depth range due to the anomalously low isotopic ratios measured in the 0.5 M HCl-extracted Fe pool from this interval. Error bar in the left panel represents a 2σ uncertainty of ± 0.13‰ in measured $\delta^{56}Fe$ values. Error bars are extrapolated for the calculated isotopic composition. Note the difference in $\Delta^{56}Fe_{ASW\text{-}0.01\ M\ HCl}$ between the top and bottom of the core corresponds to a decreased ratio of Fe(II)/Fe total with depth in the ASW phase.

Table A.3.1. Carbon and nitrogen concentration in CP core and surface sediment samples

Sample	Distance from Vent (m)	Total N (wt%)[a]	Total C (wt%)[a]	Total inorganic C (wt%)[b]	Total organic C (wt%)[c]
Core 1 top	0	0.08	0.59	bd[d]	0.59
Core 1 mid top	0	0.04	0.53	bd	0.53
Core 1 mid bottom	0	0.06	0.47	bd	0.47
Core 1 bottom	0	0.05	0.59	bd	0.59
Core 2	1.0	0.14	1.46	0.47	0.99
Core 3	2.1	0.04	0.60	0.01	0.59
Core 4	4.1	0.03	0.55	0.14	0.41
Core 5	6.8	0.06	0.91	0.39	0.52
Core 6	8.2	0.03	0.93	0.36	0.57

[a] 20 mg sample size

[b] 50 mg sample size

[c] Calculated difference between total C and total inorganic C

[d] Below detection limit

Table A.3.2a. Raw total carbon (TC) concentration data from the CP vent pool spring water

Sample[a]	TC (mg L^{-1})				Average of replicates[c]	
	Analyses[b]				TC (mg L^{-1})	1 SD
	1	2	3	4		
CP1	67.44	66.96	66.96	23.30	56.17	21.91
CP2	66.24	66.72	66.72	13.25	53.23	26.66
CP3	68.16	68.40	68.88	23.50	57.23	22.49
CP4	68.40	69.12	68.16	13.39	54.77	27.59
CP5	68.16	67.92	68.64	21.58	56.57	23.33
CP6	68.16	68.16	67.44	21.70	56.36	23.11
					55.72	*24.18*

[a] Six replicate samples of spring water were collected from the CP vent pool in Oct 2015

[b] Each sample was analyzed four times on the TOC Analyzer instrument

[c] Italicized numbers represent the grand average of analyses and variance

Table A.3.2b. Raw total inorganic carbon (TIC) concentration data from the CP vent pool spring water

Sample[a]	TIC (mg L^{-1})				Average of replicates[c]	
	Analyses[b]				TIC (mg L^{-1})	1 SD
	1	2	3	4		
CP1	63.12	62.64	44.88	1.11	42.94	29.15
CP2	62.40	62.40	36.00	0.92	40.43	29.13
CP3	65.04	65.04	45.84	1.16	44.27	30.13
CP4	64.56	64.80	35.04	0.93	41.33	30.34
CP5	64.32	64.32	43.68	1.08	43.35	29.81
CP6	64.08	63.84	46.56	1.14	43.91	29.67
					42.70	*29.71*

[a] Six replicate samples of spring water were collected from the CP vent pool in Oct 2015

[b] Each sample was analyzed four times on the TOC Analyzer instrument

[c] Italicized numbers represent the grand average of analyses and variance

Table A.3.2c. Raw total organic carbon (TOC) concentration data from the CP vent pool spring water

Sample[a]	TOC (mg L^{-1})				Average of replicates[c]	
	Analyses[b]				TOC (mg L^{-1})	1 SD
	1	2	3	4		
CP1	4.32	4.32	22.08	22.20	13.23	10.29
CP2	3.84	4.32	30.72	12.34	12.80	12.56
CP3	3.12	3.36	23.04	22.34	12.97	11.23
CP4	3.84	4.32	33.12	12.46	13.43	13.71
CP5	3.84	3.60	24.96	20.50	13.22	11.12
CP6	4.08	4.32	20.88	20.54	12.46	9.53
					13.02	*11.41*

[a] Six replicate samples of spring water were collected from the CP vent pool in Oct 2015

[b] Each sample was analyzed four times on the TOC Analyzer instrument

[c] Italicized numbers represent the grand average of analyses and variance

Table A.3.3. Raw isotopic data for aqueous Fe and sequential HCl-extracted Fe from a time series of the Fe(III)-reducing incubation

Replicate A								Replicate B									Grand average of replicates	
Elapsed time (days)	Phase	Fe(II) (µmol)	Fe(III) (µmol)	δ^{56}Fe (‰) Analyses 1	2	3	4	Elapsed time (days)	Phase	Fe(II) (µmol)	Fe(III) (µmol)	δ^{56}Fe (‰) Analyses 1	2	3	4	5	δ^{56}Fe (‰)	2σ
0	ASW							0	ASW									
	0.01 M HCl	1.11	0.01	-0.85	-0.88	-0.89	-0.97		0.01 M HCl	1.10	0.01	-0.90	-0.86	-0.94			-0.90	0.04
	0.5 M HCl	9.11	15.76	0.69	0.67				0.5 M HCl	9.11	17.54	0.72	0.72	0.67			0.70	0.05
	6 M HCl	2.01	41.25	0.84	0.76	0.73			6 M HCl	0.62	42.38	0.71	0.74				0.76	0.10
2	ASW	0.04	0.01	-0.54	-0.54			2	ASW	0.03	0.01	-0.74	-0.72	-0.35			-0.58	0.31
	0.01 M HCl	2.38	0.01	-0.61	-0.61	-0.66			0.01 M HCl	2.21	0.00	-0.60	-0.52	-0.68			-0.61	0.05
	0.5 M HCl	13.50	29.31	0.72					0.5 M HCl	12.64	33.76	0.72	0.69				0.71	0.03
	6 M HCl	2.06	39.10	0.67	0.48	0.74			6 M HCl	1.05	45.16	0.70	0.68	0.73			0.67	0.19
4	ASW	0.04	0.00	-0.61	-0.65			4	ASW	0.04	0.01	-0.46	-0.38				-0.52	0.25
	0.01 M HCl	2.53	0.01	-0.41	-0.46	-0.46			0.01 M HCl	2.40	0.02	-0.63	-0.60	-0.61			-0.53	0.10
	0.5 M HCl	17.98	20.52	0.76	0.72				0.5 M HCl	16.55	25.39	0.77					0.75	0.06
	6 M HCl	2.59	38.68	0.71					6 M HCl	1.34	44.92	0.77	0.65	0.68			0.70	0.11
6	ASW	0.06	0.00	-0.35	-0.31			6	ASW								-0.33	0.06
	0.01 M HCl	2.45	0.01	-0.10					0.01 M HCl	2.54	0.03	-0.30					-0.20	0.14
	0.5 M HCl	24.94	23.84	0.74					0.5 M HCl	23.80	35.17	0.65					0.70	0.13
	6 M HCl	2.63	39.31	0.67					6 M HCl	0.96	39.59	0.76					0.72	0.13
8	ASW	0.08	0.00	0.04	-0.01	-0.04		8	ASW	0.06	0.00	-0.18	-0.16	-0.29	-0.13		-0.11	0.23
	0.01 M HCl	2.75	0.01	0.19					0.01 M HCl	2.48	0.04	-0.22	0.07				0.01	0.42
	0.5 M HCl	33.91	26.22	0.77	0.68	0.75			0.5 M HCl	34.81	34.53	0.74	0.75				0.74	0.07
	6 M HCl	2.20	34.37	0.69	0.64				6 M HCl	1.96	39.77	0.72	0.67	0.63			0.67	0.08
10	ASW	0.10	0.00	0.35	0.30			10	ASW	0.08	0.00	0.03					0.22	0.35
	0.01 M HCl	2.99	0.04	0.44					0.01 M HCl	2.75	0.00	0.16	0.18	0.11	0.13		0.21	0.26
	0.5 M HCl	33.43	19.56	0.77					0.5 M HCl	37.15	36.91	0.73					0.75	0.06
	6 M HCl	2.92	32.48	0.57					6 M HCl	1.92	36.75	0.67					0.62	0.15
12	ASW	0.13	0.00	0.42	0.44	0.43		12	ASW	0.10	0.02	0.28					0.39	0.15
	0.01 M HCl	3.18	0.00	0.43	0.55	0.48	0.48		0.01 M HCl	2.90	0.01	0.37	0.32	0.38			0.43	0.08
	0.5 M HCl	50.27	28.25	0.81					0.5 M HCl	44.83	38.85	0.73	0.77				0.77	0.09
	6 M HCl	2.20	29.59	0.52					6 M HCl	2.11	35.78	0.62	0.70	0.54	0.57	0.60	0.50	0.13
14	ASW	0.12	0.01	0.48	0.44			14	ASW	0.11	0.01	0.49					0.47	0.05
	0.01 M HCl	3.19	0.01	0.45	0.42	0.47	0.47		0.01 M HCl	3.04	0.01	0.54					0.47	0.05
	0.5 M HCl	53.70	23.40	0.73	0.83	0.77			0.5 M HCl	45.59	26.95	0.70	0.75	0.91			0.78	0.16
	6 M HCl	2.44	30.27	0.66					6 M HCl	2.15	30.81	0.56					0.61	0.10
16	ASW	0.13	0.04	0.68	0.66	0.70		16	ASW	0.11	0.01	0.43					0.59	0.25
	0.01 M HCl	3.34	0.00	0.70					0.01 M HCl	3.13	0.00	0.65	0.65				0.67	0.06
	0.5 M HCl	58.66	21.78	0.81	0.70				0.5 M HCl	53.13	28.23	1.21	1.23	1.28			1.05	0.54

	6 M HCl	2.97	29.55	0.64				6 M HCl	0.91	33.12	0.57	0.56		0.59	0.07
22	ASW	0.07	0.00	0.77	0.88		22	ASW	0.10	0.01	0.56	0.67		0.72	0.27
	0.01 M HCl	3.43	0.00	0.90	0.91			0.01 M HCl	3.34	0.00	0.78			0.86	0.15
	0.5 M HCl	64.48	15.36	0.73	0.83			0.5 M HCl	60.18	19.04	0.77			0.77	0.10
	6 M HCl	2.44	26.95	0.61				6 M HCl	0.72	32.05	0.63			0.62	0.32
29	ASW	0.04	0.01	0.98	0.92		29	ASW	0.05	0.01	0.97			0.96	0.07
	0.01 M HCl	3.41	0.00	0.87				0.01 M HCl	3.41	0.00	0.62	0.68		0.72	0.26
	0.5 M HCl	58.47	16.50	0.78				0.5 M HCl	56.75	19.44	0.80			0.79	0.03
	6 M HCl	3.21	26.19	0.55	0.58			6 M HCl	0.77	30.53	0.64			0.59	0.09
36	ASW						36	ASW							
	0.01 M HCl	3.22	0.21	1.13	1.06	1.06		0.01 M HCl	3.34	0.19	1.05	1.04		1.07	0.07
	0.5 M HCl	60.76	11.17	1.00				0.5 M HCl	64.95	13.77	0.76	0.73	0.69	0.78	0.25
	6 M HCl	2.97	25.60	0.65	0.64			6 M HCl	0.86	28.63	0.66	0.65		0.65	0.01

Table A.3.4. Calculated isotopic composition of the Fe(III) component of the 0.5 M HCl extracted Fe phase in the Fe(III)-reducing incubation

Elapsed Time (d)	$\delta^{56}Fe_{Fe(II)\ 0.01\ M\ HCl}$ (‰)[a]	2σ	$X_{Fe(II)\ 0.01\ M\ HCl}$	low error estimate[b]	$\delta^{56}Fe_{Fe\ tot\ 0.5\ M\ HCl}$ (‰)	2σ	high error estimate[b]	$X_{Fe(II)\ 0.5\ M\ HCl}$	Extrapolated mixing line[c]						Calculated error[e]	$\delta^{56}Fe_{Fe(III)\ 0.5\ M\ HCl}$ (‰)[f]
									Low estimate				High estimate			
									Slope	Intercept[d]	Slope	Intercept[d]	Slope	Intercept[d]		
0	-0.90	0.14	0.994	0.50	0.70	0.14	0.89	0.354	-2.18	1.27	-2.49	1.58	-2.80	1.88	0.61	1.57
2	-0.61	0.14	1.001	0.51	0.71	0.14	0.91	0.293	-1.59	0.98	-1.87	1.26	-2.15	1.54	0.56	1.26
4	-0.53	0.14	0.995	0.55	0.75	0.14	0.95	0.429	-1.91	1.37	-2.26	1.72	-2.61	2.06	0.70	1.71
6	-0.20	0.14	0.992	0.50	0.70	0.14	0.90	0.452	-1.30	1.09	-1.67	1.45	-2.03	1.82	0.73	1.44
8	0.01	0.14	0.990	0.54	0.74	0.14	0.93	0.531	-1.14	1.14	-1.57	1.57	-2.00	2.00	0.85	1.55
10	0.21	0.14	0.993	0.55	0.75	0.14	0.95	0.556	-0.79	0.99	-1.24	1.44	-1.70	1.89	0.90	1.43
12	0.43	0.14	1.005	0.57	0.77	0.14	0.97	0.586	-0.34	0.77	-0.81	1.25	-1.28	1.72	0.95	1.25
14	0.47	0.14	0.997	0.58	0.78	0.14	0.98	0.664	-0.34	0.81	-0.93	1.40	-1.52	1.99	1.18	1.39
16	0.67	0.14	1.016	0.85	1.05	0.14	1.24	0.691	-0.56	1.23	-1.17	1.85	-1.78	2.47	1.24	1.89
22	0.86	0.14	1.005	0.57	0.77	0.14	0.96	0.784	1.33	-0.48	0.44	0.42	-0.46	1.32	1.80	0.42
29	0.72	0.14	1.003	0.59	0.79	0.14	0.99	0.762	0.53	0.19	-0.29	1.01	-1.11	1.84	1.65	1.02
36	1.07	0.14	0.943	0.58	0.78	0.14	0.98	0.834	4.45	-3.13	2.63	-1.41	0.80	0.31	3.45	-0.65

[a] Correction for the pure Fe(III) component of the 0.5 M HCl extracted fe phase assumes that any residual Fe(II) in the sample is of the same isotopic composition as the primarily Fe(II) 0.01 M HCl extracted phase

[b] Projected high and low errors is calculated using the square root of the sum of squares of the error associated with the measured isotopic composition of the phases, i.e. sqrt(0.14^2+0.14^2) = 0.20

[c] The isotopic composition and mol fraction of Fe(II) 0.01 M HCl is taken as one end member of the mixing line, projecting a line from this point, through the isotopic composition and mole fraction Fe(II) of the 0.5 M HCl extracted Fe, to the other end member of $X_{Fe(II)} = 0$ allows for the estimation of the isotopic composition or the pure Fe(III) component of the 0.5 M HCl extracted Fe phase

[d] Note that the Y-intercept is the estimated isotopic composition of the sample when $X_{Fe(II)} = 0$

[e] Calculated error is the difference between the projected high and low isotopic composition of the sample

[f] Calculated isotopic composition using Equation 4

Table A.3.5. Calculated system isotopic composition for the Fe(III)-reducing incubation

Elapsed Time (d)	Fe phase mol fraction				Average measured δ^{56}Fe (‰)				Mol fraction x δ^{56}Fe				Calculated $\delta^{56}Fe_{system}$ (‰)
	Aqueous	0.01 M HCl	0.5 M HCl	6 M HCl	Aqueous	0.01 M HCl	0.5 M HCl	6 M HCl	Aqueous	0.01 M HCl	0.5 M HCl	6 M HCl	
0	0.0002	0.0159	0.3679	0.6160	nd[a]	-0.90	0.70	0.76		-0.0143	0.2557	0.4666	0.71
2	0.0005	0.0253	0.4922	0.4820	-0.58	-0.61	0.71	0.67	-0.0003	-0.0155	0.3502	0.3214	0.66
4	0.0005	0.0286	0.4650	0.5059	-0.52	-0.53	0.75	0.70	-0.0003	-0.0151	0.3476	0.3549	0.69
6	0.0006	0.0257	0.5514	0.4222	-0.33	-0.20	0.70	0.72	-0.0002	-0.0052	0.3847	0.3021	0.68
8	0.0007	0.0247	0.6073	0.3673	-0.11	0.01	0.74	0.67	-0.0001	0.0003	0.4470	0.2462	0.69
10	0.0009	0.0280	0.6135	0.3577	0.22	0.21	0.75	0.62	0.0002	0.0057	0.4596	0.2221	0.69
12	0.0011	0.0254	0.6810	0.2925	0.39	0.43	0.77	0.59	0.0004	0.0109	0.5242	0.1727	0.71
14	0.0011	0.0281	0.6747	0.2961	0.47	0.47	0.78	0.61	0.0005	0.0132	0.5268	0.1795	0.72
16	0.0012	0.0271	0.6885	0.2832	0.59	0.67	1.05	0.59	0.0007	0.0181	0.7202	0.1674	0.91
22	0.0008	0.0296	0.6972	0.2725	0.72	0.86	0.77	0.62	0.0006	0.0255	0.5346	0.1681	0.73
29	0.0005	0.0311	0.6909	0.2774	0.96	0.72	0.79	0.59	0.0005	0.0225	0.5476	0.1641	0.73
36	0.0004	0.0323	0.6982	0.2691	nd	1.07	0.78	0.65		0.0345	0.5467	0.1746	0.76

[a] Not determined, insufficient Fe quantity for isotopic analysis

Table A.3.6. Raw isotopic data for spring water Fe collected from coring site locations along the flow path

Sample	Fe(II) (µmol)	Fe(III) (µmol)	δ^{56}Fe (‰)			Average of replicates	
			Analyses			δ^{56}Fe (‰)	2σ
			1	2	3		
Core 1	0.0952	0.0033	-0.93	-0.86	-0.91	-0.90	0.07
Core 2	0.0840	0.0045	-0.97				
Core 3	0.0449	0.0093	-0.98	-1.06		-1.02	0.10
Core 4	0.0037	0.0155	-0.99	-0.98	-0.94	-0.97	0.06
Core 5	0.0055	0.0498	-0.86	-0.85	-0.81	-0.84	0.06
Core 6	0.0034	0.0294	-0.86	-0.90	-0.93	-0.89	0.06

Table A.3.7. Calculated system isotopic composition for each depth interval of the sediment cores collected along the CP flow path

Sample	Depth (cm)	Fe phase mol fraction				Average measured δ^{56}Fe (‰)				Mol fraction x δ^{56}Fe				Calculated $\delta^{56}Fe_{system}$ (‰)
		ASW[a]	0.01 M HCl	0.5 M HCl	6 M HCl	ASW	0.01 M HCl	0.5 M HCl	6 M HCl	ASW	0.01 M HCl	0.5 M HCl	6 M HCl	
Core 1	1	0.0014	0.0083	0.4247	0.5656	0.55	-0.06	0.63	1.08	0.0008	-0.0005	0.2676	0.6109	0.88
	2	0.0205	0.0262	0.5354	0.4178	0.29	0.03	0.84	1.21	0.0059	0.0007	0.4479	0.5062	0.96
	3	0.0037	0.0151	0.4646	0.5165	0.27	0.05	0.12	1.19	0.0010	0.0008	0.0558	0.6154	0.67
	4	0.0069	0.0170	0.3902	0.5860	0.11	0.11	-0.95	1.01	0.0008	0.0019	-0.3707	0.5917	0.22
	5	0.0054	0.0140	0.4779	0.5027	0.62	0.16	-1.14	0.94	0.0034	0.0022	-0.5448	0.4746	-0.06
	6	0.0055	0.0138	0.5090	0.4717	0.86	-0.01	-0.05	0.88	0.0048	-0.0001	-0.0254	0.4144	0.39
	7	0.0046	0.0113	0.5840	0.4000	0.84	-0.25	0.47	0.91	0.0039	-0.0028	0.2745	0.3644	0.64
	8	0.0038	0.0151	0.5220	0.4591	0.46	-0.42	0.23	0.83	0.0017	-0.0063	0.1201	0.3811	0.50
	9	0.0109	0.0143	0.5981	0.3768	0.93	-0.48	0.06	0.80	0.0101	-0.0068	0.0359	0.3015	0.34
	10	0.0258	0.0180	0.5691	0.3871	0.85	-0.45	0.21	0.81	0.0219	-0.0081	0.1195	0.3134	0.45
	11	nd[b]	0.0205	0.4821	0.4973	0.79	-0.43	0.20	0.68		-0.0088	0.0964	0.3400	0.43
	12	0.0051	0.0164	0.4492	0.5294	0.75	-0.37	0.19	0.40	0.0038	-0.0061	0.0853	0.2143	0.30
	12.8	0.0483	0.0175	0.4589	0.4753	0.68	-0.54	0.06	0.80	0.0328	-0.0094	0.0275	0.3803	0.43
Core 2	1	0.0009	0.0000	0.1276	0.8714	0.18	-1.08	0.01	0.08	0.0002	0.0000	0.0013	0.0727	0.07
	2	0.0015	0.0000	0.1009	0.8975	-0.09	-0.29	0.10	0.02	-0.0001	0.0000	0.0101	0.0181	0.03
	3	0.0015	0.0000	0.0859	0.9126	-0.21	-0.31	0.10	-0.05	-0.0003	0.0000	0.0086	-0.0460	-0.04
	4	0.0015	0.0000	0.0684	0.9302	-0.30	-0.36	0.12	0.02	-0.0004	0.0000	0.0082	0.0203	0.03
	5	0.0018	0.0000	0.0759	0.9223	-0.37	-0.43	-0.04	-0.13	-0.0006	0.0000	-0.0030	-0.1213	-0.13
	6	0.0018	0.0000	0.1010	0.8971	-0.19	-0.40	0.07	0.03	-0.0004	0.0000	0.0071	0.0273	0.03
	6.8	0.0024	0.0003	0.1289	0.8684	-0.27	-1.78	0.34	-0.01	-0.0006	-0.0004	0.0438	-0.0105	0.03
Core 3	1	0.0011	0.0001	0.1404	0.8584	-0.89		-0.98	-0.59	-0.0010		-0.1376	-0.5087	-0.65
	2	0.0007	0.0000	0.1214	0.8778	-0.99	-1.01	-1.10	-0.43	-0.0007	0.0000	-0.1336	-0.3768	-0.51
	3	0.0005	0.0000	0.1075	0.8920	-0.89	-0.86	-1.04	-0.26	-0.0005	0.0000	-0.1117	-0.2279	-0.34
	4	0.0005	0.0000	0.0707	0.9288	-0.62	-0.48	-0.86	-0.11	-0.0003	0.0000	-0.0608	-0.1031	-0.16
	5	0.0003	0.0001	0.0451	0.9546	-0.83	-0.55	-1.14	-0.30	-0.0003	0.0000	-0.0514	-0.2843	-0.34
	6	0.0003	0.0000	0.0880	0.9117	-1.26	-0.62	-1.25	-0.37	-0.0004	0.0000	-0.1100	-0.3355	-0.45
	7	0.0005	0.0000	0.1222	0.8773	-1.25	-0.71	-1.33	-0.42	-0.0006	0.0000	-0.1626	-0.3661	-0.53
	8	0.0004	0.0000	0.1078	0.8917	-1.79	-0.69	-1.38	-0.46	-0.0008	0.0000	-0.1487	-0.4081	-0.56
	9	0.0005	0.0000	0.1296	0.8699	-1.51	-0.72	-1.33	-0.45	-0.0008	0.0000	-0.1724	-0.3952	-0.57
	10	0.0005	0.0000	0.1176	0.8819	-1.59	-0.70	-1.23	-0.37	-0.0008	0.0000	-0.1446	-0.3287	-0.47
	10.7	0.0006	0.0001	0.1615	0.8379	-1.34	-0.66	-1.11	-0.44	-0.0008	0.0000	-0.1793	-0.3664	-0.55
Core 4	1	0.0010	0.0001	0.0498	0.9490	-1.17	-0.97	-1.17	-0.52	-0.0012	-0.0001	-0.0585	-0.4978	-0.56
	2	0.0051	0.0001	0.0654	0.9294	-1.10	-1.00	-1.20	-0.48	-0.0056	-0.0001	-0.0784	-0.4494	-0.53
	3	0.0011	0.0001	0.0710	0.9278	-0.94	-0.90	-1.20	-0.41	-0.0011	-0.0001	-0.0853	-0.3812	-0.47
	4	0.0013	0.0000	0.0321	0.9666		-0.84	-0.93	-0.32		0.0000	-0.0299	-0.3062	-0.34
	5	0.0028	0.0001	0.0764	0.9207	-1.24	-0.89	-0.96	-0.40	-0.0035	-0.0001	-0.0734	-0.3640	-0.44

	6	0.0019	0.0001	0.0725	0.9255	-1.21	-0.94	-0.84	-0.34	-0.0024	-0.0001	-0.0612	-0.3163	-0.38
	7	0.0020	0.0001	0.0615	0.9365	-1.14	-1.02	-1.11	-0.48	-0.0022	-0.0001	-0.0682	-0.4525	-0.52
Core 5	1	0.0007	0.0001	0.1507	0.8485	-1.46	-1.45	-1.30	-0.52	-0.0010	-0.0002	-0.1964	-0.4428	-0.64
	2	0.0009	0.0001	0.1379	0.8611	-1.55	-1.48	-1.36	-0.71	-0.0013	-0.0002	-0.1878	-0.6090	-0.80
	3	0.0011	0.0001	0.1390	0.8598	-1.48	-1.41		-0.77	-0.0016	-0.0002	0.0000	-0.6632	-0.66
	4	0.0014	0.0002	0.1383	0.8601	-1.30	-1.25	-1.14	-0.57	-0.0019	-0.0002	-0.1582	-0.4903	-0.65
	5	0.0013	0.0003	0.1517	0.8467	-1.29	-1.31	-1.13	-0.53	-0.0017	-0.0004	-0.1709	-0.4495	-0.62
	6	0.0026	0.0005	0.1540	0.8428	-1.52	-1.48	-1.16	-0.64	-0.0039	-0.0008	-0.1794	-0.5397	-0.72
Core 6	1	0.0021	0.0003	0.2199	0.7778	-0.95	-1.14	-1.26	-0.05	-0.0020	-0.0004	-0.2778	-0.0387	-0.32
	2	0.0026	0.0004	0.1048	0.8922	-0.86	-1.10	-1.20	-0.48	-0.0023	-0.0004	-0.1259	-0.4310	-0.56
	3	0.0012	0.0002	0.2089	0.7897	-0.38	-0.52	-0.99	0.32	-0.0005	-0.0001	-0.2062	0.2496	0.04
	4	0.0017	0.0001	0.3843	0.6139	-0.10	-0.03	-0.79	0.26	-0.0002	0.0000	-0.3017	0.1576	-0.14
	5	0.0021	0.0001	0.1920	0.8058	0.35	0.23	-0.26	0.39	0.0007	0.0000	-0.0498	0.3151	0.27
	6	0.0075	0.0005	0.1506	0.8414	0.40	-0.77	-0.47	0.37	0.0030	-0.0004	-0.0714	0.3154	0.25
	7	0.0014	0.0015	0.1570	0.8401	0.35	-0.27	-0.42	0.34	0.0005	-0.0004	-0.0660	0.2865	0.22
	7.4	0.0030	0.0022	0.2081	0.7867	0.47	-0.33	-0.46	0.27	0.0014	-0.0007	-0.0953	0.2095	0.11

[a] Artificial spring water (see Fortney *et al*. 2016) extracted Fe

[b] Not determined, insufficient Fe quantity for isotopic analysis

Table A.3.8. Raw isotopic data for sequential ASW- and HCl-extracted Fe from a depth profile of CP sediment cores collected along the flow path

Sample	Depth (cm)	Phase	Fe(II) (µmol)	Fe(III) (µmol)	δ^{56}Fe (‰)						Average of replicates	
					Analyses						δ^{56}Fe (‰)	2σ
					1	2	3	4	5	6		
Core 1	**1**	ASW	4.1	6.2	0.55							
		0.01 M HCl	117.4	29.4	-0.06							
		0.5 M HCl	3930.3	3601.5	0.63							
		6 M HCl	210.5	9819.8	1.07	1.09					1.08	0.04
	2	ASW	32.0	32.6	0.28	0.30					0.29	0.03
		0.01 M HCl	152.1	40.4	-0.01	0.07					0.03	0.11
		0.5 M HCl	1835.8	2090.5	0.85	0.83	0.83				0.84	0.02
		6 M HCl	191.3	2872.7	1.21							
	3	ASW	7.0	7.7	0.27							
		0.01 M HCl	122.8	28.8	0.09	0.01					0.05	0.11
		0.5 M HCl	3162.3	1498.3	0.12	0.12					0.12	0.00
		6 M HCl	294.3	4887.4	1.19							
	4	ASW	4.9	12.1	0.13	0.09					0.11	0.05
		0.01 M HCl	92.1	28.2	0.16	0.06					0.11	0.14
		0.5 M HCl	2427.5	333.2	-0.95							
		6 M HCl	248.1	3897.9	1.01							
	5	ASW	4.5	13.2	0.62							
		0.01 M HCl	86.0	33.7	0.16	0.15					0.16	0.02
		0.5 M HCl	3831.0	270.4	-1.13	-1.15					-1.14	0.02
		6 M HCl	259.1	4055.2	0.94							
	6	ASW	2.7	16.1	0.86							
		0.01 M HCl	93.8	27.0	-0.01							
		0.5 M HCl	3018.6	1430.7	-0.05							
		6 M HCl	218.8	3904.8	0.82	0.91	0.91				0.88	0.11
	7	ASW	2.4	15.1	0.84							
		0.01 M HCl	75.2	36.5	-0.25							
		0.5 M HCl	3224.4	2560.5	0.47							
		6 M HCl	199.1	3763.4	0.91							
	8	ASW	2.0	10.0	0.46							
		0.01 M HCl	93.8	28.2	-0.42							
		0.5 M HCl	2421.5	1793.0	0.23							
		6 M HCl	152.3	3554.4	0.83							
	9	ASW	3.3	25.4	1.14	0.83	0.82				0.93	0.36
		0.01 M HCl	82.4	25.6	-0.48	-0.48					-0.48	0.01
		0.5 M HCl	2677.0	1846.1	0.06							
		6 M HCl	126.2	2723.1	0.80							
	10	ASW	4.7	37.2	0.85							
		0.01 M HCl	67.3	23.8	-0.45							
		0.5 M HCl	1675.6	1211.8	0.22	0.19					0.21	0.04
		6 M HCl	103.7	1860.3	0.81							
	11	ASW			0.78	0.81					0.79	0.04
		0.01 M HCl	62.9	21.2	-0.43							
		0.5 M HCl	1101.2	873.0	0.20							
		6 M HCl	86.7	1949.8	0.68							
	12	ASW	0.6	8.2	0.69	0.81	0.74				0.75	0.12
		0.01 M HCl	58.1	22.1	-0.37							
		0.5 M HCl	1247.4	953.1	0.19							
		6 M HCl	104.7	2488.6	0.40							

	12.8	ASW	3.9	50.2	0.68						
		0.01 M HCl	40.5	22.6	-0.59	-0.56	-0.47			-0.54	0.12
		0.5 M HCl	1007.3	651.3	0.10	0.03				0.06	0.10
		6 M HCl	460.3	1257.7	0.80	0.80				0.80	0.01
Core 2	**1**	ASW	0.5	14.1	0.12	0.24				0.18	0.17
		0.01 M HCl	0.4	0.8	-1.06	-1.11				-1.08	0.07
		0.5 M HCl	69.5	5252.6	-0.18	0.20				0.01	0.55
		6 M HCl	28.8	36317.4	0.08						
	2	ASW	3.1	17.9	0.03	-0.21				-0.09	0.33
		0.01 M HCl	0.2	1.1	-0.27	-0.32				-0.29	0.08
		0.5 M HCl	57.4	3562.8	0.09	0.11				0.10	0.03
		6 M HCl	17.8	32171.5	0.02						
	3	ASW	3.1	20.7							
		0.01 M HCl	0.0	1.1	-0.31						
		0.5 M HCl	38.3	3650.9	0.08	0.11				0.10	0.03
		6 M HCl	23.8	39169.7	-0.05						
	4	ASW	2.8	19.9	-0.30						
		0.01 M HCl	0.0	1.2	-0.33	-0.40				-0.36	0.10
		0.5 M HCl	34.0	3307.6	0.16	0.08				0.12	0.11
		6 M HCl	33.3	45425.5	0.02						
	5	ASW	3.0	24.7	-0.37						
		0.01 M HCl	0.0	1.3	-0.41	-0.45				-0.43	0.06
		0.5 M HCl	33.5	3474.0	-0.01	-0.07				-0.04	0.09
		6 M HCl	19.1	42580.9	-0.13						
	6	ASW	3.3	22.6	-0.19						
		0.01 M HCl	0.0	0.9	-0.40						
		0.5 M HCl	48.8	3821.8	0.10	0.05	0.05			0.07	0.06
		6 M HCl	13.4	34350.8	0.03						
	7	ASW	1.8	19.7	-0.23	-0.23	-0.34			-0.27	0.12
		0.01 M HCl	5.0	1.2	-1.78						
		0.5 M HCl	245.0	2958.0	0.37	0.32				0.34	0.06
		6 M HCl	7.6	21568.4	-0.01						
Core 3	**1**	ASW	0.2	1.1	-0.89	-0.90	-0.86			-0.89	0.04
		0.01 M HCl	0.0	2.9							
		0.5 M HCl	3.1	3741.1	-0.98						
		6 M HCl	8.6	22882.3	-0.62	-0.58	-0.58	-0.61	-0.58	-0.59	0.05
	2	ASW	0.1	0.9	-0.98	-1.00				-0.99	0.02
		0.01 M HCl	0.0	1.4	-1.01						
		0.5 M HCl	4.1	4432.5	-1.10						
		6 M HCl	15.2	32056.5	-0.43						
	3	ASW	0.1	1.0	-0.89						
		0.01 M HCl	0.0	2.2	-0.82	-0.90				-0.86	0.11
		0.5 M HCl	5.5	4815.8	-1.04						
		6 M HCl	27.5	39994.5	-0.23	-0.28				-0.26	0.07
	4	ASW	0.1	0.9	-0.62						
		0.01 M HCl	0.0	1.2	-0.48						
		0.5 M HCl	9.4	3327.4	-0.84	-0.89				-0.86	0.08
		6 M HCl	280.8	43579.2	-0.11						
	5	ASW	0.0	0.9	-0.83						
		0.01 M HCl	0.0	2.9	-0.50	-0.59				-0.55	0.13
		0.5 M HCl	9.4	2588.2	-1.14						
		6 M HCl	512.5	54518.9	-0.30						
	6	ASW	0.0	0.9	-1.27	-1.24				-1.26	0.04

		0.01 M HCl	0.0	1.9	-0.62						
		0.5 M HCl	14.4	4453.9	-1.25						
		6 M HCl	339.0	45968.5	-0.32	-0.42				-0.37	0.14
	7	ASW	0.2	1.0	-1.25						
		0.01 M HCl	0.0	1.1	-0.73	-0.69				-0.71	0.06
		0.5 M HCl	13.6	5721.0	-1.33						
		6 M HCl	30.5	41127.6	-0.42						
	8	ASW	0.0	1.0	-1.79						
		0.01 M HCl	0.0	1.9	-0.69						
		0.5 M HCl	8.1	4757.2	-1.38						
		6 M HCl	148.9	39278.7	-0.46						
	9	ASW	0.2	0.9	-1.51						
		0.01 M HCl	0.0	0.9	-0.73	-0.63	-0.71	-0.79	-0.76	-0.72	0.13
		0.5 M HCl	12.5	5650.3	-1.31	-1.35				-1.33	0.05
		6 M HCl	246.7	37761.9	-0.45						
	10	ASW	0.0	0.9	-1.59						
		0.01 M HCl	0.0	1.1	-0.71	-0.68				-0.70	0.04
		0.5 M HCl	13.2	4780.6	-1.23	-1.22				-1.23	0.02
		6 M HCl	231.3	35730.0	-0.37						
	11	ASW	0.2	1.5	-1.36	-1.32				-1.34	0.05
		0.01 M HCl	0.0	2.2	-0.66						
		0.5 M HCl	20.8	6197.1	-1.11						
		6 M HCl	12.4	32247.2	-0.44						
Core 4	**1**	ASW	0.0	14.1	-1.17						
		0.01 M HCl	0.0	5.0	-0.97	-0.97				-0.97	0.00
		0.5 M HCl	3.0	2086.1	-1.19	-1.15	-1.20			-1.18	0.06
		6 M HCl	13.0	39791.2	-0.55	-0.50				-0.53	0.07
	2	ASW	0.1	84.9	-1.10						
		0.01 M HCl	0.0	4.0	-1.00						
		0.5 M HCl	1.7	3751.9	-1.20						
		6 M HCl	18.3	53341.3	-0.48						
	3	ASW	0.2	18.3	-0.94	-0.93				-0.94	0.02
		0.01 M HCl	0.0	2.9	-0.90						
		0.5 M HCl	6.1	3664.5	-1.20						
		6 M HCl	14.8	47916.5	-0.41						
	4	ASW	0.1	21.3							
		0.01 M HCl	0.0	3.1	-0.84	-0.85				-0.84	0.01
		0.5 M HCl	4.8	2098.1	-0.95	-0.91	-1.00	-0.85	-0.95	-0.93	0.11
		6 M HCl	38.2	63254.7	-0.32						
	5	ASW	0.1	41.8	-1.24						
		0.01 M HCl	0.0	3.8	-0.89						
		0.5 M HCl	5.4	3243.0	-0.96						
		6 M HCl	15.9	39125.2	-0.40						
	6	ASW	0.1	29.6	-1.21						
		0.01 M HCl	0.0	3.4	-0.94						
		0.5 M HCl	5.6	3354.7	-0.84						
		6 M HCl	34.6	42883.3	-0.34						
	7	ASW	0.1	27.3	-1.14						
		0.01 M HCl	0.0	2.8	-1.07	-0.97				-1.02	0.14
		0.5 M HCl	12.5	3169.7	-1.11						
		6 M HCl	35.5	48432.8	-0.48						
Core 5	**1**	ASW	0.8	6.9	-1.46						
		0.01 M HCl	0.0	4.2	-1.41	-1.50				-1.46	0.13

	0.5 M HCl	2.4	6035.2	-1.30							
	6 M HCl	2.8	33983.3	-0.52							
2	ASW	0.7	7.5	-1.55							
	0.01 M HCl	0.1	4.7	-1.48							
	0.5 M HCl	2.2	5235.9	-1.36							
	6 M HCl	2.5	32715.5	-0.71							
3	ASW	0.9	10.3	-1.48							
	0.01 M HCl	0.1	5.7	-1.45	-1.36					-1.41	0.13
	0.5 M HCl	1.6	5694.0								
	6 M HCl	2.9	35228.8	-0.76	-0.80	-0.75				-0.77	0.05
4	ASW	1.1	16.4	-1.29	-1.31					-1.30	0.03
	0.01 M HCl	0.1	8.2	-1.30	-1.20					-1.25	0.14
	0.5 M HCl	2.6	5979.2	-1.14							
	6 M HCl	3.0	37210.1	-0.64	-0.63	-0.53	-0.48			-0.57	0.16
5	ASW	1.1	17.6	-1.29	-1.30					-1.29	0.02
	0.01 M HCl	0.2	12.4	-1.30	-1.33					-1.32	0.04
	0.5 M HCl	4.1	7089.7	-1.13							
	6 M HCl	3.1	39593.6	-0.53							
6	ASW	0.8	27.8	-1.51	-1.53	-1.45				-1.50	0.08
	0.01 M HCl	0.3	20.5	-1.48							
	0.5 M HCl	3.9	5868.3	-1.16							
	6 M HCl	2.7	32124.8	-0.64							
Core 6											
1	ASW	0.8	5.8	-0.98	-0.92					-0.95	0.08
	0.01 M HCl	0.0	5.0	-1.13	-1.16					-1.15	
	0.5 M HCl	5.1	3500.9	-1.26							
	6 M HCl	4.3	12398.9	-0.05							
2	ASW	1.1	10.4	-0.86	-0.80	-0.90				-0.86	0.10
	0.01 M HCl	0.0	8.0	-1.07	-1.10	-1.13				-1.10	0.06
	0.5 M HCl	5.5	2267.4	-1.20							
	6 M HCl	7.3	19338.7	-0.48							
3	ASW	1.0	5.6	-0.39	-0.43	-0.34	-0.38	-0.36	-0.40	-0.38	0.05
	0.01 M HCl	0.0	4.1	-0.52							
	0.5 M HCl	5.2	4807.6	-0.99							
	6 M HCl	4.8	18190.5	0.32							
4	ASW	0.9	5.9	-0.02	-0.18	-0.12				-0.10	0.16
	0.01 M HCl	0.0	1.4	-0.03							
	0.5 M HCl	7.2	5418.9	-0.79							
	6 M HCl	2.8	8664.4	0.26							
5	ASW	2.5	3.9	0.34	0.36					0.35	0.03
	0.01 M HCl	0.0	0.9	0.23							
	0.5 M HCl	2.9	1884.2	-0.26							
	6 M HCl	2.8	7918.4	0.41	0.37					0.39	0.06
6	ASW	9.1	17.9	0.45	0.35					0.40	0.13
	0.01 M HCl	4.7	0.6	-0.77							
	0.5 M HCl	177.0	1507.9	-0.47							
	6 M HCl	8.3	9408.1	0.37							
7	ASW	2.2	5.4	0.40	0.33	0.31				0.35	0.09
	0.01 M HCl	21.5	0.6	-0.27							
	0.5 M HCl	1366.1	878.2	-0.41	-0.43					-0.42	0.02
	6 M HCl	4.4	12001.5	0.34							
8	ASW	2.3	11.7	0.26	0.68					0.47	0.59
	0.01 M HCl	25.3	0.9	-0.33							
	0.5 M HCl	803.6	1639.8	-0.46	-0.46					-0.46	0.00
	6 M HCl	6.2	9232.0	0.27							

Table A.3.9. Calculated isotopic composition of the Fe(III) component of the 0.5 M HCl extracted Fe phase from core 1

Depth (cm)	$\delta^{56}Fe_{Fe(II)\ 0.01\ M\ HCl}$ (‰)[a]	2σ	$X_{Fe(II)\ 0.01\ M\ HCl}$	low error estimate[b]	$\delta^{56}Fe_{Fe\ tot\ 0.5\ M\ HCl}$ (‰)	2σ	high error estimate[b]	$X_{Fe(II)\ 0.5\ M\ HCl}$	Extrapolated mixing line[c]						Calculated error[e]	$\delta^{56}Fe_{Fe(III)\ 0.5\ M\ HCl}$ (‰)[f]
									Low estimate				High estimate			
									Slope	Intercept[d]	Slope	Intercept[d]	Slope	Intercept[d]		
1	-0.06	0.13	0.800	0.45	0.63	0.13	0.81	0.522	-1.82	1.39	-2.48	1.92	-3.14	2.45	1.06	1.38
2	0.03	0.13	0.790	0.65	0.84	0.13	1.02	0.468	-1.94	1.56	-2.51	2.01	-3.08	2.46	0.90	1.55
3[g]	0.05	0.13	0.810	-0.06	0.12	0.13	0.30	0.679	*0.87*	*-0.65*	*-0.53*	*0.48*	*-1.93*	*1.61*	*2.27*	*0.27*
4	0.11	0.13	0.765	-1.13	-0.95	0.13	-0.77	0.879	*-10.94*	*8.48*	*-9.33*	*7.25*	*-7.71*	*6.02*	*2.47*	*-8.70*
5	0.16	0.13	0.718	-1.32	-1.14	0.13	-0.96	0.934	*-6.87*	*5.09*	*-6.01*	*4.48*	*-5.16*	*3.87*	*1.22*	*-19.54*
6	-0.01	0.13	0.776	-0.23	-0.05	0.13	0.13	0.678	*2.31*	*-1.80*	*0.43*	*-0.34*	*-1.45*	*1.12*	*2.92*	*-0.14*
7	-0.25	0.13	0.673	0.29	0.47	0.13	0.65	0.557	-4.60	2.85	-6.19	3.92	-7.78	4.99	2.14	1.37
8	-0.42	0.13	0.769	0.05	0.23	0.13	0.41	0.575	-2.39	1.42	-3.34	2.15	-4.29	2.88	1.46	1.11
9	-0.48	0.13	0.763	-0.12	0.06	0.13	0.24	0.592	-2.08	1.11	-3.15	1.93	-4.23	2.75	1.64	0.84
10	-0.45	0.13	0.738	0.03	0.21	0.13	0.39	0.580	-3.01	1.77	-4.17	2.63	-5.33	3.49	1.72	1.12
11	-0.43	0.13	0.748	0.02	0.20	0.13	0.38	0.558	-2.33	1.32	-3.30	2.04	-4.27	2.76	1.45	0.99
12	-0.37	0.13	0.725	0.01	0.19	0.13	0.37	0.567	-2.39	1.36	-3.55	2.20	-4.72	3.05	1.69	0.93
13	-0.54	0.13	0.642	-0.12	0.06	0.13	0.24	0.607	*-12.01*	*7.17*	*-17.31*	*10.57*	*-22.61*	*13.98*	*6.80*	*0.99*

[a] Correction for the pure Fe(III) component of the 0.5 M HCl extracted fe phase assumes that any residual Fe(II) in the sample is of the same isotopic composition as the primarily Fe(II) 0.01 M HCl extracted phase

[b] Projected high and low errors is calculated using the square root of the sum of squares of the error associated with the measured isotopic composition of the phases, i.e. sqrt(0.13^2+0.13^2) = 0.18

[c] The isotopic composition and mol fraction of Fe(II) 0.01 M HCl is taken as one end member of the mixing line, projecting a line from this point, through the isotopic composition and mole fraction Fe(II) of the 0.5 M HCl extracted Fe, to the other end member of $X_{Fe(II)} = 0$ allows for the estimation of the isotopic composition or the pure Fe(III) component of the 0.5 M HCl extracted Fe phase

[d] Note that the Y-intercept is the estimated isotopic composition of the sample when $X_{Fe(II)} = 0$

[e] Calculated error is the difference between the projected high and low isotopic composition of the sample

[f] Calculated isotopic composition using Equation 4

[g] Note that the extrapolated and calculated isotopic compostion resulted in anomalously low $\delta^{56}Fe$ values and were thus not used in calculation of fractionation factors

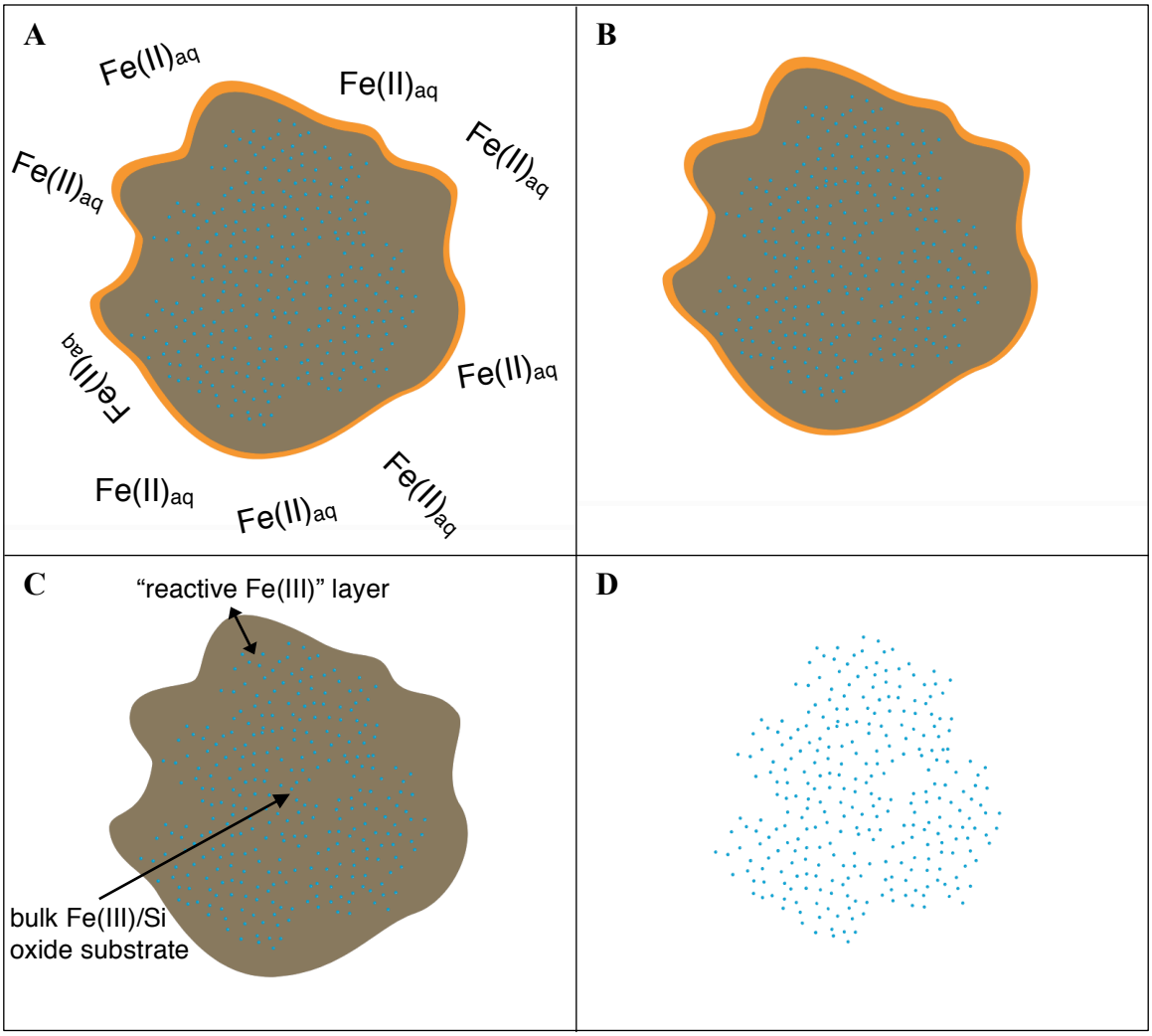

Figure A.3.1. Conceptual illustration of the sequential HCl extraction of a Fe particle to show how different Fe phases were collected from the CP core samples or in the Fe(III) reducing incubations. (A) Due to the low volume of pore fluid in the core samples, an equal mass of artificial spring water (ASW) was mixed with Fe/Si oxides to liberate any aqueous Fe(II), which was then removed by centrifugation. (B) A short, 15 minute extraction (1 hr extraction in the Fe(III)-reducing incubations) using dilute 0.01 M HCl was used to remove the sorbed Fe(II) layer, shown here as the orange rim around the Fe particle. (C) A 24 hr extraction in 0.5 M HCl was used to remove the "reactive Fe(III)" (see Crosby et al., 2005, 2007). (D) Finally, after a 24 hr extraction in concentrated 6M HCl, all of the bulk substrate Fe(III) is dissolved and removed, and all that remains is amorphous Si, shown here as blue dots.

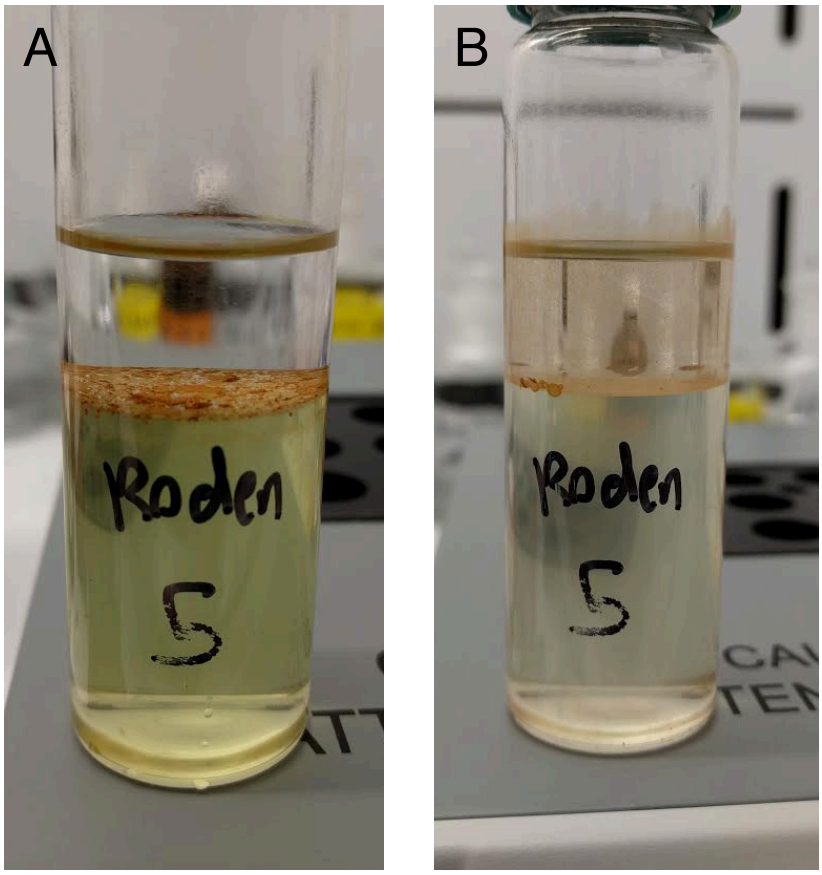

Figure A.3.2. Photos of liquid-liquid extraction vials following centrifugation showing the potential iron-organic complex formed at the interface between aqueous and organic phases during lipid extraction. Photo A shows a rust-colored layer between the 5% NaCl solution (top layer) and hexane phase (bottom layer) following base hydrolysis in 0.5 M NaOH in methanol. Photo B shows the same vial following three additional hexane extractions, acidification to pH 1-2 with HCl, and liquid-liquid extraction using 4:1 hexane:dichloromethane.

749

Figure A.3.3. Photo of coring site 2 where a variety of plant detritus including sticks (S), pinecones (P), and leaves (L) has been trapped and partially buried in the CP oxide sediment. The potential sources of lignin shown here are not readily observable at the hot spring vent.

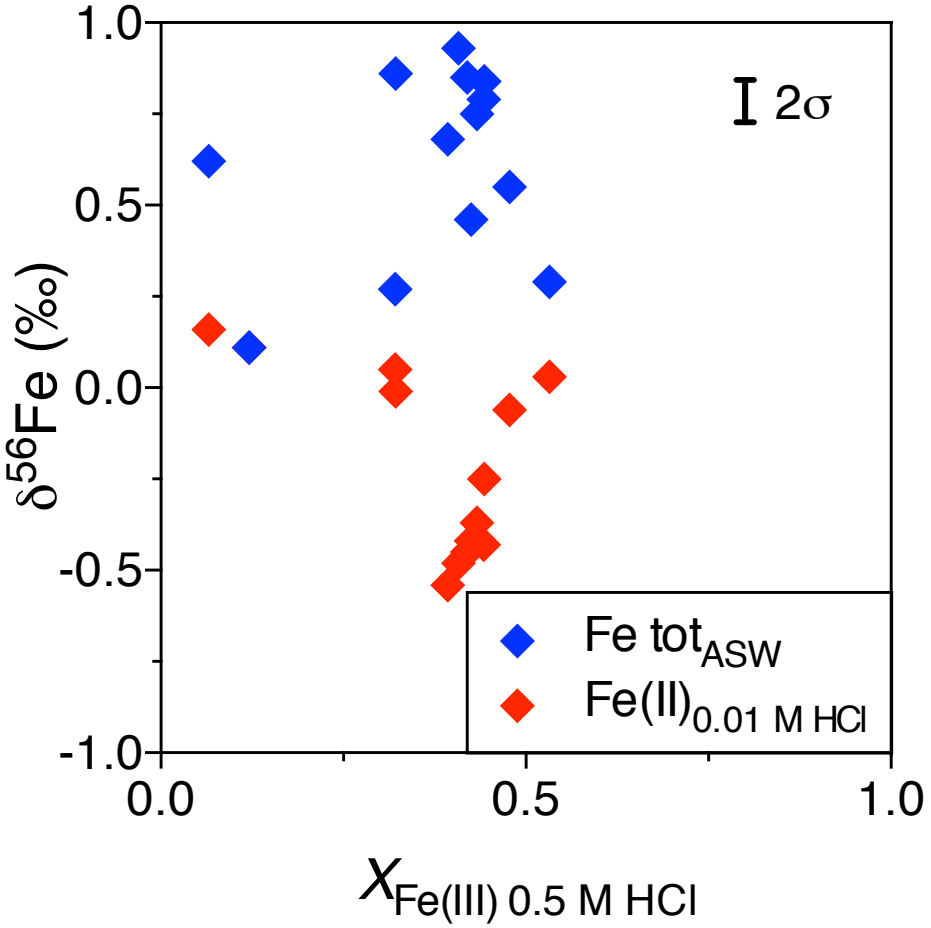

Figure A.3.4. Isotope composition of the ASW extracted total Fe and $Fe(II)_{0.01\ M\ HCl}$ versus the proportion of Fe(III) in the 0.5 M HCl extracted Fe phase from the same depth interval in core 1. Data did not fit a linear regression line, R square values of 0.08 and 0.31, respectively. Thus, estimating the Fe isotope fractionation between nominally Fe(II) phases and $Fe(III)_{0.5\ M\ HCl}$ was not possible.

CONCLUSION

The purpose of PhD research project was to identify which microbial organisms inhabit Chocolate Pots hot springs (CP), determine what genomic evidence is present to indicate their putative metabolic potential, and measure the isotopic composition of *in situ* samples to investigate whether or not stable Fe isotope analyses are a valid technique for identifying past of present microbial Fe redox activity.

This project has been a continuation of my MS research which investigated the microbial Fe(III) reduction potential of an enrichment culture derived from CP using the native Fe/Si oxides as an electron acceptor. A robust Fe(III)-reducing community was established was established, however the question of how representative of the *in situ* environment in terms of both the microbial community members and their distribution remained. We hypothesized that microbial Fe(III) reduction would be active at CP, be implicated in organisms related to those we identified previously in the enrichment culture experiment like *Geobacter*, *Melioribacter*, and *Thermodesulfovibrio*, and that these organisms would encode enzymes putatively involved in Fe redox transformations. Further on, we hypothesized that a complete Fe redox cycle was operative at CP, that is, both an Fe(III)-reducing and Fe(II)-oxidizing microbial was present and active. Finally, with more of a direct astrobiological connection, we hypothesized that microbial activity, e.g. Fe(III)-reduction, would leave behind biosignatures in the form of stable Fe isotope ratios that could be used to inform us in investigations of early life on Earth, or theoretical ancient life on Mars.

High levels of Fe(III) reduction were observed in sediment samples collected from the CP vent pool, however the activity level dropped off substantially within a few meters of the vent. Even under acetate amended incubations, suggesting the microbial community further

downstream is less primed for Fe(III) reduction. The most important discovery of this experiment was that activity levels were comparable in incubations without additional electron donor. This suggested that whatever the carbon and electron donor was *in situ* it was sufficient to support an active Fe(III)-reducing microbial community. Although this then raised the question of what the source of carbon was *in situ*, and that investigation is still underway.

The stable isotope probing (SIP) experiments were a success in that we probed for and stimulated members of the microbial community capable of reducing Fe(III) coupled to acetate oxidation. However, the prominent taxon in these incubations was related to *Geobacter*, which we lovingly refer to as being a "weed" and is well known for rapid growth and out competing other members of the microbial community when fed small amounts of acetate. This is incredibly useful for bioremediation application, where *Geobacter* species are naturally abundant in only trace numbers, but when given acetate, their population explodes, and are able to help remediate contaminated groundwater and sediments, e.g. uranium contamination. Here too at CP *Geobacter* is present in the native microbial community, but in very trace numbers such that we question the environmental significance of these organisms. The unamended control in the SIP experiment revealed an increase in *Thermodesulfovibrio* and Ignavibacteria related taxa in incubations that demonstrated Fe(III) reduction activity. Granted, it was less activity than in the acetate stimulated and *Geobacter*-containing incubations, but this gave us the first indication of which members of the microbial community may be involved in Fe(III) reduction *in situ*. Metagenomic sequencing results from these incubations showed *Thermodesulfovibrio* and Ignavibacteria related taxa to encode putative extracellular electron transfer (EET) pathways as further support of their involvement in Fe redox transformations. A more thorough investigation of potential EET systems was conducted in these experiments as compared to the bioinformatics

approach taken in my MS research, and set the stage for subsequent direct investigations of the *in situ* microbial community.

In order to avoid any potential biases introduced from conducting incubation experiments, i.e. *Geobacter* outcompeting all other Fe(III)-reducers, we studied the *in situ* environment by collecting sediment and spring water directly CP and using shotgun metagenomic sequencing to study the native microbial community composition and distribution. By using metagenomic read coverage as a proxy for abundance *in situ* we were able to surmise which taxa were prominent members of the microbial community. Several reconstructed genomes identified as relatives of Ignavibacteria were identified as well as a couple *Thermodesulfovibrio* relatives, all of which encoded putative EET pathways. Curiously, several of these taxa appeared to be abundant in the more distal core sections, yet little Fe(III) reduction activity was observed here. This highlights the disconnect between putative abundance of an organism, its apparent activity *in situ*, and its overall function in the microbial community. These results also make a case for the importance of direct measures of *in situ* levels of activity of a particular organism using techniques like transcriptomics. Some additional putative Fe(III)-reducing taxa, which had not previously been observed in the incubation studies, were identified including relatives of *Caldithrix* and *Deferrisoma*. The Fe(III)-reducing microbial community at CP is complex and dynamic, and not just comprised of a single prominent Fe(III) reducer as we previously thought.

The microbial community responsible for the other side of the Fe cycle, lithoautotrophic Fe(II) oxidizers, appear to be present at CP as well. Reconstructed genomes identified as a relative of *Sideroxydans* encoded both an EET system and CO_2 fixation pathway, supporting its role as a putative Fe(II) oxidizer. The relatively low abundance of these organisms was not

unexpected considering the poor energy yields of Fe(II) oxidation at neutral pH, but it was unclear how significant of a role these organisms played *in situ*. Ultimately we concluded that the vast majority of Fe(II) oxidation likely occurred indirectly by reacting with atmospheric oxygen, or biogenic oxygen from the cyanobacterial community. These cyanobacteria are also the most likely source of fixed carbon for the heterotrophic microbial community, although this investigation is still underway.

To be blunt, the analysis of stable Fe isotope ratios was not a useful geochemical tool to assess the Fe(III) reduction activity at CP. Fractionation between Fe(II) and Fe(III) phases in the rock record (e.g. banded iron formations) has been cited as evidence for relic microbial activity. Additionally, under controlled laboratory experiments, dissimilatory Fe(III) reduction has been shown to produce significant fractionation on the order of -3‰ between aqueous Fe(II) and the reactive Fe(III) phase. However, the environmental variability of *in situ* investigations, such as the work done at CP, introduces too many uncertainties into the results to gain any clear understanding. For instance, in the relatively controlled conditions of the Fe(III)-reducing incubation experiments used to track changes in Fe isotope composition through time as Fe(III) reduction proceeds, conditions were so varied between experiments that it was difficult to compare results. In my MS work, we conducted a similar experiment using processed CP oxides (derived from a different location at the hot spring), inoculated with a sample of the enrichment culture, and incubated for about three days. Here, we used the fine-grained portion of the natural CP oxides that contained members of the native microbial community at their natural levels abundance, and incubated for close to three months. The former study revealed expected Fe isotope fractionation factors as a result of Fe(III) reduction, yet here even though overall trends in the data were apparent, the error associated with the data were large.

As for potentially investigating Fe(III) reduction *in situ*, the analysis of stable Fe ratios in CP materials was even more obscured. Fe(II) was nonexistent in samples collected beyond the CP vent, therefore no fractionation calculations were possible. This was not too unsurprising or discouraging, since these results corroborated the microbial community analysis of Fe(III) reduction activity. Aqueous Fe(II) was not measurable in the sediment cores, and the wash step with artificial groundwater may have only liberated colloidal Fe(III) phases, and not been representative of the aqueous Fe(II) that might have been present *in situ*. Dilute acid extractions using 0.01 M HCl were not digested for a sufficiently long enough time to remove all "sorbed" Fe(II). As a result, very high Fe(II) concentrations were measured in 0.5 M HCl-extracted phases that were nominally supposed to be comprised of Fe(III). Once again, these high uncertainties made it difficult to interpret the Fe isotope ratios. A negative fractionation between primarily Fe(II) and primarily Fe(III) phases near the surface of the core collected at the CP vent was apparent, and suggestive of Fe(III) reduction. However it was difficult to report a fractionation factor with certainty and compare the *in situ* results with experimental studies. Unless variation in oxygen versus oxygen-free conditions, microbial community composition, mixed and undefined Fe oxide substrates, silica concentrations, and extent of reduction can be accounted for and controlled in laboratory settings, the inability to confidently relate *in situ* results to experimental result makes the Fe isotope composition of a sample an unreliable biosignature.

In summary, we identified putative members of the CP microbial community that are responsible for Fe(III) reduction *in situ*, *Thermodesulfovibrio* and Ignavibacteria. There may be other organisms contributing to this process, but these two have been identified repeatedly and appear to be prominent members of the microbial community. The metabolic potential for lithoautotrophic Fe(II) oxidation by relatives of *Sideroxydans* is present at CP, however further

investigation is required to understand how active this process is *in situ*. The Fe isotope composition of a sample appears to be an unreliable biosignature for Fe(III) reduction activity, and *in situ* analyses introduces to many variables and uncertainty in the data.

To any potential future graduate students studying Chocolate Pots, I recommend a thorough transcriptomic investigation of the sediment and water column microbial communities at the CP vent. Coassemble a bunch of deeply sequenced metatranscriptomes and look for the increased expression of genes in EET systems and CO_2 fixation pathways. As for the identity of the *in situ* Fe(III) reducers, I think this is most likely accomplished by a consortium of organisms, but I'm still curious what they are. I attempted an isolation campaign of the *Melioribacter* relative from the enrichment cultures from my MS, but ultimately abandoned that line of inquiry. I now think that the *Thermodesulfovibrio* relative may contribute more *in situ*, so maybe you can take that approach? If you're involved in any Mars missions, that's awesome! I also recommend against using stable Fe isotopes as potential biosignature. As of now, we don't know the bulk Martian crustal average, and as I described above, the range of variables makes the results difficult to interpret. Maybe in combination with other tools it could be advantageous, carbon isotopes, microfossils, etc. Thanks for reading, and good luck in your future endeavors.

APPENDIX

“Dissertation Fuel”

Completing a PhD is a tremendous amount of work and incredibly difficult research wise, and probably even more so mentally taxing. I can't count the number of times I wanted to throw in the towel and move on with something else, and this feeling was only exacerbated by the anxiety and depression I faced as a graduate student. I'm glad I didn't quit. I have many people to thank for that, primarily my wife, Katie, and my children, Charlie and Max. They encouraged and motivated me when I was at my lowest points and most importantly have given a reason to continue with my program. I also need to thank my therapist and the inventors of *Citalopram* for helping regulate my mental health. I'm proud of what I've accomplished and I hope that it opens doors for me such that I'm able to better provide for my family in the future. I have created this appendix as a means of recording a few of the things that have helped these past several years.

> "I have robbed my family of my time in order to please people whose affections and loyalty will never approach that which my family offers so freely."
>
> – Andrew Barlow, *Fatherly*

> "Life is more than time passing before death, it is the sum and total of all we make of it. Decisions may not be easy, but many is the time when not making a decision, not taking action is worse than a poor decision."
>
> – Elegos A'kla, *I Jedi*

These two quotes capture much of the struggle I've felt as a graduate student, trying to balance work and family, and trying to be satisfied with my career choice. My family is the most important aspect of my life. As such, I've decided that academia is not the path for me, as I fear it would require more time, and take more time from my family, than I am willing to give. In turn, this decision made my question my choice to enter graduate school all the more. I'm satisfied with my decision to earn my PhD, and I view it now as an opportunity to provide for my family in such a way that I can maintain balance.

I like beer. Homebrewing is a hobby I picked up early in my graduate career, and it's lapsed recently as I've worked on completing this document, but I hope to more regularly create new brews in the near future. My field site was called Chocolate Pots hot spring, primarily due to the deep orange-brown color of the iron oxide deposits, but I always thought it'd be fun to play on that and do something with chocolate related to my graduate research. A little over a year ago I had some filtered spring water from my hot spring leftover from an experiment and thought using in in a batch of homebrew would be rather symbolic. I also think it's appropriate that I apparently made this batch of beer on May 22, 2017, a year to the day before my PhD defense.

Brew & Bed & Breakfast (B^3) Brewing

"Dissertation Fuel" Coffee Stout (because beer and coffee keep us going)
"Primordial Soup" Chocolate Stout

1. All grain
    a. 8 lbs 2-row
    b. 1 lb rye malt
    c. 1 lb roasted barley
    d. 1 lb dark chocolate malt
2. Step infusion 1 qt/lb
    a. 11 qt (2.75 gal) water, including 2 L Chocolate Pots spring water
3. Add grain to 145°F water and 350 g fresh (frozen) whole Cascade hops from the Roland Lee hop farm in Fort Atkinson, hold for 30 min
4. Raise temperature to ~155°F with 5 qt boiling water, hold for 45 min
5. Add 2 qt boiling water to raise temperature to ~167°F for final conversion, hold for 20 min
6. Sparge with 3 gal 170°F water
7. Bring wort to a boil and split into 2.5 gal batch for coffee stout, and 6 gal for chocolate stout
8. Add Newport hops, 60 min boil remaining
    a. 10 g for coffee
    b. 18 g for chocolate
9. Add 56 g baking chocolate to chocolate stout, 60 min boil remaining
10. Add UK Challenger hops, 10 min boil remaining
    a. 10 g for coffee
    b. 18 g for chocolate
11. Add Irish moss, 5 min boil remaining
    a. 0.3 g for coffee
    b. 1 g for chocolate

12. Add 56 g Trader Joe's Guatemalan extra dark roast to coffee stout wort post-boil
13. Wyeast 1084 Irish Ale yeast
14. Ferment for 10 wk
15. Rack to secondary fermentor
    a. Add 2 oz. cacao nibs extracted in 1 c vodka to chocolate
16. Brewer's Friend estimate: 60 IBU, 4.5% ABV

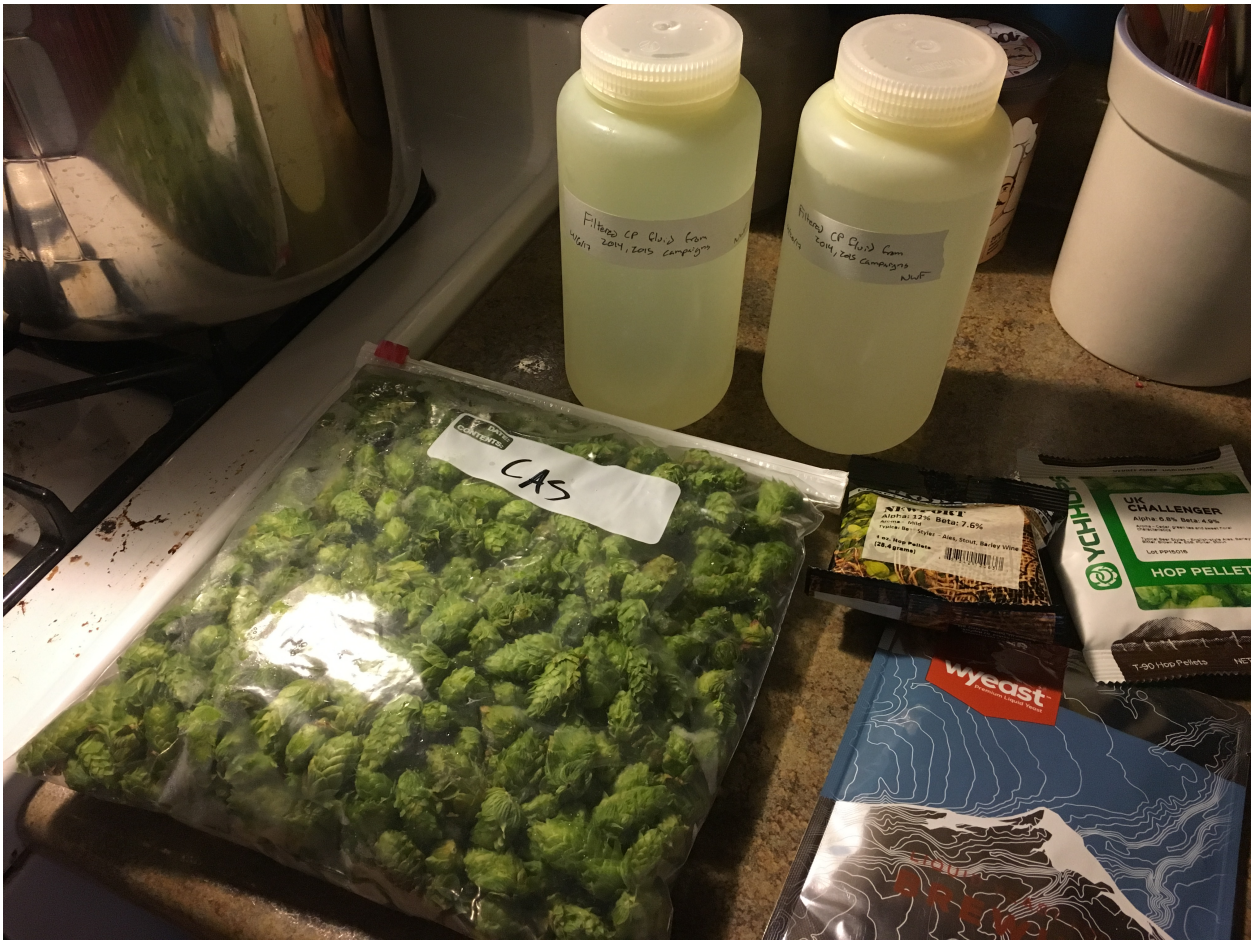

The ingredients

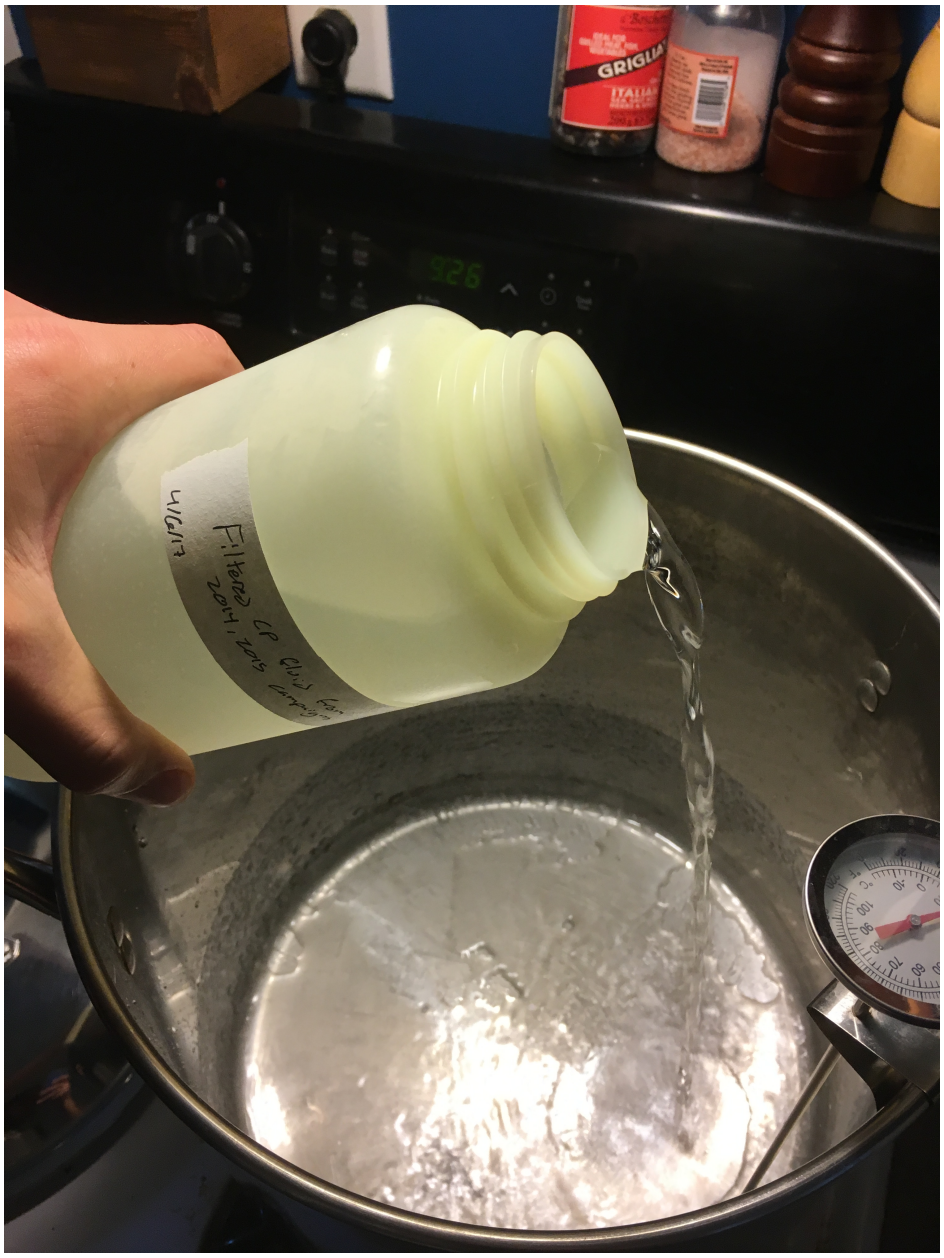

Adding the spring water

Mixing in the grain

My brewing assistant!

Transferring the wort

Sparging the grain

Vodka extracted cacao nibs

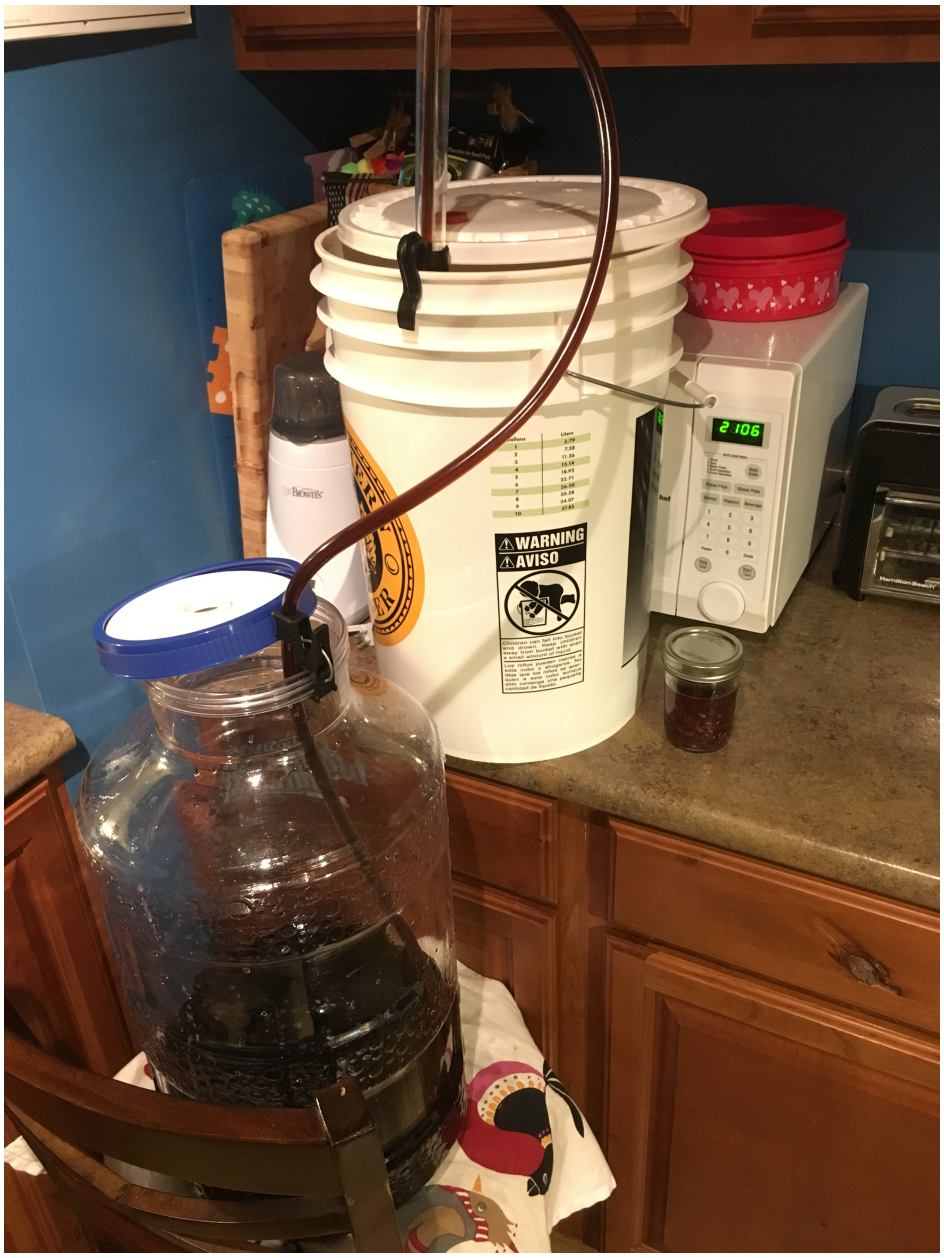

Racking to the secondary

Lovely day for a B^3 original!